UCRL-18313

cy. 2

RECEIVED
LAWRENCE
RADIATION LABORATORY
NOV 6 1968
LIBRARY AND
DOCUMENTS SECTION

University of California

Ernest O. Lawrence Radiation Laboratory

TWO-WEEK LOAN COPY

This is a Library Circulating Copy which may be borrowed for two weeks. For a personal retention copy, call Tech. Info. Division, Ext. 5545

CHARGE AND ENERGY DISTRIBUTION OF RECOIL ATOMS FROM THE ALPHA DECAY OF TH^{226}

Karlene Corbit Klages Gunter

(Ph.D. Thesis)

September 1968

Berkeley, California

UCRL-18313
cy. 2

DISCLAIMER

This document was prepared as an account of work sponsored by the United States Government. While this document is believed to contain correct information, neither the United States Government nor any agency thereof, nor the Regents of the University of California, nor any of their employees, makes any warranty, express or implied, or assumes any legal responsibility for the accuracy, completeness, or usefulness of any information, apparatus, product, or process disclosed, or represents that its use would not infringe privately owned rights. Reference herein to any specific commercial product, process, or service by its trade name, trademark, manufacturer, or otherwise, does not necessarily constitute or imply its endorsement, recommendation, or favoring by the United States Government or any agency thereof, or the Regents of the University of California. The views and opinions of authors expressed herein do not necessarily state or reflect those of the United States Government or any agency thereof or the Regents of the University of California.

UCRL-18313

UNIVERSITY OF CALIFORNIA

Lawrence Radiation Laboratory
Berkeley, California

AEC Contract No. W-7405-eng-48

CHARGE AND ENERGY DISTRIBUTION OF RECOIL ATOMS FROM THE ALPHA DECAY OF TH^{226}

Karlene Corbit Klages Gunter

(Ph. D. Thesis)

September 1968

CHARGE AND ENERGY DISTRIBUTION OF RECOIL ATOMS FROM THE ALPHA DECAY OF TH^{226}

Contents

Abstract 1

I. Introduction

A. General Theory and Previous Work 1

B. Purpose of the Experiment 5

C. General Outline of Experiment and Nomenclature 8

II. Experimental Procedure

A. U^{230} Source Preparation 13

B. Th^{226} Source Preparation 15

C. Experimental Apparatus 18

D. Identification of Recoils

1. Introduction 29

2. Production of Two and Three-Pronged Events--Theory and Experiment 32

3. Interference of Ra^{222} Recoils--Theory and Experiment 48

4. A Check of the Theory using Data from the Thin Plates and Experimental Determination of the Probability Curve 57

E. Energy Calibration of the Double Focusing Alpha Spectrograph for Regular Plates 62

III. Source and Pressure Effects on the Charge Energy Distributions of Th^{226} Recoils

A. Source Effects--Theory and Experiment 67

B. Pressure Effects--Theory and Experiment 74

IV. Results

A. Th^{226} Alpha Spectrum and Half Life.

1. Theory and Experiment 81

2. Conclusions 89

B. Comparison of Different Methods of Making Thin Alpha Sources

1. Experimental Results and Hypotheses 91

2. Theory 125

3. Conclusions and Future Experiments 134

C. Charge and Energy Distributions of Th^{226} Recoils

1. Experimental Results 138

2. Theory 194

3. Conclusions and Future Experiments 196

V. Error Analysis 198

Acknowledgments 200

References 201

CHARGE AND ENERGY DISTRIBUTION OF RECOIL ATOMS FROM THE ALPHA DECAY OF TH^{226}

Karlene Corbit Klages Gunter

Lawrence Radiation Laboratory
University of California
Berkeley, California

ABSTRACT

The charge and energy distribution of Th^{226} recoils from thin, electrostatically collected recoil sources were studied with a 180 deg double focussing alpha spectrograph. It was determined that the energy distributions so obtained were the result of collisions between the recoils and atoms on or in the source plate. The charge distribution of the recoils associated with $Th^{226}\alpha_0$ peaked at a charge of +1 whereas those associated with the electron conversion process following the emission of a $Th^{226}\alpha_{111}$ peaked at a charge of +11. These charge distributions are likely not too different from those which would be obtained from the decay of gaseous Th^{226}.

In order to insure that the recoils sources used for the above study were thin, a series of experiments were carried out to determine the best method of preparing consistently thin alpha sources. Three techniques were investigated: vacuum sublimation, electrostatic parallel plate collection and cylindrical electrostatic collection on a thin edge. Of these three, parallel plate collection produced the thinnest sources by far. The best such plates were made by collecting recoils in air at STP onto clean Pt employing the smallest possible source-collector separation and the minimum electric field intensity needed for total collection.

In connection with this work, more accurate values were obtained for the intensities of the various alpha groups of Th^{226} than are presently

in use. The intensity of the 111.1 keV γ ray was also obtained along with evidence that the present level assignments for the third and fourth excited states of Ra^{222} are correct.

I. INTRODUCTION

A. General Theory and Previous Work

When alpha decay occurs, the daughter or recoil atom suffers an extensive readjustment of the atomic electrons surrounding it. The end result of such an adjustment can be a recoil with a relatively high net positive charge. The final charge is generally the result of several different processes.

Midgal[1] in 1941 was the first to tackle the theoretical problem of the effects of alpha decay upon the atomic electrons. In 1953, J. S. Levinger[2] further discussed and extended Midgal's theory and demonstrated the areas where it tended to break down with a comparison between theory and experiment. In 1955, H. M. Schwartz[3] suggested a change in coordinate systems which further clarified the theory. Unfortunately, all of the theory that has been developed thus far deals with the inner shell electrons. The ionization of these inner shell electrons during alpha decay is the least probable of events, and hence contributes little to the final charge distribution of recoils.

For a basic understanding of the problem, the atomic electrons surrounding a nucleus can be divided into three groups: the inner shell electrons which travel much faster than the alpha particle, the outer shell electrons which travel much slower than the alpha particle, and the intermediate electrons.

For the inner shell electrons, alpha decay is an adiabatic process. One could treat alpha decay for these electrons by using molecular orbital theory where the daughter nucleus and alpha particle are treated as separate nuclei. This is not necessary, however, for heavy atoms because the potential due to the alpha particle is so much smaller than the potential

due to the nucleus that it can be treated as a perturbation. One can calculate the ionization probabilities for various inner shell electrons by this technique. In so doing it is essential to take into account the physical recoil of the nucleus. This leads to ionization probabilities per alpha decay on the order of 1×10^{-7} for the K shell electrons and 0.6×10^{-4} for the L shell electrons for an atom such as Po^{210}, whereas the experimental values are 2.0×10^{-6} and 2.9×10^{-4} respectively.[2] As one works outward away from the nucleus, the two assumptions (a) that this is an adiabatic process, and (b) that perturbation theory can be used, become poorer and poorer and the resulting transition probabilities agree less and less with experimental values.

The problem of the intermediate electrons has not been handled theoretically at all except for some statements to the effect that the probability of ionization due to a direct "collision" between the alpha particle and an atomic electron is greatest when the atomic electron's velocity is approximately the same as that of the alpha particle.

The outer shell electrons generally see alpha decay simply as a sudden change in the nuclear charge unless the alpha particle happens to directly collide with them. Unfortunately, no one has made these theoretical calculations for alpha decay although Migdal[1] and Green[4] have both calculated the sudden approximation for beta decay.

Once the direct effects of the alpha decay have been calculated, the process is still not complete. Holes in any shell other than the outermost shell will tend to fill either by an x-ray transition or by an Auger transition.[5-7] Such Auger processes further increase the net charge of the recoil atom. Furthermore, the vacancy cascades in themselves will perturb the orbits of electrons further out and hence can cause electrons

to be ejected that are not taking direct part in the Auger or x-ray transition. The lifetimes of such Auger transitions are on the order of 10^{-13} to 10^{-15} sec whereas the "lifetimes" of the direct alpha particle induced ionizations is of the order of the time it takes the alpha particle to leave the vicinity of the recoil atom, or about 10^{-17} sec.

If the alpha decay leaves the daughter nucleus in an excited state which can decay by electron conversion, we have a further process by which the final charge of the recoil atom is greatly increased. This is because electron conversion takes place in the innermost electron shells and will inititate a vacancy cascade which may greatly increase the net charge of the recoil atom.

Little work has been done on the charge or energy distribution of recoils resulting from alpha decay[8-10] and no work, has been published in the available literature on the energy distribution of very thin recoil sources. This lack of data on the charge and energy distribution of recoils from alpha decay is mainly due to two factors. First, a gas is the ideal subject for such a study because the resulting charge and energy distribution will be the direct result of the alpha decay and not the result of some interaction between the recoil and the backing material on which the alpha source is placed. This in turn limits one to a large extent to the rare gases, most of which undergo beta decay[11-15] rather than alpha decay. Second, atoms with few electrons are more easily analyzed theoretically and hence amenable to a comparison between theory and experiment, but they do not decay by alpha emission.

In addition to work done on the charge distribution of the recoil as a whole, some work has been done on Po^{210} on the formation of particular vacancies in the inner electron shells due to alpha decay. This was done as a means of checking Migdal's and Leveringer's theories.[17-18]

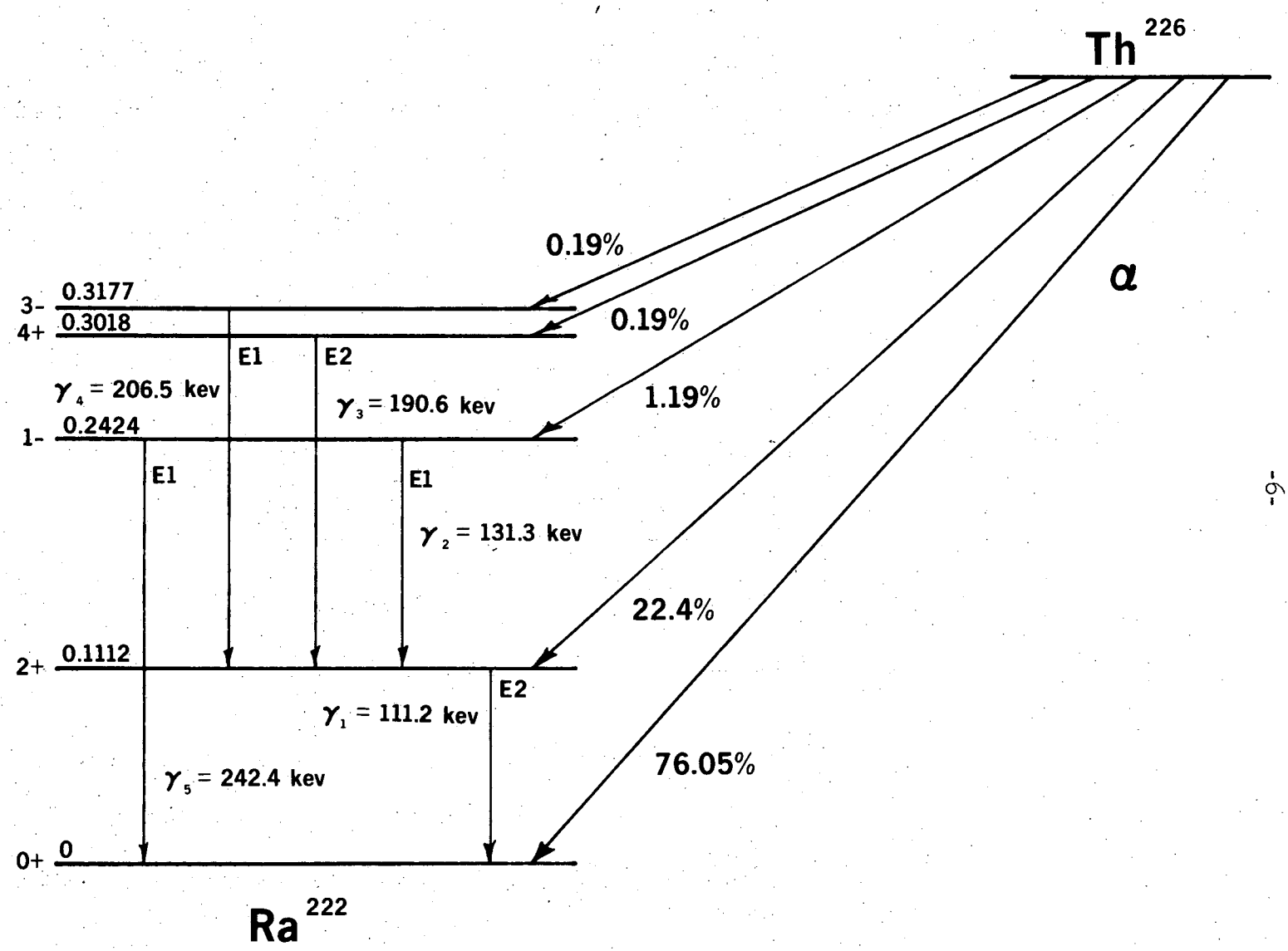

XBL 686-1088

Figure 1. Alpha decay scheme of Th^{226}.

resulting from electron conversion in the inner electron shells.

C. General Outline of Experiment and Nomenclature

The Th^{226} recoil sources were made by a variety of techniques which are extensively discussed in the section on Th^{226} source preparation. The recoils were studied using a 180 deg double focusing alpha spectrograph in conjunction with photographic emulsions for dection.[26-28] The alpha particles appear in the emulsion as nearly parallel tracks of approximately the same length. The recoils appear in the emulsion as two or three alpha tracks of varying length and direction coming from a common vertex on the surface of the emulsion (2- and 3-pronged events)(see Fig. 10, page 30). These 2- and 3-pronged events represent only a portion of the total number of recoils striking the plate.

It was necessary to employ two different techniques to obtain the desired information. The first technique used the alpha spectrograph in the normal manner (see Fig. 2), to obtain both the energy distributions of charges +2 through +20 and the ratios between recoils of those charges which were recorded as 2- and 3-pronged events and their corresponding alpha peaks. The information concerning the energy distribution for any given charge was obtained directly off the photographic emulsion by plotting number of events vs. position on the emulsion. Because of the variation of field with radius the distance along the plates is almost a linear function of the energy of the particles striking the plate. The ratios could not be obtained quite so directly because it is impossible to get recoils of charge +n and the corresponding alpha peak on the same plate at the same time except when n = 2. Therefore, in order to obtain the desired ratios, a plate was made containing recoils of charge +n followed by a plate containing charge +2 recoils and all the alpha peaks. These plates employed the same Th^{226} recoil source and careful records were kept

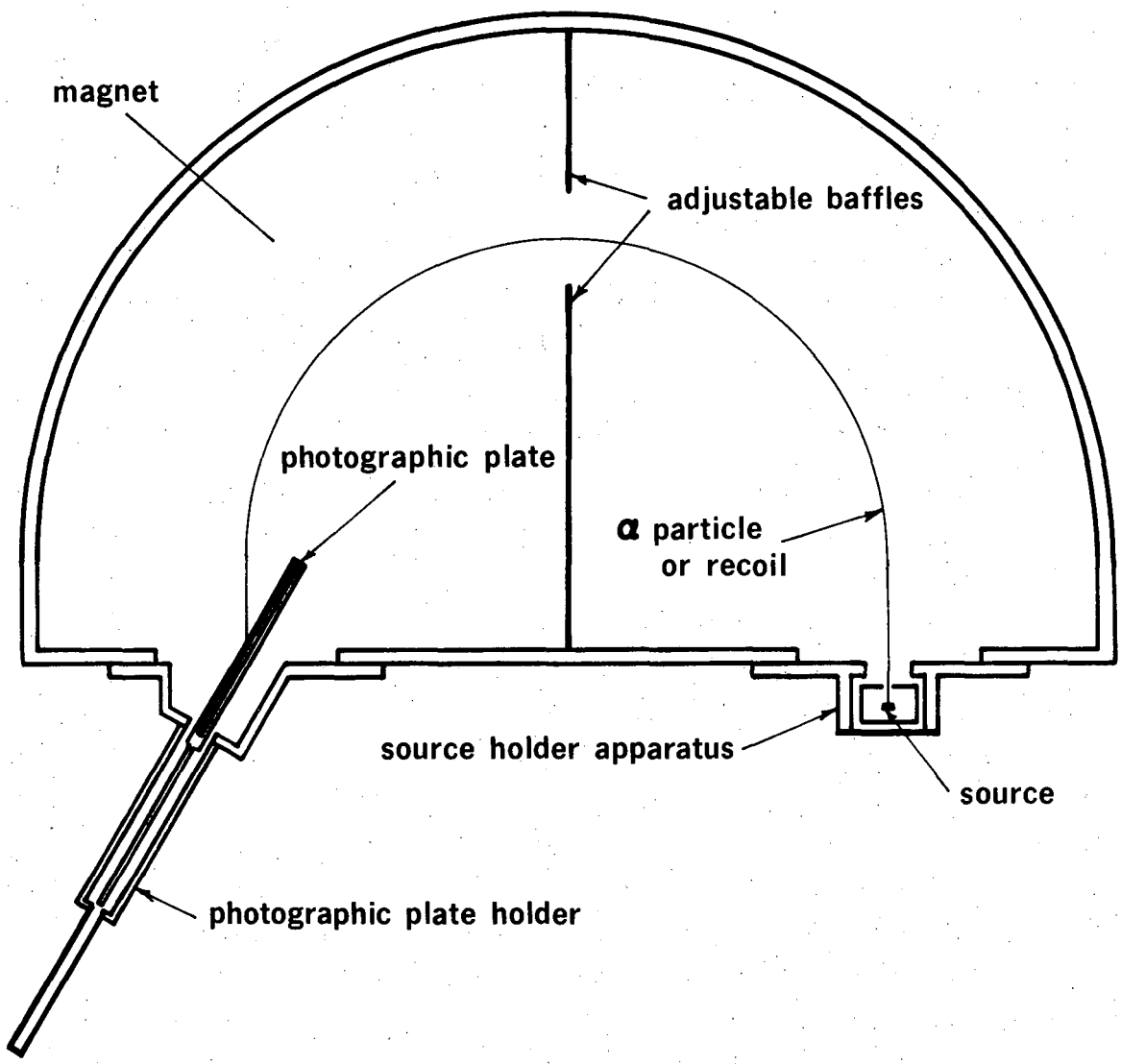

XBL 686-1086

Figure 2. Schematic diagram of the 180 deg double focusing alpha spectrograph when used in the "regular" plate configuration.

of time of exposure for both plates. Thus, a correlation could be made between the number of alpha decays that occurred during the exposure of the +n recoil plate and the actual number of alphas counted on the second plate.

Unfortunately, the magnetic field of this spectrograph is not strong enough to enable one to investigate charges +1 or -1 by this technique and of course charge zero recoils are not affected by a magnetic field at all. Thus, it was necessary to follow another technique to investigate these charges and to correlate them with the higher charges. This was done by designing an apparatus to hold a photographic plate in between the pole tips of the alpha spectrograph in direct line with the source (see Fig. 3). This apparatus made it possible to obtain the charge zero recoils along with several higher charges depending upon the magnetic field that was employed. In order to separate the various charges, a slit system was employed corresponding to a slit at the source and a collimating slit 4.75 cm in front of the source. This apparatus produced what are called "thin" plates because they are so much narrower than the plates that are normally used in the alpha spectrograph. It has several drawbacks. First, various charges hit the plate at different angles and since the ratio of the number of 2- plus 3-pronged events to the total number of recoils depends upon the angle of incidence of the Th^{226} recoil, some means of obtaining this ratio as a function of angle had to be found. This problem did not arise for the regular plates because the Th^{226} recoils always hit the photographic emulsion at approximately the same angle regardless of their charge. Second, one can not obtain a direct ratio between recoils and alphas because the alpha peak at charge +2 contains not only the Th^{226} alphas but also the alphas of all the daughter atoms

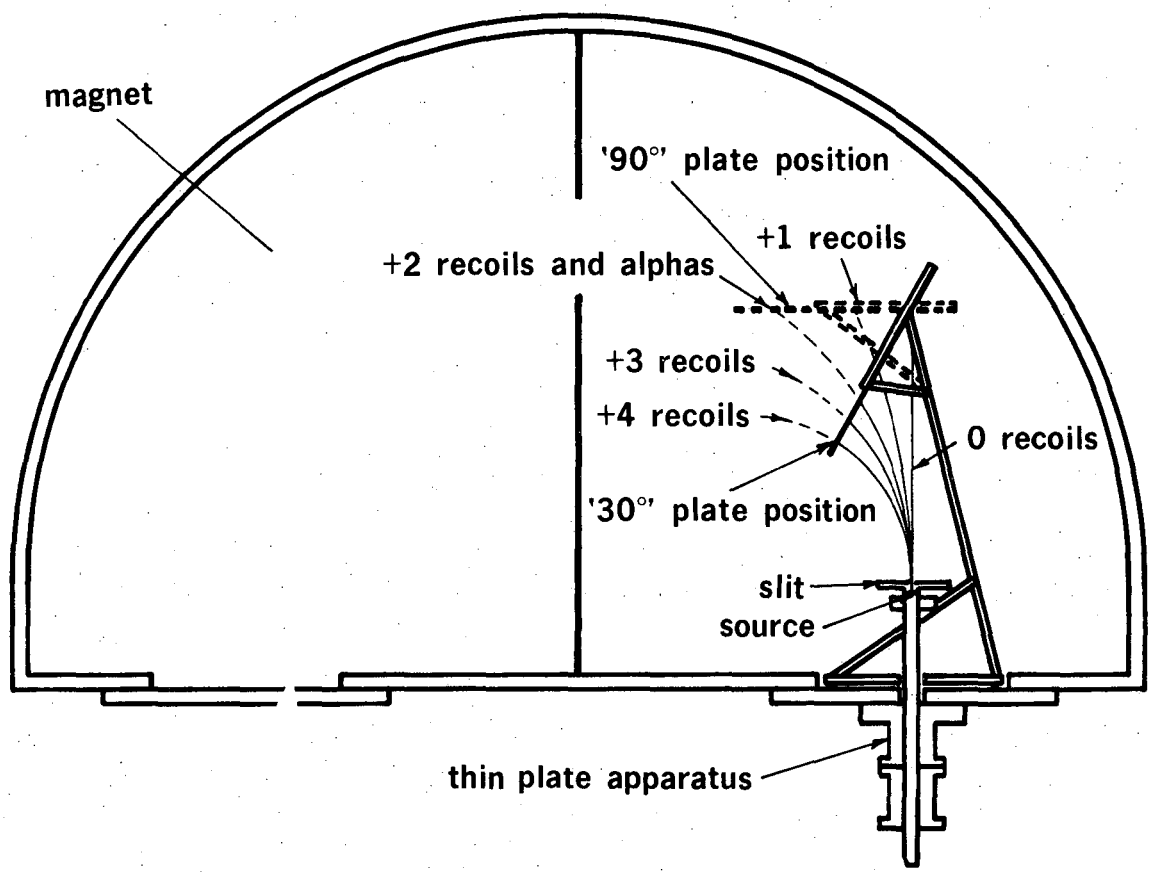

XBL 686-1087

Figure 3. Schematic diagram of the 180 deg double focusing alpha spectrograph when used in the "thin" plate configuration.

in the decay chain. Third, one can not obtain energy distributions from these plates because the intrinsic width of various peaks due to the width of the two collimating slits is much greater than the width due to the recoil's energy distribution.

For ease in discussing the data from these two kinds of sources, the following nomenclature was adopted. Recoil peaks are identified by the notation $A\ R_{Ex}^{+n}$ where A represents the decaying atom such as Th^{226}, R indicates recoil, n indicates the charge of the recoils, E indicates the energy in keV of the excited state of the recoil nucleus populated by the alpha decay of A, and x is either γ or e depending upon whether the excited state decayed by γ emission or by electron conversion. Furthermore, the following is true:

$$A\ R_{Ex} \equiv \sum_{\text{all } n} A\ R_{Ex}^{+n}$$

$$A\ R_{E}^{+n} \equiv AR_{E\gamma}^{+n} + AR_{Ee}^{+n}$$

$$AR^{+n} \equiv \sum_{\text{all excited state}} AR_{E\gamma}^{+n} + AR_{Ee}^{+n}.$$

Variations of these, follow the same pattern. Likewise $A\ \alpha_E$ indicates an alpha peak from the alpha decay of atom A which leaves the daughter or recoil nucleus in the E keV excited state. $A\gamma_i$ indicates all the γ rays designated by i that are given off by the excited nucleus A. For example, it can be seen from Fig. 1 that

$$Ra^{222}\gamma_1 = Th^{226}R_{111\gamma_1} + Th^{226}R_{242\ \gamma_2\gamma_1} + Th^{226}R_{242\ e_2\gamma_1}$$

$$+ Th^{226}R_{302\ \gamma_3\gamma_1} + Th^{226}\ R_{302\ e_3\gamma_1} + Th^{226}\ R_{318\ \gamma_4\gamma_1}$$

$$+ Th^{226}\ R_{318\ e_4\gamma_1}$$

II. EXPERIMENTAL PROCEDURE

A. U^{230} Source Preparation

The U^{230} sources used in this work were produced by bombarding disks of Th^{232} metal, which were 18-mils thick by 1 1/4-in. in diameter, with up to 378.5 μamp-hours of 50 MeV deuterons in the 88-in. cyclotron. The 378.5 μamp-hour bombardment yielded a source of U^{230} corresponding to approximately 2×10^9 alpha disintegrations/min. 28 days after bombardment. Information contained in W Meinke's thesis[29] was used to determine the μamp-hours necessary to produce sources of the desired intensity of U^{230}.

A few days after the bombardment the thorium metal was dissolved and the Pa fraction was separated from all the other components by means of an HCl anion-exchange column.[27] Approximately 28 days later, the U fraction was removed from most of the other components by means of HCl anion-exchange columns. An 8M HNO_3 anion exchange column was then used to separate the U fraction from the Fe that had originally been in the thorium metal disk since U remains strongly absorbed on the column at 8M HNO_3 whereas Fe does not. This column was then followed by another HCl column which was used as a final cleanup column.

The uranium's activity was then evaporated from a hydrocloric acid solution onto a clean platinum plate by means of vacuum sublimation.[27] The resulting sources were practically mass free and usually invisible to the unaided eye.

Since it is desirable to collect as many Th^{226} recoils as possible for any given experimental set up, it was necessary to locate the exact position of the U^{230} on the Pt source disk. The activity was located by marking the source plate and then exposing a photographic plate to it by means of direct contact. The resulting photograph then showed the exact position, size and

distribution of the U^{230}. The U^{230} sources were generally 5/32-in. wide by 1/2-in. long.

B. Th^{226} Source Preparation

Th^{226} sources were prepared by electrostatic recoil collection or by vacuum sublimation. There were two basic kinds of electrostatic collectors used; these are shown in Fig. 4.

The first kind sets up a uniform electric field. Type a, the parallel plate collector shown in Fig. 4, is of this kind. The U^{230} source, a 1-in. dia. platinum disk, is placed between parts (c) and (d) with the activity located below the slit in (c). The slit in (c) was located in the center and was 3/16-in. wide by 1 1/4-in. long. The cardboard (c) was of several different thicknesses in order to vary the distance between the U^{230} source and the Th^{226} collector plate. These were 0.1 cm, 0.4 cm, and 0.7 cm respectively. (b) was removable and held in place by Scotch tape. It contained a slit which was used to determine the configuration of Th^{226} recoils on the collector plate which was placed between (a) and (b). All of the pieces are 2 1/2-in. wide by 3 1/2-in. long except for (a) and (b) which are slightly smaller.

When this collector was used to make sources for the production of "regular" plates (see page 18, the slit in (b) was generally 1-in. long by 1/8-in. wide. The collector plate itself was 1-in. long by 3/8-in. wide and it was placed over the slit in (b) in such a way as to produce a source of recoils that was centered down the middle of the collector plate. When this collector was used to make sources for the production of "thin" plates (see page 21), the slit in (b) was 7/16-in. long by 1/8-in. wide or 3/16-in. long by 1/8-in. wide depending upon the shape of the source slit to be used in the machine. The collector plates were 5/8-in. long by 1/4-in. wide and were placed over the slit in (b) in the same manner as for the production of the regular plates.

(a) flat metal plate with + pole attached
(b) a piece of paper with a slit
(c) variable thickness of cardboard with a large slit in the middle
(d) flat metal plate with - pole attached
(e) insulating piece of cardboard

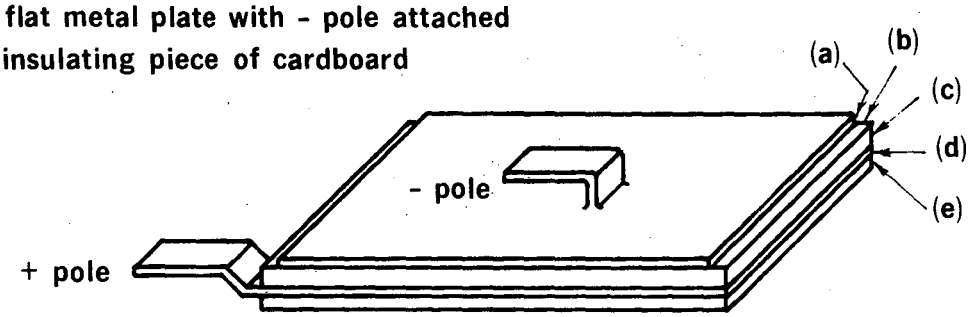

Type a — parallel plate

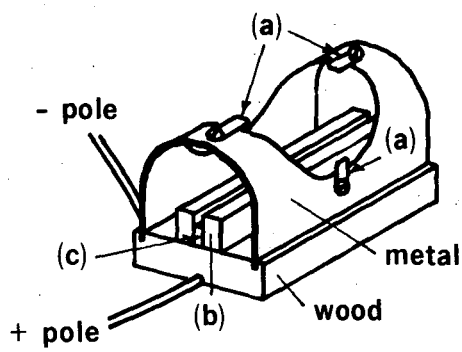

(a) source clamps
(b) lucite collector holder with slit for target
(c) copper conductor in lucite for electrial connection between collector and - pole

Type b — 'small dog house'

(a) hole for source
(b) lucite collector holder with slit for target
(c) metal connector between collector and - pole

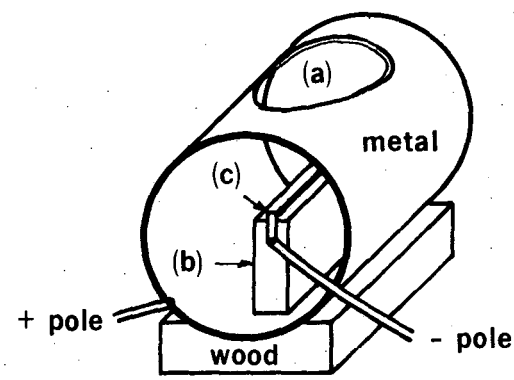

Type c — 'large dog house'

XBL 686-1085

Figure 4. The three types of electrostatic recoil collectors that were used in various experiments.

Collectors type b and type c, shown in Fig. 4, are of the second kind. They set up cylindrical fields that are approximately radial.

The "small dog house" has a radius of 1.27 cm and a length of 2 inches. Th^{226} recoils are collected on the edge of a piece of aluminum 0.011-in. thick by 1-in. long and 3/16-in. wide. The U^{230} source when held in place by the four source clamps completes the cylindrical geometry of the collector.

The "large dog house" has a radius of 3.7 cm and a length of 3-in. The aluminum collector, which is 0.011-in. thick by 1-in. long by 3/16-in. wide, forms the entire negative pole and hence the cylindrical field is rather imperfect with the field lines tending to concentrate at either end of the collector. The U^{230} source is held in place over the source hole by masking tape.

Recoil collection always took place at atmospheric pressure. If some collecting media other than air was desired, the entire collector was placed in a bell jar which was evacuated and then filled with the appropriate gas. Provisions were made to heat the various parallel plate collection plates to a high temperature in order to remove surface impurities.

All collections took place in a Berkeley box due to the high intensity of the U^{230} sources.

Some Th^{226} sources were made by collecting recoils in the parallel plate collector picking up the resulting activity with 4 M HCl and evaporating it onto a clean platinum plate by means of vacuum sublimation.[27] The platinum plate was 3/8-in. wide by 1-in. long and was masked by a collimating plate to produce a source of Th^{226} recoils 1/8-in. wide by 1-in. long centered down the middle of the above platinum plate. The distance between the source and collector varied from about 0.4 cm to 1 cm.

C. Experimental Apparatus

Some of the information used in determining the alpha spectrum of Th^{226} was obtained using a standard Frisch gridded ion chamber. A silicon solid state detector was used in the half-life determination of Th^{226}. It was also used in conjunction with a lithium-diffused germanium detector to obtain the intensity of some of the gamma rays of the U^{230} family.

The double focusing alpha spectrograph has been extensively discussed elsewhere.[26-28] Suffice it to say that this instrument has an optical radius of 35 cm and has an inhomogeneous field which produces vertical as well as horizontal focusing. In its normal mode of operation, the path of the recoils or alpha particles is as shown in Fig. 2. The focal properties of the field produce an approximate image of the source at the detector when the intrinsic half width of the peak is less than the physical width of the source. As shown in Fig. 2, nuclear-emulsion photographic plates were used as detectors and are designated as "regular" plates. These plates are type K-1 emulsion produced by Ilford Limited of Ilford, England and are 1 15/64-in. wide by 9-in. long with an emulsion thickness of 25 microns $\pm$ 10%. The beam strikes the plates at approximately the same angle irrespective of location along the length of the plate or the value of the magnetic field.

The baffles were set at $\pm$ 5 cm for all regular plates. For proper operation, it was found to be necessary to provide a copper conductor between the upper and lower pole faces of the magnet and to flush the system between runs with air. This was done to prevent a build up of positive charges on either pole face. It was found experimentally that without such precautions, such a build up did occur for intense sources

and although it did not affect the paths of the alpha particles, it did affect the paths of the recoils.

The source holder apparatus is shown in Fig. 5. It is designated as the "quick change" source because it is possible to change sources without destroying the vacuum in the rest of the machine. Using this holder it is possible to remove and replace a source in less than two minutes. The cold trap was added to the source holder apparatus to decrease the background caused by Rn^{218} and it indeed decreased the background by a factor of about 36.

The lucite and metal source holder shown in Fig. 5 was used to hold Th^{226} recoil sources which were made either by the vacuum sublimation technique or by the parallel plate electrostatic collector. The sources were placed under the source clamping plate which was then held shut by the spring clip at the tip of the source holder. The copper conductor connecting the metal part of the lucite holder with the main metallic part of the source holder was used to prevent the build up of a net negative charge on the Th^{226} recoil source plate. Lucite spacers were used to vary the absolute height of the source in order to center the recoils and alpha particles of interest on the detecting photographic plate.

During operation the main part of the apparatus was bolted to the face of the alpha spectrograph with the main seal O-ring acting as a vacuum seal between the holder apparatus and the main part of the machine. The source holder was inserted into the main part of the holder apparatus and the chamber containing it evacuated. The cut off valve was then opened and the source slid into the cold box which is open to the main part of the machine. This sequence is reversed to remove a source.

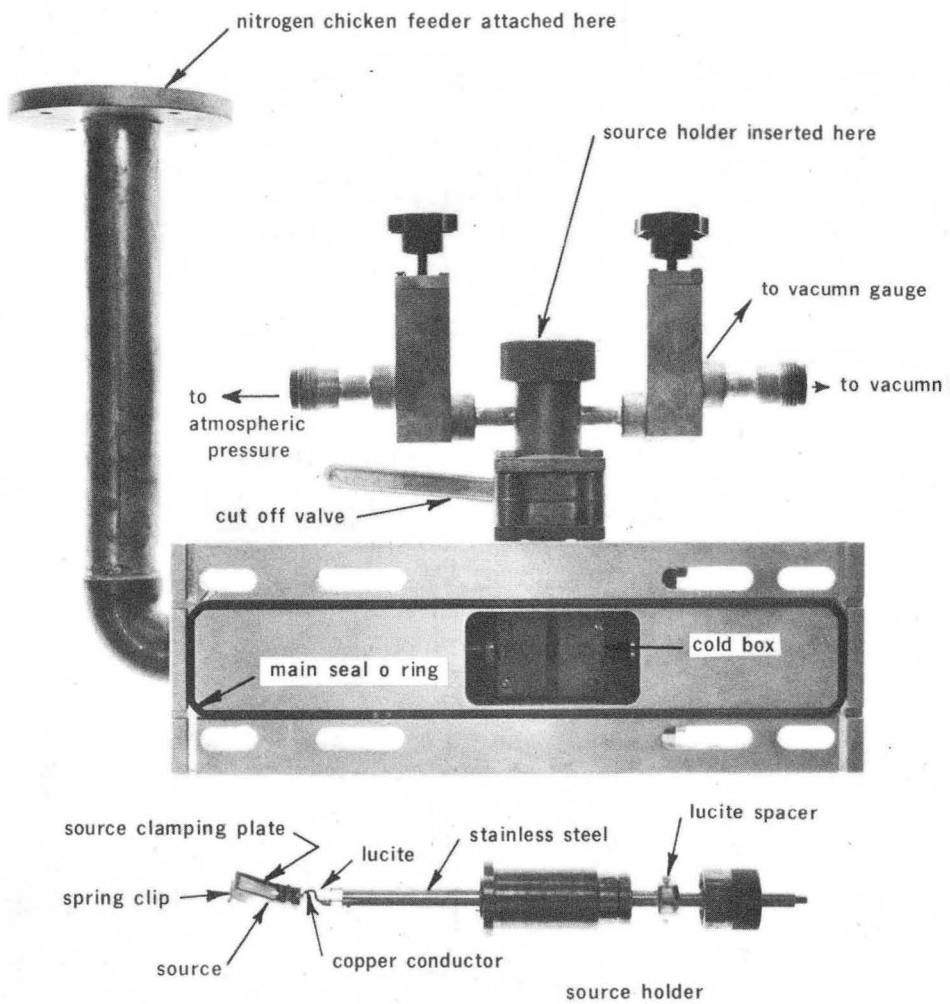

XBB 687-4055

Figure 5. A quick change source holder apparatus that is attached to the 180 deg double focusing alpha spectrograph for the production of "regular" plates. This apparatus is used for sources that are on a flat surface.

The metal source holder shown in Fig. 6 was used to hold Th^{226} recoil sources which were made in either the "small dog house" collector or the "large dog house" collector. It was used in the same way as that described above.

Ratios between charges -2 through +4 were obtained by using the thin plate apparatus shown in Fig. 7 in conjunction with the double focusing alpha spectrograph. It was attached in the same manner as the other holders. The paths followed by the recoils for a particular field are shown schematically in Fig. 3 along with the two possible plate positions.

These two plate positions are designated as the "30 deg" and "90 deg" plate positions. The angle used in the designation indicates the approximate angle at which the charge zero recoils will hit the plate. The exact angle depends upon the relative positions of the source slit and the collimating slit which can vary from plate to plate. However, the actual angles are closer to 29.71 deg and 88.63 deg rather than 30 deg and 90 deg.

The sources themselves, are made by collecting recoils on Pt plates 3/8-in. by 1/4-in. through a collimating slit. The source is then held in place at the end of the source holder shown in Fig. 7 by means of the source clamping plate. The source slit itself is made from a thin Al plate. It is then glued to the back of the source clamping plate in such a manner as to place it between the source clamping plate and the recoil source. The source slit is separate from the recoil sources in order to insure the proper alignment between it and the collimating slit for all recoil sources. It is removable because different source slits were used to produce different kinds of plates.

During an actual run, the entire thin plate apparatus must be removed and replaced inside the main part of the spectrograph each time a

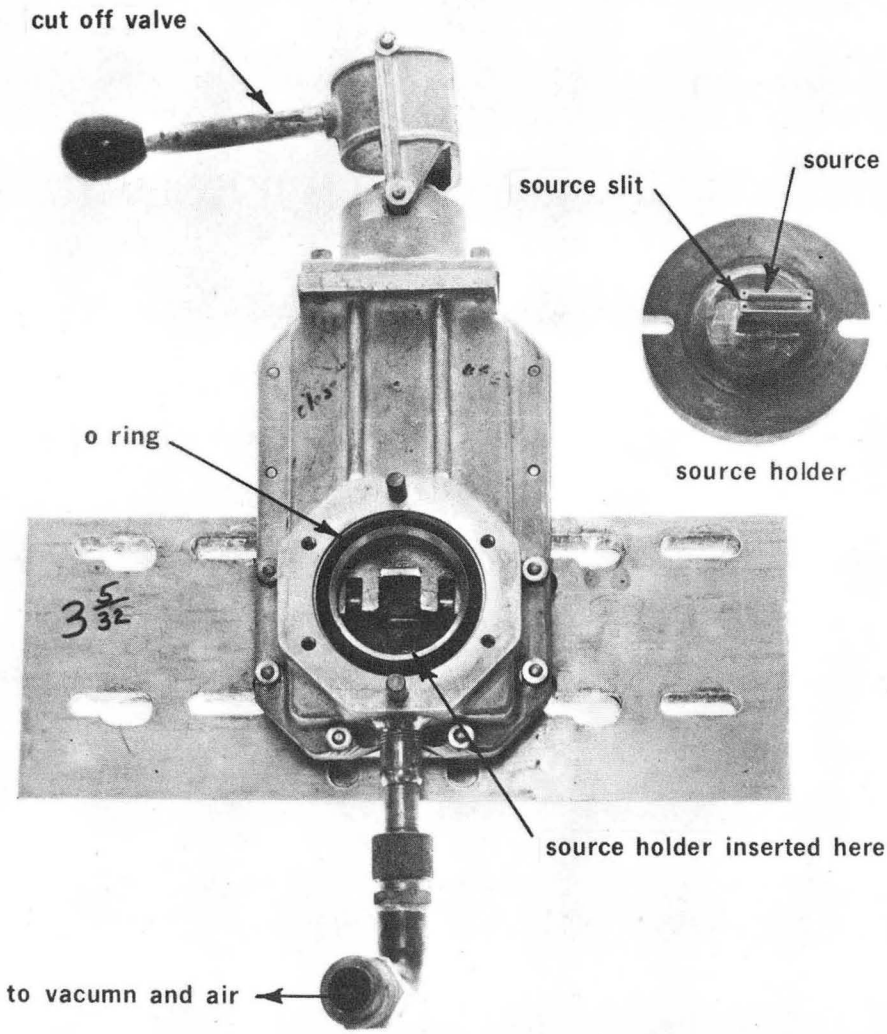

XBB 687-4054

Figure 6. A quick change source holder apparatus that is attached to the 180 deg double focusing alpha spectrograph for the production of "regular" plates. This apparatus is used to hold sources that are on the edge of a thin plate.

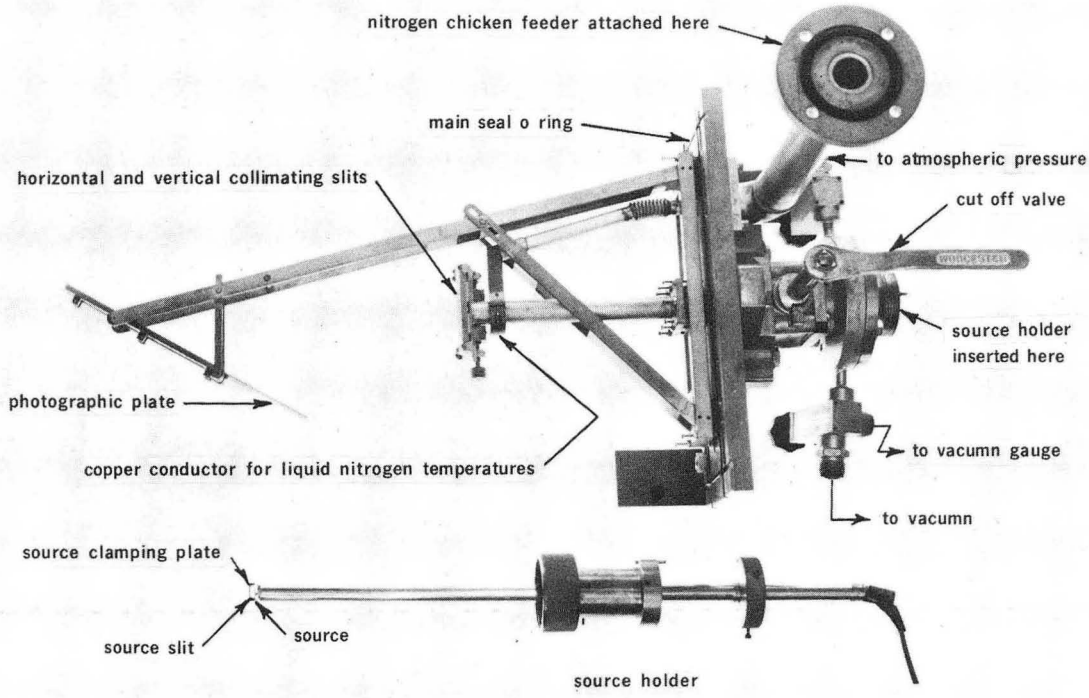

XBB 687-4053

Figure 7. Apparatus that is attached to the 180 deg double focusing alpha spectrograph for the production of "thin" plates.

new photographic plate is to be used. (This entire operation must be carried out in the dark in order to prevent exposure of the emulsion.) Once the thin plate apparatus is attached to the machine and the main chamber of the machine has been evacuated to operating pressure (about 10^{-5} mm of Hg), the actual production of a thin plate commences. The source is placed in the source holder which is inserted into the main part of the thin plate apparatus. The chamber containing the source is evacuated, the cut off valve is opened, and the source is slid into position in the main part of the machine. This process is repeated for as many sources as are needed to produce one plate.

It was found by experience that operating the entire apparatus at room temperature (approximately 72° F) yielded a very high random background of Rn^{218} on the plate. This background was decreased by a factor of about 20 by adding the copper conductor and auxiliary equipment shown in Fig. 7 to lower the temperature of the tube surrounding the source and the collimating slit apparatus to slightly above liquid nitrogen temperature (77° K). It was found that this cooling apparatus not only cooled the region around the source but it also tended to cool the source itself down to about 32° F. Since the regular sources are at approximately 72° F and the effects of temperature are unknown, some thin plates were made by heating the source. The heater raised the source temperature to about 100° to 110° F. Thin plates produced under these circumstances were designated as "cold" and "warm" plates respectively.

In order to prevent recoils of different charges from landing in the same area of the plate, it was necessary to collimate the recoil and alpha beam by means of the source slit and the collimating slit. If one assumes that the magnetic field is homogeneous and in the vertical direction:

i.e. $\vec{B} = B_0\hat{z}$ then the paths followed by the recoils in the x-y plane are circles of radii,

$$r = p/qB_0$$

where p = the momentum of the recoil and q = the charge of the recoil. (Although the magnetic field is not strictly homogeneous, the recoil paths which are calculated for the thin plates will not be much different from the actual flight paths.) Using the above formula for r plus the further condition that the transmission for any given magnetic field is to be a maximum consistent with the condition of no overlap between recoil peaks of different charges, it is possible to calculate the optimal widths of the vertical source and collimating slits.

When the beam is collimated with vertical slits only (vertical is the $\hat{z}$ direction), then the situation shown in Fig. 8 is obtained. This slit situation is designated by ▯ and is quite useful because the transmission is high. Actually the beam is defined in the vertical direction too. This is done at the source by the source clamping plate which is 1/2-in. high and at the photographic plate by the height of the plate which is 3/4-in. high. However, because the flight paths for different charged recoils are different, the transmission for each charge recoil is different and unknown. Thus, in order to obtain direct ratios between ratios of different charges, it is necessary to collimate the beam in the vertical direction also. This situation is shown in Fig. 9 and is designated by □ . The relative and absolute heights of the slits in the vertical direction are determined by the following two conditions. First, the transmission to the plate for the Th^{226} recoils must be the same regardless of charge. And second, the transmission must be as large as possible. The □ plates can be used to find the direct ratios between Th^{226} recoils of different charges and

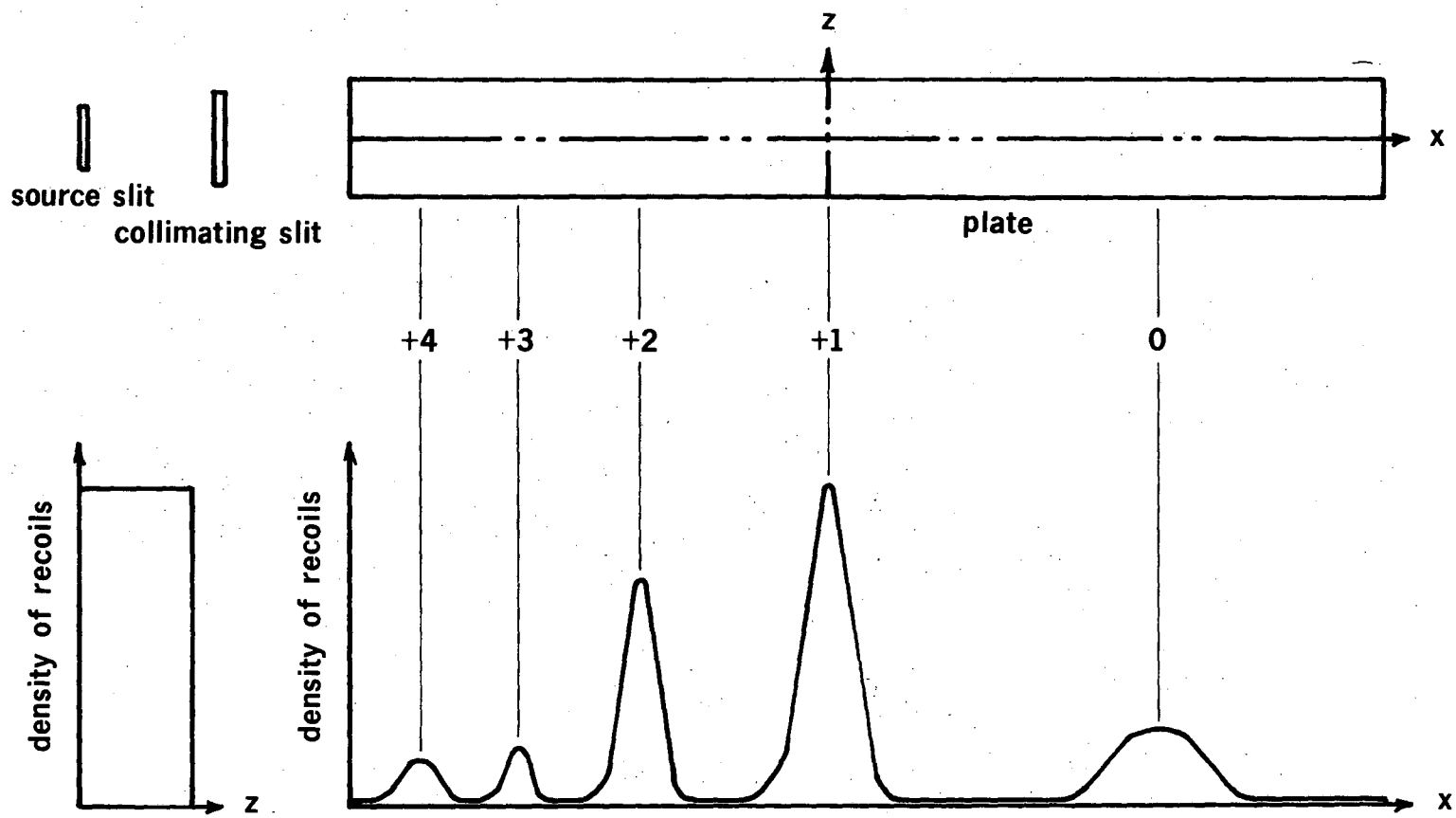

XBL 686-1089

Figure 8. A schematic diagram of the density of recoils along the length and width of the "thin" plate in the 30 deg position when the recoil beam is collimated with vertical slits only.

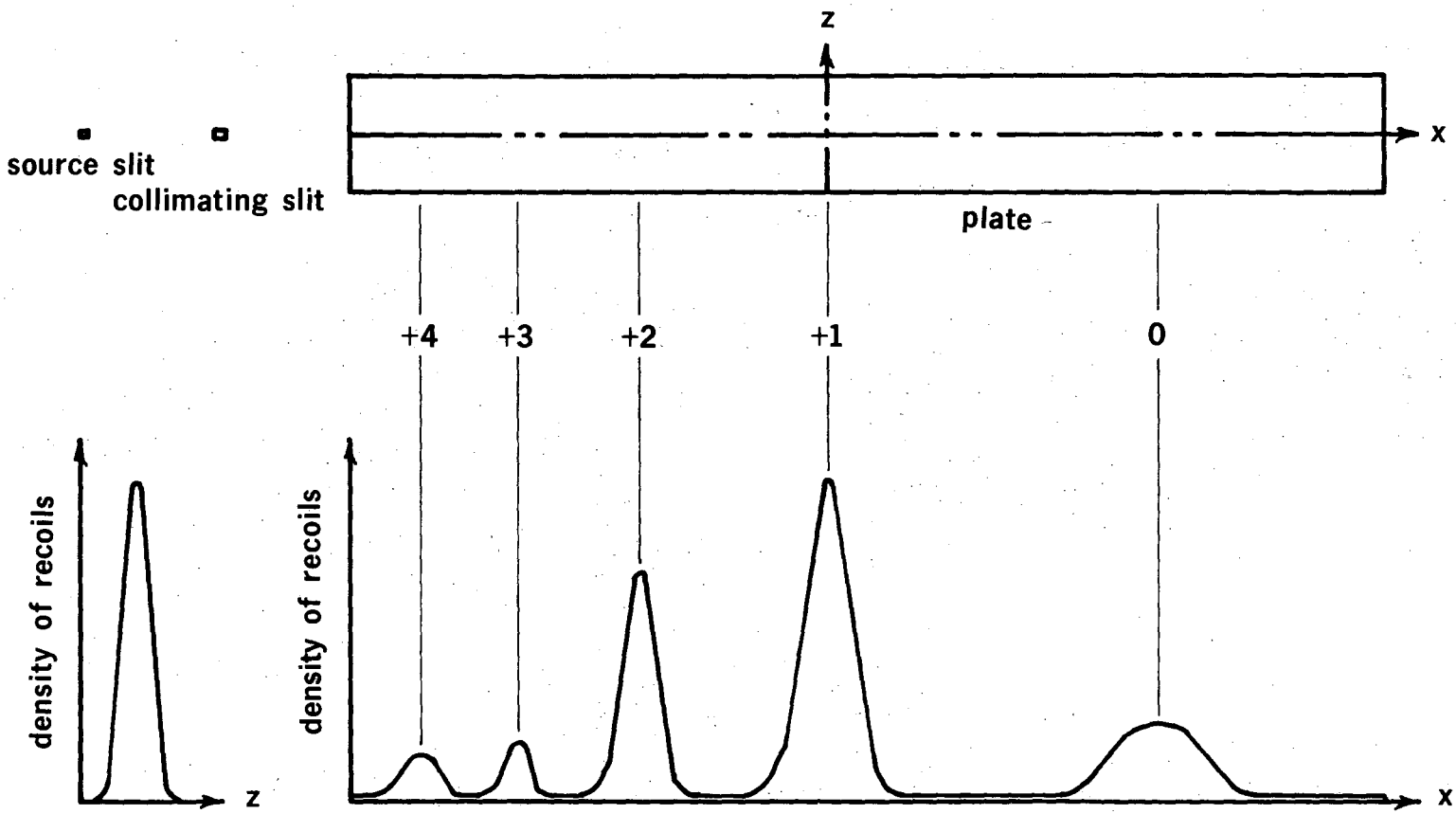

XBL 686-1090

Figure 9. A schematic diagram of the density of recoils along the length and width of a "thin" plate in the 30 deg position when the recoil beam is collimated with vertical and horizontal slits.

and these ratios can be used to determine the relative transmissions for various charges for plates.

The transmission for plates was only 1/25 that for plates, and hence with weak sources it was necessary to use plates.

D. Identification of Recoils

1. Introduction

As has previously been mentioned, photographic emulsions are used to detect the recoils of Th^{226}. Actually however, the tracks left by the recoils themselves are so short that they cannot be seen, even with the highest power available.* Instead, what is actually seen is the alpha tracks of the Th^{226} recoil daughter products as shown in Fig. 10, which shows what is called a three-pronged event. It also indicates why this detection technique requires a radioactive series which has a long decay chain containing many alpha decays. The energies and half lives of the U^{230} decay chain are as follows:

	U^{230}	
21 days	↓	α = 5.89 MeV (67.5%) 5.82 MeV (31.9%)
	Th^{226}	
30.5 min.	↓	α = 6.34 MeV (76%) 6.23 MeV (22%)
	Ra^{222}	
38 sec	↓	α = 6.57 MeV (97%) 6.23 MeV (3%)
	Rn^{218}	
35 msec	↓	α = 7.14 MeV (≈ 100%)
	Po^{214}	
164 μsec	↓	α = 7.69 MeV (≈ 100%)
	Pb^{210}	
21 years	↓	β^-
	Bi^{210}	

*Tracks or gaps of 1/4 μ could be distinguished, but no such were observed. This is to be expected from the rough estimates (of the order of .02μ) that can be made from experimental recoil ranges in other media.[30]

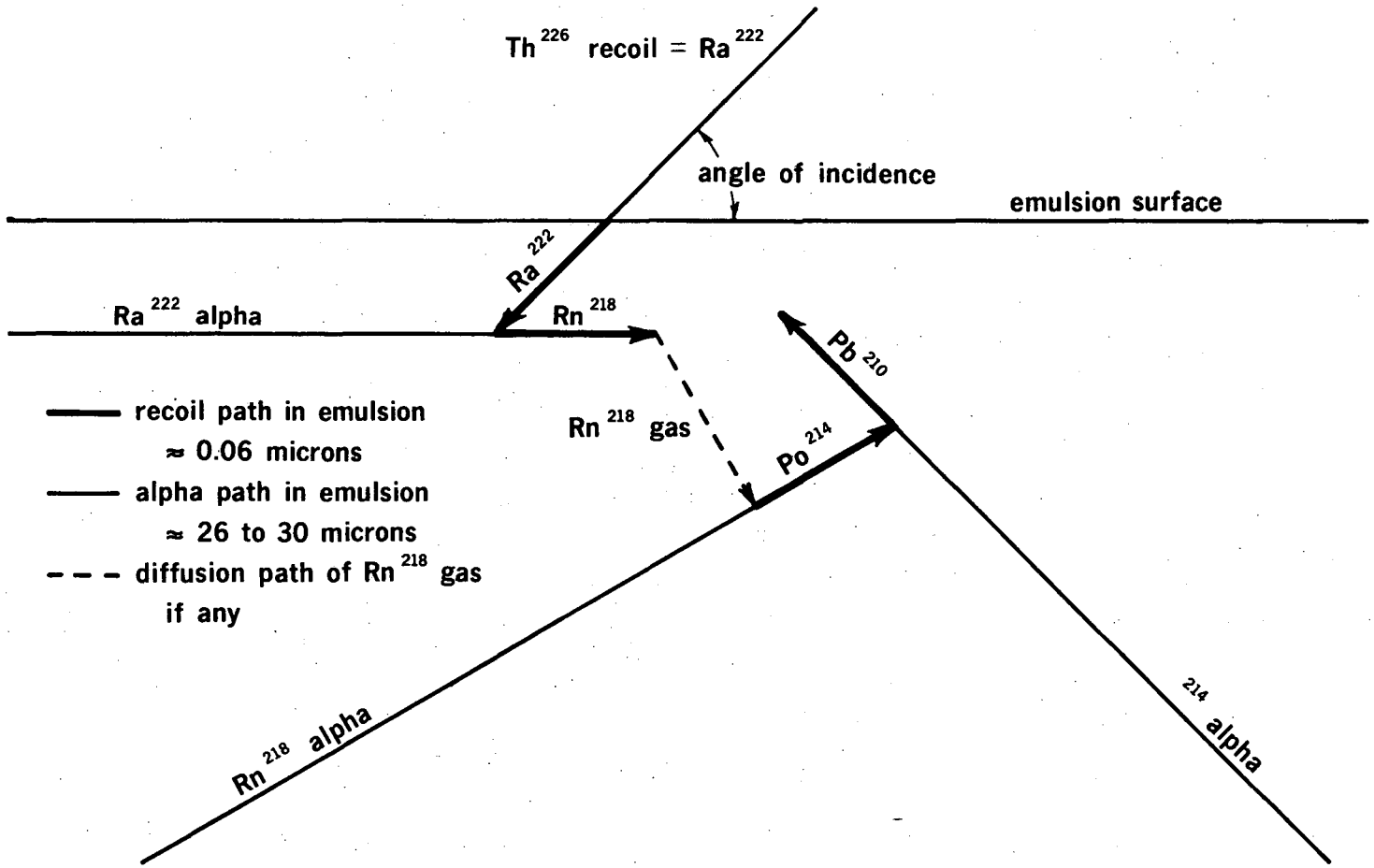

XBL 686-1091

Figure 10. Schematic of a 3-pronged event produced by the decay of the various daughter products of Ra^{222} in emulsion.

The number of alpha tracks to be seen in the emulsion following the alpha decay of Ra^{222} ranges from zero to 3. Since the recoil paths are so short, the resulting alpha tracks will appear to come from a common center on the surface of the emulsion. Neither zero pronged nor one pronged events can be identified, one pronged events because there is no way of distinguishing them from the normal background of random alpha tracks which also enter the emulsion. However, two and three pronged events can be identified by the existence of an apparent common entry point on the surface of the emulsion.

If all of the data could be obtained using the "regular plate" technique, then it would be unnecessary to know the relative probabilities of obtaining zero, one, two or three pronged events. The angle of incidence of the initial recoil is approximately the same for all regular plates, and the above relative probabilities can only be a function of the angle of incidence of the initial recoil and the diffusion length or path of the Rn^{218} gas, if any. The diffusion length or path of the Rn^{218} gas should only be a function of the type and condition of the emulsion used and not a function of the initial charge of the Th^{226} recoil. (This appears to be confirmed experimentally and is discussed under Part 2 of this section.) The emulsions used for all experiments were the same (Ilford K-1) and they were stored in a vacuum. Thus, the condition of the emulsion was always the same.

However, all the information could not be obtained using the "regular plate" technique and one of the characteristics of the "thin plate" technique is the variation in the angles of incidence of the Th^{226} recoils for different charges. Thus, it is necessary to obtain the relative probabilities of zero, one, two, and three pronged events either experimentally or theoretically in order to relate the data for charges 0 and

$\pm$ 1 to charges $\pm$ 2 through + 20.

2. Production of Two and Three Pronged Events--Theory and Experiment.

The ideal way to obtain the relative probabilities of getting zero, one, two and three pronged events is to devise a theory for their production and then check the theory experimentally. Such a theory must make at least two assumptions. The first concerns the directionality of the alpha decays; the second conerns the actions of the Rn^{218} gas in the emulsion after it loses its recoil energy.

With respect to the first, it is simplest to assume that the alphas decay isotropically. Since all the nuclei have spin 0, except for the 3% branch in Ra^{222}, there should be no possibility of a non-isotropic alpha emission. Also the charge deposited by the recoil is not sufficient to influence the alpha direction, as is demonstrated by Fig. 11 which shows that the ratio Prob(3α)/Prob($2\alpha + 3\alpha$)* is independent of the charge of the recoil for the regular plates for which the angle of incidence does not vary with the charge. The best fit from Fig. 11 to this ratio is 0.136. Using the assumption that alpha emission is isotropic, the simplest theory assumes the Rn^{218} gas is trapped. This theory was then checked by plotting Prob (3α)/Prob ($2\alpha + 3\alpha$) = Number (3α)/Number ($2\alpha + 3\alpha$) vs. the angle of incidence of the Th^{226} recoil as shown in Fig. 12. It can be seen from the graph that this first theory is totally inadequate. Other simple assumptions concerning the Rn^{218} gas can be made. The passage of a recoil through the emulsion is likely to be very destructive. Thus, it could be that the Rn^{218} gas instead of being trapped at the end of its recoil flight path can

*Prob(3α, β deg) $\equiv$ probability of obtaining 3-pronged events for an incidence angle of β deg. Prob($2\alpha + 3\alpha$, β deg) $\equiv$ probability of obtaining 2- or 3-pronged events for an incidence angle of β deg.

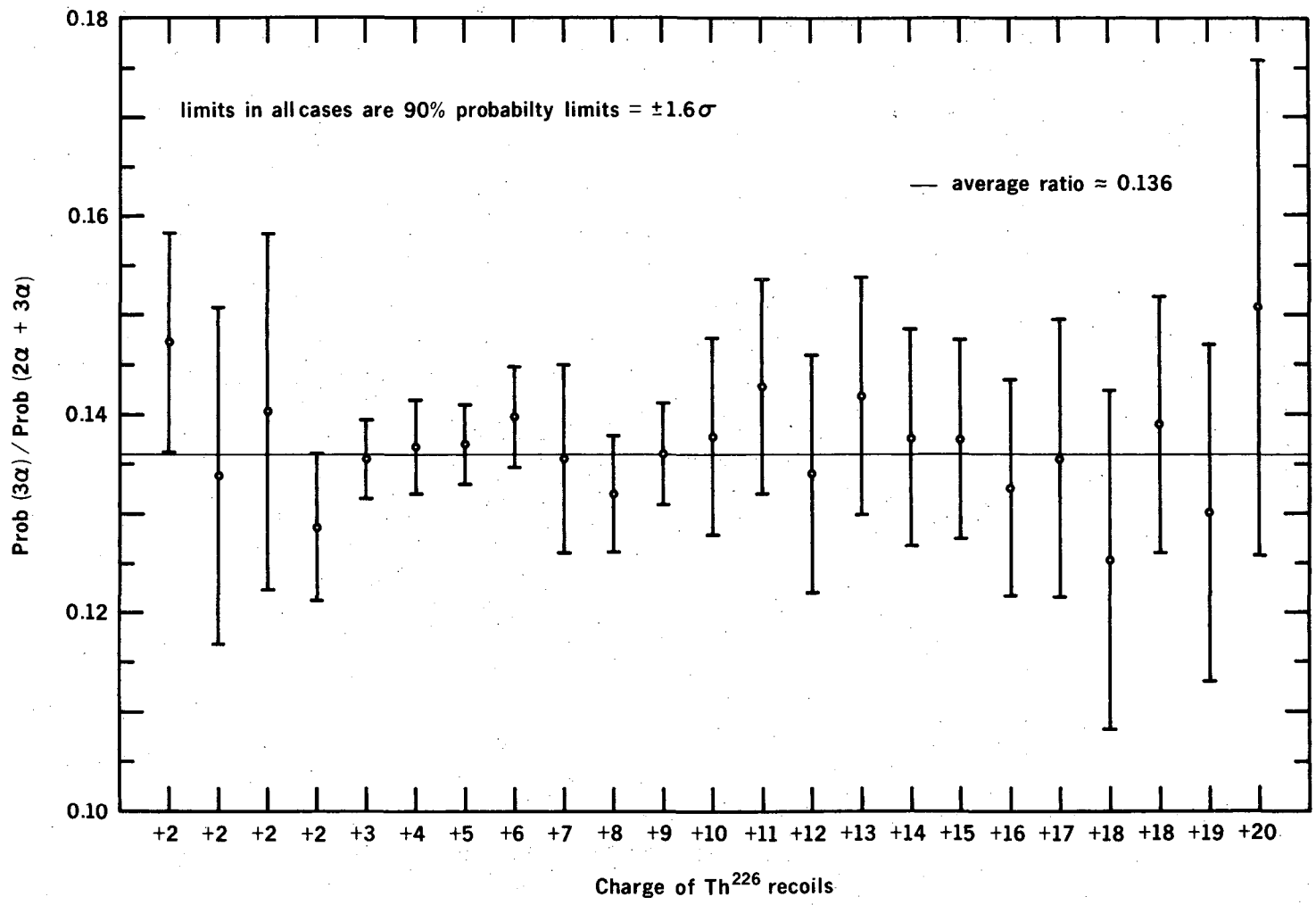

XBL 687-1167

Figure 11. Plot of Prob(3α)/Prob(2α + 3α) for Th^{226} recoils as a function of charge. Each point represents data from a single plate. Several +2's were indicated to prevent overlaps of the experimental points.

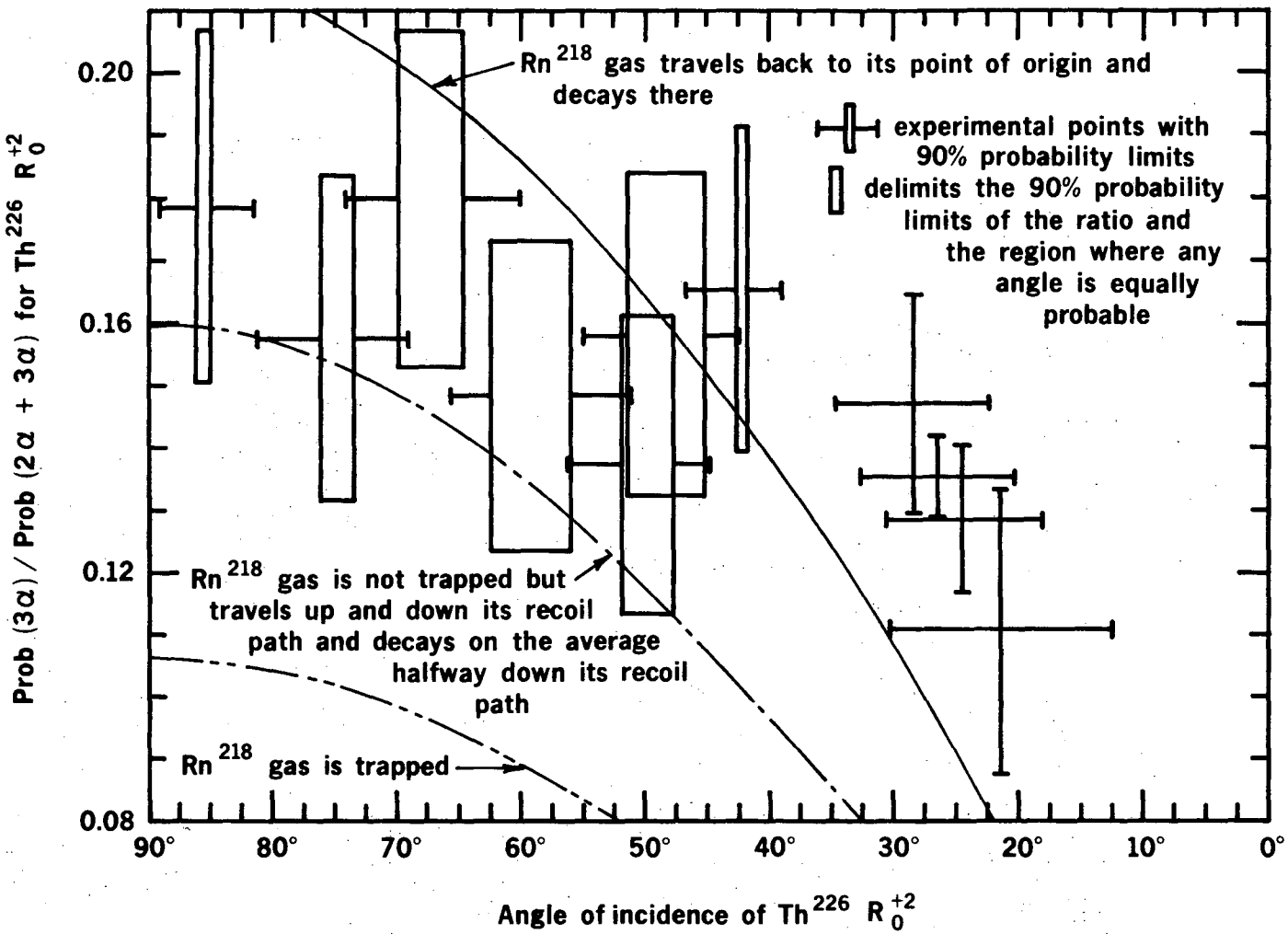

Figure 12. Plot of Prob(3α)/Prob(2α + 3α) for $Th^{226}R^{+2}$ as a function of the angle of incidence of the $Th^{226}R^{+2}$ for three different theories as well as for the experimental points. Large angles in addition to having the usual 90% probability limits also include a region where any angle is as probable as any other angle. This is due to the uncertainty in the thickness of the emulsion for the particular plate involved.

travel up and down this path of destruction and consequently decay, on the average, halfway down its recoil path. Or for some strange reason, it could be that the Rn^{218} gas travels back to its point of origin and decays there. It can be seen from Fig. 12 that neither of these assumptions is adequate either.

Before going on to discuss a theory which appears to fit the experimental data, something should be said about how the experimental data was obtained.

Charge +2 plates were made in the regular plate configuration with the exception that the angle of incidence of the Th^{226} recoils was varied from about 20 deg to about 90 deg. For each plate, the angle of incidence was determined along with the ratio No. (3α)/No. $(2\alpha + 3\alpha)$. The latter number could be obtained directly by counting two and three pronged events but the former number had to be obtained in a somewhat indirect manner because the angle at which the beam strikes the regular plates is only approximately known.

These angles were calculated in the following manner from the Th^{226} α_0 tracks which were on the experimental plates along with the Th^{226} recoil two and three pronged events. Since the emulsion thickness is less than the distance that Th^{226} α_0's can travel in such a media, two different situations can occur. For sufficiently shallow angles, the alpha particle never leaves the emulsion and its entire flight path appears in the emulsion as an ionized track. This situation is shown as Case a in Fig. 13. It can be seen from the figure that if the distance traveled by Th^{226} α_0's in Ilford K-1 emulsion is known, then the angle of incidence can be determined by simply measuring the distance x, since cos a = x/d. For Case b, the alpha travels through the emulsion and on into the glass behind it. In this case

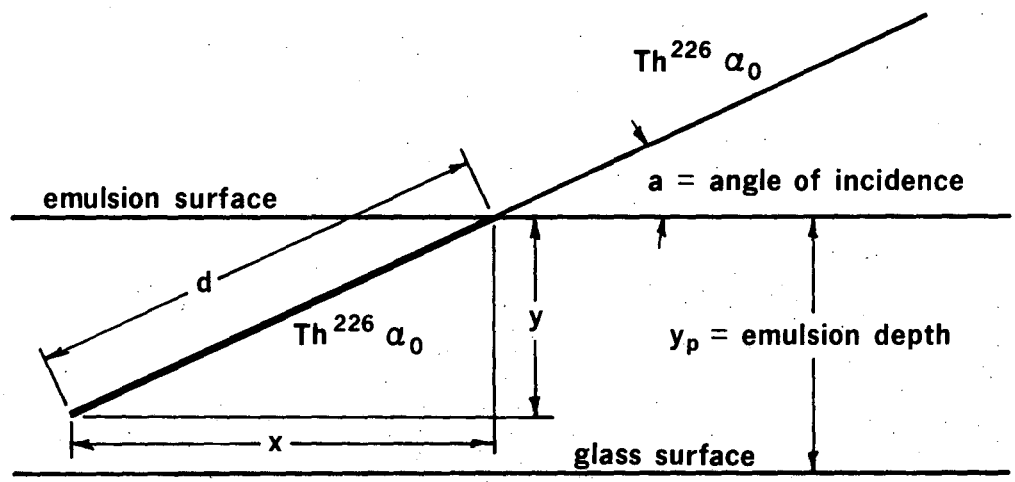

Case a — small angles of incidence

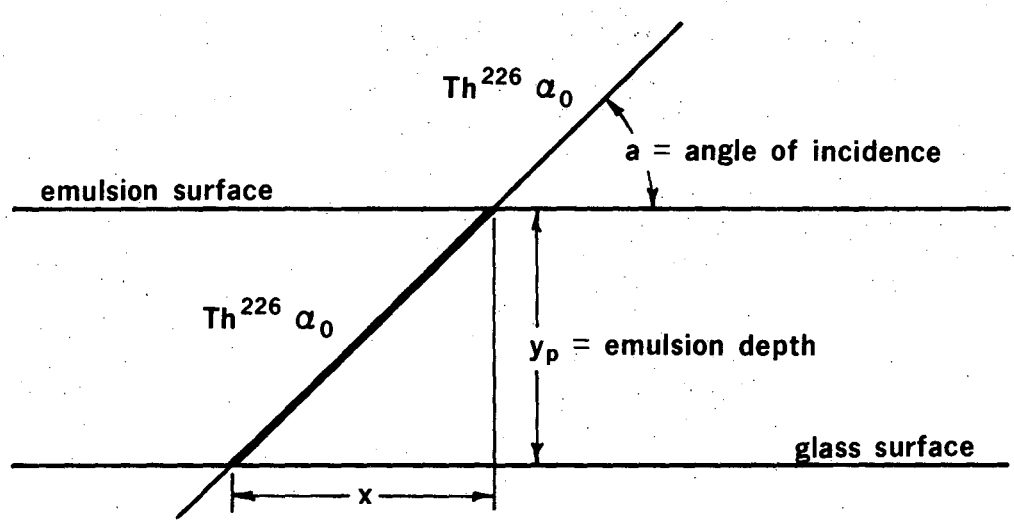

Case b — large angles of incidence

XBL 687-1309

Figure 13. Schematic of the production of alpha tracks in emulsion. In case a, the alpha particle does not penetrate the entire depth of the emulsion and so d is equal to its range in emulsion. In case b, it travels through the emulsion and on into the glass below where it leaves no visible track before stopping.

$$\tan a = y_p/x$$

where both x and y_p must be found.

Several articles[31-34] treat the range of α's in emulsion. A graph for Ilford C-1 emulsion was given but none was given for Ilford K-1 emulsion at 0% humidity. The humidity is important not only because it changes the density of the emulsion and hence its stopping power[33-35] but also because it changes the emulsion depth y_p.[35] According to the literature, the curve for Ilford K-1 emulsion at 0% humidity should have the same shape as the Ilford C-2 emulsion curve but it will be shifted.

This shifted curve was found in the following manner. The alpha tracks which make up the two and three pronged recoil events often appear to be parallel or nearly parallel to the surface of the emulsion. Although development and later storing of the emulsion causes swelling and shrinkage of the emulsion, such changes can only affect the depth of the emulsion y_p since the bonding between the emulsion and the glass below prevents any significant changes in the x direction. Thus the lengths of the above surface alpha tracks will correspond to the ranges of either $Po^{214}\alpha_0$, $Rn^{218}\alpha_0$ or $Ra^{222}\alpha_0$ in Ilford K-1 emulsion at 0% humidity. The lengths of these tracks were measured using an x97 oil immersion lens on a microscope where the field of view was divided into 100 small divisions. The length of these small divisions was measured and found to correspond to 1.1324 microns. Figure 14 shows a plot of the length of these tracks in divisions vs. number of alphas with these lengths. It can be seen from the figure that these lengths do fall into three distinct peaks corresponding to the ranges of $Ra^{222}\alpha_0$, $Rn^{218}\alpha_0$ and $Po^{214}\alpha_0$. These ranges were then converted into microns and plotted on a graph along with the range energy curve for Ilford C-2 emulsion.[32] (See Fig. 15.) An experimental range energy curve for

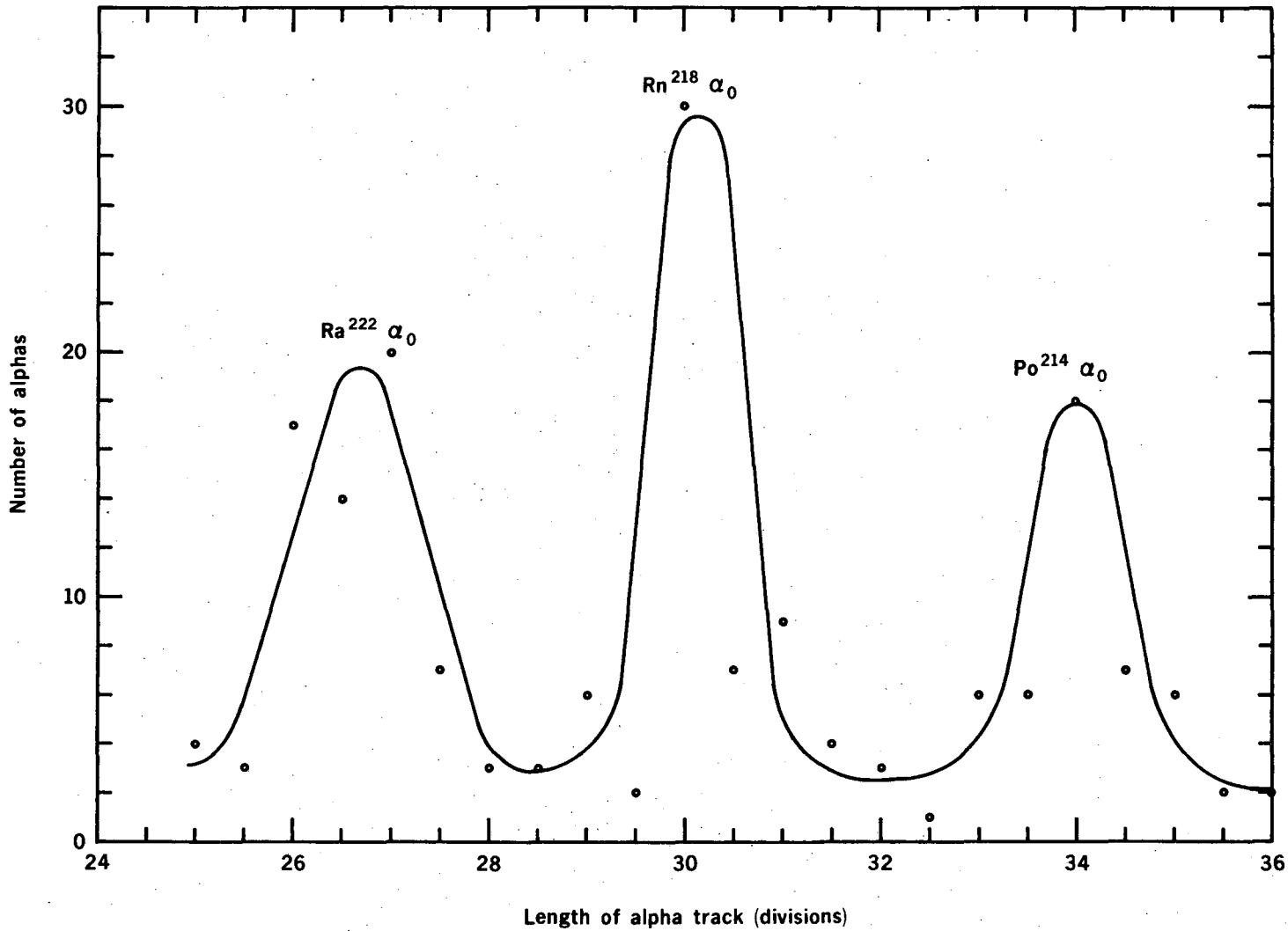

XBL 687-1166

Figure 14. Plot of the number of alpha tracks of a given length as a function of track length. The peaks indicate the source of the alpha particles.

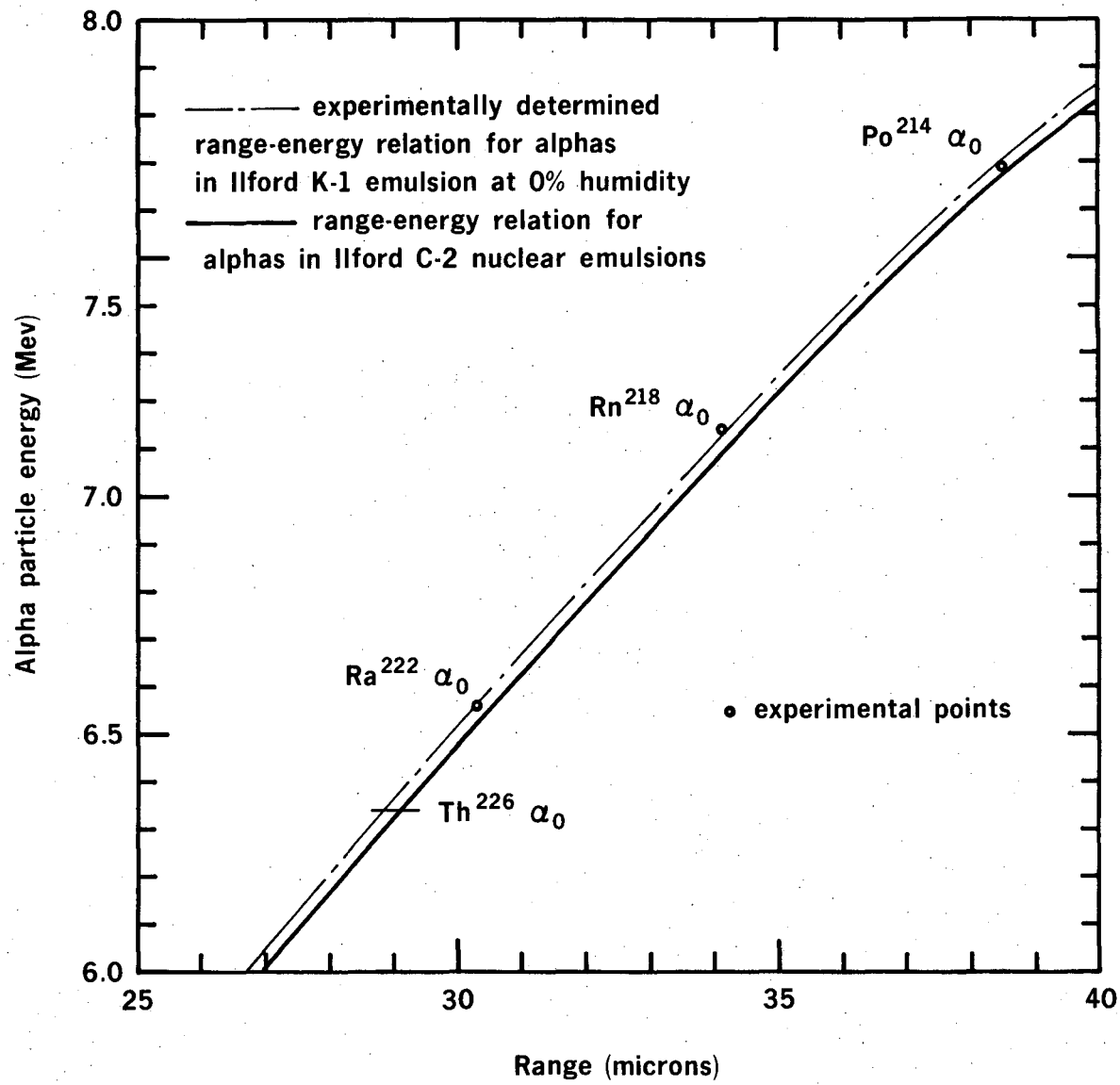

XBL 687-1163

Figure 15. Experimentally determined range curve of alphas in Ilford K-1 emulsion at 0% humidity along with a similar curve for alphas in Ilford C-2 emulsions.[32]

Ilford K-1 emulsion at 0% humidity was then determined and from it the range d of $Th^{226}\alpha_0$ was found. This distance along with measured values of x was then used to determine the angle of incidence for photograph plates where the angle of incidence is small and hence corresponds to Case a in Fig. 13. In order to find the angle of incidence for large angles (Case b), it was necessary to determine the emulsion depth y_p. The manufacturers state that the plates are 25 μ thick ± 10% at an unknown humidity. This unknown humidity is probably somewhere between 50 and 60%. Thus the actual plate thickness at 0% humidity is probably 23μ ± 2.5%.[35]

Experimental emulsion thickness at the time of exposure was found by the following technique. Alphas known to fall into Case a (small angles of incidence) were used to determine the emulsion depth of a given plate since y can be both directly measured in terms of focal divisions and calculated in terms of microns using the known value of d and the measured value of x. (See Fig. 13.) Using this calibration, y_p was then directly measured by measuring y for alpha tracks known to fall into category b (large angles of incidence). It was found that emulsion thickness at the time of exposure varied from 18 to 23μ and varied by as much as 10% or so in a single plate. Thus it is necessary to assume that emulsion thickness ranges from plate to plate from 18 to 23μ and is known only to within these limits.

This uncertainty results in an uncertainty in the angle of incidence for large angles indicated in Figs. 12 and 16.

Since neither of the previous theories fit the data, it was though that perhaps the Rn^{218} gas diffuses equally in all directions from the end of its recoil flight path.[36-38] This situation is shown in Fig. 16 where theoretical curves for diffusion lengths for Rn^{218} gas corresponding to 0.12, 0.10 and 0.08 μ are shown. These values for the diffusion length

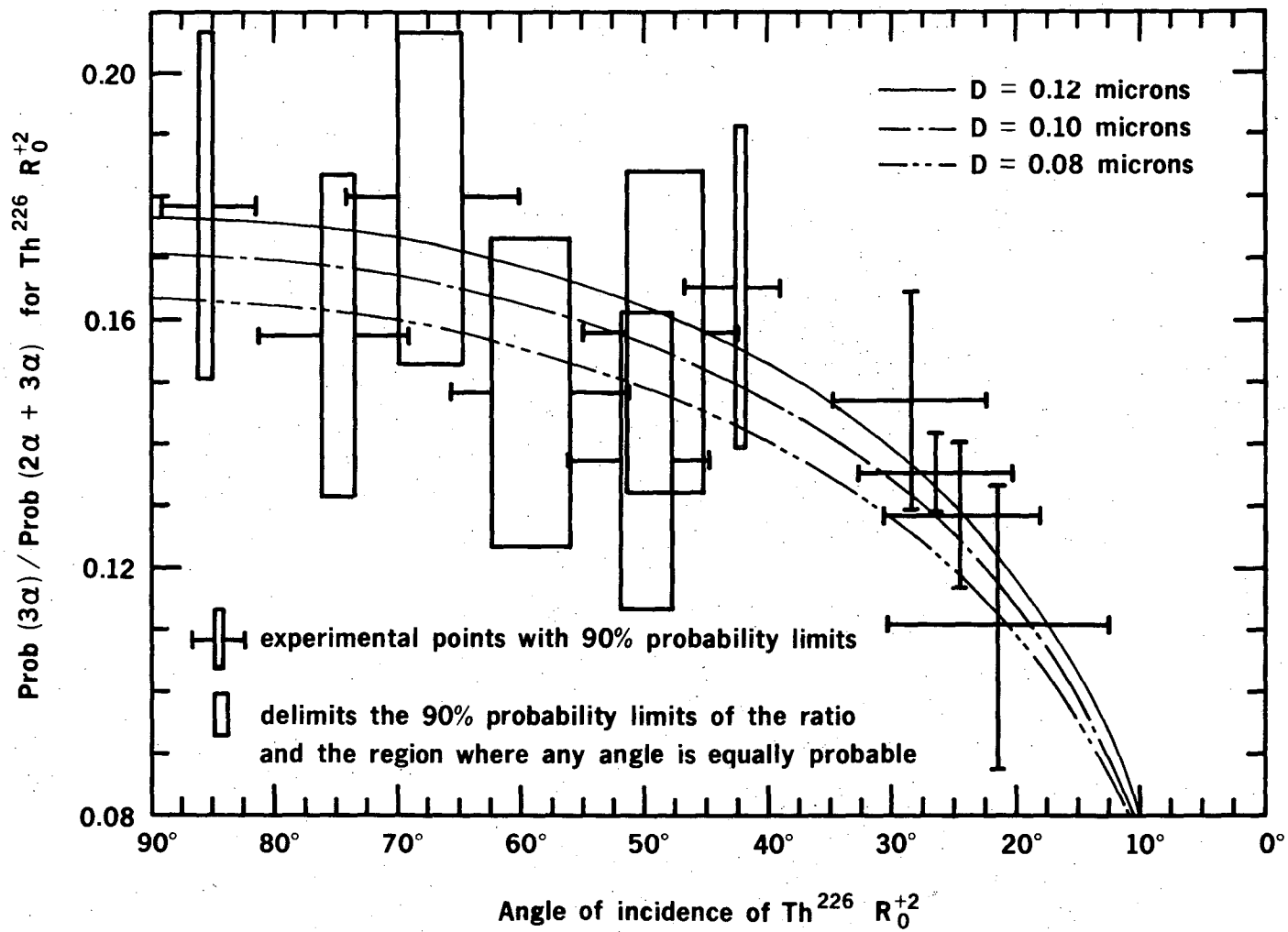

XBL 687-1310

Figure 16. Plot of Prob(3α)/Prob(2α + 3α) for $Th^{226}R^{+2}$ as a function of the angle of incidence of the $Th^{226}R^{+2}$ for the Rn^{218} diffusion theory as well as for the experimental points. Large angles in addition to having the usual 90% probability limits also include a region where any angle is as probable as any other angle. This is due to the uncertainty in the thickness of the emulsion for the particular plate involved.

of the Rn^{218} gas in Ilford K-1 emulsion at 0% humidity correspond to the assumption that the range of $Th^{226}R_0^{+2}$ in Ilford K-1 emulsion at 0% humidity is 0.0650 μ. It can be seen from Fig. 16 that this theory appears to fit the experimental situation very well. A least squares fit of the experimental data to the theoretical curves indicates that D = 0.10μ.

A further check on this theory was made using information obtainable from the regular plates. A plot of No. $(2\alpha + 3\alpha)$ for $Th^{226}R_{111e}^{+n}$ [≡ No. $Th^{226}R_{111e}^{+n}(2\alpha + 3\alpha)$] divided by the No. α_{111e} vs. n (see Fig. 85) indicates that

$$\frac{[\text{No. } Th^{226}R_{111e}(2\alpha + 3\alpha)]}{(\text{No. } \alpha_{111e})} \approx \sum_{n=+3}^{+20} \left[\frac{[\text{No. } Th^{226}R_{111e}^{+n}(2\alpha + 3\alpha)]}{(\text{No. } \alpha_{111e})}\right] .$$

But

$$\frac{(\text{No. } Th^{226}R_{111e})}{(\text{No. } \alpha_{111e})} = \left[\frac{[\text{No. } Th^{226}R_{111e}(2\alpha + 3\alpha)]}{[\text{No. } \alpha_{111e}][\text{Prob}(2\alpha + 3\alpha)]}\right]$$

should equal one. Hence, we should have

$$\text{Prob } (2\alpha + 3\alpha) = \sum_{n=+3}^{+20} \left[\frac{[\text{No. } Th^{226}R_{111e}^{+n}(2\alpha + 3\alpha)]}{(\text{No. } \alpha_{111e})}\right] .$$

This gives an independent measure of the value for D since the angle of incidence for the regular plates is known to be 26.5 ± 2.0 deg. However, the value of D obtained by this means is D = 0.035μ ± 0.010μ and this value is far different from the value obtained from Fig. 16 which was D = 0.10μ.

The final test of this theory is to see how well it fits the data from the thin plates. This in turn means that the angle at which recoils of different charges strike the thin plates must be determined. In the case of charge +2 this angle can be determined directly from the plates in the same way that it was determined on the regular plates by use of the alphas

which strike the plate in the same region. The angle at which charge 0 hits the thin plates is purely a matter of the geometry of the thin plate apparatus and hence it too can be determined directly. However, the angles at which charges $\pm$ 1, - 2, + 3 and + 4 hit the plates can only be calculated using the knonw geometry of the thin plate apparatus and certain assumptions concerning the magnetic field in the spectrograph.

These assumptions are as follows. First, the magnetic field is assumed to be of the form $\vec{B} = B_0\hat{z}$. Because the distances involved are so small, this assumption is not too inaccurate. The second assumption concerns the shape of the fringing field. The actual shape of the fringing field at the point of entry of the particles for the fields employed is shown in Fig. 17. This field shape is approximated by assuming that $\vec{B} = B_0\hat{z}$ for $y \geq -1.5$ cm and $= 0$ for $y \leq 1.5$ cm, where the y axis is perpendiuclar to $\hat{z}$ and the edge of the pole face at which point $y = 0$.

The geometry of the situation is shown in Fig. 18. It can be seen from the figure that the slit is not always located in the same place relative to the source and the photographic plate. However, the collimating slit and the stop for the photographic plate are fixed and so it is possible to calculate x_s for each plate by comparing the actual position of the zero charge peak to its position if x_s were zero, i.e., the distance $z_0 = \sqrt{x_2^2 + y_2^2}$ is measured. z is the distance from the peak of charge +n to the place where the peak of charge zero would be located if $x_s = 0$. It, along with the known value of the angle C, is used to find x_1 and y_1.

Once the recoil enters the magnetic field it follows a circular path and we have

$$(x - a)^2 + (y - b)^2 = r^2$$

where $a = -r\cos c + 3.75 \tan c \approx -r + 3.75\, c$ and $b = r \sin c \approx rc$ since

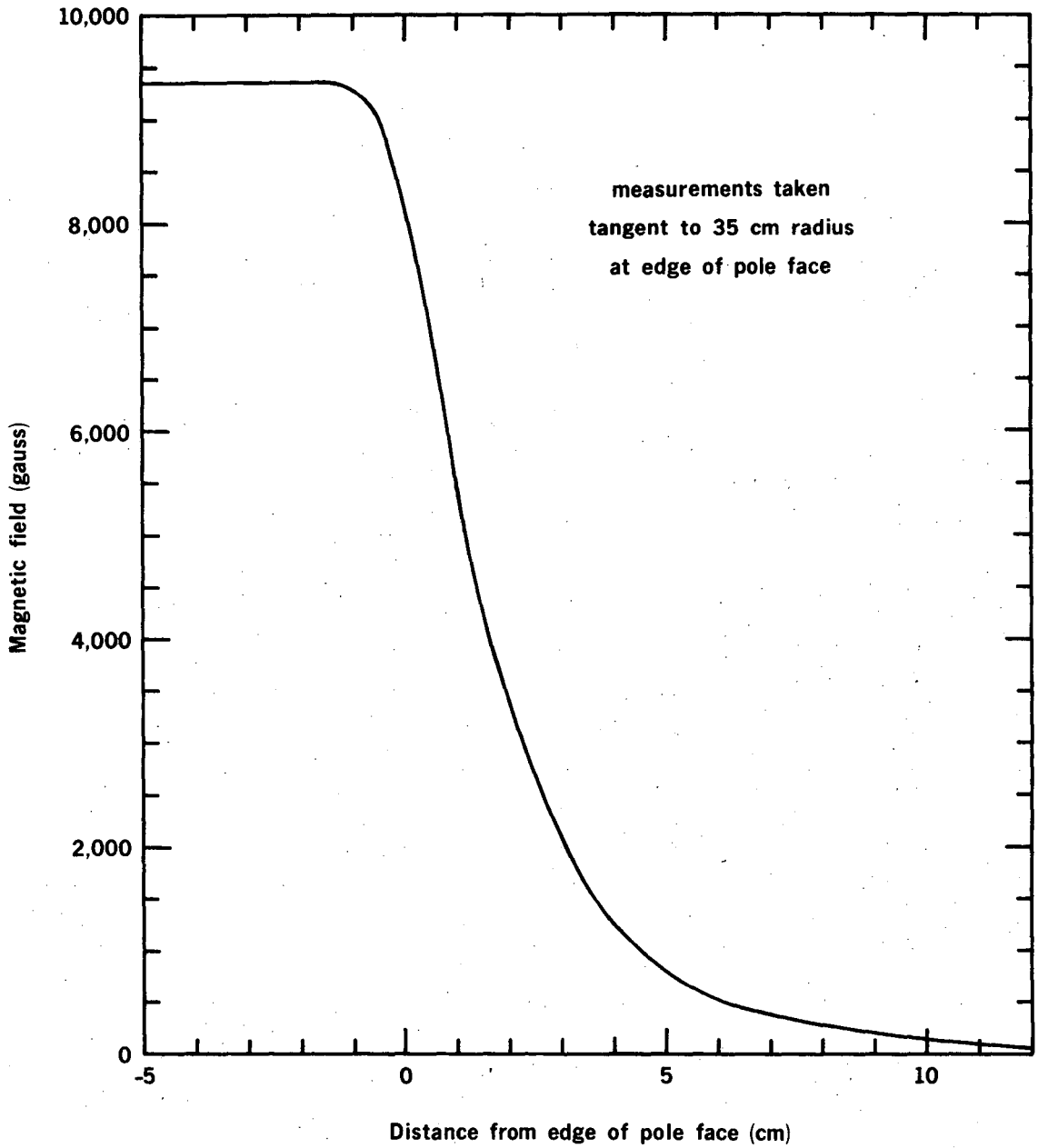

XBL 687-1307

Figure 17. Fringing field of the 180 deg double focusing alpha spectrograph at a radius of 35 cm.

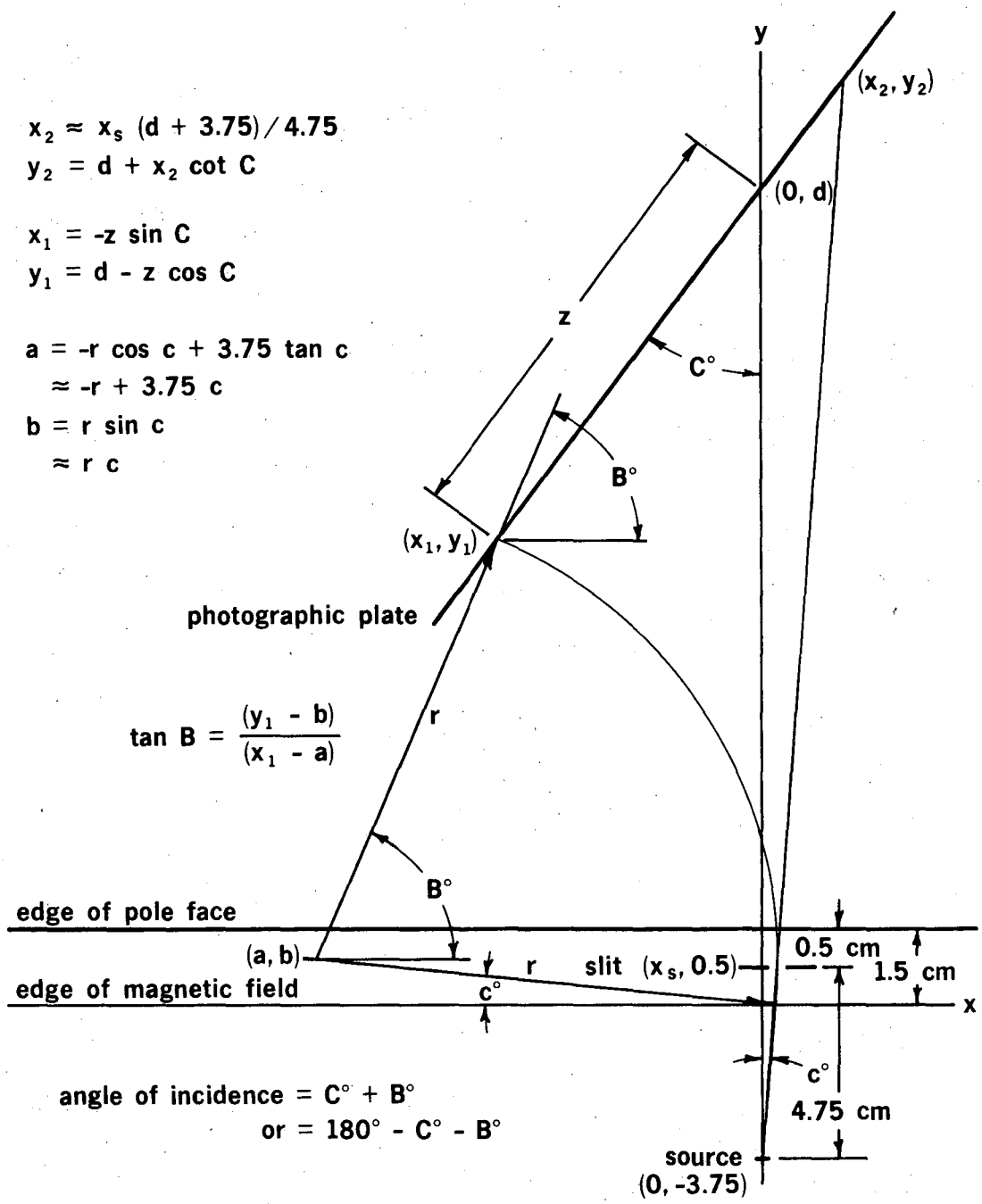

XBL 687-1308

Figure 18. Diagram of the physical relationships of various quantities used in calculating the angle of incidence of Th^{226} recoils for both "90 deg" and "30 deg" thin plates. Some angles and distances illustrated are exaggerated to different degrees in the interests of clarity.

c is a very small angle. We thus have two equations,

$$(x_1 - a)^2 + (y_1 - b)^2 = r^2$$

and

$$(x_s - a)^2 + (0.5 - b)^2 = r^2,$$

and two unknowns, r and c. Using these equations we can calculate r and c and hence we can find the angle B where

$$\tan B = \frac{y_1 - b}{x_1 - a} \quad .$$

The angle of incidence for recoils of charge + n where n = $\pm$ 1, $\pm$ 2, + 3 or +4 is then equal to B + C for the "30 deg" plates and 180 deg - B - C for the "90 deg" plates.

These calculated values for the angles of incidence can be checked in two ways. First, the angle of incidence for recoils of charge +2 can be measured directly according to the procedure mentioned on page 35 . This was done for various of the thin plates and it was found that the calculated value was always well within the experimental range of angles. The variations between experimental and calculated values for "30 deg" plates and "90 deg" plates indicate that the theoretical values for n = +2 are off by a maximum of 1 deg in either case.

Second, if the field really were homogeneous, we would have

$$nr = mv/B = \text{constant}.$$

A comparison between the calculated values of r and what we should have if the field really were homogeneous indicates that for the case under consideration, the field is homogeneous to within 2.4% or less.

Thus the calculated angles of incidence can be used to test how well the data from the thin plates fits the theory for the production of two and

three pronged events assuming diffusion of the Rn^{218} gas in all directions. The easiest test to make is that of the ratio No.(3α)/No.($2\alpha + 3\alpha$). Table I shows these data and shows an obvious discrepancy.

Table I. Comparison of experimental and theoretical values for the ratio No.(3α)/No.($2\alpha + 3\alpha$) for different charges for several thin plates.

Plate	Charge	Experimental No.(3α)/No.($2\alpha + 3\alpha$)	Theoretical No.(3α)/No.($2\alpha + 3\alpha$)
α-2-985			
"30 deg"	0	.081±.005	.139
▫ cold	+1	.127±.005	.150
	+2	.135±.007	.165
	+3	.123±.014	.169
	+4	.142±.018	.170
α-2-992			
"30 deg"	0	.084±.007	.134
▯ cold	+1	.134±.005	.150
	+2	.144±.008	.165
	+3	.124±.016	.169
	+4	.146±.020	.170
α-2-1015	0	.076±.007	.134
"30 deg"	+1	.139±.006	.150
▯ warm	+2	.152±.008	.165
	+3	.125±.017	.169
	+4	.142±.021	.170
α-2-990	0	.097±.007	.170
"90 deg"	+1	.136±.006	.169
▫ cold	+2	.126±.008	.161
	+3	.131±.024	.141

Errors are 90% probability limits

There are two possible causes for the discrepancy. The first involves the possible existence of Ra^{222} recoils which would give rise to extra 2-pronged events and hence decrease the effective ratios. The second involves the fact that the thin plates are in a strong magnetic field

whereas the regular plates are not. This could result in some alignment effects that in turn affect the relative production of 2- and 3-pronged events and hence also affects the ratio No.(3α)/No.($2\alpha + 3\alpha$). If this were true, then the ratio No. $Th^{226}R^{+2}$(3α, 27 deg)/No. $Th^{226}\alpha_0$ would be different for thin plates and regular plates. However, if one calculates this ratio for both thin and regular plates, one finds that the resulting ratios are well within the experimental errors. This in turn indicates that the mechanism for the formation of 2- and 3-pronged events is the same for thin and regular plates and hence, only the existence of Ra^{222} recoils could explain the differences in the ratio No.(3α)/No.($2\alpha + 3\alpha$) for thin and regular plates.

3. <u>Interference of Ra^{222} Recoils-Theory and Experiment</u>

Since the Th^{226} recoils are emitted isotropically, this means that half the Th^{226} recoils leave the source plate and half go into the source plate. The ones which leave the source plate either strike the sides of the brass tube which encloses the area between the source and the collimating slit (see Fig. 7), strike the back side of the source slit or collimating slit, get through both slits and strike the thin plate emulsion, or

get through both slits and are lost somewhere in the alpha spectrograph. In order to get through both slits, the recoils must leave the source at an angle of approximately 90 deg. This fact is very important because the Th^{226} recoils which remain in the source plate will decay and produce Ra^{222} recoils and any of these recoils which are emitted in the proper solid angle will pass through the two slits because their energy is greater than that of the Th^{226} recoils. That is, if x Th^{226} recoils leave the source and strike the emulsion, 1/2 x Ra^{222} recoils will do the same. Once the Ra^{222} recoils strike the emulsion they will further decay and produce 2-, 1- or

0-pronged events. The probability of producing any particular number of prongs will be a function of the angle of incidence of the Ra^{222} recoil, its remaining recoil energy when it first strikes the emulsion, and the behavior of the Rn^{218} gas in the emulsion. When certain assumptions are made concerning the range vs. energy curve of Rn^{218} in the source plate and it is further assumed that Rn^{218} gas diffuses equally in all directions in the emulsion with a diffusion length equal to 0.10μ, the Prob(2α) for Ra^{222} recoils ranges from about .09 to .16; that is, some of the 2-pronged events on the emulsion are definitely formed by Ra^{222} recoil decay rather than by Th^{226} recoil decay. The only question that remains concerns the probable charges of these Ra^{222} recoils.

Since most of the Ra^{222} recoils travel through a considerable amount of source plate (in this case platinum) and then have a certain probability of colliding with C, N or O on the surface of the Pt plate, their charge distribution will be a result of the collisions in the Pt metal and with C, N and O rather than being just a result of the alpha decay they undergo. According to Burhop,[39] the probable charge an ion or atom obtains after colliding with another ion, atom or electron depends upon four things. The first is the initial charges of the colliding objects, the second is their relative velocity, the third is their ionization potentials if they are atoms or ions, and the fourth is their impact parameter. Their relative velocity is important because the smaller it is, the longer the two systems have to react with each other. If their relative velocity is large, the two systems are unlikely to have time to effect a change of charge. This factor is of particular importance in the interaction between the Ra^{222} recoils and the conduction electrons in the Pt metal. It is unlikely that the Ra^{222} recoils will be able to trap conduction electrons into a bound

state unless their relative velocity is small.

In the case of a collision between Rn^{218} (the Ra^{222} recoil) and Pt, C, O, or N, temporary molecular orbitals are set up. The final charges of the two systems very much depend upon the ionization potentials of Rn^{218} and Pt, C, N or O. Table II lists some of these ionization potentials.

Table II. Some of the ionization potentials of C, N. O, Pt, Rn and Ra.

Element	Ionization potential in eV			
	I	II	III	IV
C	11.26	24.38	47.87	64.48
N	14.53	29.59	47.43	77.45
O	13.61	35.11	54.89	77.39
Pt	9.0	18.56	≈ 30	
Rn^{218}	10.75	≈ 19	≈ 30	≈ 42
Ra^{222}	5.28	10.15	≈ 44	≈ 46

The charge of the Rn^{218} could vary from 0 to +9. The charge of C, N, and O will, in general, be zero. The charge of Pt will be +2. From these probably charges along with the various ionization potentials, it becomes apparent that the most probable charge for Rn^{218} is either +1 or 0. Rn^{218} with a charge of +2 is also possible although its probable occurence will be much less than that of charge 0 or +1. Rn^{218} with a charge of +3 or more will be highly unlikely. Furthermore, as Rn^{218} loses more and more of its energy through collisions in the Pt source plate, a charge of zero becomes more and more probable whereas the probabilities of charges +1 or +2 decrease because the probability of picking up a conduction electron will increase. In particular, the probability of $Ra^{222}R^{+2}$ will be approximately zero as soon as any appreciable amount of energy has been lost.

From Table I, on the assumption that the excess 2-pronged events are caused by Ra^{222} recoils, it is apparent that there are indeed a large

number of $Ra^{222}R^{0}$ and $Ra^{222}R^{+1}$. However, there also appears to be a considerable number of $Ra^{222}R^{+2}$, $Ra^{222}R^{+3}$ and $Ra^{222}R^{+4}$ on plates α-2-985, α-2-992 and α-2-1015 although α-2-991 appears to have only $Ra^{222}R^{+2}$ but no $Ra^{222}R^{+3}$. This, of course, is in direct contradiction with what was just stated as the most probable charge distribution.

However, there is another possible cause for these apparent Ra^{222} recoils with charges +2, +3 and +4. They are only apparent for two reasons. First, the "30 deg" plates (α-2-985, α-2-902, α-2-1015) appear to have $Ra^{222}R^{+3}$ whereas the "90 deg" plates do not appear to have $Ra^{222}R^{+3}$. Second, a plot of No.(3α)/No.(2α + 3α) vs. charge for the regular plates (see Fig. 11) indicates that any $Ra^{222}R^{+n}$ for $n \geq +2$ that exists must be so small that it doesn't materially affect the ratio No.(3α)/No.(2α + 3α). This means that it is likely that

$$\frac{\text{No. } Ra^{222}R^{+2}}{\text{No. } Th^{226}R^{+2} + \text{No. } Ra^{222}R^{+2}} \leq .05$$

$$\frac{\text{No. } Ra^{222}R^{+3}}{\text{No. } Th^{226}R^{+3} + \text{No. } Ra^{222}R^{+3}} \leq .02$$

and

$$\frac{\text{No. } Ra^{222}R^{+4}}{\text{No. } Th^{226}R^{+4} + \text{No. } Ra^{222}R^{+4}} \leq .02$$

(see Fig. 11).

A glance at Figs. 19 through 21 indicates that the solution to this problem must involve a source of collimated Ra^{222} recoils that just happen to hit the emulsions at the same spot that another peak does because the background between the various charged peaks is too low to account for the discrepancies in the ratios No.(3α)/No.(2α + 3α) for charges +2, +3 and +4. A further glance at these graphs will disclose another peculiarity. The plot of number of alphas vs. distance along the plate indicates an alpha

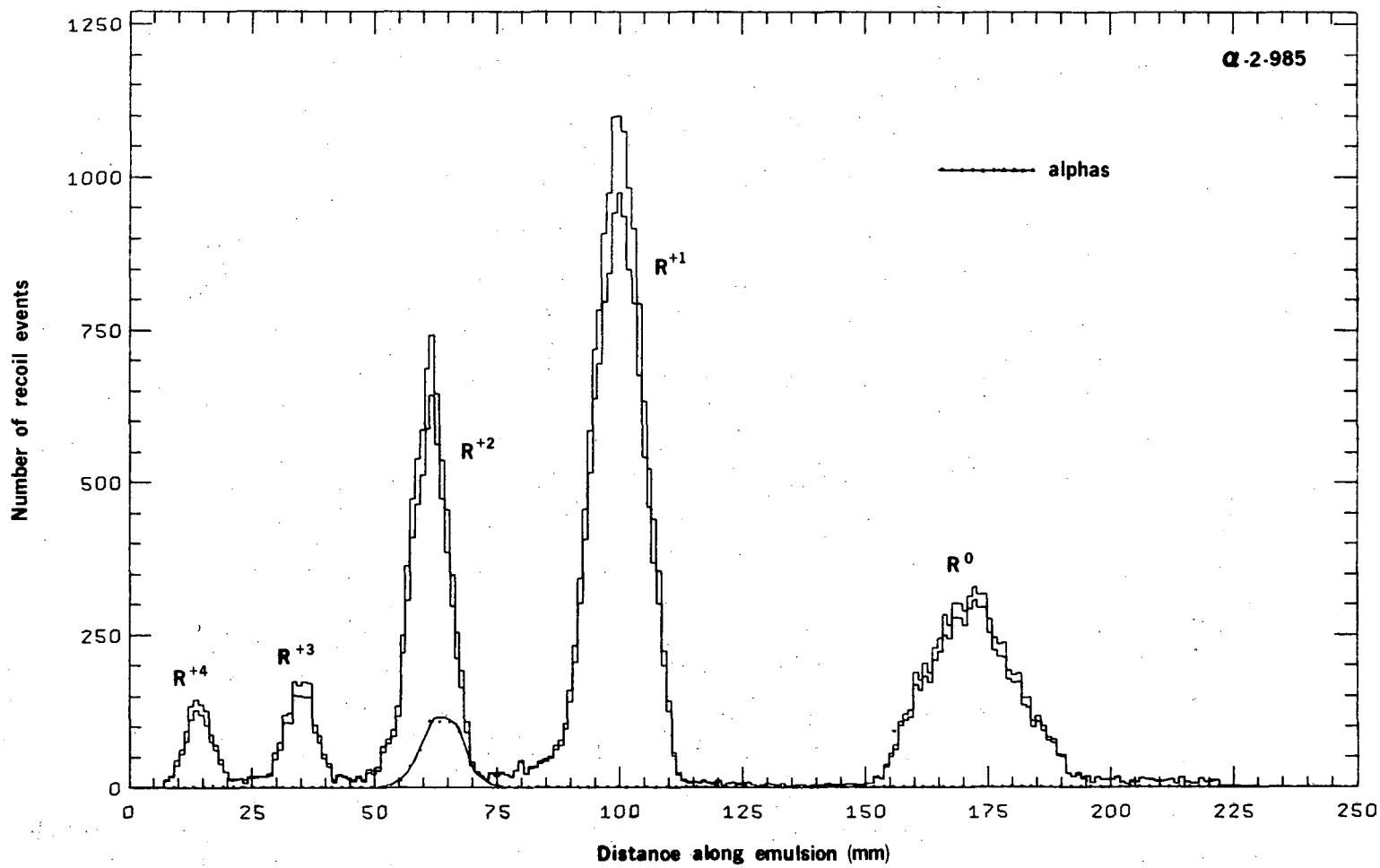

XBL 687-1225

Figure 19. Recoil spectrum of Th^{226} taken with alpha particle spectrograph in "thin plate" configuration. Alpha peak is reduced by a factor of 35. The number of 2- and 3-pronged events are indicated separately. α-2-985 is a "30 deg" α_{cold} plate.

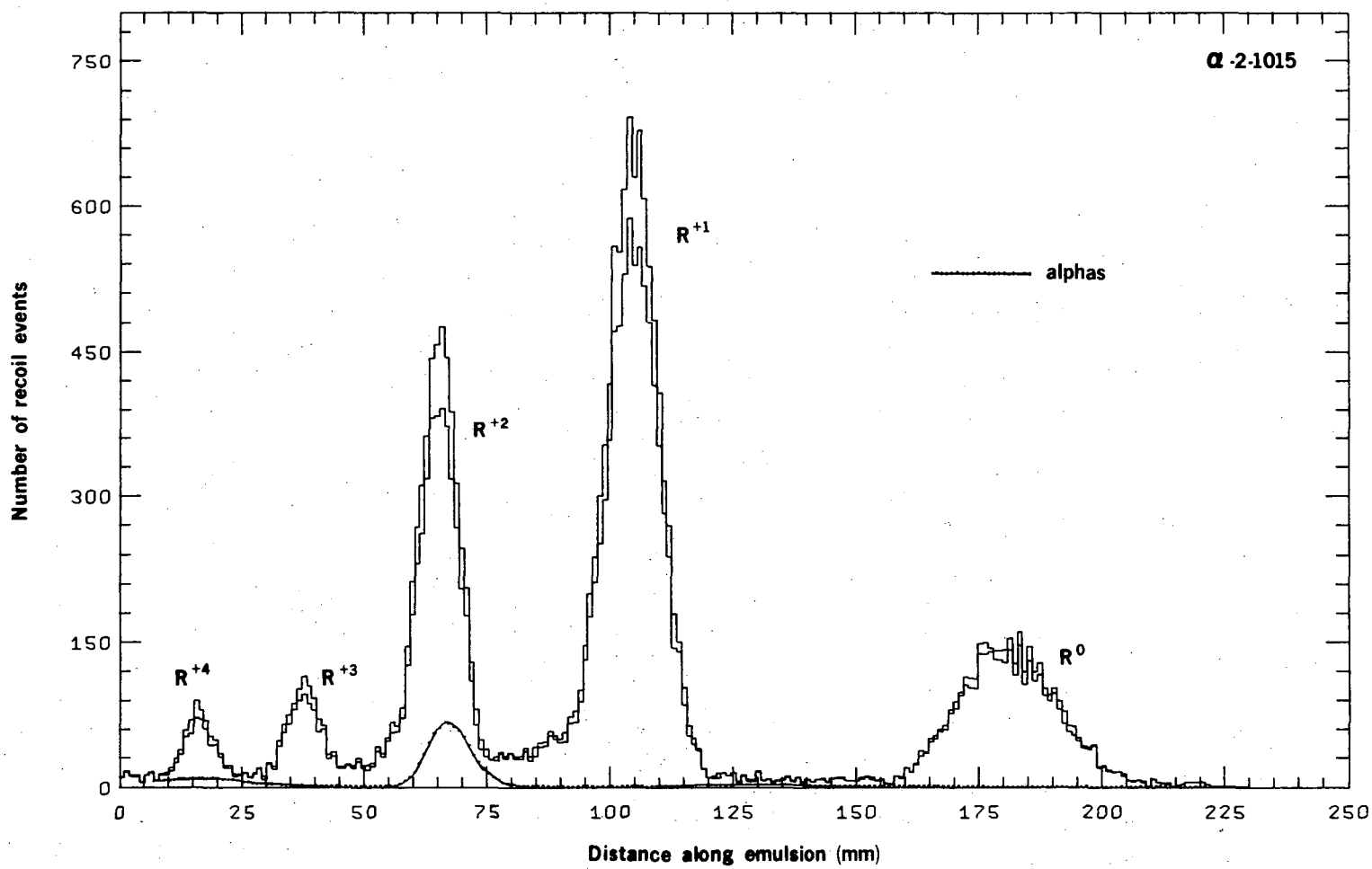

XBL 687-1217

Figure 20. Recoil spectrum of Th^{226} taken with alpha particle spectrograph in "thin plate" configuration. Alpha peak is reduced by a factor of 50. The number of 2- and 3-pronged events are indicated separately. α-2-1015 is a "30 deg" $\square_{warm}$ plate.

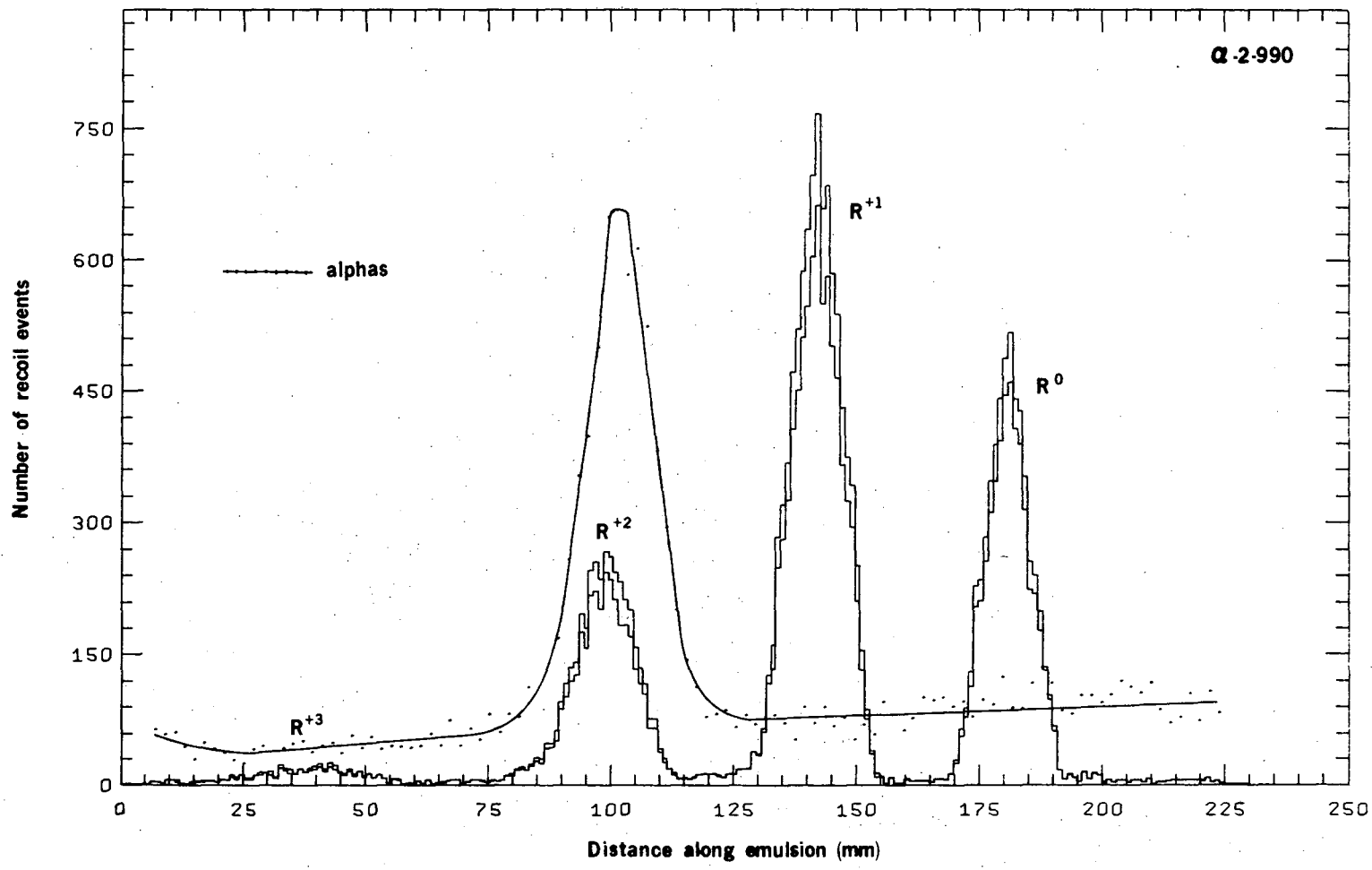

XBL 687-1215

Figure 21. Recoil spectrum of Th^{226} taken with alpha particle spectrograph in "thin plate" configuration. Alpha peak is to scale. The number of 2- and 3-pronged events are indicated separately. α-2-990 is a "90 deg" cold plate.

peak at charge +4 on all of the "30 deg" thin plates. Such a peak can be the result of only two possible causes. The first possibility is that the peak represents alphas whose energy is about 1.6 MeV. Since no such alpha energy occurs naturally, such energies must be the result of normal alphas from the source passing through a thickness of material that causes them to lose 4.8 MeV on the average. The only such material available is the source slit plate which is of such a thickness that alphas in order to penetrate it and still have 1.6 MeV left over would have to initially have 12 MeV of energy which is impossible. Furthermore, since range straggling for alphas is small, we should have

$$\frac{\text{No. 1.6 MeV alphas}}{\text{No. 6.3 - 7.14 MeV alphas}} = \frac{\text{area of source - area of source slit}}{\text{area of source slit}}$$

$$\approx 2 \text{ for } \alpha\text{-2-1015}$$

$$\approx 20 \text{ for } \alpha\text{-2-985.}$$

But, from the graphs it can be seen that this ratio $\approx 1/5$ for α-2-1015 and $\approx 1/20$ for α-2-985. So not only are the actual ratios far too small but that of α-2-985 is smaller than that of α-2-1015, and it should be the other way around. Hence, the alphas at the +4 position can't possibly be 1.6 MeV alphas. However, there is one other possibility and the above ratios fit into this hypothesis very well. As was mentioned on page 48, some of the recoils which leave the source land on the sides of the brass tube which encloses the area between the source and the slit. These recoils in turn decay into alphas and some of these decay particles will escape through the collimating slit and possibly hit the thin plate emulsion. A study of the geometry of the situation gives the following results: (see Figs. 7 and 18)

1. 6.33 to 7.14 MeV alphas will strike the "30 deg" plates at the +4 Th^{226} recoil position and will not strike the "90 deg" plates at all.

2. The ratio, No. of such alphas/No. alphas directly from the source, will be less than one, and furthermore this ratio should be larger for α-2-1015 than for α-2-985.

3. $Ra^{222}R^{0}$ recoils which come from the sides of the brass tube will strike the "30 deg" and "90 deg" plates at the $Th^{226}R^{+2}$ position only.

4. $Ra^{222}R^{+1}$ recoils which come from the sides of the brass tube will strike the "30 deg" plate at the $Th^{226}R^{+3}$ position only and will not strike the "90 deg" plate at all.

5. $Ra^{222}R^{+2}$ recoils which come from the sides of the brass tube follow the same path as the alphas.

A check with experiment shows that every one of these conditions is fulfilled and also explains why the ratio No.(3α)/No.$(2\alpha + 3\alpha)$ for the +3 peak is correct for the "90 deg" plates but is too small for the "30 deg" plates. Furthermore, although $Ra^{222}R^{+2}$ on the order of 5% of the number of $Th^{226}R^{+2}$ does little to affect the ratio No. (3α)/No.$(2\alpha + 3\alpha)$ for charge +2 and hence does not show up on the regular plates as an effect, $Ra^{222}R^{+2}$ on the order of 5% of the number of $Th^{226}R^{+4}$ has a large affect on the ratio No.(3α)/No.$(2\alpha + 3\alpha)$ for charge +4 because No. $Th^{226}R^{+2}$/No. $Th^{226}R^{+4} \approx 6.1$.

The only curious aspect of the whole business is the fact that the half width of the peaks formed by these alphas and Ra^{222} recoils is so small.

Since there is no way to calculate the expected number of extraneous Ra^{222} recoils at any particular spot on the thin plates, it becomes necessary to ignore all 2-pronged events and only use the 3-pronged events. This is safe to do because 3-pronged events can only be formed by Th^{226} recoil decay and all Th^{226} recoils come directly from the source. These 3-pronged events were then used to check the theoretical Prob(3α) discussed in Sec. 2 in the next section.

4. <u>A Check of the Theory using Data from the Thin Plates and Experimental Determination of the Probability Curve</u>.

As was discussed in Sec. 2, the only theory for the production of 2- and 3-pronged events in emulsion that fits any of the experimental data assumes that the alphas decay isotropically and that Rn^{218} gas diffuses isotropically from the end of its recoil path with a diffusion length equal to 0.10μ. However, although the experimental values of Prob(3α)/Prob(2α + 3α) vs. angle of incidence fit this theory very well, the experimental value of Prob(2α + 3α) for the regular plates obtained from the relation

$$\text{Prob}(2\alpha + 3\alpha) = \sum_{n=+3}^{+20} \left(\frac{\text{No. } Th^{226}R^{+n}_{111e} \ (2\alpha + 3\alpha)}{\text{No. } \alpha_{111e}} \right)$$

indicates that the diffusion length D = 0.035 ± 0.010μ instead of 0.10μ. This discrepancy necessitates a further check of this theory and since the entire purpose of this theory is to make it possible to find the ratios No. $Th^{226}R^{+n}$/No. $Th^{226}R^{+2}$ for n = ± 1 or 0, data from the thin plates should be used to check the validity of this theory.

In the case of the thin plates designated by □ (see the section on the thin plate apparatus starting on page 21 for an explanation of the nomenclature used in this section), all of the Th^{226} recoils of charges 0 through +3 or +4 that get through both source and collimating slits strike the thin plate emulsion. Hence, in the case of □ thin plates, we have

$$\frac{\text{No. } Th^{226}R^{+n}}{\text{No. } Th^{226}R^{+2}} = \frac{[\text{No. } Th^{226}R^{+n}(3\alpha)]/[\text{Prob}(3\alpha, \text{ angle } +n)]}{[\text{No. } Th^{226}R^{+2}(3\alpha)]/[\text{Prob}(3\alpha, \text{ angle } +2)]} .$$

If we assume the isotropic Rn^{218} diffusion theory for the production of 2- and 3-pronged events and further assume that the diffusion length D = 0.10μ, we get the results shown in Table III.

Table III. Comparison of the ratios No. $Th^{226}R^{+n}$/No. $Th^{226}R^{+2}$ for several different values of n for two different thin plates.

Plate	n	No. $Th^{226}R^{+n}$/No. $Th^{226}R^{+2}$
α-2-985	0	1.185±.104
cold "30 deg"	+1	2.425±.158
	+3	0.172±.024
	+4	0.131±.019
α-2-990	0	0.907±.093
cold "90 deg"	+1	2.210±.182
	+3	0.191±.050

90% probability limits are given for the ratio

It can be seen immediately that the experimental data does not fit the theory since the ratio for a given n should be the same for the two plates. The remaining solution is to throw all the theories out and find an experimental Prob(3α) vs. angle of incidence curve from the data on plates α-2-985 and α-2-990. Such an experimental probability curve is shown on Fig. 22 along with the theoretical probability curve with D = 0.10μ. This curve was found by assuming the following:

1. Prob(3α, 29.8 deg) = 0.0310
2. the curve must be smooth
3. Prob(3α, a deg) ≥ Prob(3α, b deg) for a deg ≥ b deg.

The curve was then found using only the following data:

1. $\frac{\text{No. } Th^{226}R^{0}(3\alpha)}{\text{No. } Th^{226}R^{+2}(3\alpha)}$ from α-2-985
2. $\frac{\text{No. } Th^{226}R^{0}(3\alpha)}{\text{No. } Th^{226}R^{+2}(3\alpha)}$ from α-2-990
3. $\frac{\text{No. } Th^{226}R^{+1}(3\alpha)}{\text{No. } Th^{226}R^{+2}(3\alpha)}$ from α-2-985

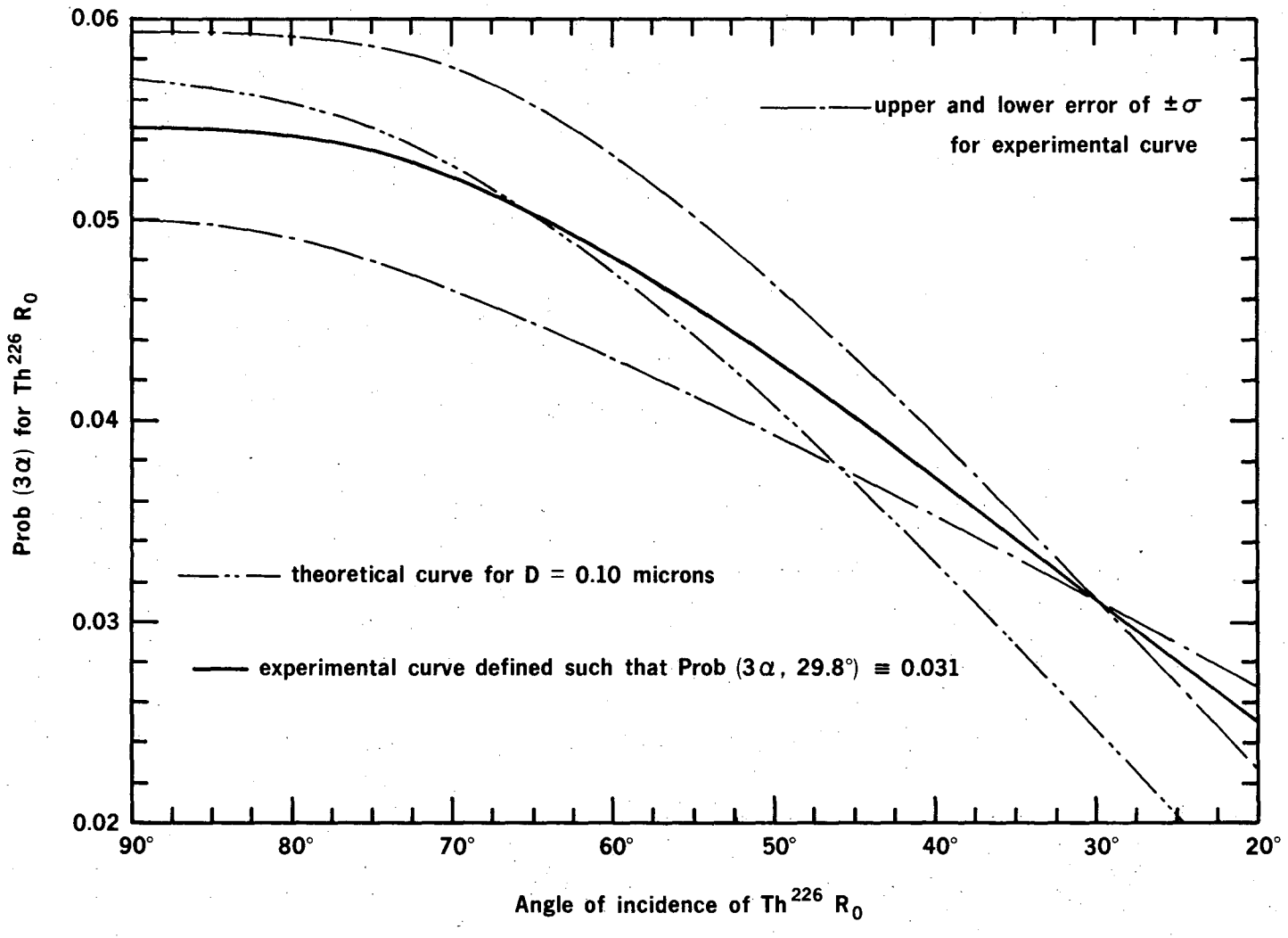

Figure 22. Theoretical and experimental curves of Prob(3α) for $Th^{226}R_0$ as a function of the angle of incidence of the recoils.

4. $\dfrac{\text{No. } Th^{226}{}_{R}{}^{+1}(3\alpha)}{\text{No. } Th^{226}{}_{R}{}^{+2}(3\alpha)}$ from α-2-990

in the following two equations

$$\frac{\text{No. } Th^{226}{}_{R}{}^{0}}{\text{No. } Th^{226}{}_{R}{}^{+2}} = \left(\frac{\text{No. } Th^{226}{}_{R}{}^{0}(3\alpha)}{\text{No. } Th^{226}{}_{R}{}^{+2}(3\alpha)}\right)_{\alpha\text{-2-985}} \left(\frac{\text{Prob}(3\alpha,\ 59.7\text{ deg})}{\text{Prob}(3\alpha,\ 29.8\text{ deg})}\right) \quad (1)$$

$$= \left(\frac{\text{No. } Th^{226}{}_{R}{}^{0}(3\alpha)}{\text{No. } Th^{226}{}_{R}{}^{+2}(3\alpha)}\right)_{\alpha\text{-2-990}} \left(\frac{\text{Prob}(3\alpha,\ 61.6\text{ deg})}{\text{Prob}(3\alpha,\ 86.8\text{ deg})}\right)$$

where Prob(3α, 59.7 deg) $\approx$ Prob(3α, 61.6 deg) and Prob(3α, 29.8 deg) = 0.310

and

$$\frac{\text{No. } Th^{226}{}_{R}{}^{+1}}{\text{No. } Th^{226}{}_{R}{}^{+2}} = \left(\frac{\text{No. } Th^{226}{}_{R}{}^{+1}(3\alpha)}{\text{No. } Th^{226}{}_{R}{}^{+2}(3\alpha)}\right)_{\alpha\text{-2-985}} \left(\frac{\text{Prob}(3\alpha,\ 59.7\text{ deg})}{\text{Prob}(3\alpha,\ 46.6\text{ deg})}\right)$$

$$= \left(\frac{\text{No. } Th^{226}{}_{R}{}^{+1}(3\alpha)}{\text{No. } Th^{226}{}_{R}{}^{+2}(3\alpha)}\right)_{\alpha\text{-2-990}} \left(\frac{\text{Prob}(3\alpha,\ 61.6\text{ deg})}{\text{Prob}(3\alpha,\ 78.2\text{ deg})}\right) \quad (2)$$

where Prob(3α, 59.7 deg) $\approx$ Prob(3α, 61.6 deg). Successive approximations were made until a curve was found that caused the two equations to be satisfied exactly. The curve was then checked by finding No. $Th^{226}{}_{R}{}^{+3}$/ No. $Th^{226}{}_{R}{}^{+2}$ from both α-2-985 and α-2-990 using the experimental curve and comparing the two numbers. It was found that

1. $$\left(\frac{\text{No. } Th^{226}{}_{R}{}^{+3}}{\text{No. } Th^{226}{}_{R}{}^{+2}}\right)_{\alpha\text{-2-985}} = \left(\frac{\text{No. } Th^{226}{}_{R}{}^{+3}(3\alpha)}{\text{No. } Th^{226}{}_{R}{}^{+2}(3\alpha)}\right)_{\alpha\text{-2-985}} \left(\frac{\text{Prob}(3\alpha,\ 59.7\text{ deg})}{\text{Prob}(3\alpha,\ 70.8\text{ deg})}\right)$$

$$= .177 \pm .025^{*}$$

and

*Error limits for all experimental numbers are $\pm$ 90% probability limits unless otherwise indicated.

1. $$\left(\frac{\text{No. } Th^{226}R^{+3}}{\text{No. } Th^{226}R^{+2}}\right)_{\alpha\text{-}2\text{-}990} = \left(\frac{\text{No. } Th^{226}R^{+3}(3\alpha)}{\text{No. } Th^{226}R^{+2}(3\alpha)}\right)_{\alpha\text{-}2\text{-}990} \left(\frac{\text{Prob}(3\alpha,\ 61.6\text{ deg})}{\text{Prob}(3\alpha,\ 39.0\text{ deg})}\right)$$

$$= .171 \pm .045.$$

As can be seen, these numbers compare very favorably with each other and hence this experimental probability curve along with the experimental ratio, Prob(3α, regular plate angle = 26.5 deg)/Prob($2\alpha + 3\alpha$, 26.5 deg) = 0.136, were used exclusively in determining the relative ratios of various charged recoils.

The failure of any of the simple theories to explain the experimental data is unfortunate and should provide an interesting problem for future experiments.

E. Energy Calibration of the Double Focusing Alpha Spectrograph for Regular Plates.

If the magnetic field were homogeneous, then it would be true that to a very good approximation

$$mv^2/r = qvH,$$

where H = the magnetude of the magnetic field, m = the mass of the particle in question, v = its velocity, q = its charge, and r is the radius of its path. Furthermore, if x is the distance along the emulsion from the high energy end to the place on the emulsion where the particle lands, then

$$r = c_1x + c_2,$$

where c_1 and c_2 are constants. Thus

$$mv = qrH$$

$$= qH(c_1x + c_2)$$

or

$$E = (qH)^2/2m \quad (c_1x + c_2)^2,$$

where E is the energy of the particle. However, the field is not homogeneous and can not be measured directly. Thus, a better approximation is to assume that

$$E = (B/2)^2 \; F \; (A_o + B_ox + C_ox^2)$$

where F is defined such that $H = \sqrt{F} \; B$, B is the magnitude of the observed magnetic field in Mc/sec for a Li probe, E is in kV, x is in mm and A_o, B_o and C_o are constants. In order to determine the values of A_o, B_o and C_o it is first necessary to find F as a function of B. This was done for the double focusing alpha spectrograph and the results are shown in Fig. 23. The discontinuities occur at the points where it is necessary to change the current range of the magnet. It can be seen that the value of F to be used

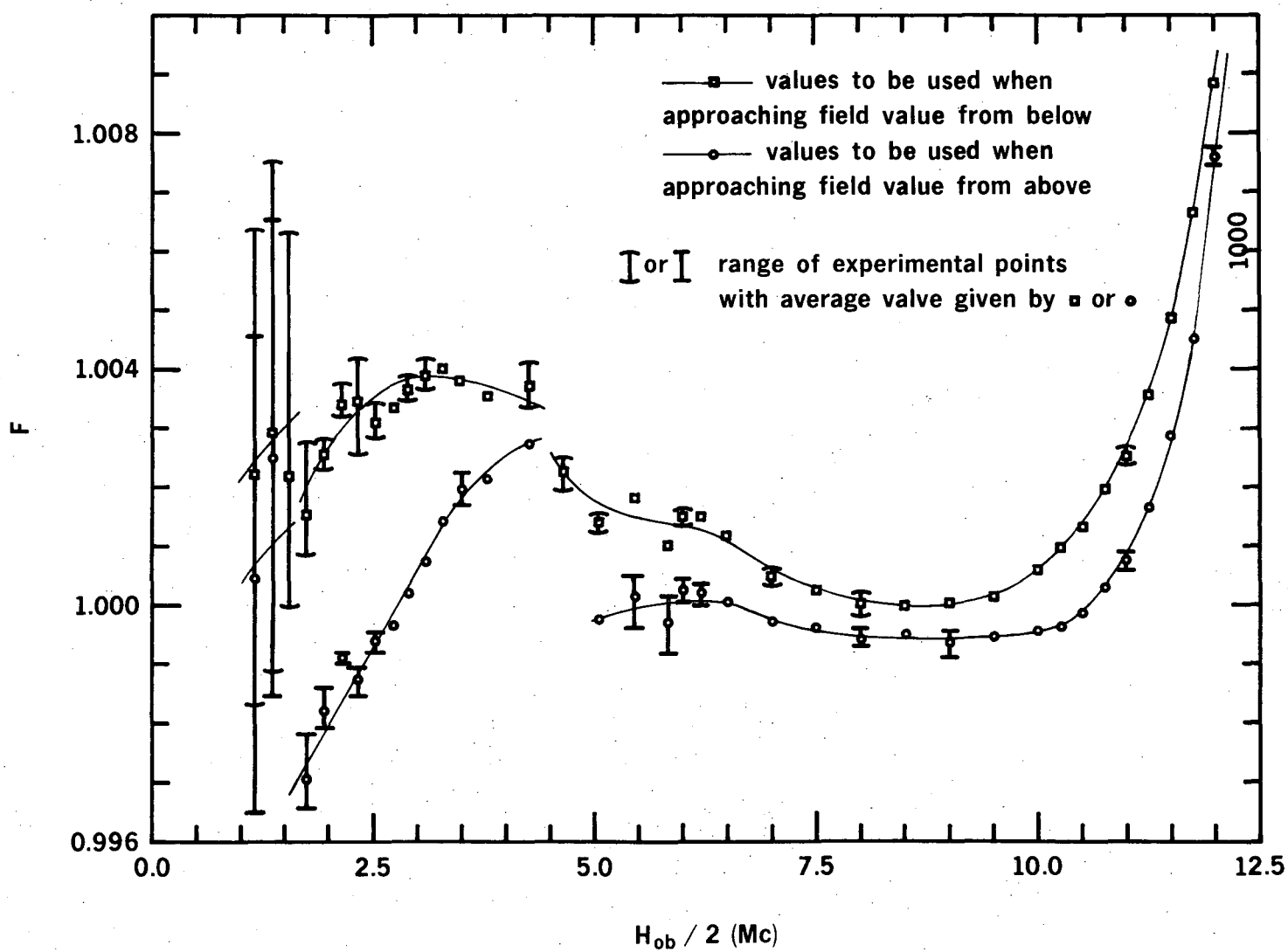

Figure 23. F as a function of H_{ob} where H_{ob} is designated as B in the text and is given in terms of Mc/sec for a Li probe. The magnitude of the magnetic field along the path of the particle for regular plates is given by $H = \sqrt{F}\ H_{ob}$ XBL 687-1165

depends upon whether the field in question was approached from above, i.e., from a higher field value, or from below, i.e. from a lower field value. At very low field values, the residual magnetic field causes the value of F to flucutate widely.

Plates containing peaks whose energy is fairly well known were then used to find the values of A_o, B_o and C_o using a least squares fit for various sets of data. The values thus found were

$$A_o = 54.976$$

$$B_o = -\ 2.7903 \times 10^{-2}$$

$$C_o = -\ 2.7590 \times 10^{-5} \text{ for alpha particles.}$$

The least squares fit for B_o and C_o independent of A_o was very good indicating that the relative energies between two peaks on the same plate can be obtained to within $\pm$ 0.75% using the above values for B_o and C_o. However, the least squares fit for A_o, B_o and C_o was poor giving values for the absolute energy which were consistently low by about 200 keV. This problem was solved by assuming the above values of B_o and C_o and then using a least square fit to find a value for A_o which was consistent with known alpha peak energies. This value of A_o is the one given above and with it the absolute energies can be found to within $\pm$ 0.24%. Although this appears to be fairly accurate, 0.24% of 6 MeV is 14.4 keV and the machine was designed to give better accuracy than this. After some investigation, the cause of the difficulty was found to arise from the method in use to measure the frequency of the Li probe resonance and hence the values of B given for the various plates were accurate to $\pm$ .05% only. This was highly unfortunate because no two recoil peaks were on the same regular plate and hence the center of any particular recoil peak with respect to the center of any other peak cannot be known with any accuracy. This point is amply demonstrated

in Fig. 24 which shows calculated energies versus charge for many different plates. However, since the calculated energies of the centers of the various recoil peaks do not show any apparent trend with respect to an increase in charge, it is very likely that the energies of all the $Th^{226}Ro^{+n}$ peaks are approximately the same regardless of the value of n and that the same holds true for the energies of the $Th^{226}R_{111e}^{+n}$ peaks. However, irrespective of absolute energies, the energy distributions of the various peaks are accurate to $\pm$ 0.75% as mentioned before and hence peak shapes can be compared accurately.

In changing the formula

$$E = (B/2)^2 F(A_o + B_o x + C_o x^2)$$

to the old form of

$$\Delta E = (B/2)^2 F D_o(1 + cx) \Delta x 10^{-2}$$

where ΔE , $E_2 - E_1$, $\Delta x = x_2 - x_1$, and $x = (x_1 + x_2)/2$, we find that

$$D_o = - B_o 10^2 = 2.7903$$

and

$$C = 2 C_o/B_o = 1.9775 \times 10^{-3}.$$

This compares with the old values of

$$D_o = 2.815$$

and

$$C = 1.79 \times 10^{-3}.$$

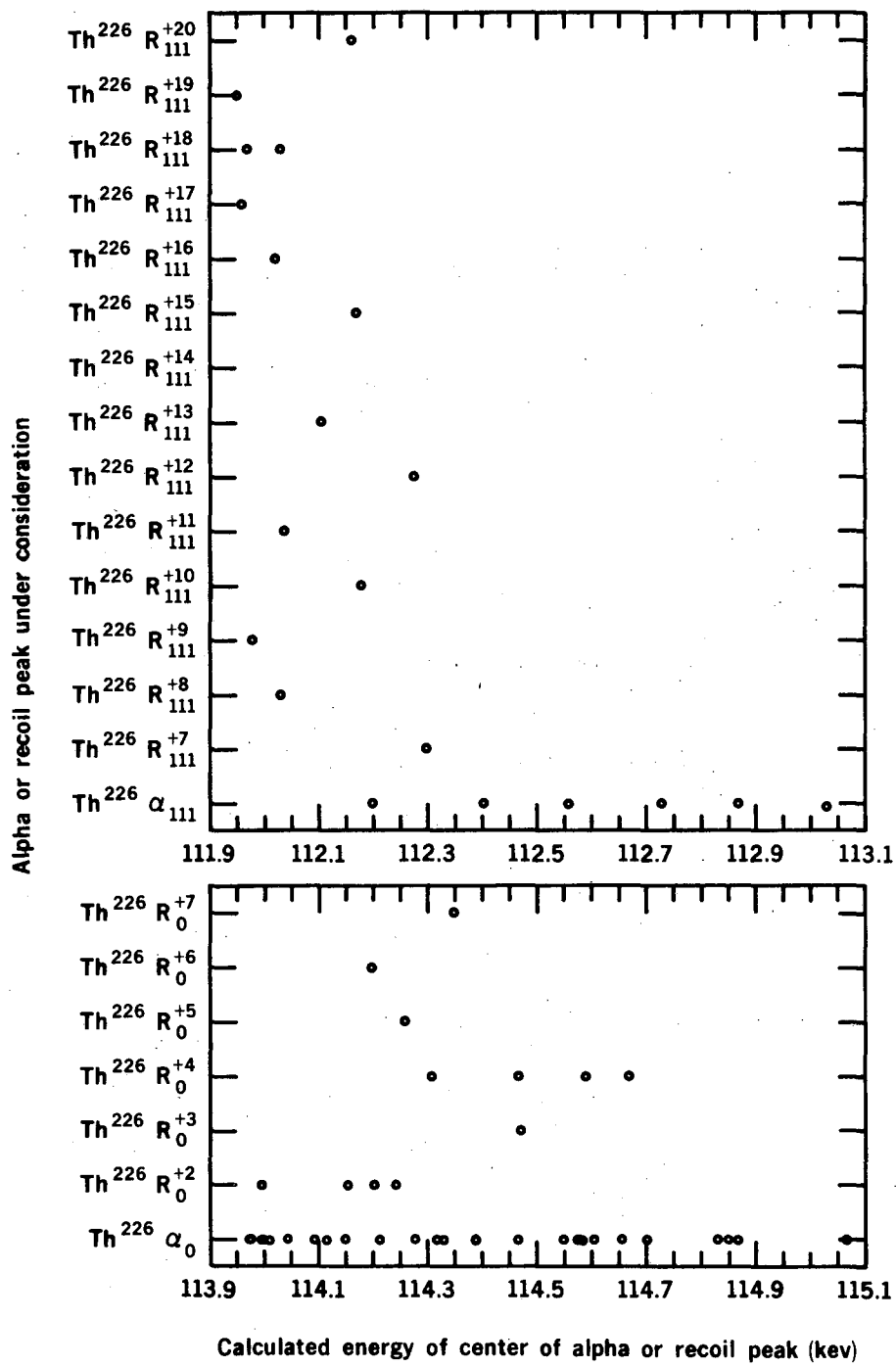

Figure 24. Plot of the calculated energies of the centers of various recoil and alpha peaks; each point represents a peak from a different plate. The alpha peak energies are given in terms of the energy they would have if they were Th^{226} recoil peaks in order to make a comparison between the positions of both recoil and alpha peaks.

III. SOURCE AND PRESSURE EFFECTS ON THE CHARGE ENERGY DISTRIBUTIONS OF Th^{226} RECOILS

A. Source Effects--Theory and Experiment

Since the Th^{226} recoils investigated do not result from the decay of gaseous Th^{226} but rather result from the decay of Th^{226} which has been deposited upon a source plate of some material, it is important to ascertain how dependent the charge and energy distributions obtained for Th^{226} recoils are upon this circumstance. Since the Th^{226} deposits on these source plates do not tend to fall off, it is apparent that there is at least some force causing it to adhere to the source plate. When the Th^{226} decays, these forces must modify the recoil's initial charge and energy.

It is highly likely that a fair amount of the Th^{226} is actually buried under one or more layers of Pt metal. In addition, some C, N, or O in the form of various compounds is likely present as a contamination on the surface of the Pt. Thus the Th^{226} recoil in escaping the source plate can have collisions with metallic Pt, the conduction electrons, or simple inorganic compounds containing C, N or O. These collisions in turn affect the initial charge and energy distribution of the Th^{226} recoils. Thus it is important to have an idea of what kind of changes are likely to be made.

As was mentioned before in the section on the interference of Ra^{222} recoils (see page 48) four things are important in ionic or electronic collisions:[39]

1. relative velocity of the two species involved in the collision,
2. the impact parameter of the collision,
3. the initial charges of the two species, and

4. the various ionization potentials of the two species.

In general, all of the electrons of Ra^{222}, Pt, N, O, and C are moving much faster than the Ra^{222} atom and hence will have time to set up molecular orbitals when Ra^{222} collides with Pt, N, O or C. The possible exceptions to this are the two outermost electrons of Ra^{222}. The initial charge of Pt will be +2 whereas that of N, C and O will likely be either 0 or +1. The initial charge of Ra^{222} can vary but it will have some limits. These limits are very important on the effect the collisions will have on the final charge distribution of Ra^{222}. This initial charge distribution will be discussed later. A glance at Table II on page 50 shows that any collisions between Ra^{-2}, Ra^{-1} or Ra^{+0} and C^{+1}, N^{+1}, O^{+1} or Pt^{+2} will almost surely cause these Ra ions to become Ra^{+1} or Ra^{+2}. A collision between Ra^{+1} and Pt^{+2} will likely result in Ra^{+2}. A collision between Ra^{+1} and C^{+1}, N^{+1}, or O^{+1} will likely yield Ra^{+2}. However, Ra^{+2} has a relatively high probability of picking up conduction electrons as does Ra^{+1} to a much lesser extent. Thus, it is probable that, in general, the possible collision processes will favor Ra^{+1} rather than Ra^{+2}. Collisions between Ra^{+n} for $n \geq +3$ and Pt, C, N, O, or conduction electrons will almost certainly yield Ra^{+m} where $m < n$ because the ionization potentials for Ra^{+n} where $n \geq +3$ are so large. Thus the probability of the following collision is approximately zero:

$$Ra^{+n} + \text{Pt, C, N, O or electron} \rightarrow Ra^{+m} \quad \begin{matrix} n \geq +2 \\ m > n \end{matrix} .$$

Thus, on the whole, collisions will tend to change Ra^{-2}, Ra^{-1}, and Ra^{0} to Ra^{+1} or Ra^{+2}, and change Ra^{+n} where $n \geq +3$ to Ra^{+1} or Ra^{+2}. Ra^{+1} and Ra^{+2} will tend to exchange charges back and forth. However, since (as will be seen in Sec. IV. C. on experimental results) No. $Th^{226}R^{0} \approx$ No. $Th^{226}R^{+2}$ and No. $Th^{226}R^{+1} \approx 2 \times$ No. $Th^{226}R^{+2}$, collisions on the whole

will probably cause a net gain in the total number of Ra^{+2}'s. All of these collision processes will involve some decrease in the velocity of the Ra atom. Therefore, collisions in the source plate, in addition to enhancing the number of $Th^{226}R^{+1}$ and $Th^{226}R^{+2}$, will reduce the peak energies and broaden all the recoil peaks. This will be particularly true of the $Th^{226}R^{+1}$ and $Th^{226}R^{+2}$ peaks since recoils which undergo multiple collisions will, in general, have a final charge of either +1 or +2.

These charge changes will not have as drastic an effect as it might seem initially because a fair amount of the readjustment of the Th^{226} recoil to the effects of the alpha decay occur away from the source plate and its contaminations. The recoil has an energy of about 114 keV which corresponds to a velocity of about 3×10^7 cm/sec. The velocity of the alpha particle is about 55 times greater than this. This means that the direct ionization effects due to the alpha particle emission will occur before the recoil has a chance to move. At most, this emission will probably cause the direct removal of 3, 4 or possibly 5 electrons. Of these, two will certainly be the outermost Th^{226} electrons since these electrons would not be tightly bound to Ra^{222}. The next most likely electrons to be removed are the valence electrons of Ra^{222}. In addition, one or possibly two electrons might be removed from the P, O or N shells. Thus, the initial charge of Ra^{222} is likely to range from 0 to +3 or +4 at the most. These holes will eventually be filled by Auger processes[5] which have lifetimes of the order of 10^{-13} to 10^{-15} sec. In 10^{-15} sec, the recoil will have traveled a distance of about 3×10^{-8} cm which is about equal to the diameter of a Pt atom. In 10^{-13} sec, the recoil will have traveled 100 times the diameter of a Pt atom and hence will have escaped the source plate before the Auger process occurs. Therefore Auger processes can occur

either in the source plate or well away from it. If these processes occur in the plate, then the charge distribution will be strongly affected by the collisions which can occur in leaving the source plate, because recoils which would have had a final charge of +5 or +6, etc. will have their charges decreased through these collisions and hence show up in the low energy tails of recoil peaks with smaller charges. On the other hand, if the Auger processes occur outside the source plate, a recoil, which would have a final charge of +5, +6, etc. due to Auger processes, can undergo collisions in the source plate without affecting its final charge and simply increase the low energy tail of the higher charge recoil peaks.

Changes in source temperature can have two affects. First, an increase in source temperature will change the electron population levels associated with the Th^{226} atom in Pt. Because the temperature change is small, it will affect at most the population levels of the outermost four electrons which will likely be involved in various molecular orbitals with nearest neighbor atoms or possibly in the conduction band. Since the ionization effects due directly to the emission of the alpha particle are highly dependent upon the electron configuration, increases in source temperature could change the initial charge distribution due to the alpha particle's emission. In general, an increase in temperature will result in a shift in this initial charge distribution towards higher charges if any shift occurs. Second, any change in the population levels of the Th^{226} atom as a result of an increase in temperature will also affect the electron population levels of the recoil atom. Since the lifetime of an Auger process depends entirely upon the overlap of the initial electronic state and the final electronic state, changes in the electron population levels will

certainly affect the lifetimes of the Auger processes. Such changes may involve either an increase or a decrease in the lifetime of the Auger processes. If the Auger lifetimes tend to increase with an increase in source temperature, then the final charge distribution will tend to peak toward higher charges. If the Auger lifetimes tend to decrease with an increase in source temperature, then the final charge distribution will tend to peak toward lower charges. The lifetime of the 110 keV excited state is on the order of 10^{-9} to 10^{-10} sec. During this time the recoil will have traveled from 0.00315 mm to 0.315 mm, and consequently, the electron conversion process will always occur well away from the source plate. Since the Auger electron cascade following such a process is the primary influence in forming the charge distribution of $Th^{226}R_{111e}$, collisions which occur to $Th^{226}R_{111e}$ while they are leaving the source will not materially affect the $Th^{226}R_{111e}$ distribution.

Collisions in the plate will cause peak broadening through the formation of a low energy tail. Before the electron conversion process occurs, $Th^{226}R_{111e}$ will have the same charge distribution as $Th^{226}R_0$. Since the most probable charge of $Th^{226}R_0$ is +1 (see Fig. 91) the energy distributions of all of the $Th^{226}R_{111e}$ will have approximately the same shape as the energy distribution of $Th^{226}R_0^{+1}$. The energy distribution of $Th^{226}R_0$ will vary depending upon the charge of the recoils and the temperature of the source plate. The energy distributions of higher charged $Th^{226}R_0$ will have smaller half widths and smaller low energy tails than those of lower charges. $Th^{226}R_0^{+1}$ will probably have the largest tail and half-width followed by $Th^{226}R_0^{+2}$.

A check of experimental data verifies these conclusions. (See Figs. 60 and 80). The half widths of the $Th^{226}R_{111e}^{+n}$ peaks for n = +9

to +20 are all about 900 eV and larger than the half width of $Th^{226}R_0^{+2}$ peak which is 675 eV, which is in turn larger than that of the $Rh^{226}R_0^{+3}$ peak which is 450 eV and that of the $Th^{226}R_0^{+6}$ peak which is 390 eV.

The importance of these collisions is further confirmed by evidence from the "warm" and "cold" thin plates. As was discussed before on pages 1 and 24, the sources for the "cold" thin plates were approximately 32° F, the sources for the regular plates were at approximately 72° F and the sources for the "warm" thin plates were at approximately 100° to 110° F. Now, the following ratios occurred:

$$(\text{No. } R^{+3}/\text{No. } R^{+2})_{\text{cold}} = .177 \pm .017$$

$$(\text{No. } R^{+3}/\text{No. } R^{+2})_{\text{reg. plate}} = .229 \pm .008$$

$$(\text{No. } R^{+3}/\text{No. } R^{+2})_{\text{warm}} = .156 \pm .028$$

and

$$(\text{No. } R^{+3}/\text{No. } R^{+4})_{\text{cold}} = 1.29 \pm .17$$

$$(\text{No. } R^{+3}/\text{No. } R^{+4})_{\text{reg. plate}} = 1.402 \pm .069$$

$$(\text{No. } R^{+3}/\text{No. } R^{+4})_{\text{warm}} = 1.40 \pm .34.$$

It can be seen that the number of +2 recoils with respect to the number of +3 recoils is indeed affected by the temperature of the source. From these results it appears that an increase in temperature does shift the initial charge distribution toward higher charges. Furthermore, it appears that an increase in temperature tends to decrease the lifetimes of the Auger processes involved and hence to cause an eventual shift in the charge distribution towards lower charges. The sum of these two effects is to cause an increase followed by a decrease in the ratio No. $Th^{226}R^{+3}$/No. $Th^{226}R^{+2}$ as the source temperature increases from 32° F to 72° F to 110° F. Further evidence for this hypothesis is given by the

fact that the ratio (No. $Th^{226}R^{0}$/No. $Th^{226}R^{+2}$) decreases as the temperature increases as does the ratio (No. $Th^{226}R^{+1}$/No. $Th^{226}R^{+2}$).

The above hypotheses are, of course, speculative and it would be very interesting to check the speculation by means of detailed experiments.

B. Pressure Effects--Theory and Experiment

The pressure in the alpha spectrograph was measured by an ordinary ion gauge and so it is not known with extreme accuracy. However, according to the ion gauge the pressure ranged from 2 or 3 x 10^{-5} mm of Hg to 5 x 10^{-6} mm of Hg. The maximum actual pressure was probably no more than 4 or 5 x 10^{-5} mm of Hg and it would be that high only for a short time during the first part of any source run. These pressure values correspond to the mean free paths of the recoil atoms ranging from 556 cm for 5 x 10^{-5} mm of Hg to 5560 cm for 5 x 10^{-6} mm of Hg. The path followed by the alphas or recoils before striking the regular plates is about 160 cm.

As far as the alpha particles are concerned, even the highest possible pressure of 5 x 10^{-5} mm of Hg is insignificant. For such a pressure, the probability that an alpha is deflected through an angle greater than .5 deg assuming Rutherford scattering is about 8 x 10^{-8}. Deflections of less than .5 deg will certainly have no noticeable affects on the shape of the alpha peak since such collisions will have little effect in changing the charge of the alpha particles involved.

For recoils, the situation is somewhat different. Using modified Rutherford scattering, the maximum angle of deflection is about 3 deg. This angle is generally insignificant because of the double focusing properties of the magnet except perhaps insofar as the recoils might hit the magnet pole tips. The probability of a collision of some kind, somewhere along the path of the recoil is 29% for a pressure equal to 5 x 10^{-5} mm of Hg and is 3% for a pressure of 5 x 10^{-6} mm of Hg. However, the probability of having a collision which causes the energy of the recoil to decrease by 4 keV is only 0.4% for a pressure of 5 x 10^{-5} mm of Hg. This probability corresponds to all collisions whose angles of deflection are greater than

1.5 deg. In fact, for a pressure of 5×10^{-5} mm of Hg, the probability of having a collision that results in the recoil being deflected through an angle ≥ 0.5 deg with an energy loss ≥ 0.02 keV, is only 1.1%. Thus, it is obvious that if the only result of a collision between a recoil with a gas molecule along its path were a change in the energy and direction of the recoil, then the effects of such collisions would be negligible. However, there are other results.

The charge of the recoil may, even will probably, be changed in a collision. Table IV shows possible charge changes for collisions into O and N in air. Table IV is constructed by considering the ionization potentials in the same way as is done in Secs. II.D.3. and III.A. This table gives the maximum possible charge changes to obtain these maxima.

For example, in a collision between $Th^{226}R^{+15}$ and an N atom, as the atoms come closer and closer to each other, the outermost electrons of the N atom set up molecular orbitals about the $Th^{226}R^{+15}$-N pair. The electrons in these orbitals will have approximately the same energy that they had in the N orbitals from which they came.[39] Hence, in general, these electrons will be in excited molecular orbital states. The number of such orbitals which are set up depends upon the impact parameter because such an orbital can not be created unless the atoms get close enough. As the atoms move apart, the electrons go into atomic orbitals about either the recoil or the N atom. Of course, more than one electron can not occupy the same orbital and this limitation restricts the maximum charge exchange which can occur. In the case of $Th^{226}R^{+15}$ colliding with N, this maximum is 5 and can be ascertained by studying the relative ionization potentials of N^{+5}, N^{+6} and Ra^{+15}. As the atoms separate, the atom about which the electron in its molecular orbital spends more time is the one more likely to keep the electron. In the case of Ra^{+15} and N, the Ra generally keeps the

Table IV. Possible changes in charge which could occur to $Th^{226}R^{+n}$ during a collision with gaseous O or N.

Atom recoil collides with	n	Possible changes in n which could occur
O	$n \geq +13$	n could decrease by 6
N	$n \geq +13$	n could decrease by 5
N or O	n = +12	n could decrease by 5
N or O	n = +11	n could decrease by 4 or 5
N or O	n = +10	n could decrease by 3 or 4
N or O	n = +9	n could decrease by 3
N	n = +7, +8	n could decrease by 3
O	n = +7, +8	n could decrease by 2 or 3
N or O	n = +3 to +6	n could decrease by 2
N or O	n = +2	n would not change
N or O	n = 0, +1	n could increase by 1 or 2 if $Th^{226}R^{+n}$ hits a charged molecule or O_2.

electron; however, as the orbitals adjust to the changing situation, the outermost electrons spend less and less relative time near the Ra atom as the charge of Ra decreases and that of N increases. Even assuming that Ra acquires the maximum number of electrons from O or N, this does not mean that it maintains this charge because these acquired electrons are generally in excited atomic orbitals and in the de-excitation, the probability of electron loss by Auger processes is very large. Depending upon circumstances, a collision between $Th^{226}R^{+15}$ and N could yield $Th^{226}R^{+n}$ where n ranges from + 14 to +10.

The question immediately arises as to whether or not it would be possible to have a collision without having a change in charge even though it is possible with a sufficiently small impact parameter. The definition of collision in this section means that the impact parameter is $\leq 1.5 \times 10^{-8}$ cm. Now,

$$E_{ion} \approx \left(\frac{z_{eff}}{n}\right)^2 \quad (13.6 \text{ eV})$$

and

$$r \approx \frac{n^2}{z_{eff}} \quad (.5 \times 10^{-8} \text{ cm})$$

where E_{ion} = the ionization, potential, z_{eff} = the charge of the Th^{226} recoil, n = the principal quantum number, and r = the radius of electron orbital. Hence, for $Th^{226}R^{+15}$ colliding with N_2,

$$E_{ion} \text{ of } N_2 = 15.5 = (15/n)^2(13.6)$$

yields $n \approx 15$ which yields $r = 15\ (.5 \times 10^{-8} \text{ cm}) = 7.5 \times 10^{-8}$ cm. Thus, $Th^{226}R^{+15}$ can always acquire at least one electron for an impact parameter $\leq 1.5 \times 10^{-8}$ cm. This holds true for $Th^{226}R^{+n}$ down to n = +3 or +4. In fact, it indicates that for the higher charge recoils, this collision parameter is too small and hence the actual probability of collision is somewhat larger than that used above.

However, when one considers that a large impact parameter means a small "collision time" and that the smaller the collision time, the less the probability of setting up the molecular orbital, etc., the use of 1.5×10^{-8} cm may still be reasonable.

Thus, although the maximum possible charge changes shown in Table IV may not occur, it is very unlikely that recoils with charges $\geq +5$ will not acquire at least one electron and it is probable that $Th^{226}R^{+3}$ and $Th^{226}R^{+4}$ will also acquire at least one electron.

The question immediately arises as to what happens to the recoils which change their charges during their time-of-flight in the alpha spectrograph. The flight paths of recoils which strike the regular plate emulsion can be considered in three separate parts (see Fig. 2). The total flight path is about 160 cm long. The first 24.5 cm of this distance occurs outside the magnetic field. Any changes in charge which occur in this region will result in the recoil behaving as if it had had that particular charge all along. The probability of a collision occurring in this region is 4.4% for a pressure of 5×10^{-5} mm of Hg. Such collisions will not likely affect the charge distributions for the regular plates with the possible exception of $Th^{226}R_0$ charge distribution. This is because no charge +2 recoils will be lost as a result of such collisions, and hence there could be a net gain in the total number of +2 recoils as a result of collisions along this portion of the recoil flight path. The second portion of the recoil flight path is 111 cm long and occurs wholly inside the magnetic field of the spectrograph. Any recoil which gains an electron in this region will be totally lost because any such recoil either misses the photographic emulsion entirely or has an equal probability of striking the emulsion anywhere along its length which classifies it as part of the

background. The third region of the recoil flight path is again outside the magnetic field and is about 24.5 cm long. Any collisions which occur in this region of the flight path will have, in general, no affect on the subsequent path of the recoil.

Hence, collisions which occur to the particles along their flight paths in the spectrograph for the production of regular plates, have the following effects. First, 20% or more of the recoils whose charges are $\geq +5$ will be totally lost through collisions while in the magnetic field. Second, 20% or more of the recoils whose charges are 0, +1, +3 or +4 could be totally lost through collisions in the same region although it is unlikely that the percentage is so high, particularly for charges 0 and +1. Third, essentially no alphas or charge +2 recoils are lost due to collisions. This in turn means that although the experimental ratio No. $Th^{226}R_0^{+2}$/No. α_0 will be correct, No. $Th^{226}R^{+n}$/No. α will be up to 20 or more percent too small for $n \geq +5$, where this unknown percent will be approximately the same for all $n \geq +5$. In addition No. $Th^{226}R_0^{+n}$/No. α_0 for n = +3 or +4 can also be up to 20 or more percent too small and this unknown percent can be different from that of $n \geq +5$ and that of each other. Thus, the vacuum pressure in the spectrograph probably has little or no affect on the charge and energy distribution of $Th^{226}R_{111e}^{+n}$ other than changing the experimental value of Prob($2\alpha + 3\alpha$) as discussed below. However, it can affect the charge distribution of $Th^{226}R_0^{+n}$ as far as the relative percentages of $Th^{226}R_0^{+n}$ for $n > +2$ with respect to n = +2 is concerned. It does not affect the relative percentages of $Th^{226}R_0^{+1}$ or $Th^{226}R_0^{0}$ with respect to $Th^{226}R_0^{+2}$ because these ratios are obtained from the thin plates where the probability of a recoil undergoing a collision in flight before striking the thin plate is only 4.4% for a vacuum pressure

of 5×10^{-5} mm of Hg and the errors involved in calculating No. $Th^{226}R_0{}^{+1}$ or 0/ No. $Th^{226}R_0{}^{+2}$ are greater than 4.4%.

The differences in the quantities

$$\text{Prob}(2\alpha + 3\alpha,\ 26.5\ \text{deg})_{111e} = \sum_{n=+3}^{+20} \left(\frac{\text{No.}\ Th^{226}R_{111e}{}^{+n}(2\alpha + 3\alpha)}{\text{No.}\ \alpha_{111e}} \right)$$

and

$$\text{Prob}(2\alpha + 3\alpha,\ 26.5\ \text{deg})_0 = \sum_{n=-2}^{+10} \left(\frac{\text{No.}\ Th^{226}R_0{}^{+n}(2\alpha + 3\alpha)}{\text{No.}\ \alpha_0} \right)$$

(see page 189) indicates that the vacuum pressure effects are such that the probability of a collision along the flight path of a recoil going to a regular plate is about 22.2%.

IV. RESULTS

A. Th^{226} Alpha Spectrum and Half Life

1. Theory and Experiment

Alpha spectra of Th^{226} were obtained using both a silicon solid state alpha detector and a 180 deg double focusing alpha spectrograph. The previously reported alpha energies and their intensities are:[43]

$Th^{226}\alpha_0$ = 6.34 MeV, 79% of total

$Th^{226}\alpha_{111}$ = 6.23 MeV, 19% of total

$Th^{226}\alpha_{242}$ = 6.11 MeV, 1.7% of total

$Th^{226}\alpha_{302 + 318}$ = 6.04 MeV, 0.6% of total.

The spectra obtained using the solid state counter were merely used to check the results found with the alpha spectrograph. This was done because the spectra produced by the alpha spectrograph are much more accurate than those produced by the solid state counter. The absolute energies of the Th^{226} alphas were not determined for the reasons outlined in Part E of Sec. II. However, it is apparent from Fig. 24, that the energy of $Th^{226}\alpha_0$ lies somewhere between 6.33 and 6.43 MeV. Furthermore, since the most accurate frequency measurements were made for the later plates, the actual energy of $Th^{226}\alpha_0$ probably lies somewhere between 6.34 and 6.36 MeV. Th^{226} was collected from a U^{230} source using the parallel plate collector at 22.5 volts with an electric field of 225 volts/cm. This source was then run in the solid state counter yielding the spectrum shown in Fig. 25. Since the $Th^{226}\alpha_{111}$ peak is combined with the $Ra^{222}\alpha_{325}$ peak, it was necessary to also obtain an alpha spectrum of Ra^{222} in order to analyze the alpha spectrum of Th^{226}. A Th^{226} source was produced as before and then Ra^{222} was collected from it by the same technique. This source was then run in the solid state counter yielding the alpha spectrum

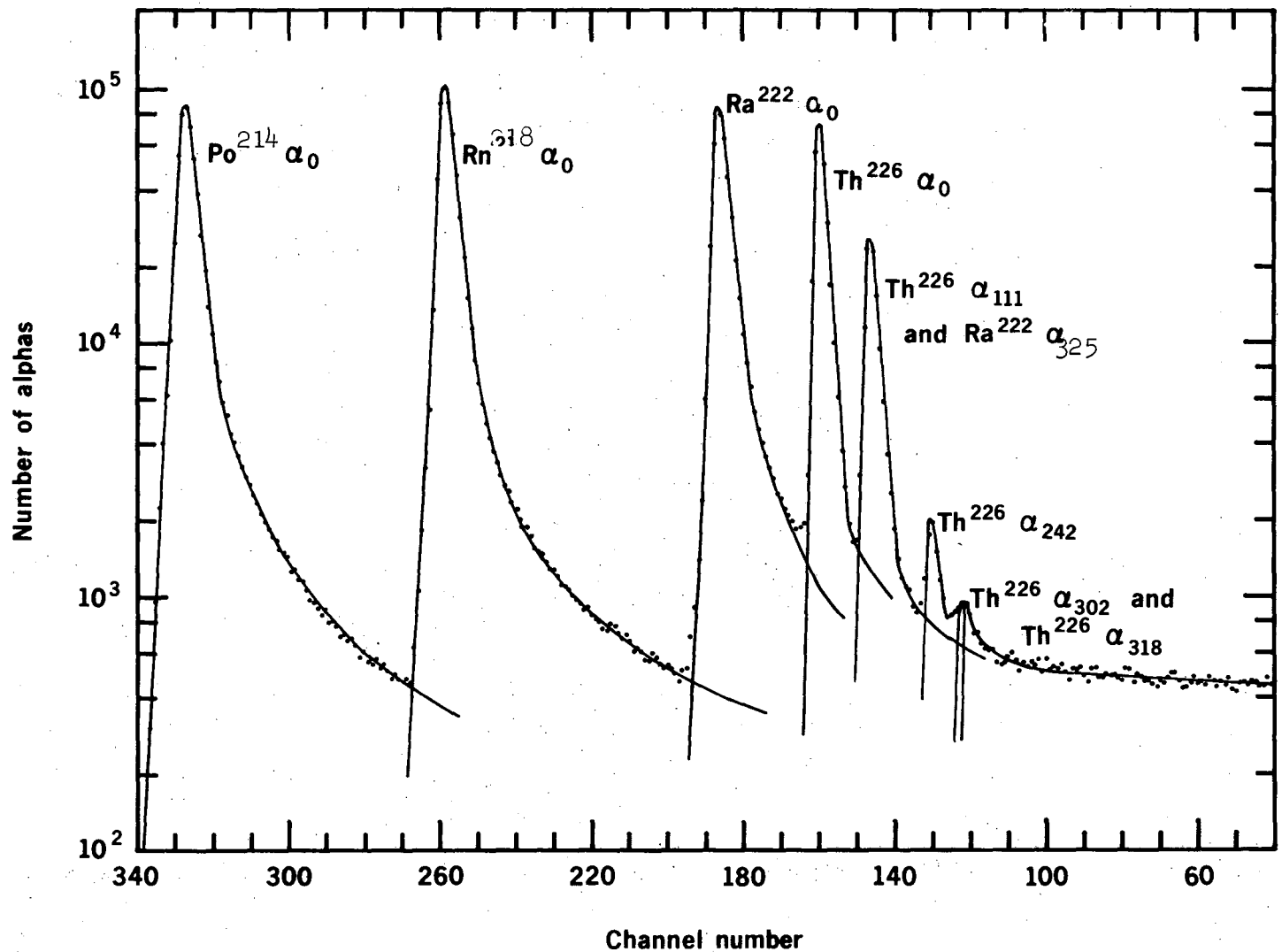

XBL 687-1515

Figure 25. Alpha spectrum of the Th^{226} family taken with a silicon counter.

shown in Fig. 26.

If it is assumed that the $\%Ra^{222}\alpha_0 + \%Ra^{222}\alpha_{325} \approx 100\%$, then

$$\% \; Ra^{222}\alpha_0 = 96.9\%$$

$$\% \; Ra^{222}\alpha_{325} = 3.11\%$$

and $$Ra^{222}\alpha_{325}/Ra^{222}\alpha_0 = 0.03208 \pm 0.00086.$$

If it is assumed that the $\% \; Th^{226}\alpha_0 + \% \; Th^{226}\alpha_{111} + \% \; Th^{226}\alpha_{242} + \% \; Th^{226}\alpha_{302} + \% \; Th^{226}\alpha_{318} = 100\%$, then

$$\% \; Th^{226}\alpha_0 = 76.37 \pm .42\%$$

$$\% \; Th^{226}\alpha_{111} = 21.85 \pm .39\%$$

$$\% \; Th^{226}\alpha_{242} = 1.29 \pm .15\%$$

and $$\% \; Th^{226}\alpha_{302} + \alpha_{318} = .49 \pm .15\%.$$

These numbers are calculated merely as a check of the figures found using the double focusing alpha spectrograph, and they agree quite well with those obtained from the alpha spectrograph within the error limits involved. The Th^{226} spectra found using the double focusing alpha spectrograph are shown in Figs. 27 and 28. It can be seen that the resolution is much greater than that obtained from the Frisch gridded ion chamber (see Fig. 25). In fact, it is possible to separate the two peaks $Th^{226}\alpha_{302}$ and $Th^{226}\alpha_{318}$. The distortions in the peaks at the high energy end of the spectrum are due to distortions in the focusing properties of the alpha spectrograph. The half widths of all of the alpha peaks are reflections of the half width of the source, which was 1/16-in. and corresponds to about 13.3 keV on the alpha particle energy scale.

If we again assume that $\% \; Th^{226}\alpha_0 + \% \; Th^{226}_{111} + \% \; Th^{226}\alpha_{242} + \% \; Th^{226}\alpha_{302} + \% \; Th^{226}\alpha_{318} = 100\%$, we get from α-2-935

$$\% \; Th^{226}\alpha_0 = 75.93 \pm .25\%$$

$$\% \; Th^{226}\alpha_{111} = 22.53 \pm .25\%$$

$$\% \; Th^{226}\alpha_{242} = 1.155 \pm .048\%$$

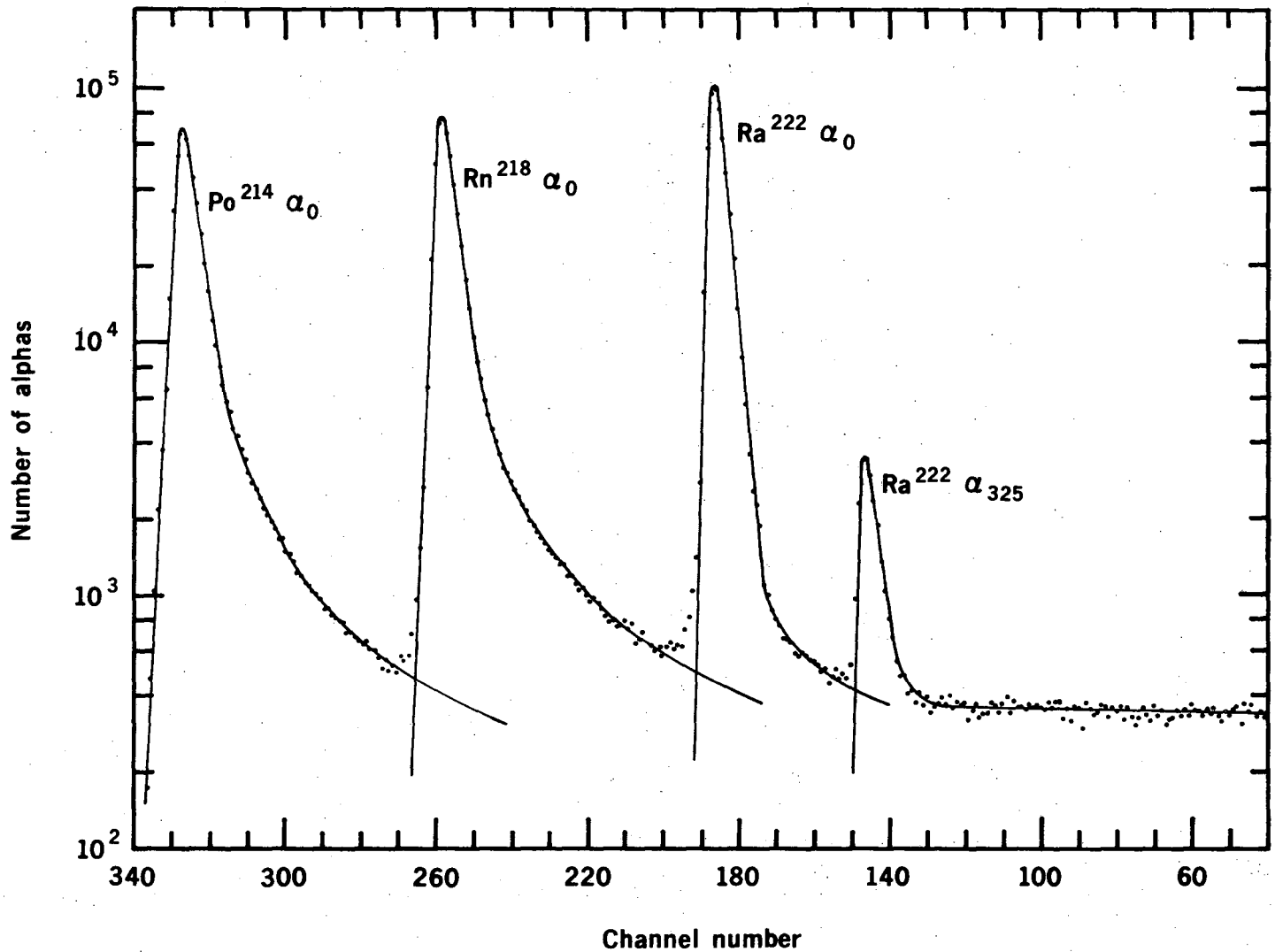

XBL 687-1314

Figure 26. Alpha spectrum of the Ra^{222} family taken with a silicon counter

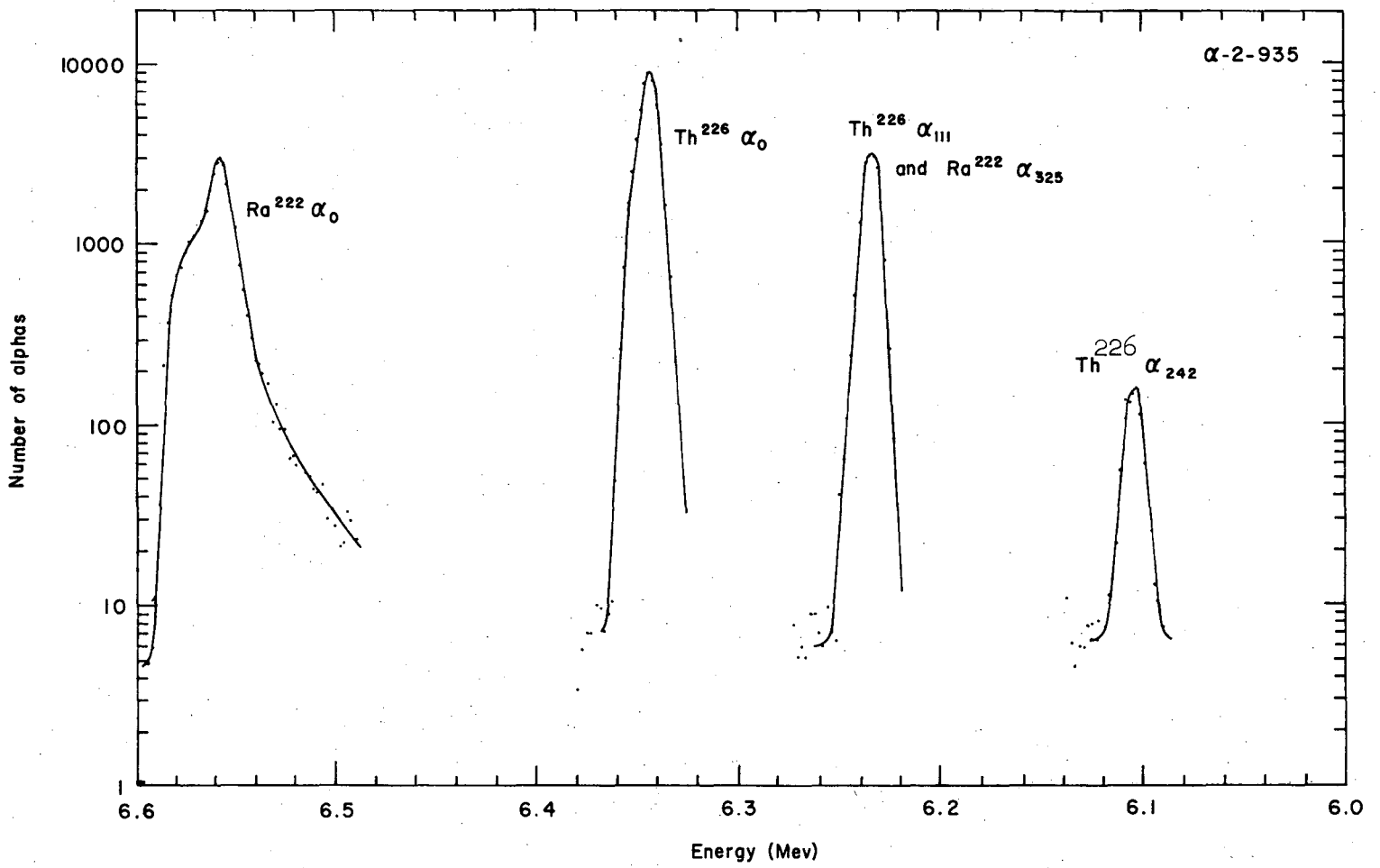

XBL 687-1388

Figure 27. Alpha spectrum of the Th^{226} family taken with a 180 deg double focusing alpha spectrograph.

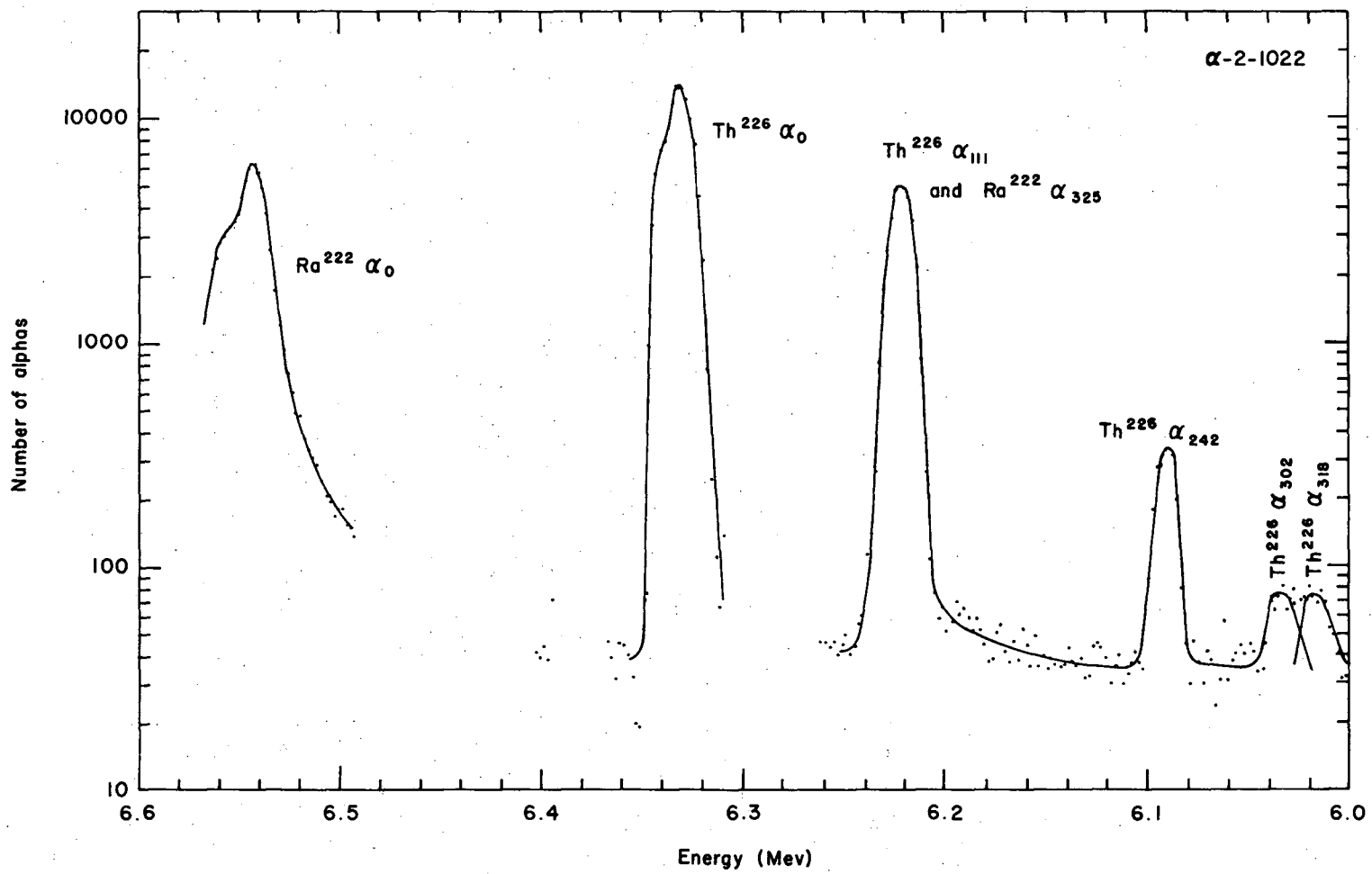

XBL 687-1389

Figure 28. Alpha spectrum of the Th^{226} family taken with a 180 deg double focusing alpha spectrograph.

and from α-2-1022

$$\% \ Th^{226}\alpha_0 = 76.13 \pm .29\%$$

$$\% \ Th^{226}\alpha_{111} = 22.27 \pm .26\%$$

$$\% \ Th^{226}\alpha_{242} = 1.215 \pm .054\%$$

$$\% \ Th^{226}\alpha_{302} = 0.190 \pm .040\%$$

$$\% \ Th^{226}\alpha_{318} = 0.190 \pm .040\%.$$

Combining the two sets of data, one obtains

$$\% \ Th^{226}\alpha_0 = 76.05 \begin{smallmatrix} + .28 \\ - .21 \end{smallmatrix}\%$$

$$\% \ Th^{226}\alpha_{111} = 22.38 \begin{smallmatrix} + .16 \\ - .25 \end{smallmatrix}\%$$

$$\% \ Th^{226}\alpha_{242} = 1.190 \begin{smallmatrix} + .042 \\ - .029 \end{smallmatrix}\%$$

$$\% \ Th^{226}\alpha_{302} = 0.190 \pm .040\%$$

$$\% \ Th^{226}\alpha_{318} = 0.190 \pm .040\%.$$

The various Ra^{222} gamma ray intensities were calculated using the conversion co-efficient tables of both Hager and Seltzer[41] and Pauli.[42] If we assume that $Ra^{222}\gamma_1$ and $Ra^{222}\gamma_3$ are E_2 transitions and that $Ra^{222}\gamma_2$, $Ra^{222}\gamma_4$, and $Ra^{222}\gamma_5$ are E_1 transitions (see Fig. 1), then we obtain the following total conversion co-efficients:

$$Ra^{222}\gamma_1\alpha_T = 6.78$$

$$Ra^{222}\gamma_2\alpha_T = 0.267$$

$$Ra^{222}\gamma_3\alpha_T = 0.756$$

$$Ra^{222}\gamma_4\alpha_T = 0.0934$$

$$Ra^{222}\gamma_5\alpha_T = 0.0652.$$

These figures were calculated in the following manner. The K, L and M conversion co-efficients were found directly from the conversion coefficient tables.[40,41] To a good approximation $N_\ell/M_\ell \approx (3/4)^3 = .422$, $O_\ell/M_\ell \approx (3/5)^3 = .216$, $P_\ell/M_\ell \approx (3/6)^3 = .125$ and $Q_\ell/M_\ell \approx (3/7)^3 = .079$.

Since the shell construction of Ra is as follows:

$$KL_1L_2L_3M_1M_2M_3M_4M_5N_1N_2N_3N_4N_5N_6N_7O_1O_2O_3O_4O_5P_1P_2P_3Q_1,$$

we get

$$N_T \approx .422\ (M_1 + M_2 + M_3 + M_4 + M_5) = .422\ M_T$$

$$O_T \approx .216\ (M_1 + M_2 + M_3 + M_4 + M_5) = .216\ M_T$$

$$P_T \approx .125\ (M_1 + M_2 + M_3)$$

and

$$Q_T \approx .079\ M_1.$$

Thus the total conversion co-efficient α_T for any transition of Ra^{222} is as follows:

$$\alpha_T = K_T + L_T + M_T + N_T + O_T + P_T + Q_T$$

$$\approx K_T + L_T + 1.638\ M_T + .204\ M_1 + .125\ (M_2 + M_3).$$

The following gamma ray intensities were then calculated using the experimental alpha intensities and the calculated conversion co-efficients:

$$Ra^{222}\gamma_1 = 2.963 \begin{smallmatrix} + .047 \\ - .053 \end{smallmatrix}\% \text{ of total } \alpha \text{ decay}$$

$$Ra^{222}\gamma_2 = 0.226 \pm .016\% \text{ of total } \alpha \text{ decay}$$

$$Ra^{222}\gamma_3 = 0.108 \pm .022\% \text{ of total } \alpha \text{ decay}$$

$$Ra^{222}\gamma_4 = 0.174 \pm .035\% \text{ of total } \alpha \text{ decay}$$

and

$$Ra^{222}\gamma_5 = 0.849 \pm .060\% \text{ of total } \alpha \text{ decay.}$$

From the gamma ray intensity of $Ra^{222}\gamma_1$, we find that $Th^{226}\alpha_{111\gamma}$ = $2.877 \begin{smallmatrix} + .045 \\ - .051 \end{smallmatrix}\%$ of the total α decay and $Th^{226}\alpha_{111e} = 19.51 \begin{smallmatrix} + .30 \\ - .35 \end{smallmatrix}\%$ of the total alpha decay. These values are designated as the "theoretical" values.

As a check, the gamma intensity of $Ra^{222}\gamma_1$ was determined experimentally using two different U^{230} sources. A silicon solid state detector

was used to find the total number of U^{230} atoms present from the alpha count. This number was then used to calculate the alpha disintegration rate of Th^{226} as a function of time. A lithium diffused germanium detector was then used to find the $Ra^{222}\gamma_1$ disintegration rate. The gamma intensity of the $Ra^{222}\gamma_1$ peak was then calculated from these two pieces of information. The two sources gave:

$$\% \; Ra^{222}\gamma_1 = 2.90 \pm .18\% \text{ of total } \alpha \text{ decay}$$

and $$\% \; Ra^{222}\gamma_1 = 2.84 \pm .30\% \text{ of total } \alpha \text{ decay, respectively.}$$ These compare very favorably with the "theoretical" value of $2.963 \begin{smallmatrix} + .047 \\ - .053 \end{smallmatrix}\%$ of the total α decay.

The half-life of Th^{226} was then measured using the same silicon solid state detector and it was found that $Th^{226}T_{1/2} = 30.52 \begin{smallmatrix} + 1.08 \\ - 0.96 \end{smallmatrix}$ min.

2. Conclusions

A comparison of the values obtained above for the alpha intensities of Th^{226} and the gamma intensities of Ra^{222} with those presently in use,[43] indicates quite a change from the old values. Unfortunately, the intensities of the U^{230} sources available did not make it possible to obtain direct experimental values for any of the Ra^{222} gamma intensities other than $Ra^{222}\gamma_1$. However, if the new value obtained for the intensity of the $Ra^{222}\gamma_1$ peak is used to correct the present[43] experimental values for the other $Ra^{222}\gamma$ intensities, one obtains the following experimental values.

If

$Ra^{222}\gamma_1 = 2.96\%$ of the total α decay,

then $Ra^{222}\gamma_2 = 0.23\%$ of the total α decay

$Ra^{222}\gamma_3 = 0.10\%$ of the total α decay

$Ra^{222}\gamma_4 = 0.17\%$ of the total α decay

and $Ra^{222}\gamma_5 = 0.81\%$ of the total α decay.

No error is given since no errors are given in the experimental values used.[42] All of these numbers compare favorably with the "theoretical" values shown on page 88; and hence, the assumption in present use that $Ra^{222}\gamma_3$ is an E_2 transition and $Ra^{222}\gamma_4$ is an E_1 transition rather than the other way around is probably correct. This in turn means that the level assignment shown in Fig. 1, is probably correct.

B. Comparison of Different Methods of Making Thin Alpha Sources

1. Experimental Results and Hypotheses

As was discussed previously under Th^{226} Source preparation, two different methods were employed to produce Th^{226} alpha sources. The first was electrostatic collection of Th^{226} and the second was vacuum sublimation of Th^{226} onto a Pt plate. (See Sec. II. B. on Th^{226} source preparation.)

If an attempt is made to collect recoils in the parallel plate collector without the presence of an electric field few recoils are obtained, even at the closest collection distance of 0.1 cm. The reason for this is clear upon making a simple calculation. All electrostatic recoil collections were made at standard pressure and temperature. Under these conditions, the mean free path for U^{230} recoils is about 5.6×10^{-3} cm in air, 5.3×10^{-3} cm in Ar and 37×10^{-3} cm in He, and hence it is obvious that few recoils would be found on the plate. The maximum collection voltage used for parallel plate collection is about 1000 volts/cm which means that the recoils can acquire only 0.04 to 0.06 eV between collisions for an electric field of this magnitude. This gain is much smaller than the average energy loss per collision, and consequently it is clear that recoils do not reach the collector plate because the applied voltage increases their energy. Instead, it is apparent that for sometime after reaching thermal velocities, the recoils maintain their charge and hence their ability to drift towards the collector. An examination of the first ionization potentials of Th, H_2O, N_2, O_2, Ar and He shows that the first ionization potential of Th is about 7 or 8 eV whereas the first ionization of H_2O, N_2, O_2, Ar or He is greater than or equal to 12.5 eV. Thus, it is

very unlikely for a reaction of the type

$$Th^{+1} + X \rightarrow Th + X^{+1}$$

where X = N_2, O_2, H_2O, Ar or He to occur. Hence, the only way a charged Th atom can become neutral is through one of the following two reactions:

$$Th^{+1} + X^{-} \rightarrow Th + X$$

or

$$Th^{+1} + e^{-} \rightarrow Th.$$

That such reactions can occur is clearly shown by Fig. 29; otherwise any voltage at all would be sufficient to collect all possible recoils. It is also apparent from the figure that not only is the electric field important for collecting the maximum number of recoils but so is the separation between the U^{230} source and the Th^{226} collector in that the "plateau" is reached more rapidly when the separation distance is small.

Since the drift velocity of an ion increases linearly with an increase in the electric field strength, this figure indicates that the number of Th ions in a group drifting towards the collector decreases as a complex function of time; however, the existence of a "plateau" indicates that it is not profitable to increase the electric field potential beyond a certain point.

At the time the experiments for finding the best technique for making thin alpha sources were run, it was not realized that there were quite so many variables and so the data is difficult to interpret with certainty. This difficulty was further increased by the fact that reasonably large changes in these variables apparently causes only small changes in the thinness of the alpha source produced. The most probable reason for this insensitivity will be discussed in the next section on theory.

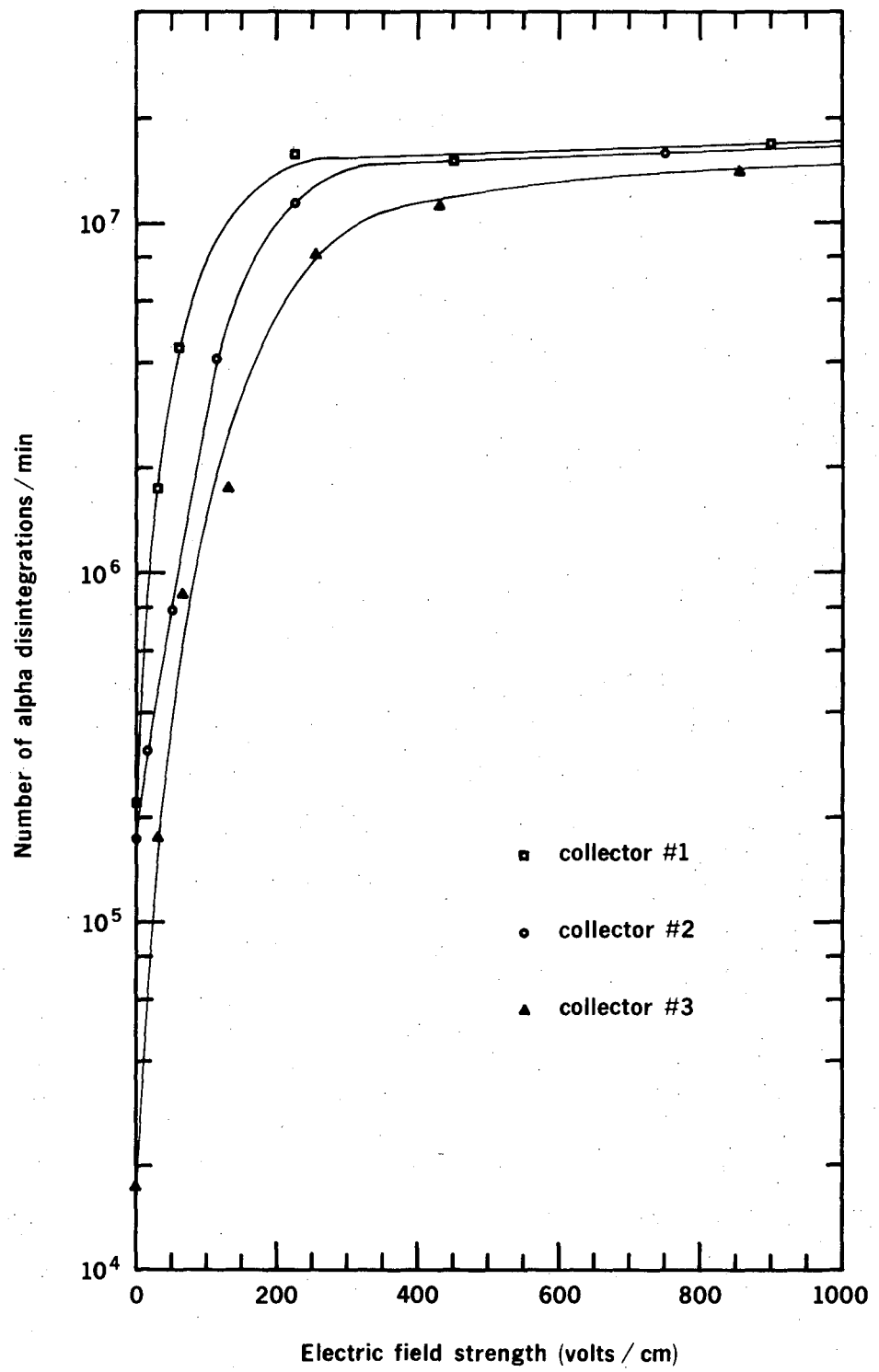

XBL 687-1162

Figure 29. Collection efficiency of various parallel plate collectors as a function of electric field strength. Collectors Nos. 1, 2 and 3 have source-collector separations of 0.1, 0.4 and 0.7 cm, respectively. Collection was made in air at STP.

Comparison was made between different methods of preparing sources by studying the energy distribution of $Th^{226}R^{+2}$ and the ratio No. $Th^{226}R^{+2}$ $(2\alpha + 3\alpha)$/No. $Th^{226}\alpha_0$. The No. $Th^{226}R^{+2}(2\alpha + 3\alpha)$ used was not actually all of the $Th^{226}R^{+2}(2\alpha + 3\alpha)$ available but were only those in the energy region from 375 eV on the high energy side of the α_0 peak to 3000 eV on the low energy side of the α_0 peak. This was done in order that the ratio might better reflect any differences in the thinness of the various sources.

The energy distributions of the recoils discussed in this section were obtained by counting the number of 2- and 3-pronged events in 1/4 mm strips, and then converting to counts per energy of the recoil by the relation: 1 mm ≈ 75 eV. The alphas were measured in the same way and plotted directly on the graphs where the energies of alphas given on the graphs are really the calculated energies of the corresponding recoils. The recoil points plotted on the graphs are actually averages over the nearest three points so that if:

No. $Th^{226}R^{+2}(2\alpha + 3\alpha)$ between 114.000 and 114.075 keV = a

No. $Th^{226}R^{+2}(2\alpha + 3\alpha)$ between 114.075 and 114.150 keV = b

No. $Th^{226}R^{+2}(2\alpha + 3\alpha)$ between 114.150 and 114.225 keV = c

No. $Th^{226}R^{+2}(2\alpha + 3\alpha)$ between 114.225 and 114.300 keV = d

No. $Th^{226}R^{+2}(2\alpha + 3\alpha)$ between 114.300 and 114.375 keV = e

then

No. $Th^{226}R^{+2}(2\alpha + 3\alpha)$ plotted between 114.075 and 114.150 keV = $\frac{a+b+c}{3}$

No. $Th^{226}R^{+2}(2\alpha + 3\alpha)$ plotted between 114.150 and 114.225 keV = $\frac{b+c+d}{3}$

No. $Th^{226}R^{+2}(2\alpha + 3\alpha)$ plotted betwwen 114.225 and 114.300 keV = $\frac{c+d+e}{3}$

etc.

Several different variables were considered in this study; they are as follows:

1. collection time,
2. material collection plate is composed of,
3. treatment of collection plate before it is used for collection,
4. media through which recoils pass in order to be collected--collection media,
5. electric field intensity,

and 6. distance between collector plate and source.

It appears that the following factors are also important and unfortunately, at the time the data were taken, their importance was not known:

1. intensity of the source,
2. presence of small amounts of impurities in the collection media, in particular, the percentage of water vapor present, and also O_2 in Ar or He.

A study of the experimental data from parallel plate collection and related information indicates the following hypotheses:

1. When the parallel plate electrostatic collector is used at STP and a reasonable electric field intensity, the U^{230} recoils can not penetrate the collection plate material very deeply as a result of their impact energy. Even under the most favorable circumstances for such penetration such as collecting in He with an electric field of 1000 volts/cm, the recoils will have on the average an energy of only 0.06 eV upon impact. The worst half width for the $Th^{226}R^{+2}$ peak for any source made with a clean collector plate is only 900 eV. Of this 900 eV, 250 eV is due to the physical width of the Th^{226} source. This is a very small loss of energy since the average energy loss per collision in Pt, Mo, Al or Fe is on the order of 710, 540, 320 and 470 eV, respectively. (Keep in mind that the most probable energy loss is

much smaller than the average energy loss.) These figures were obtained by assuming that the average energy loss/collision = $E_A\lambda/R$ where E_A is the total energy which is lost through collisions[44] and R and λ are the calculated range[30] and mean free path of the recoils in the collecting plate material, and hence, they may be off by a factor of two in either direction. In addition, the worst value for the ratio No. $Th^{226}R^{+2}(2\alpha + 3\alpha)$/No. $Th^{226}\alpha_0$ is only 25% smaller than the best value where the 90% probability limits on these particular ratios are 4.7% and 8.0% respectively. Since the ratio No. $Th^{226}R^{+2}(2\alpha + 3\alpha)$/No. $Th^{226}\alpha_0$ varies not only as a function of source thickness but also as a function of source composition, the small variation in the value of the ratio indicates that the sources are very thin.

2. The positive ions formed in the collecting media by the passage of both recoils and alphas will travel towards the collection plate in the presence of the electric field and may form compounds which become a surface layer of contamination.

3. Since Th^{226} maintains a charge of at least +1 during its passage through the collecting medium, and since the components of the surface contamination are the same as those of the collecting medium, it is likely that the charged Th^{226} atoms pass completely through the surface contamination under the influence of the electric field and do not stop until they come into contact with the metallic surface of the collection plate.

4. An increase in the electric field does not noticeably increase the amount of surface contamination. In fact, the "plateau" for collection of surface contamination appears to be reached well before that for collection of recoils is. This point is demonstrated by plates α-2-820, α-2-821, and α-2-822 shown in Figs. 30, 31 and 32 respectively. Note that Fig. 32 shows α_0 rather than α_{111}. These plates were made using Th^{226} sources

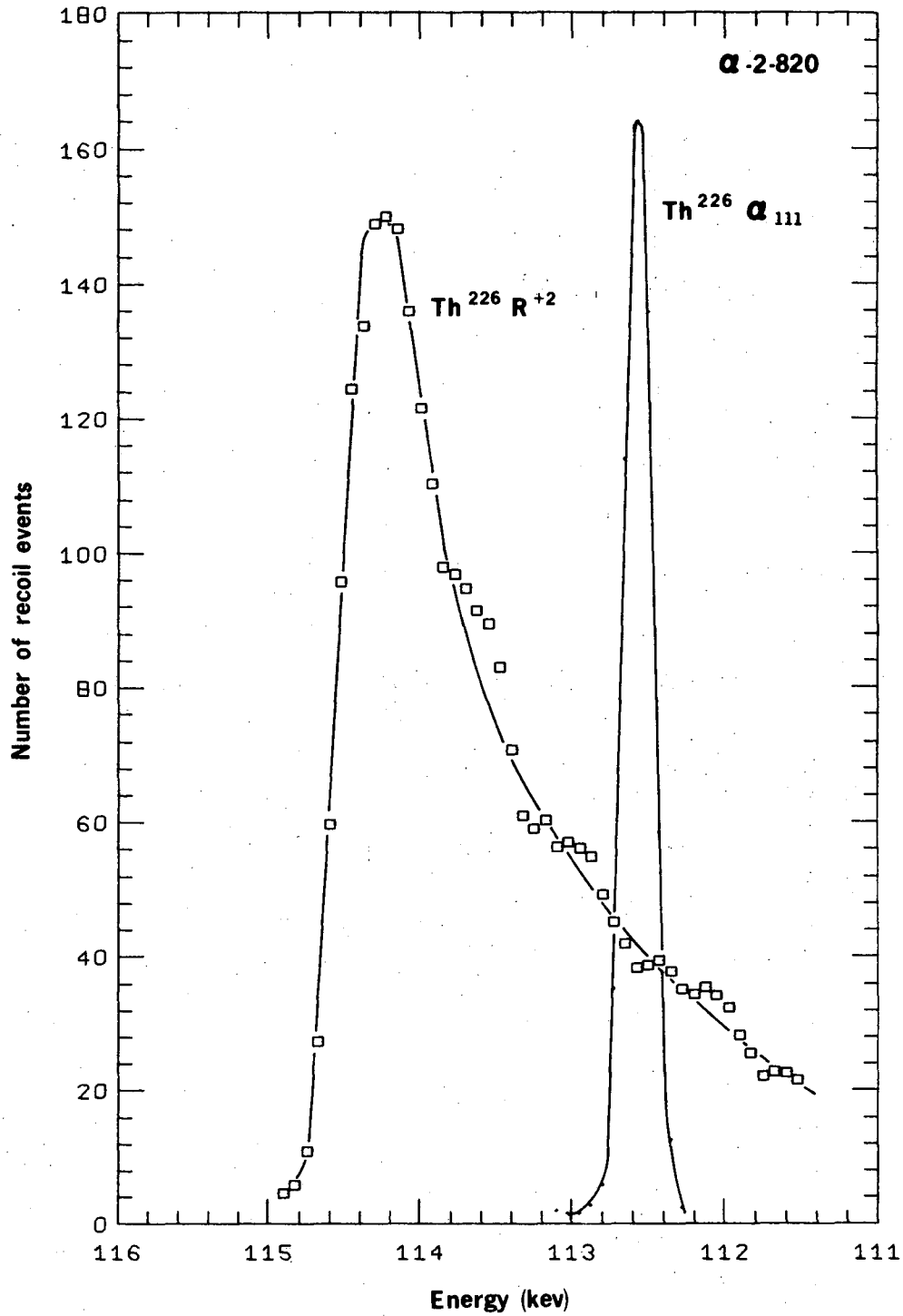

XBL 687-1148

Figure 30. $Th^{226}R^{+2}$ spectrum taken with alpha particle spectrograph in "regular plate" configuration. Alpha peak reduced in scale by a factor of 35. Spectrum made using a source which was collected for 1 1/2 hours in air onto Pt using a parallel plate collector with a separation of 0.1 cm and an electric field of 900 volts/cm.

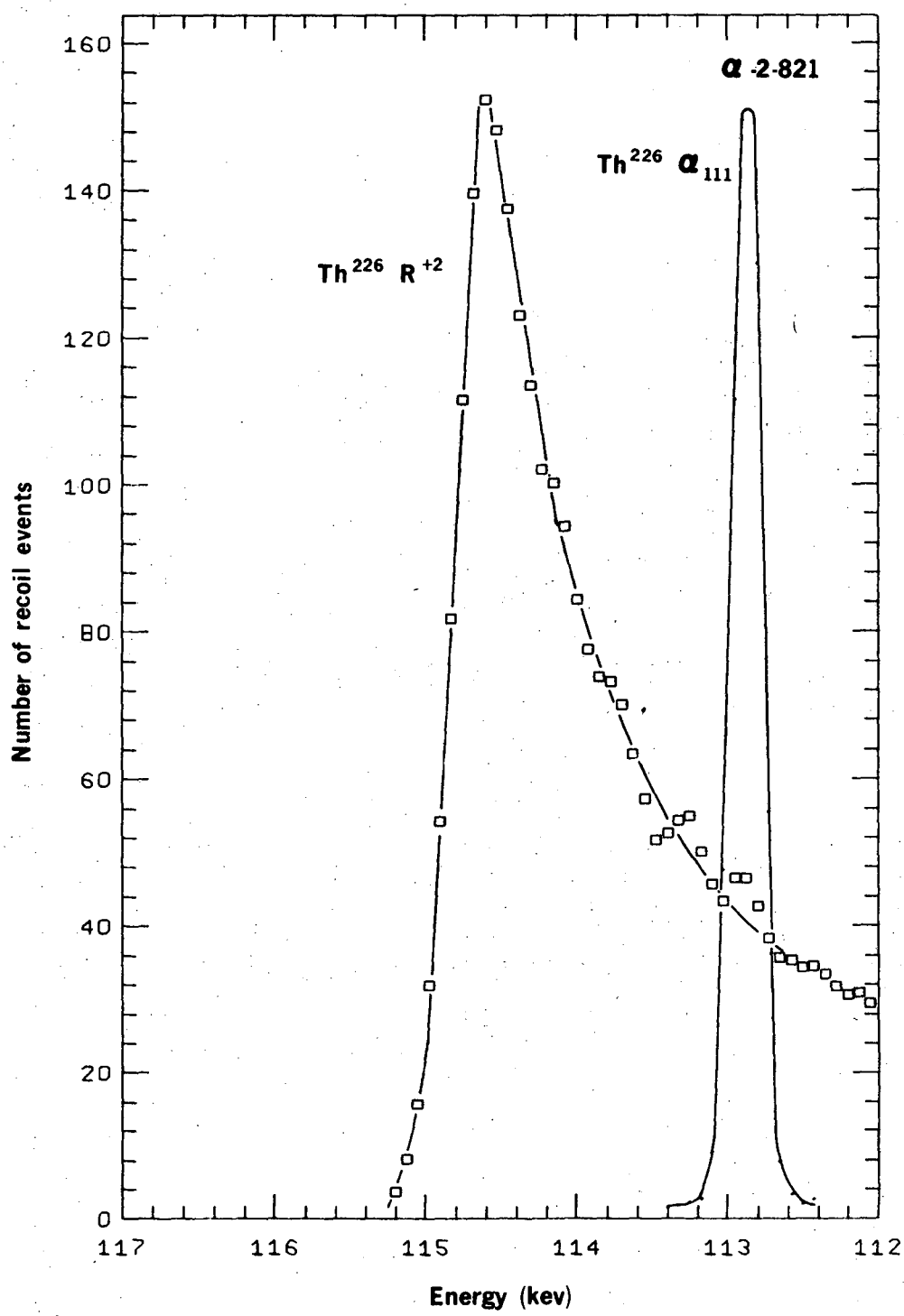

XBL 687-1160

Figure 31. $Th^{226}R^{+2}$ spectrum taken with alpha particle spectrograph in "regular plate" configuration. Alpha peak reduced in scale by a factor of 33. Spectrum made using a source which was collected for 1 1/2 hours in air onto Pt using a parallel plate collector with a separation of 0.1 cm and an electric field of 225 volts/cm.

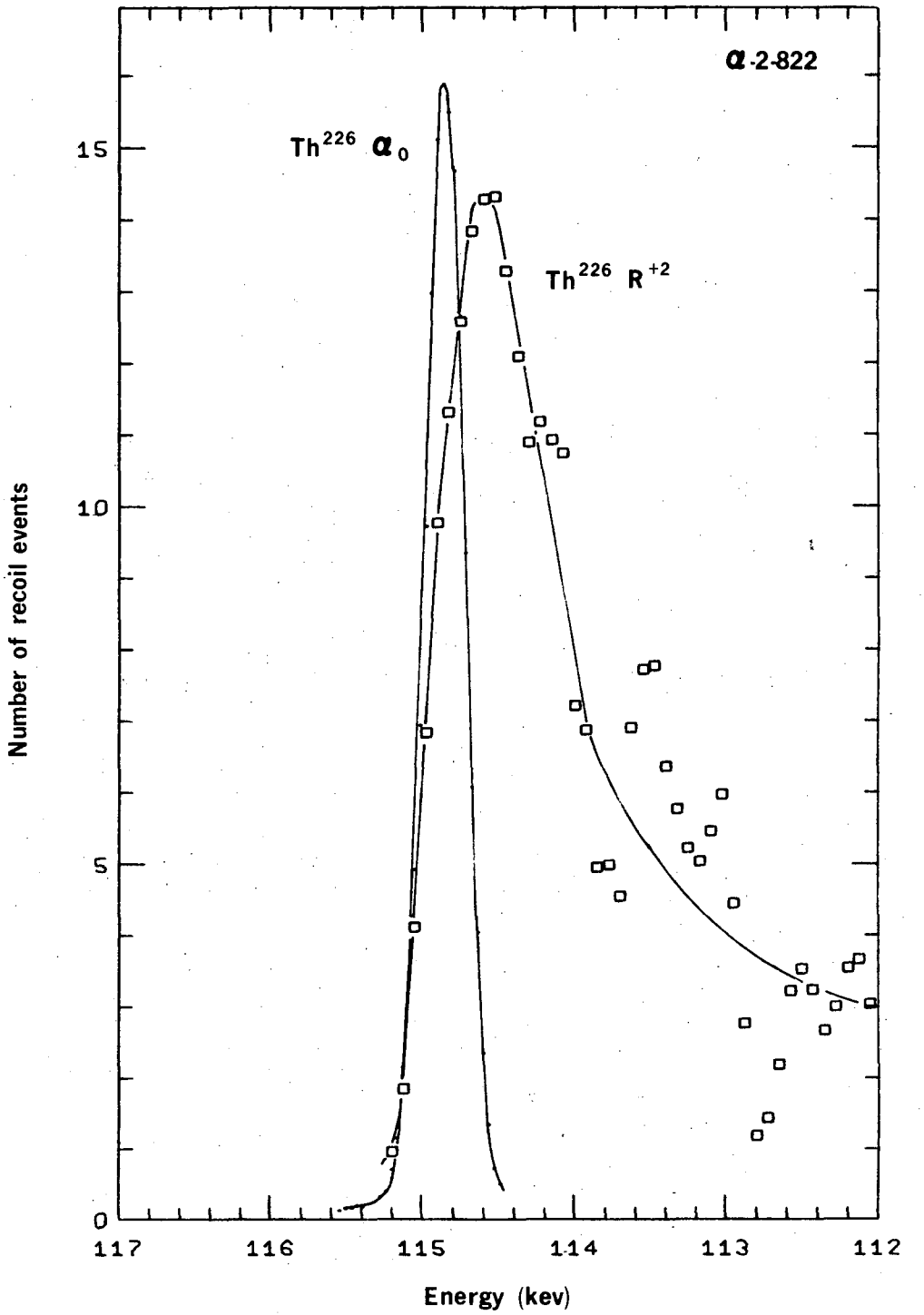

XBL 686-1092

Figure 32. The $^{226}R^{+2}$ spectrum taken with alpha particle spectrograph in "regular plate" configuration. Alpha peak reduced in scale by a factor of 75. Spectrum made using a source which was collected for 1 1/2 hours in air onto Pt using a parallel plate collector with a separation of 0.1 cm and an electric field of 30 volts/cm.

which were collected one after another from the same U^{230} source and so the source intensity is the same for each source. Further details of the source collection is given in the captions. The point to be made here is that the ratios No. $Th^{226}R^{+2}(2\alpha + 3\alpha)$/No. $Th^{226}\alpha_0$ which were .0495 ± .0022, .0515 ± .0023 and .0535 ± .0056 for 900, 225 and 30 volts/cm, respectively, are approximately the same within the error limits involved, and the energy distributions are also approximately the same. However, the recoil collection efficiencies for 900 and 225 volts/cm, which are about the same, are each 11 times that for 30 volts/cm. In other words, the recoil collection "plateau" has not been reached at 30 volts/cm whereas the surface contamination "plateau" has been reached.

5. An increase in the separation between source and collection plate in the parallel plate collector causes more surface contamination to be acquired per unit time if all the other variables are held constant. This is due to the fact that the mean free paths of the alphas involved in the U^{230} decay chain which are on the order of 5 cm in air and Ar and 28 cm in He are greater than the maximum source-collection separation used. This point is demonstrated by plates α-2-1026 and α-2-1027 shown in Figs. 33 and 34, respectively. Since these sources were consecutive, the intensity of the U^{230} source was about the same for each, and so the primary difference between these two plates is the source-collector separation, which was 0.4 and 0.1 cm respectively. (See captions for further details of source collection.) The ratios No. $Th^{226}R^{+2}(2\alpha + 3\alpha)$/No. $Th^{226}\alpha_0$ are .0616 ± .0043 and .0645 ± .0051 for α-2-1026 and α-2-1027 respectively, and so do not differ by a large amount. However, the energy distribution of α-2-1027 is much better than that of α-2-1026, and thus indicates the validity of the hypothesis.

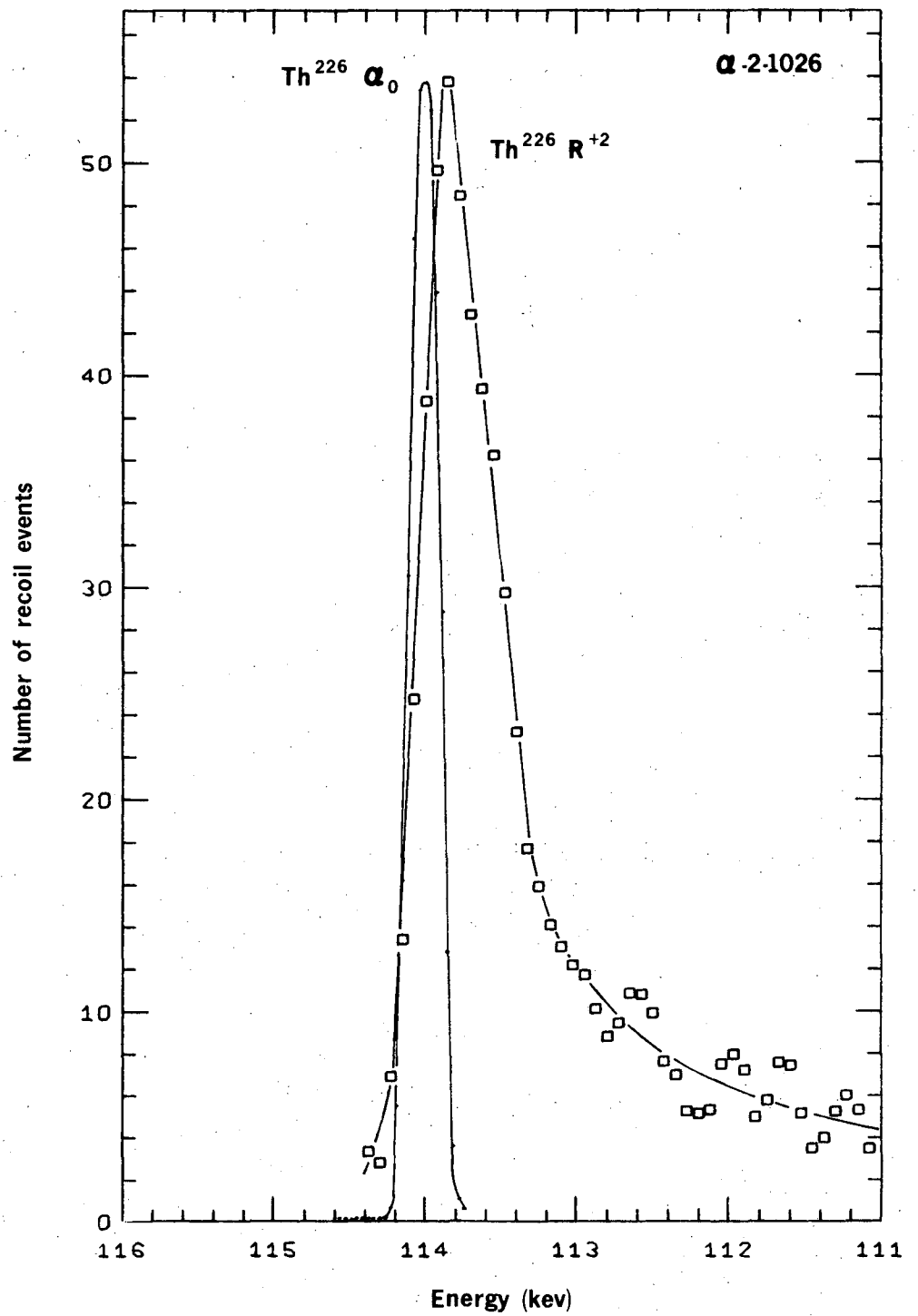

XBL 686-1098

Figure 33. $Th^{226}R^{+2}$ spectrum with alpha particle spectrograph in "regular plate" configuration. Alpha peak reduced by a factor of 60. Spectrum made using a source which was collected for 5/6 hour in air onto "flashed" Pt using a parallel plate collector with a separation of 0.4 cm and an electric field of 750 volts/cm.

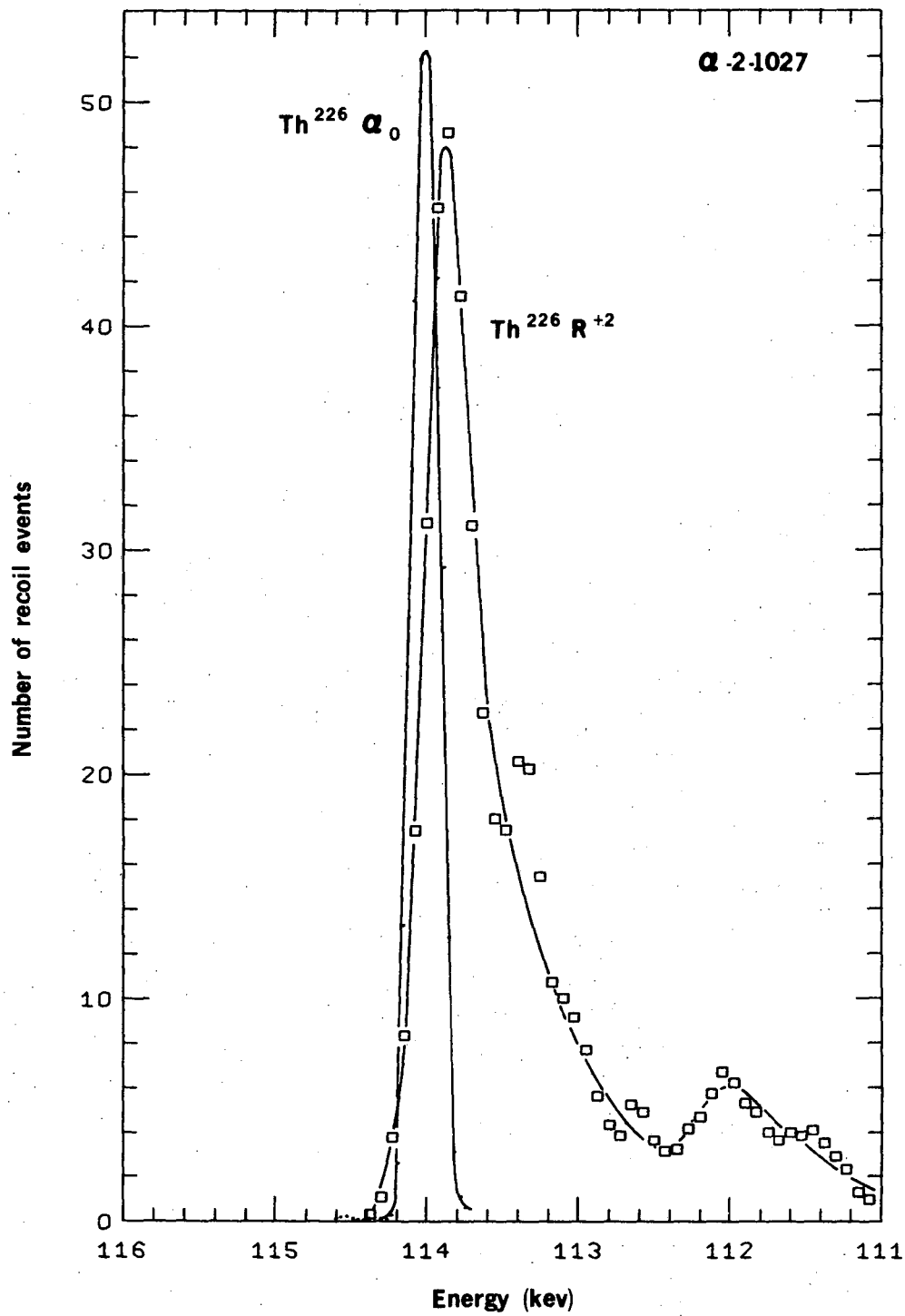

XBL 687-1145

Figure 34. $Th^{226}R^{+2}$ spectrum with alpha particle spectrograph in "regular plate" configuration. Alpha peak reduced in scale by a factor of 45. Spectrum made using a source which was collected for 5/6 hour in air onto "flashed" Pt using a parallel plate collector with a separation of 0.1 cm and an electric field of 600 volts/cm.

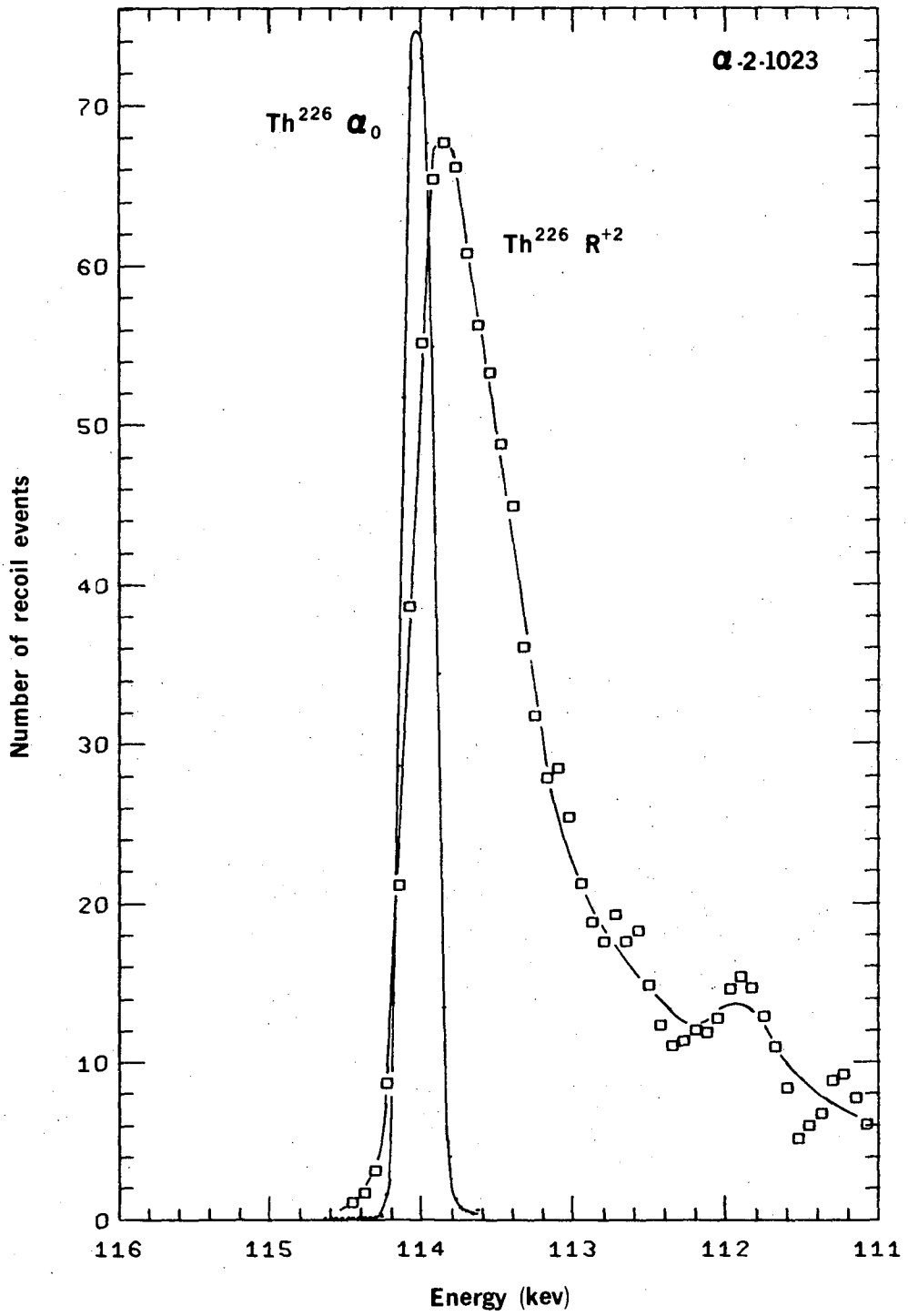

XBL 686-1108

Figure 35. $Th^{226}R^{+2}$ spectrum using alpha particle spectrograph in "regular plate" configuration. Alpha peak reduced in scale by a factor of 75. Spectrum made using a source which was collected for 1 1/2 hours in air onto "flashed" Pt using a parallel plate collector with a separation of 0.1 cm and an electric field of 60 volts/cm.

6. An increase in collection time, when all other variables are held constant, will also increase the thickness of the surface contamination providing hypothesis No. 3 is valid. This point is demonstrated by comparing plates α-2-1027 and α-2-1023 (See Figs. 34 and 35). The only differences between the Th^{226} sources used to produce these two plates are a variation in collection time, which was 5/6 hr. for α-2-1027 and 1 1/2 hrs. for α-2-1023, and a similar variation in the electric field intensity which has already been shown to have no effect on source thickness. The ratio $Th^{226}\alpha_0$ is .0645 ± .0051 for α-2-1027 and .0567 ± .0030 for α-2-1023. That is, the ratio for α-2-1027 is much better than that of α-2-1023; furthermore, the energy distribution of α-2-1027 is also much better than that of α-2-1023 as can be seen from Figs. 34 and 35.

7. An increase in the intensity of the U^{230} source appears to cause a decrease in the amount of surface contamination, all else being equal. The reason for this effect is not known. However, since the differences are small, this observation which is demonstrated by plates α-2-1023 and α-2-935 in Figs. 35 and 36 may be the result of a quirk in statistics. Again, according to the previous hypothesis, the only significant differences between the Th^{226} sources used to produce α-2-935 and α-2-1023 is that the source used for α-2-935 was collected for two hours from a U^{230} sample ten times more intense than that used for α-2-1023 which was collected for 1 1/2 hours. The difference in collection times indicates that the source for α-2-935 should be thicker than that for α-2-1023. However, the ratio No. $Th^{226}R^{+2}(2\alpha + 3\alpha)$/No. $Th^{226}\alpha_0$ (.0567 ± .0030 for α-2-1023 and .0620 ± .0021 for α-2-935) and the $Th^{226}R^{+2}$ energy distributions for the two plates (see Figs. 35 and 36) indicates just the opposite although the difference is not large.

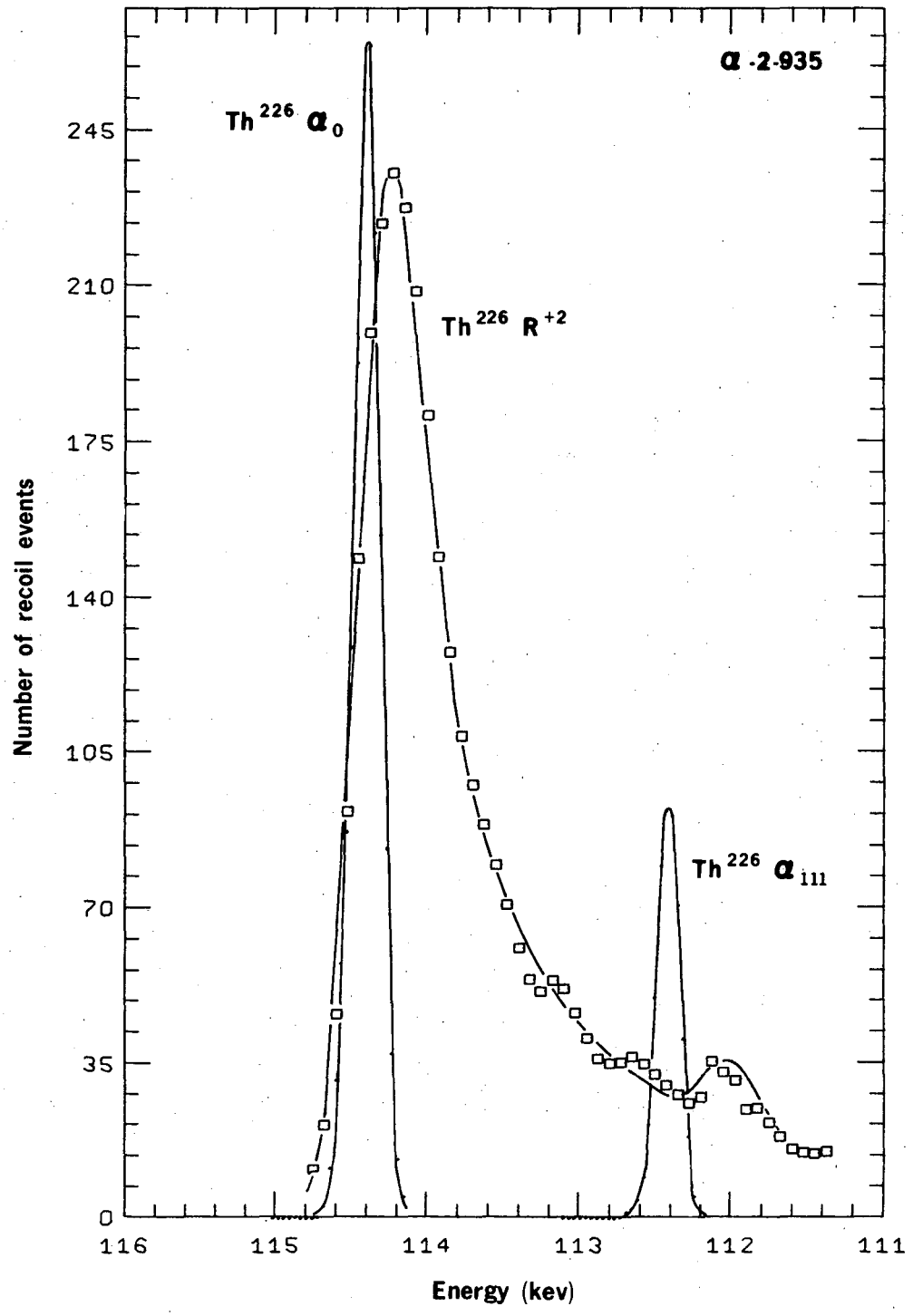

XBL 687-1144

Figure 36. $Th^{226}R^{+2}$ spectrum taken with alpha particle spectrograph in "regular plate" configuration. Alpha peak reduced in scale by a factor of 66. Spectrum made using sources which were collected for 2 hours in air onto "flashed" Pt using parallel plate collector with a separation of 0.1 cm and an electric field of 225 volts/cm.

8. Collector plates that are not carefully cleaned of all surface contamination before being used, produce sources of variable thickness depending upon the initial amount of surface contamination. Furthermore, the ratio No. $Th^{226}R^{+2}$/No. α_0 can be affected not only by the amount of the initial surface contamination but also by its composition. For example, the presence of Na could decrease the ratio No. $Th^{226}R^{+2}(2\alpha + 3\alpha)$/No. $Th^{226}\alpha_0$ because Na has a first ionization potential of only 5.1 eV and consequently any collision between it and a $Th^{226}R^{+2}$ will yield a $Th^{226}R^{+1}$. Thus, its presence would decrease the number of $Th^{226}R^{+2}$ without increasing the thickness of the Th^{226} source.

One of the best techniques of cleaning collector plates is to heat them to a red heat. Plates that have undergone this cleaning technique are called "flashed" plates. "Unflashed" designates plates which have not undergone this cleaning technique although they may have undergone some other cleaning technique. In general, the "unflashed" Pt plates were not cleaned before each use and hence are contaminated to varying degrees compared to the "flashed" Pt plates. A comparison of "flashed" and "unflashed" Pt plates consistently shows that "flashed" plates are better than "unflashed" plates. Examples of this are given in Figs. 37, 38 and 31. The sources used to produce these plates differed in the following way: Source α-2-863 (Fig. 37) and α-2-860 (Fig. 38) were collected on "flashed" and "unflashed" Pt plates for 1 1/2 and 1 hours while α-2-821 (Fig. 31) was on an "unflashed" plate for 1 1/2 hours with a U^{230} source 12 times more intense.

According to the above information in conjunction with hypotheses Nos. 6 and 7, the sources for both α-2-821 and α-2-860 should be better than that for α-2-863 if "flashing" had no effect. Instead, although

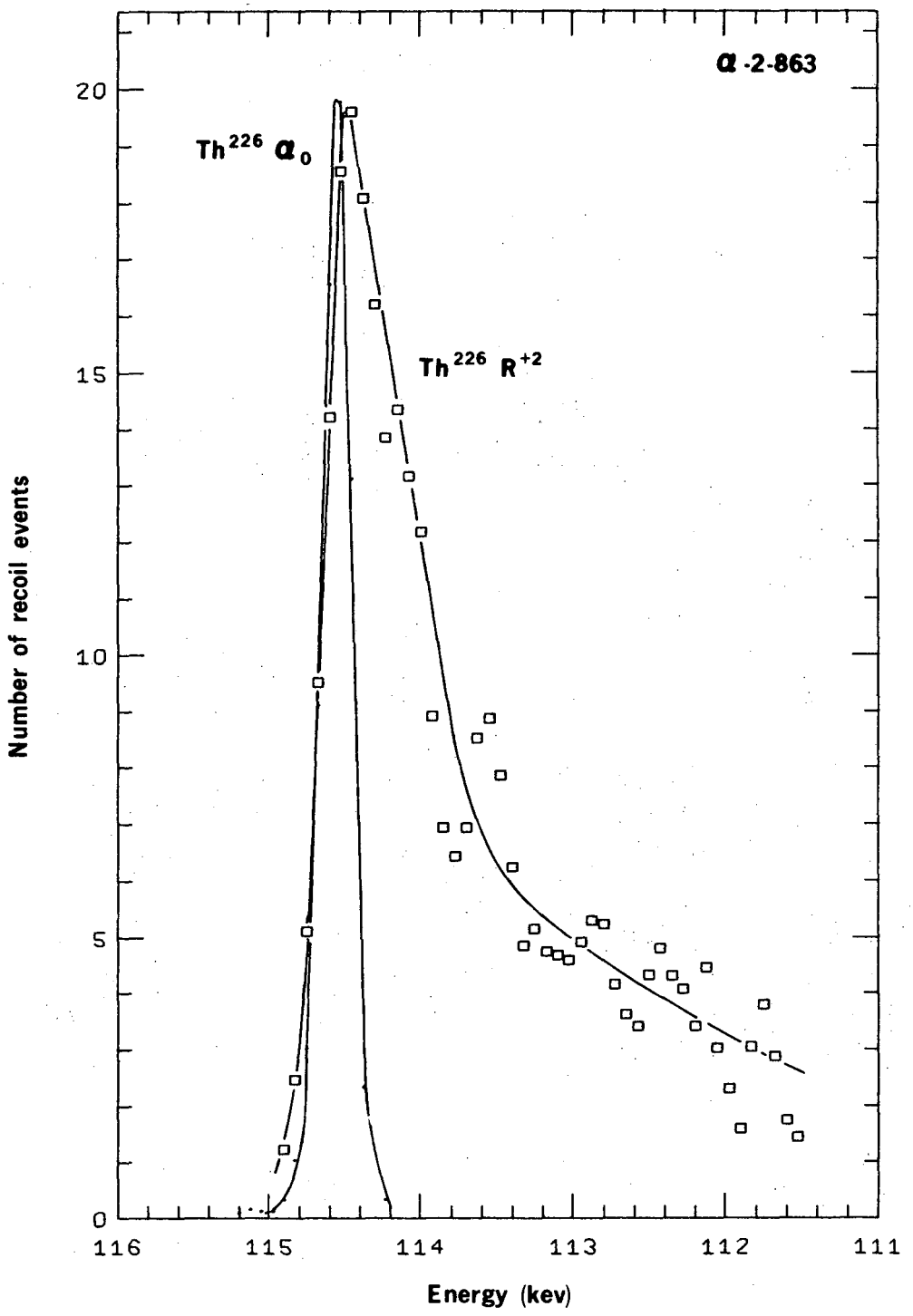

XBL 687-1156

Figure 37. $Th^{226}R^{+2}$ spectrum using alpha particle spectrograph in "regular plate" configuration. Alpha peak reduced in scale by a factor of 75. Spectrum made using sources which were collected for 1 1/2 hours in air onto "flashed" Pt using parallel plate collector with a separation of 0.1 cm and an electric field of 225 volts/cm.

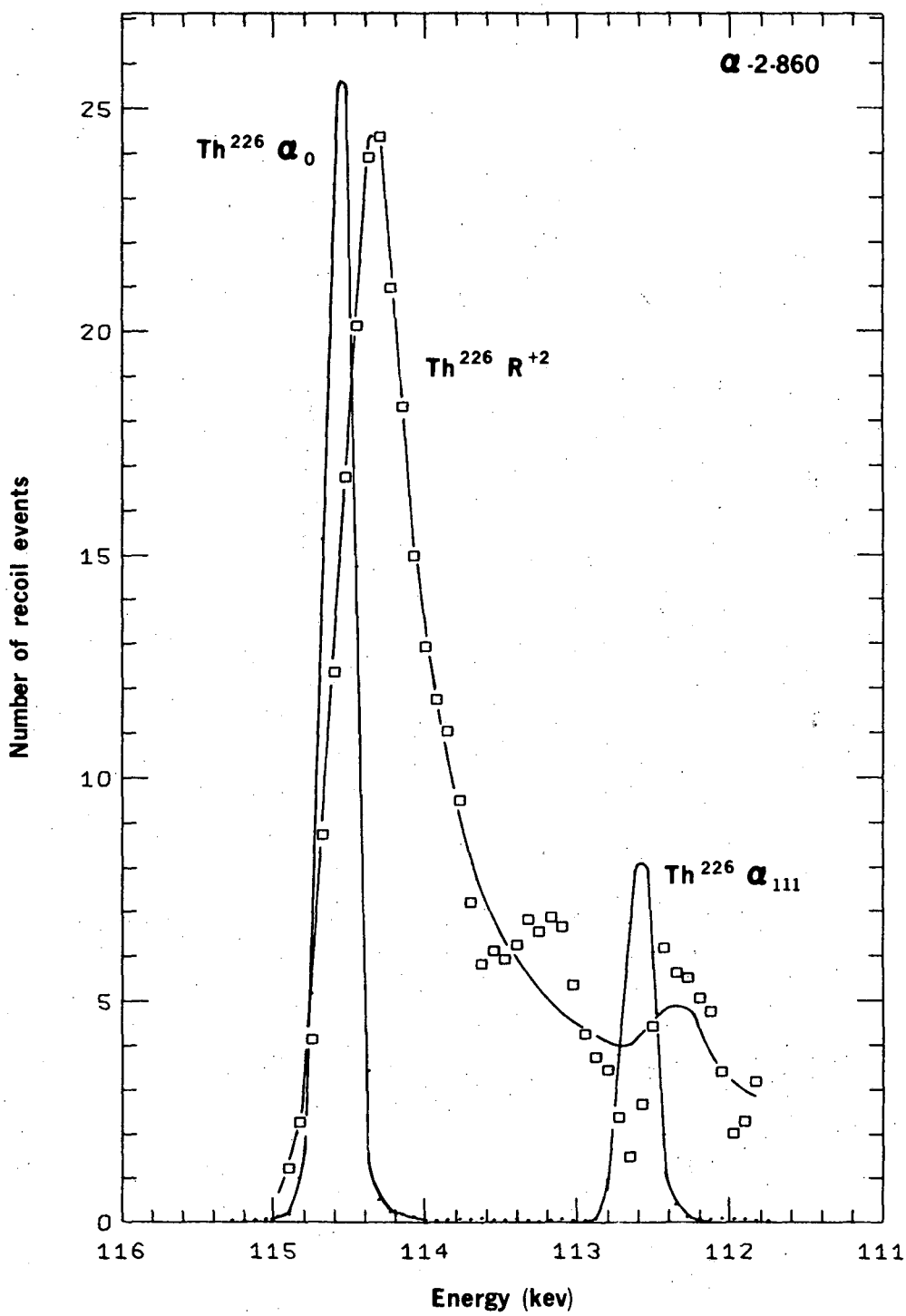

XBL 687-1158

Figure 38. $Th^{226}R^{+2}$ spectrum using alpha particle spectrograph in "regular plate" configuration. Alpha peak reduced in scale by a factor of 75. Spectrum made using sources which were collected for 1 hour in air onto "unflashed" Pt using parallel plate colletor with a separation of 0.1 cm and an electric field of 225 volts/cm.

α-2-860 has a better energy distribution than α-2-863 (see Figs. 37 and 38) its ratio No. $Th^{226}R^{+2}(2\alpha + 3\alpha)$/No. $Th^{226}\alpha_0$, .0490 $\pm$ .0048, is worse than that of α-2-863, .0614 $\pm$ .0061. Hence, although it may be a thinner source, it has some contamination which changes $Th^{226}R^{+2}$ into $Th^{226}R^{+n}$ where n is probably equal to +1.

α-2-821 not only has a worse $Th^{226}R^{+2}$ energy distribution than that of α-2-863 but its ratio No. $Th^{226}R^{+2}(2\alpha + 3\alpha)$/No. $Th^{226}\alpha_0$ is also worse being .0515 $\pm$ .0023 compared to .0614 $\pm$ .0061 for α-2-863. This indicates that the surface contamination of the α-2-821 source is much greater than it is on the α-2-863 source which in turn can only be the result of greater surface contamination before the U^{230} recoils were collected.

9. When the collections are made in air, the first Th^{226} source collected after a period of time when no sources have been made is more intense than the succeeding source, and each succeeding source is slightly less intense than the preceeding one. The probable reason for this is as follows. Air normally has a fairly high concentration of water vapor and H_2O is highly electronegative. Therefore, when the electrostatic field is on, H_2O^- ions travel to the positive plate (the U^{230} source) where they lose their charge and remain as a film of water. As the length of time the field is on increases, this film increases and causes the number of U^{230} recoils that escape and hence the intensity of the Th^{226} to decrease with time. When the field is turned off, this water film slowly sublimates and if enough time elapses between the time the field is turned off and then turned on again, the film may disappear completely. However, in general, no such time lapse occurred and so the process continued until some equilibrium was reached. Further indication that such a process is really occurring is the fact that it would have no effect on the thickness of the

resulting Th^{226} sources. This appears to have indeed been the case.

In addition to the above hypotheses, some information was obtained for the parallel plate collector concerning the effects of using plates made of materials other than Pt and collecting in media other than air. Mo, Al, and stainless steel were tried in addition to Pt. These sources yielded the $Th^{226}R^{+2}$ spectra which are shown in Figs. 39, 40, and 41. The $Th^{226}R^{+2}$ spectrum of a flashed Pt source that was collected and run in the spectrograph immediately after the first three is shown in Fig. 42 for comparison. Each one of these sources was collected under the same conditions except for the kind of collecting plate and its cleaning. The Mo, Al and stainless steel plates were carefully cleaned in acetone and alcohol rather than "flashed" because the apparatus used for flashing plates, an induction heater, was not capable of heating them to a sufficiently high temperature. The Pt plate was flashed. A study of the data and figures gives the following results. The ratios No. $Th^{226}R^{+2}(2\alpha + 3\alpha)$/ No. $Th^{226}\alpha_0$ were $.0534 \pm .0032$, $.0536 \pm .0037$, $.0426 \pm .0029$ and $.0551 \pm .0034$ for α-2-1018 (Mo), α-2-1019 (Al), α-2-1020 (stainless steel) and α-2-1021 (Pt), respectively. Thus, Pt has the best ratio although the ratios for Mo and Al are not much different. An investigation of the energy distributions again indicates that Pt makes the best collecting plate material followed by Al and then Mo. Both the ratio and the energy distribution of α-2-1020 indicates that stainless steel should not be used. However, the curious double peak seen in Fig. 41 could have been caused by a streak of surface contamination over part of the Th^{226} source and hence removable. This same hypothetical streak could also have caused a reduction in the ratio as dicussed in the eighth hypothesis. Thus, stainless steel should be investigated further before any definite decision can be made concerning

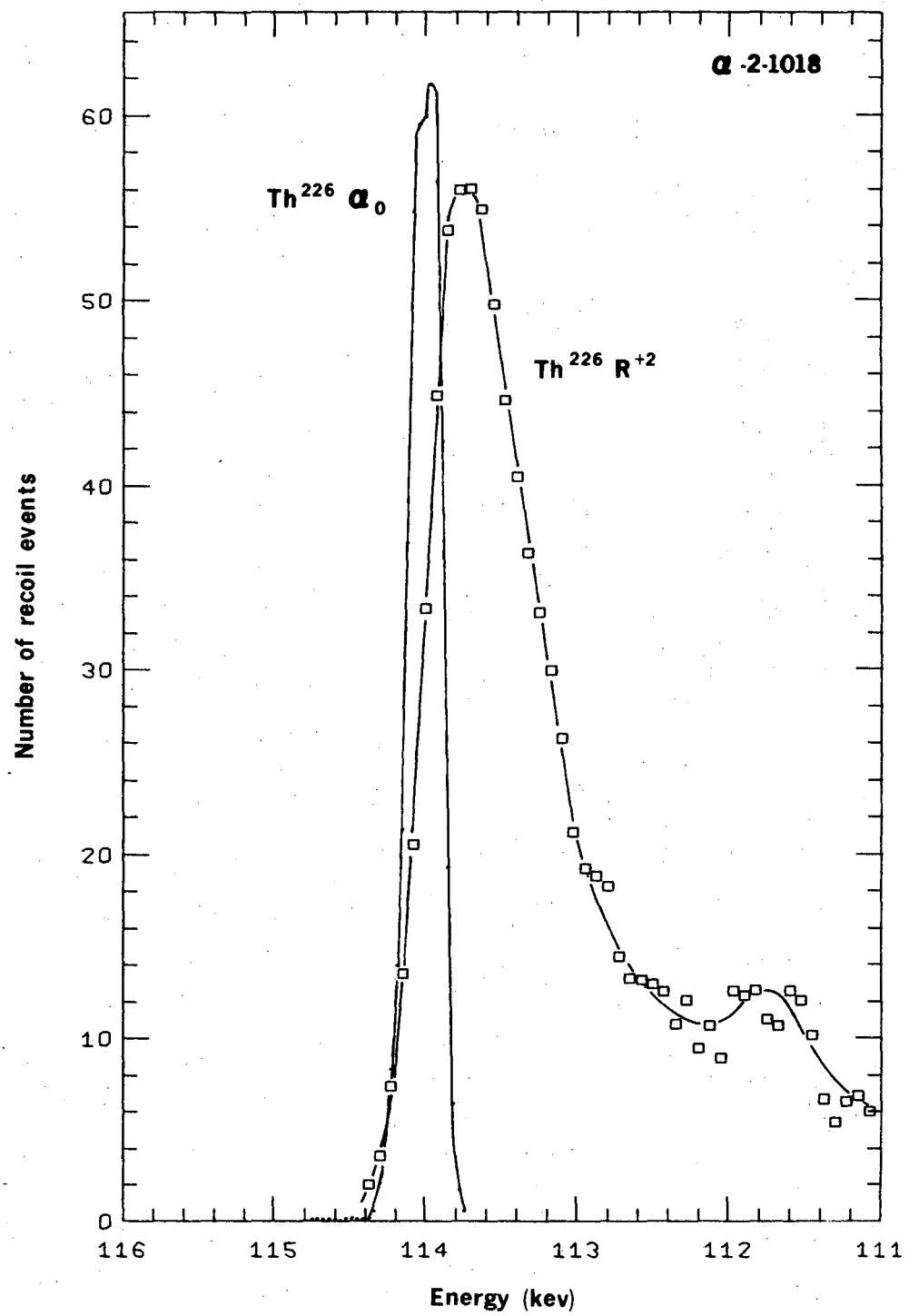

XBL 687-1155

Figure 39. $Th^{226}R^{+2}$ spectrum taken with alpha particle spectrograph in "regular plate" configuration. Alpha peak reduced in scale by a factor of 70. Spectrum made using a source which was collected for 5/6 hour in air onto "unflashed" Mo using parallel plate collector with a separation of 0.1 cm and an electric field of 225 volts/cm.

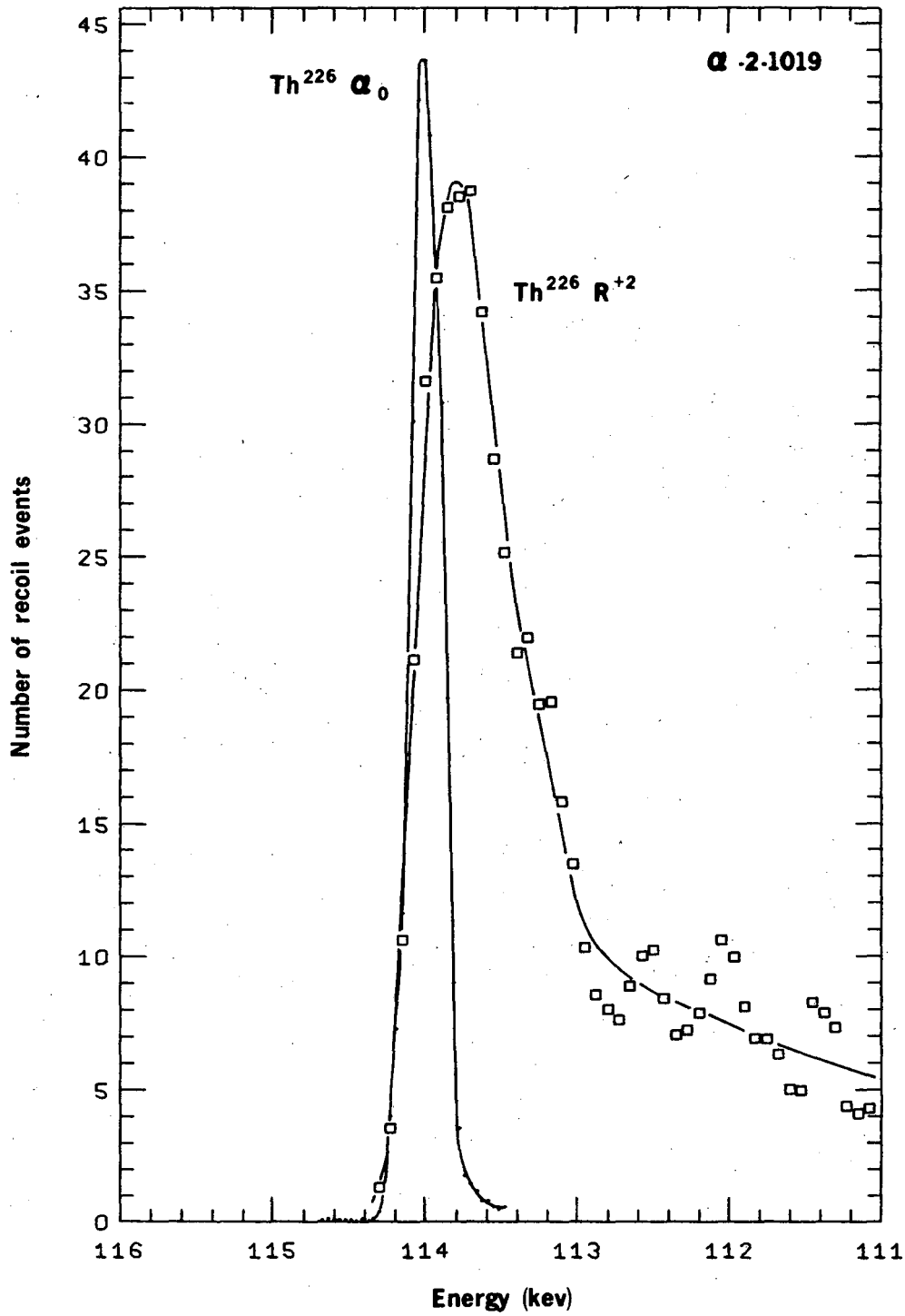

XBL 686-1094

Figure 40. $Th^{226}R^{+2}$ spectrum taken with alpha particle spectrograph in "regular plate" configuration. Alpha peak reduced in scale by a factor of 75. Spectrum made using a source which was collected for 5/6 hour in air onto "unflashed" Al using parallel plate collector with a separation of 0.1 cm and an electric field of 225 volts/cm.

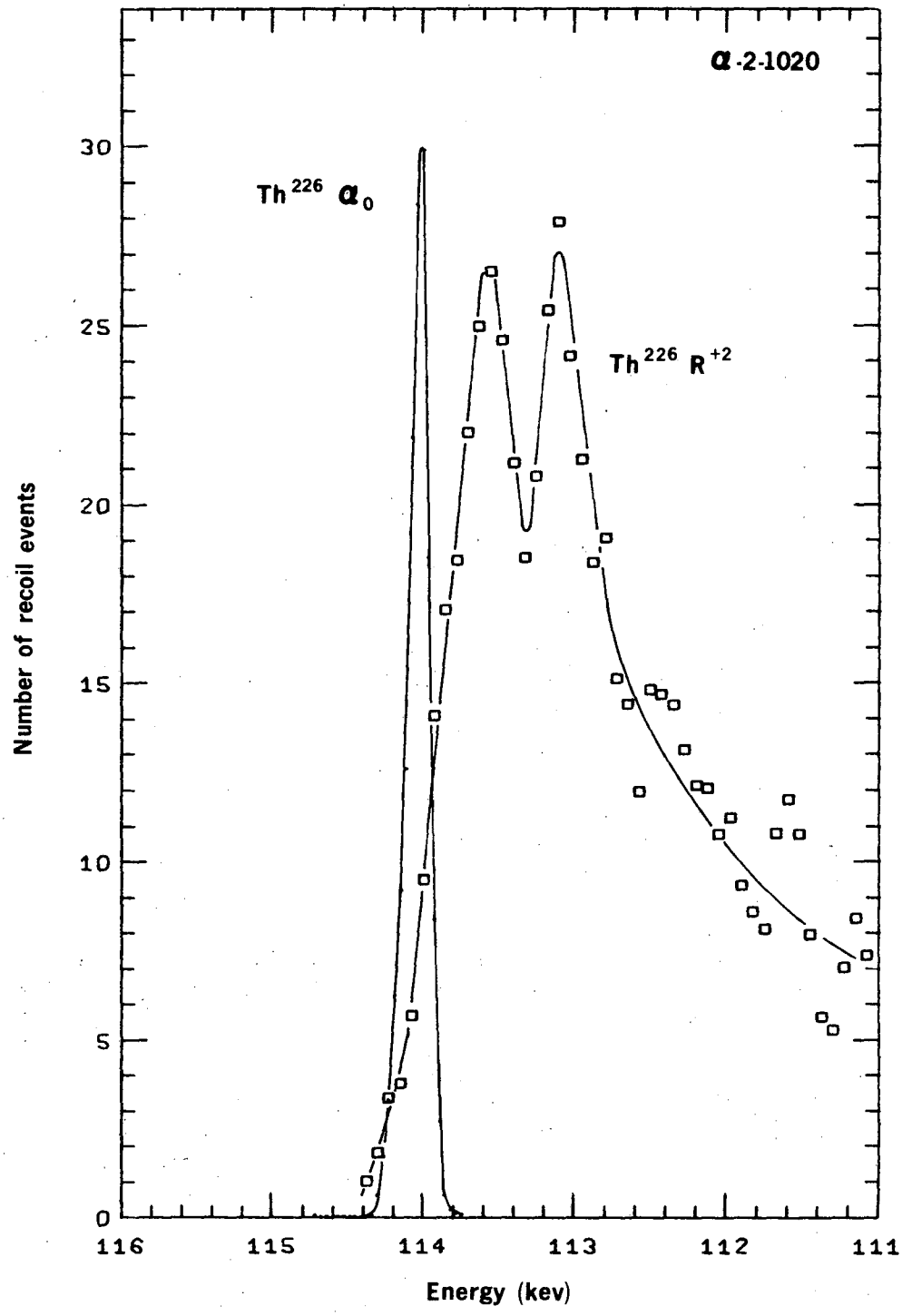

XBL 686-1105

Figure 41. $Th^{226}R^{+2}$ spectrum taken with alpha particle spectrograph in "regular plate" configuration. Alpha peak reduced in scale by a factor of 200. Spectrum made using a source which was collected for 5/6 hour in air onto "unflashed" stainless steel using parallel plate collector with a separation of 0.1 cm and an electric field of 225 volts/cm.

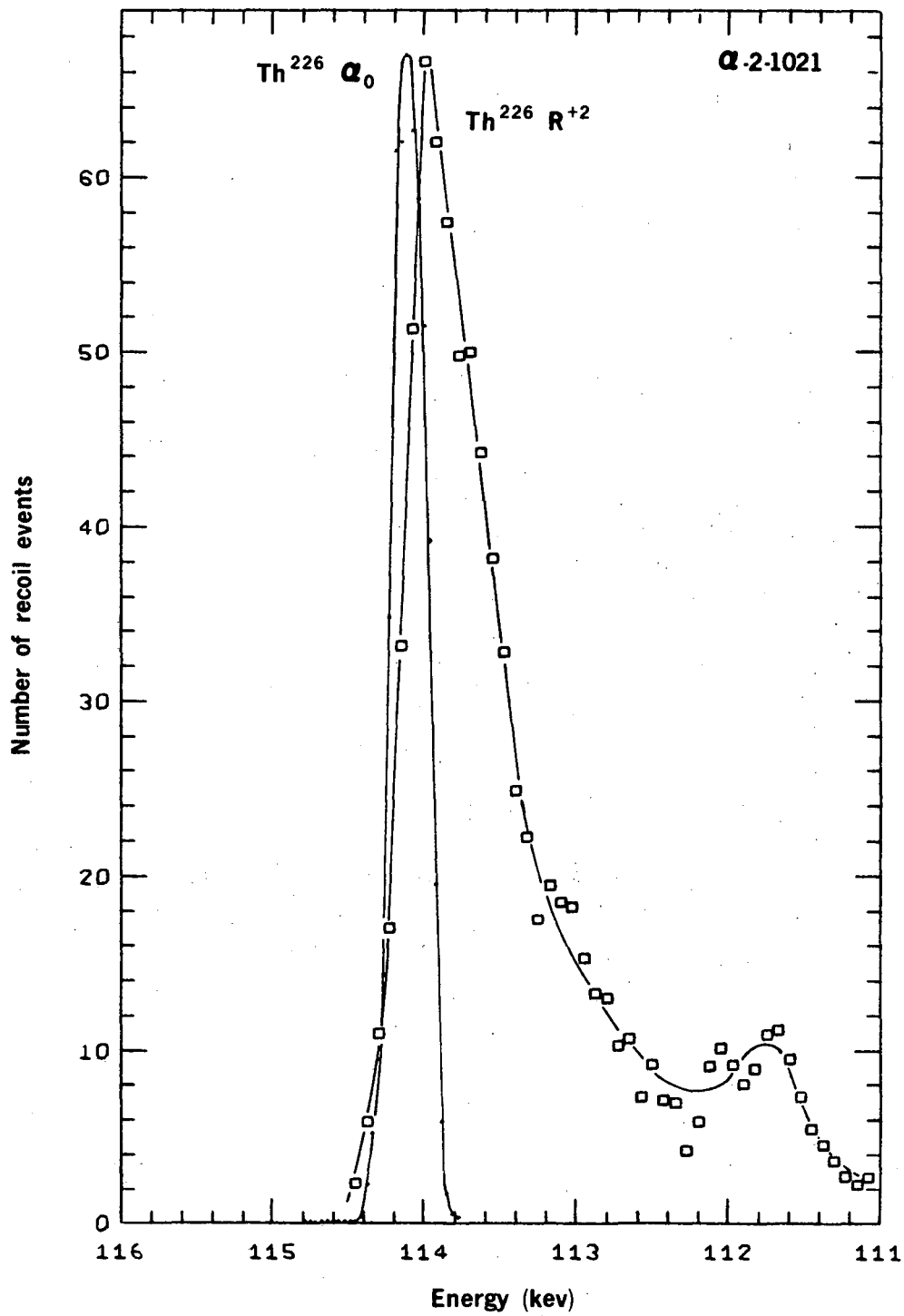

XBL 686-1101

Figure 42. $Th^{226}R^{+2}$ spectrum taken with alpha particle spectrograph in "regular plate" configuration. Alpha peak reduced in scale by a factor of 60. Spectrum made using a source which was collected for 5/6 hour in air onto "flashed" Pt using a parallel plate collector with a separation of 0.1 cm and an electric field of 225 volts/cm.

its usefullness as a collector plate material.

Even though Pt did yield the thinnest Th^{226} source, there was very little variation between it and Al and Mo. This result is probably due to the fact that in the metallic form Al has three conduction electrons per atom, Mo probably has two and Pt has two. Thus, a Th^{226} atom undergoing a collision with these atoms in the metallic state would see Al^{+3}, Mo^{+2}, and Pt^{+2}. For each of these cases, the ionization potentials are such that $Th^{226}R^{0}$ and $Th^{226}R^{+1}$ could become $Th^{226}R^{+2}$ but $Th^{226}R^{+2}$ could not become $Th^{226}R^{+3}$. Hence, since the surface contamination is the same in each case, the charge and energy distributions should be approximately the same for Al, Mo or Pt collector plates, particularly since most of the thickness effects arise from collisions with the molecules and atoms which make up the surface contamination. However, in choosing a collector plate material, Al should probably be avoided because any Al oxide present makes it difficult to obtain good electrical contact. This fact was demonstrated several times during attempts to collect recoils on Al and in Fig. 40 the intensity of the Th^{226} source collected on Al was 13.5% less than that of the Th^{226} sources collected on Mo, stainless steel, and Pt.

An attempt was made to compare sources which were collected in air, Ar + 4% CO_2, pure Ar (contained less than 5 ppm N_2, 2 ppm O_2, 1 ppm H_2, 0.5 ppm CO_2, 0.5 ppm hydrocarbons and 0.22 ppm H_2O) and pure He (contained less than 3 ppm H_2O, 8.8 ppm Na, 1 ppm N_2, 0.2 ppm O_2, 0.05 ppm Ar and 0.05 ppm CO_2). Unfortunately most of these collections were made on "unflashed" Pt and consequently the results are not too reliable. However, the resulting ratios and $Th^{226}R^{+2}$ energy distributions varied only slightly which seems to indicate that the collecting medium used is not very important.

The purity of both the He and Ar was maintained by placing the collecting apparatus in a vacuum tank which was emptied and filled with either He or Ar twice before the actual collection was begun.

Much stronger conclusions can be drawn concerning the advisability of using a cylindrical electrostatic field such as that formed in the "small" and "large dog houses" (see Fig. 4). The "dog houses" were investigated because the activity is collected on the edge of a thin plate making it possible to obtain very narrow alpha peaks by eliminating the peak widening due to the physical width of the source. In particular, if the technique had yielded very thin sources it would have been possible to use such sources to study the intrinsic half width of alpha decay. However, it rapidly became apparent that the disadvantages of such a collection outweigh its possible advantages at the present time for making thin alpha sources. The first such disadvantage is indicated by a comparison of Figs. 29 and 43. Figure 43 shows a plot of the intensity of the Th^{226} source collected as a function of the voltage at an arbitrary radius of 1 cm for the small and large dog houses. Since the U^{230} source was about 5/32 by 1/2-in. and the collector was about .011 by 1-in, collections made parallel to the source yielded Th^{226} sources which were .011 by 1/2-in. whereas collections perpendicular to the source yielded Th^{226} sources which were .011 by 5/32-in. Figure 29 shows the similar plot for parallel plate collection. A direct comparison of the Th^{226} source intensities obtainable by the three different collecting techniques shows that the maximum intensity obtained for the "small doghouse" is a factor of 8.5 smaller than that obtained by parallel plate collection. This discrepancy could be the result of several causes:

1. The collectors used for dog house collection were made of Al and

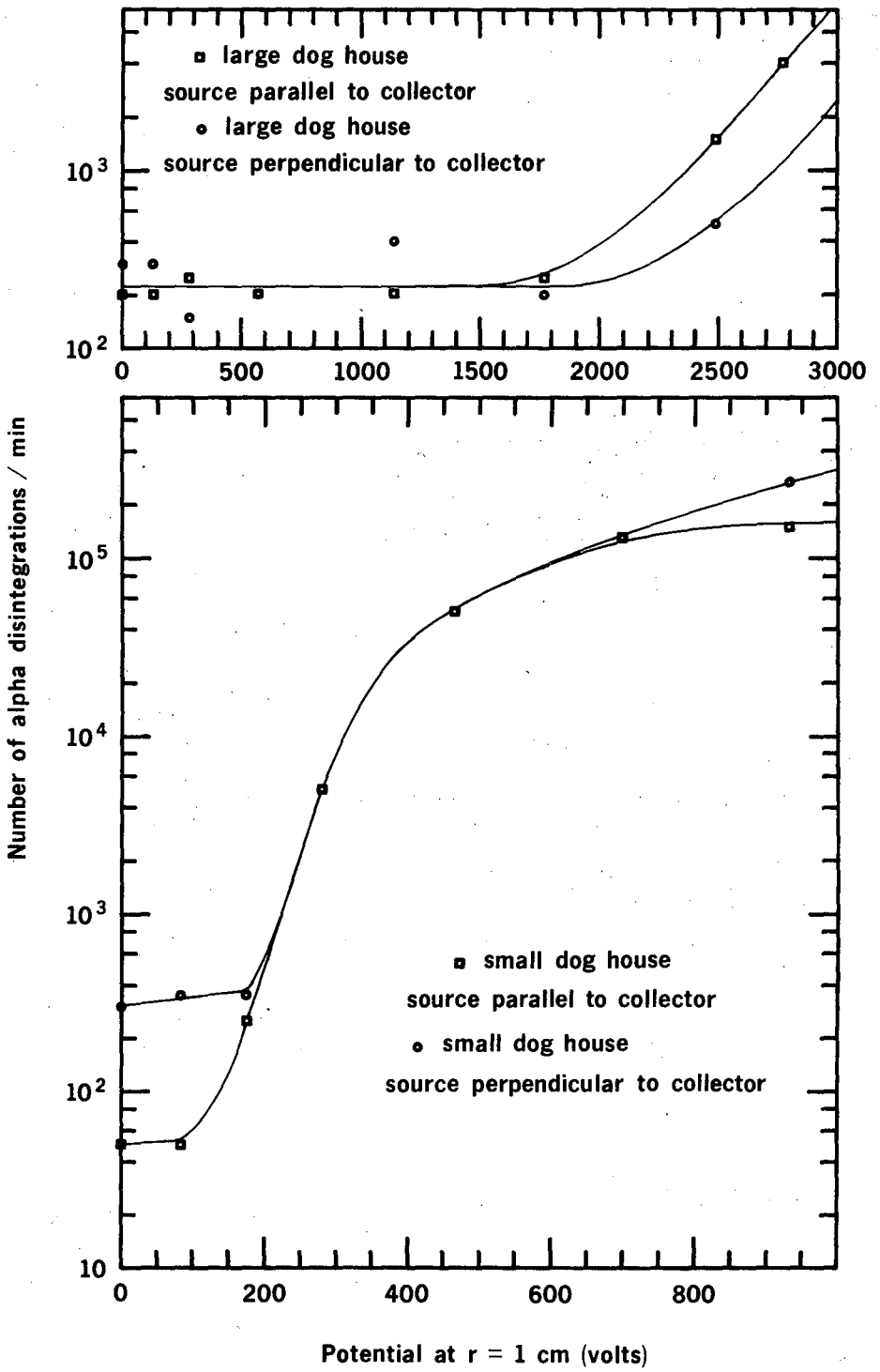

XBL 687-1164

Figure 43. Collection efficiency of both the "large dog house" and the "small dog house" as a function of the potential at a radius of 1 cm. Collections were made in air at STP.

hence the discrepancy would be due to poor electrical contact. This certainly did occur in some cases.

2. It is not clear from Fig. 43 that the plateau for the "small dog house" has been reached. This is particularly true since the last point on the high voltage side for having the source parallel to the collector could be due to poor electrical contact. It is obvious from the figure that the plateau for the "large doghouse" has not been reached. (Note that the flat regions on the low voltage sides of all four curves in Fig. 43 are merely the background count.) The plateau value, when it is reached, could be as high as for the parallel plate collection. Such a possibility is confirmed by the fact that recoils have previously been collected electrostatically with little decrease in final source intensity from distances up to 5 cm away, as long as the collecting voltage is sufficiently high.[40] Under optimum conditions (a very thin source) a collection efficiency of approximately 50%, which is the maximum efficiency possible, has been obtained.[40] Thus the plateau indicated in Fig. 29 probably represents a 50% collection efficiency. A direct check of this possibility was impossible to obtain in this case because the U^{230} sources used were too intense to be accurately measured.

3. It could be that the pattern of the electric field lines cause some of the recoils to collect on the sides of the collecting plate rather than on the edge. If this is the case, then the "plateau" for collection in either of the dog houses would be less than that for the parallel plate collector. However, if this were the case, then for any given voltage, the intensity of a Th^{226} source made with the source parallel to the collector would always be greater than the intensity of a Th^{226} source made with the source perpendicular to the collector. Since this is clearly not

the case for the "small dog house," this explanation does not apply to it. However, according to Fig. 43, this is a distinct possibility for the "large dog house" which has a different field configuration.

If, however, the lower maximum intensity obtained with the "dog houses" is intrinsic to their field configurations, then this could become a problem when collecting recoils from a low intensity primary source.

A further difficulty with the "dog houses" is indicated in Fig. 43. The actual radii of the "large dog house" and "small dog house" are 3.7 and 1.27 cm respectively. This means that to obtain 3000 volts at r = 1 cm for the "large dog house" it is necessary to apply 3800 volts to the terminals. Even so, at this voltage, the intensity of the resulting Th^{226} source is a factor of 560 times smaller than the maximum obtainable intensity using a parallel plate collector at far smaller applied voltages. For the "small dog house," 1000 volts at r = 1 cm requires an application of 1055 volts at the terminals, and the intensity is 8.5 times smaller as mentioned previously.

The problems presented by voltages of such magnitude are twofold. First, a high voltage dc supply must be available whereas parallel plate collection can be achieved with simple dry cell batteries. Second, the application of 3800 volts to the terminals of the "large dog house" means that the collected recoils will, in general, acquire 257 eV between their last collision and the time they hit the collector plate. Similarly the figure for the "small dog house" is 86 eV. With such high impact energies, it is certain that Th^{226} recoils in leaving such a source must lose at least that much energy in order to escape, and hence such sources will always be thick. Since the surface contamination increases with distance and since in the "dog house" configurations, the distances are larger, the

parallel plate configuration has an advantage.

Thus, sources produced in these "dog houses" at STP are bound to be thick. This prediction is born out by experiment. Figure 44 shows one such plate made using a source produced in the "small dog house." This source collected in Ar + 4% CO_2 but those collected in air or other media were not very different from this one. It can be seen from the figure that the energy distribution of the Th^{226} R^{+2} peak is poor. In addition, the ratio No. $Th^{226}R^{+2}(2\alpha + 3\alpha)$/No. $Th^{226}\alpha_0$ is .0078 ± .0012 which is 88% smaller than the best ratio obtained with the parallel plate collector.

Th^{226} sources produced by vacuum sublimation under the best circumstances are also thick. (The "best circumstances" means that the Th^{226} which was sublimated was practically mass free having been obtained by parallel plate collection. The primary source of extraneous mass was the small amount of HCl used to remove the Th^{226} from the collector plate in order to place it in the W trough for sublimation.) This point is clearly demonstrated by Figs. 45, 46, and 47. The only difference between the sources used to produce these plates is that the distance between source and collector for Figs. 45, 46, and 47 was about 0.2 cm, 0.4 cm, and 1.0 cm respectively. None of the energy distributions shown are good but they do seem to improve as the separation between source and collector increases. The ratios No. $Th^{226}R^{+2}$ $(2\alpha + 3\alpha)$/No. $Th^{226}\alpha_0$ which are .0008 ± .0046, .025 ± .004, and .021 ± .039 seem to bear this out. However, none of these sources is nearly as good as the worst parallel plate produced source. Furthermore, if it is necessary to use larger source-collector distances, the intensity of the collection will decrease due to solid angle reduction.

The above discussion, of course, covers relatively mass free vacuum sublimation sources and still they show the effects of source thickness in

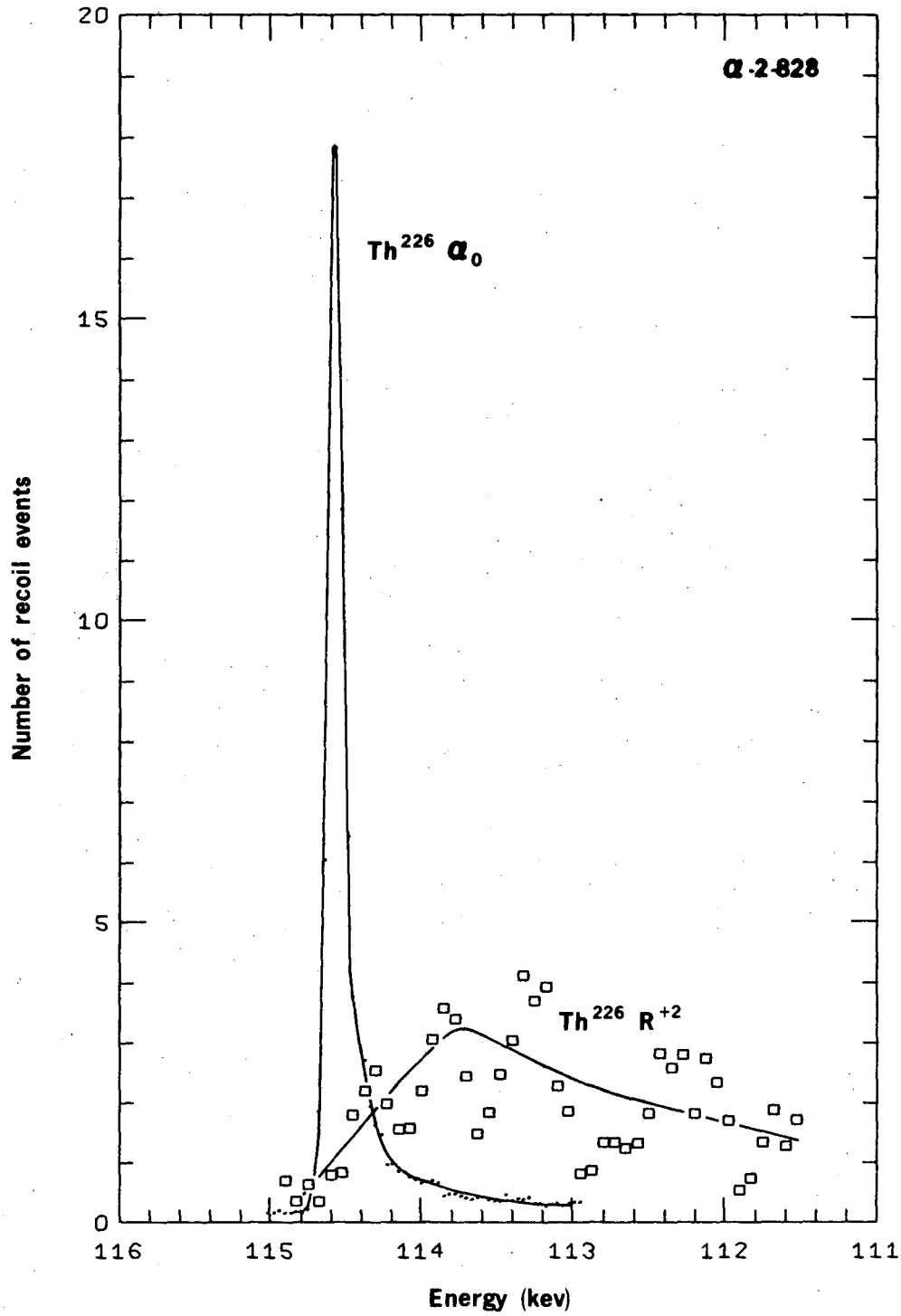

XBL 687-1151

Figure 44. $Th^{226}R^{+2}$ spectrum taken with alpha particle spectrograph in "regular plate" configuration. Alpha peak reduced in scale by a factor of 240. Spectrum made using a source which was collected for 1 hour in Ar + 4% CO_2 onto Al using "small dog house" at a potential of 1000 volts.

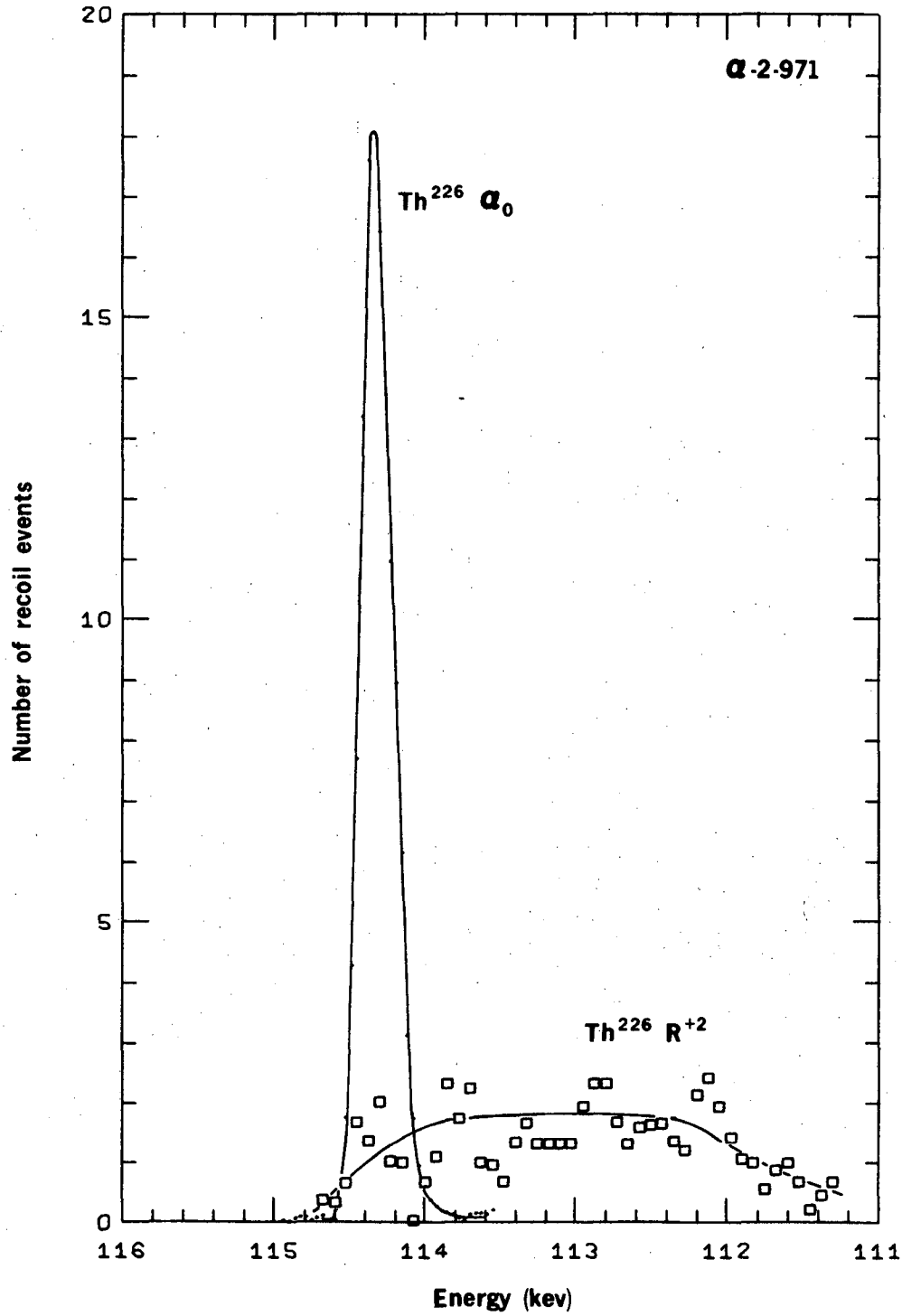

XBL 687-1161

Figure 45. $Th^{226}R^{+2}$ spectrum taken with alpha particle spectrograph in "regular plate" configuration. Alpha peak reduced in scale by a factor of 80. Spectrum made using a source which was vaporized onto Pt at a distance of about 0.2 cm.

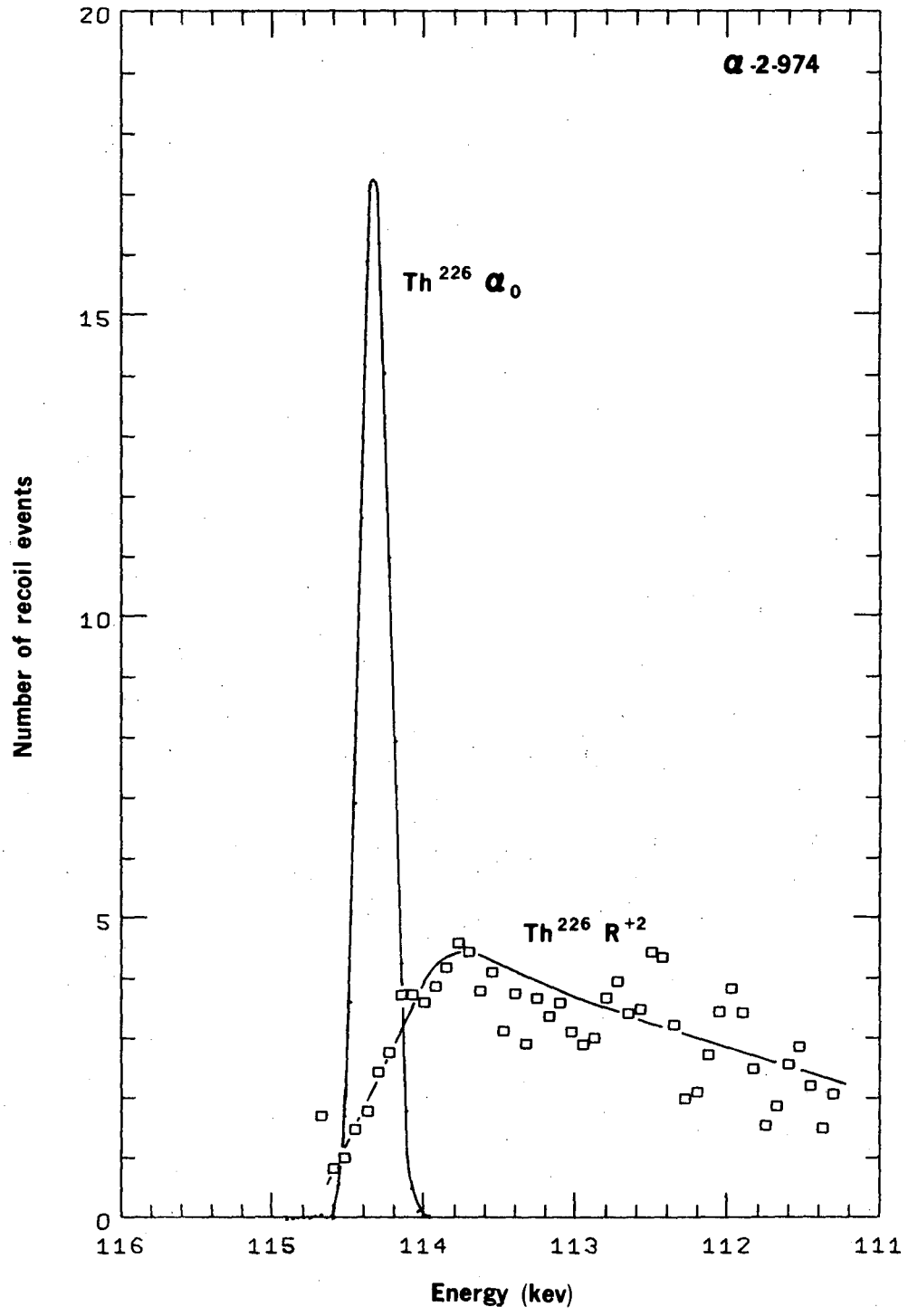

XBL 687-1150

Figure 46. $Th^{226}R^{+2}$ spectrum taken with alpha particle spectrograph in "regular plate" configuration. Alpha peak reduced in scale by a factor of 80. Spectrum made using a source which was vaporized onto Pt at a distance of about 0.4 cm.

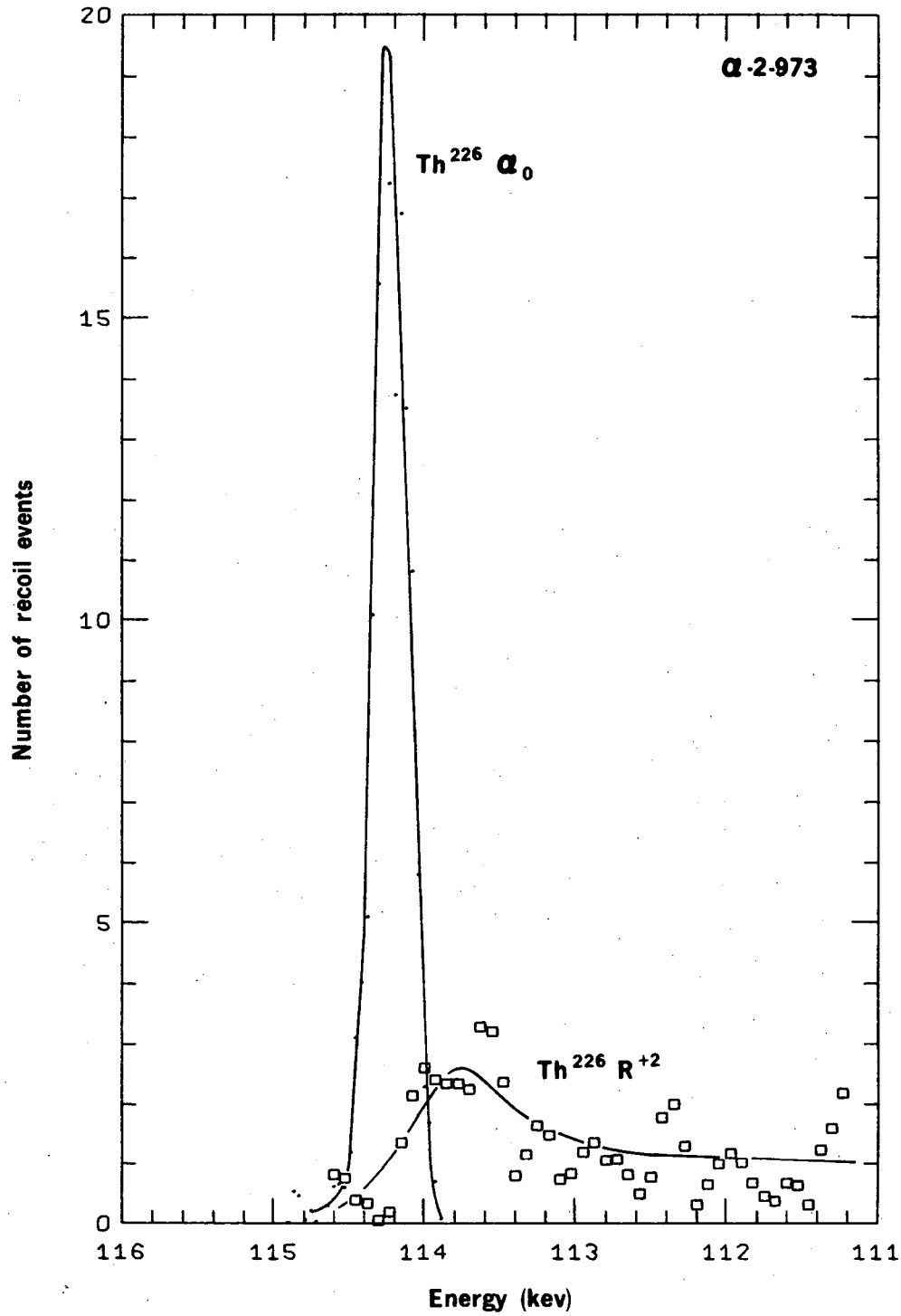

XBL 687-1152

Figure 47. $Th^{226}R^{+2}$ spectrum taken with alpha particle spectrograph in"regular plate" configuration. Alpha peak reduced in scale by a factor of 80. Spectrum made using a source which was vaporized onto Pt at a distance of about 1.0 cm.

the "tails" of the alpha peaks. (See Figs. 45, 46, and 47.) In general, sources produced by the vacuum sublimation technique will not be nearly as mass free as the sources used here and consequently they will be even thicker.

2. Theory

In order to get an idea of the total amount of surface contamination possible for any particular collection situation, it is necessary to know how many positive ions are available for collection since any surface contamination will likely arise as the result of such ions striking the surface and adhering to it. Since the range of the recoils is small at STP (on the order of 5×10^3 cm for air, Ar or CO_2 and 4×10^{-2} cm for He), all of the ions resulting from the passage of the recoils will be available for collection. The number of such ions per recoil for the energies involved is probably on the order of 3×10^3 or $\frac{113,000}{32}$. If the number of alpha disintegrations/min for the U^{230} source is designated by y and it is assumed that the number of recoils/min is about 1/3 y, then the number of ions produced/min by the passage of the recoils is on the order of 1×10^3 y. The number of ions produced by the alpha particles and available for collection is calculated as follows: the number of ions produced per alpha is of the order of 2×10^5; a source of y alpha disintegrations/min will produce $2 \times 10^5 y/(4/3)\pi r^3$ ions/min/unit volume where r is the range of the alphas in the collection media involved. (r is on the order of 5 cm for air, Ar and CO_2 and on the order of 28 cm for He.) Hence, the number of ions/min available for collection from the passage of the alpha particles is of the order of $(2 \times 10^5\ y/(4/3)\pi r^3)$(collection volume = V_o) $\approx 350\ V_o y$ ions/min for air, Ar or Ar + 4% CO_2, and $\approx 2\ V_o y$ for He. Since V_o is on the order of .5 h cm^3 for the parallel plate collector

where h is the separation between source and collector and ranged from 0.1 cm to 0.7 cm, it is clear that the majority of the ions collected during parallel plate collection were produced by the recoils and hence practically independent of the separation of source and collector. For example, if $y = 2 \times 10^{11}$ dis/min (as it did for the hottest U^{230} sources), then the number of ions available for collection in air or Ar at STP/min ≈ 1.04×10^{14}/min for h = 0.1 cm, 1.14×10^{14}/min for h = 0.4 cm, and 1.25×10^{14}/min for h = 0.7 cm and the number of ions available for collection in He at STP/min ≈ 1×10^{14}/min in all three cases. These figures clearly indicate the validity of hypothesis No. 5 while explaining why increases in the separation from 0.1 cm to 0.7 cm did not have a more drastic effect. It also helps to explain the fact that the apparent source thickness for collection in He at STP was about the same as that for collection in air at STP when the parallel plate collector was used. Of course, He and Ar are noble gases and are not expected to form compounds which could add to the surface contamination. However, it was indicated on page 115 that "pure" Ar contains about 10 ppm of contaminants which can form such compounds whereas "pure" He contains about 13 ppm of such contaminants. Since STP implies the existence of about 3×10^{19} atoms/cm^3, this means that the pure gases had about 3×10^{14} atoms/cm^3 available to form contaminating compounds. This corresponds to 0.15×10^{14} atoms for h = 0.1 cm, 0.6×10^{14} atoms for h = 0.4 cm and 1.1×10^{14} atoms for h = 0.7 cm. Additional contamination will be available from outgassing of the parallel plate collector itself and from diffusion. Furthermore, although the vast majority of ions formed initially will be either Ar^+ or He^+, any collisions between these two ions and neutral O_2, N_2, H_2O, CO_2, etc. will yield the following:

$(Ar^+ \text{ or } He^+) + (\text{neutral contaminant}) \rightarrow (Ar \text{ or } He) + (\text{contaminant})^+$

because the first ionization potentials of Ar and He are 15.7 and 24.5 eV respectively whereas those of O_2, N_2, H_2O, and CO_2 are 12.5, 15.5, 12.5 and 14.4 respectively. Thus, sources collected in Ar or He will be no thinner than those collected in air, particularly as the separation increases.

If all of the available ions are added to the surface contamination, the parallel plate collection for one hour would produce a source whose surface contamination was on the order of 10 atomic layers thick (assuming the contaminating "ions" are not in the form of large clusters of atoms) whereas one hour of collection in the small dog house would produce a source whose surface contamination was on the order of 840 atomic layers. This calculation clearly indicates a reason for the sources produced in the dog houses to be so thick.

Of course, it is not known whether all the available ions were collected. Thus, it is important to understand just what is happening to both recoils and ions during the electrostatic collection process.

In the presence of an electric field, positive ions such as the recoils will drift towards the negative electrode. Their average velocity towards the electrode is their drift velocity u. $u = kE$ where k is defined as the mobility of the ion and E is the magnitude of the electric field. In general, k is approximately proportional to $(\lambda/P)\sqrt{\frac{m + M}{m}}$ where λ is the mean free path of the ion, m is its mass, M is the mass and P is the momentum of the gas through which the ion is moving. Thus, if k_g is the mobility of a gas ion moving through the gas, then the mobility of a heavy recoil such as Th^{226} will approximately be equal to $k_g\sqrt{\frac{m + M}{2m}} \approx \frac{k_g}{\sqrt{2}}$. That is, the drift velocity of a heavy recoil travelling through air or any

other light gas will be about 1.4 times smaller than the drift velocity of the positive ions of the gas. Sample mobilities are 2.7 cm^2/volt-sec for air, 2.7 to 3 cm^2/volt-sec for Ar and 22 cm^2/volt-sec for He.[46] The drift velocities of negative ions are on the same order of magnitude. The drift velocity for electrons is not a simple linear function of the electric field[46] and hence is not included here.

As the ions and electrons drift towards their respective electrodes, they undergo a large number of collisions during which the following processes are possible:

1. $A^+ + B \rightarrow B^+ + A$

if the first ionization of B is less than or not much greater than that of A.

2. $A_+ + B^- \rightarrow A + B$ or AB

3. $A + e^- \rightarrow A^-$

and 4. $A^+ + e^- \rightarrow A$.

Processes (2) and (4) are recombination processes whereas (3) is a so-called "attachment" process.[45] These four processes can cause an ionized gas to eventually become neutral. Thus, if the drift velocity of the gas ions and recoils is sufficiently small, most of the ions and recoils will be lost before they strike the collector plate. This is just what happens at low electric fields as indicated in Figs. 29 and 43.

If n_r is the concentration of positive recoils with thermal energy, n_{ro} is the concentration of neutral recoils with thermal energy, n_+ is the concentration of positive gas ions, n_- is the concentration of negative gas ions, and n_e is the concentration of electrons, then we have

$$\frac{dn_r}{dx} = \frac{1}{u_r} \left\{ q_r - \alpha_r n_- n_r - R_r n_e n_r + e_r n_{ro} n_+ \right\} \qquad (1)$$

$$\frac{dn_{ro}}{dt} = q_{ro} - e_r n_{ro} n_+ + R_r n_e n_r + \alpha_r n_- n_r \tag{2}$$

$$\frac{dn_+}{dx} = \frac{1}{u_+} \left\{ q_+ - \alpha_+ n_- n_+ - R_+ n_e n_+ + e_r n_{ro} n_+ \right\} \tag{3}$$

$$\frac{dn_-}{dx} = - \frac{1}{u_-} \left\{ q_- + a_- n_e n - \alpha_+ n_- n_+ - \alpha_r n_- n_r \right\} \tag{4}$$

and

$$\frac{dn_e}{dx} = - \frac{1}{u_e} \left\{ q_e - R_+ n_e n_+ - R_r n_e n_r - a_- n_e n \right\} \tag{5}$$

where x is distance from U^{230} source to Th^{226} collector, u_i is the drift velocity of i, q_i is the rate at which i is formed from the passage of alphas or recoils, α_i is the recombination co-efficient for negative ions and i, R_i is the recombination co-efficient for electrons and i, e_r is the transformation co-efficient for the process gas ion + $R^0 \rightarrow$ gas atom or molecule + R^+, a_- is the co-efficient of attachment for process (4) and n is the concentration of neutral gas atoms or molecules. These equations can certainly not be solved exactly, particularly since the q_i's and n_i's are complicated functions of the distance between the electrodes and the n_i's are also functions of the magnitude of the electric field at any point. However, they can be approximately solved. The approximate values of the various coefficients for air, Ar, or He at STP are as follows: α_r, α_r and e_r are on the order of 10^{-6} cm^3/sec, R_r and R_+ are on the order of 10^{-10} cm^3/sec, a_- is on the order of 10^{-15} cm^3/sec for O_2 and H_2O at STP but equals zero for N_2, Ar and He,[45] and $n = 3 \times 10^{19}$ atoms/cm^3 at STP. Since e_r is finite, n_+ is never zero in the recoil range region and the third and fourth terms in Eq. (2) are small compared with the second, any neutral recoil will eventually become charged and travel towards the negative electrode, Thus Eq. (2) can be ignored and its effects taken

care of by including the term $e_r n_{ro} n_+$ in q_r for Eq. (1) since the decrease in n_+ due to the process will not be noticeable because $n_{ro} \gg n_+$. The q_i's have the form:

$$q_i = y_{\alpha i} + y_{ri} \quad \text{for } x \leq \lambda_r$$
$$= y_{\alpha i} \quad \text{for } d \geq x \geq \lambda_r$$

where $y_{\alpha i}$ = number of i ions produced/sec-cm^3 by alphas, y_{ri} = number of i ions produced/sec-cm^3 by recoils, λ_r = range of recoils and d = distance between electrodes. If y = number of alpha disintegrations/min, then $y_{\alpha+} = 6y$ in air and Ar; ≈ 0.032 y in He, $y_{r+} \approx 3200$ y in air and Ar; ≈ 485 y in He, $y_{\alpha-} \equiv c_\alpha y_{\alpha+}$, $y_{r-} \equiv c_r y_{r+}$, $y_{\alpha e} = (1 - c_\alpha) y_{\alpha+}$ and $y_{re} = (1 - c_r) y_{re}$, where c_α, $c_r < 1$, and $y_{\alpha r} = 0$, $y_{rr} \approx 1$ y. (Assume for simplicity that $c_\alpha = c_r = c$.)

If no ions were lost in transit, then we would collect all of the ions produced and obtain

$$n_{i\ max} = n_i(\text{at collection plate})_{max} = y_{\alpha i} \frac{d}{u_i} + y_{ri} \frac{\lambda_r}{u_i} .$$

In air at STP, $u_e \approx 5 \times 10^5$ cm/sec for an electric field intensity E_o ranging from 20 to 500 volts/cm. If we assume that $y = 2 \times 10^{11}$ dis/min, which was its maximum value, and c = .5, then we get:

$$n_{e\ max} \approx 5 \times 10^6 \text{ electrons/cm}^3 \text{ for } d = 0.1 \text{ cm}$$
$$\approx 10^7 \text{ electrons/cm}^3 \text{ for } d = 5 \text{ cm}$$
$$n_{+\ max} \approx \frac{2 \times 10^{12}}{E_o} \text{ ions/cm}^3 \text{ for } d = 0.1 \text{ cm}$$
$$\approx \frac{6 \times 10^{12}}{E_o} \text{ ions/cm}^3 \text{ for } d = 5 \text{ cm}$$
$$n_{-\ max} = \frac{1}{2} n_{+\ max}$$

and

$$n_{r\ max} \approx \frac{5 \times 10^7}{E_o} \text{ ions/cm}^3$$

where $u_i = k_i E_o$ and $k_+ = k_- = 2$, $k_r \approx 2/\sqrt{2}$ for air.

From the above, it is clear that $n_e \ll n_+$ and n_- unless $c \ll 1$, the condition if it is impossible to form negative ions at all. In the situation that n_- is zero we would have the following:

$$\frac{dn_r}{dx} = \frac{\sqrt{2}}{2E_o} \left\{ q_r - R_r n_e n_r \right\}$$

$$\frac{dn_+}{dx} = \frac{1}{2E_o} \left\{ q_+ - R_+ n_e n_+ \right\}$$

$$\frac{dn_e}{dx} - \frac{1}{u_e} \left\{ q_e - R_+ n_e n_+ - R_r n_e n_r \right\}$$

$$\approx - \frac{1}{u_e} \left\{ q_e - R_+ n_+ n_e \right\}$$

since $u_+ \approx u_- \approx \sqrt{2}\, u_r \approx 2E_o$ for air at STP. Since there are no negative ions (by definition), it is clear that if all the electrons are collected, then all the positive ions and recoils are also collected.

Consider the case where $R_+ n_+ n_e$ is small, then

$$n_+ \approx \text{const} \approx \frac{10^{12}}{E_o} \text{ ions/cm}^3 \equiv n_{+1} \text{ for } \lambda_r \geq x \geq 0$$

$$\approx \frac{10^{12} + 3 \times 10^{11}\, d}{E_o} \text{ ions/cm}^3 \equiv n_{+2} \text{ for } d \geq x \geq \lambda_r$$

for $y = 2 \times 10^{11}$ dis/min which is its maximum value. From this, we obtain for the number of electrons collected/cm^3-sec $= u_e n_e(0)$ for a parallel plate collector

$$u_e n_e(0) = \frac{(y_{\alpha+} + y_{r+})}{R_+ n_{+1}} \left\{ 1 - e^{-\frac{R_+ n_{+1}}{u_e} \lambda_r} \right\} u_e$$

$$+ \frac{y_\alpha + u_e}{R_+ n_{+2}} \left\{ e^{-\frac{R_+ n_{+1}}{u_e} \lambda_r} - e^{-\frac{R_+}{u_e} \left[n_{+2} d + (n_{+1} - n_{+2}) \lambda_r \right]} \right\}$$

Obviously, as E_o becomes large (that means large u_e and small n_{+1} and n_{+2}) essentially all ions will be collected. This is approximately true when

$\frac{R_+ n_{+1}}{u_e} \lambda_r \lesssim .1$ and $\frac{R_+}{u_e} \left[n_{+2} d + (n_{+1} - n_{+2}) \lambda_r\right] \leq .1$. The former occurs when $E_o \geq .03$ volts/cm, the latter when $E_o \geq \sqrt{2 \times 10^{-2}(10 + 3d)d} = 1.6$ volts/cm for d = 5 cm. Since total collection was never achieved at such a low voltage, even for "pure" Ar and "pure" He, it is clear that negative ions must exist and play a major part.

In this case we neglect n_e terms in Eqs. (1), (3) and (4) and get

$$\frac{dn_r}{dx} \approx \frac{\sqrt{2}}{2E_o} \left\{ q_r - \alpha_r n_- n_r \right\} \tag{6}$$

$$\frac{dn_+}{dx} \approx \frac{1}{2E_o} \left\{ q_+ - \alpha_+ n_- n_+ \right\} \tag{7}$$

$$\frac{dn_-}{cx} \approx - \frac{1}{2E_o} \left\{ q_- - \alpha_+ n_- n_+ \right\} \tag{8}$$

and

$$\frac{dn_e}{dx} \approx - \frac{1}{u_e} \left\{ q_e - a_- n n_e \right\} .$$

The solution to this last equation yields

$$u_e n_e(0) = \frac{u_e(1-c)}{a_- n} \left\{ y_{r+} \left(1 - e^{-\frac{a_- n}{u_e} \lambda_r} \right) + y_{\alpha+} \left(1 - e^{-\frac{a_- n}{u_e} d} \right) \right\}$$

which $\approx (1 - c)(y_r + \lambda_r + y_\alpha + d)$ when $\frac{a_- n}{u_e} \lambda_r$ and $\frac{a_- n}{u_e} d$ are small.

This occurs when $E_o/d \geq 100$ volts/cm^2. Thus, for most of the voltages used practially all of the electrons were collected but at low voltages, a fair number of the electrons produced by the alphas were converted into negative ions for $5 \geq d \geq 1$ cm.

In general, the solution to Eqs. (6), (7) and (8) is not easy to obtain. However, in the region where most of the ions are collected, it is not too inaccurate to assume that

$$n_- \approx \text{const} \approx \frac{3 \times 10^{11} dc}{E_o} \text{ ions/cm}^3 \equiv n_{-1} \text{ for } d \geq x \geq \lambda_r$$

$$\approx \frac{(10^{12} + 3 \times 10^{11} d)c}{E_o} \text{ ions/cm}^3 \equiv n_{-2} \text{ for } \lambda_r \geq x \geq 0$$

where $y = 2 \times 10^{11}$ dis/min. Using this we obtain,

$$\frac{2E_o}{\sqrt{2}} n_r(d) = \frac{y_{rr} 2E_o}{\alpha_r n_{-2} \sqrt{2}} \left\{ e^{-\frac{\alpha_r n_{-1}}{2E_o}\sqrt{2}\,(d - \lambda_r)} - e^{-\frac{\alpha_r \sqrt{2}}{2E_o}\left[n_{-1} d + (n_{-2} - n_{-1})\lambda_r\right]} \right\}$$

and

$$2E_o n_+(d) = \frac{y_{\alpha+}\, 2E_o}{\alpha_+ n_{-1}} \left\{ 1 - e^{-\frac{\alpha_+ n_{-1}}{2E_o}(d - \lambda_r)} \right\}$$

$$+ \frac{(y_{r+} + y_{\alpha+}) 2E_o}{\alpha_o n_{-2}} \left\{ e^{-\frac{\alpha_+ n_{-1}}{2E_o}(d - \lambda_r)} - e^{-\frac{\alpha_+}{2E_o}\left(n_{-1} d + \left[n_{-2} - n_{-1}\right]\lambda_r\right)} \right\}.$$

Since $\frac{2E_o}{\sqrt{2}} n_r(d)$ = number of recoils collected/cm^{2}sec, most of the recoils will be collected when $\frac{\alpha_r n_{-1}}{2E_o}\sqrt{2}\,(d - \lambda_r)$ and $\frac{\alpha_r \sqrt{2}}{2E_o}\left[n_{-1} d + (n_{-2} - n_{-1})\lambda_r\right]$ are small or inserting numberical values from above $E_o \gg d\sqrt{2.1 \times 10^{10}\, \alpha_r c}$ and $\sqrt{\alpha_r c(2.1 \times 10^{10} d^2 + 3.5 \times 10^8)}$. Likewise, most of the positive ions will be collected when $E_o \gg 1 \times 10^5 d \sqrt{\alpha_+ c}$ and $\sqrt{\alpha_+ c\,(1.5 \times 10^{10}\, d^2 + 2.5 \times 10^5)}$.

From this it can be seen that the pattern of the curves in Fig. 29 is confirmed by the theory since if the "plateau" is reached at 100 volts/cm for d = .1 cm, it will be reached at 260 volts/cm for d = .4 cm and 440 volts/cm for d = .7 cm assuming $c_r = c_\alpha$. If $c_r > c_\alpha$, then these numbers

will be even closer together. Furthermore, it is clear that the "plateau" for the collection of either ions or recoils is actually the collection of all the ions or recoils. If $\alpha_r > \alpha_+/\sqrt{2}$, then all of the positive ions will be collected before all of the recoils are. This appears to be true and is not too unexpected since the lower ionization potential of Th^{226} means that it will be less likely to lose an attached electron than the gas ion with the higher ionization potential. It can also be seen from the theory that the general shape of the curve in Fig. 29 is also correct. In addition, as the intensity of the U^{230} source decreases, so does the "plateau" voltage.

Thus, the theory confirms the validity of the hypotheses Nos. 2, 3, 4,5, and 6 presented in the experimental section and furthermore shows that the "plateau" represents the collection of all available recoils and positive ions. It also indicates that negative ions must be present, even in the pure He and Ar otherwise the minimum total collection voltage would have been much smaller. Furthermore, it shows that it is entirely possible to collect all available recoils at distances greater than or equal to 5 cm as long as a sufficiently large electric field intensity is maintained in the regions defined by the ranges of the alphas and recoil, and this necessary electric field intensity decreases as the square root of the source intensity. It indicates that the reason such large collecting voltages were needed to collect all of the recoils using a dog house is because the electric field intensity in the region near the source increases very slowly as the total applied voltage increases and hence most of the recoils are lost before they leave the vicinity of the source.

3. Conclusions and Future Experiments

It is clear from the experimental results that electrostatic collection

is far superior to vacuum sublimation as a means of producing thin alpha sources. Furthermore, the resulting thickness of a vacuum sublimation source seems to be inherent in the technique in that excess mass is always present.

Although improvement can be made in parallel electrostatic collection, the values of the various parameters are not too critical as far as producing a thin source goes. However, the following appears to be true:

1) An increase in U^{230} source intensity yields slightly thinner sources.

2) Water vapor in the collecting media tends to accumulate on the U^{230} source thus decreasing its apparent intensity although it has no effect on the thickness of the recoil source.

3) The electric field intensity is important only in so far as it must be sufficient to collect all of the recoils but not so large as to give the recoils a large impact energy.

4) An increase in the separation between source and collector for a parallel plate collector does increase the thickness of the source but not greatly for small separations.

5) An increase in collecting time increases source thickness.

6) A variation in collector medium appears to have little effect on source thickness.

7) Electrostatic collection at STP in "dog houses" yields sources that are much thicker than those made by parallel plate collection, both because of the increased number of collected positive ions and because of the increased impact energy of the recoils.

8) Pt appears to be the best material of those tested to use for collector plates although it does not appear to be a great deal better

than Al or Mo.

9) It is very important to use clean collector plates in order to minimize source thickness.

The results of the experiments in this section suggest a large number of experiments to test various aspects of the problem. Several such experiments are listed below.

1) The intensity hypothesis (i.e., more intense U^{230} sources yield thinner Th^{226} sources) should certainly be tested since it is so tentative.

2) As was discussed under the section on the material used for collectors, those used appeared to yield sources of comparable thickness with the possible exception of stainless steel. This result was explained by comparing the ionization potentials of these materials with those of Th. If this is indeed the proper explanation, then it would be of interest to compare the $Th^{226}R_0$ charge and energy distributions produced by using Cu with those produced using Pt, Al, and Mo because Cu in the metallic form has an apparent charge of +1 which should cause a decrease in the ratio No. $Th^{226}R^{+2}$/No. ($Th^{226}R^{+1}$ + $Th^{226}R^{0}$). These charge and energy distributions should be compared at STP and at a lower pressure such that d is only slightly greater than λ_r and with several different values of the electric field intensity in order to vary the impact energy. A comparison of the results at STP and the lower pressure should give an indication of the relative importance of collisions in the collector material with those in the surface contamination, since at lower pressure the surface contamination should be greatly reduced. An increase in the impact energy will cause the recoils to become more deeply imbedded in the collector plate material and hence the importance of collisions in

the collector plate for various materials on the charge distribution can be investigated.

3) The effects and relative importance of surface contamination should be tested by checking the charge and energy distributions of $Th^{226}R_0$ as a function of air gap (up to 5 cm) at STP and a lower pressure such that $d \approx \lambda_r$ where the collecting field intensity is kept at the minimum necessary to collect all of the recoils.

5) More experiments should be made using various collecting media such as air, Ar, N_2, He, and Ne in order to see if indeed it is of little importance. These experiments should be carried out at STP and the lower pressure mentioned before. The effects of the source-collector gap should also be studied for these various gases.

6) The importance of the presence of water vapor should also be tested, both in its effects on the thickness of the recoil source and in its effects on the apparent intensity of the U^{230} source.

7) An attempt should be made to improve the sources made in "dog houses." This can be done in the following ways. First, the dog house itself can be made smaller. This solution is limited by the size source you desire to collect from. Second, insulator baffles can be placed in the "dog house" about the source in such a way that the minimum number of positive ions is collected without preventing the total collection of recoils. Third, recoils should be collected at a lower pressure such that $d \approx \lambda_r$ with the absolute minimum electric field intensity needed for total recoil collection.

C. Charge and Energy Distribution of Th^{226} Recoils

1. Experimental Results

The results of the experiments discussed up to this point were used to determine the best technique of making sources to investigate the charge and energy distribution of Th^{226} recoils. Hence all of these sources were made by collecting recoils on flashed Pt in air at STP in the parallel plate collector with a separation of 0.1 cm and an electric field intensity of 225 volts/cm.

As has been previously discussed, the energy distribution for any charge can only be obtained from a regular plate and hence, no energy distributions were obtained for charges 0, +1 and -2. In order to insure that the energy distributions obtained from the regular plates were real and not the result of a change in the transmission of the machine as a function of distance along the plate, the transmission of the alpha spectrograph was checked. The resulting transmission curves are shown in Fig. 48 where the baffle setting used in this work was $\pm$ 5 cm. It can be seen from the curves that the transmission appears to be constant along the plate, particularly for a baffle setting of $\pm$ 3 cm.

The raw data for the energy distributions is shown in Figs. 49 through 71. The data was counted and plotted in the same way as was discussed for the graphs shown in the section on producing thin alpha sources except that the recoil points are not the average over the nearest three points but rather the direct number of recoils per 75 eV.

Four spectra for $Th^{226}R^{+2}$ were included in this group because the final data for $Th^{226}R^{+2}$ was obtained by adding the data from these four curves to form one composite peak in order to improve the statistics. The acceptable intensity of $Th^{226}R^{+2}$ peaks was limited by the necessity of

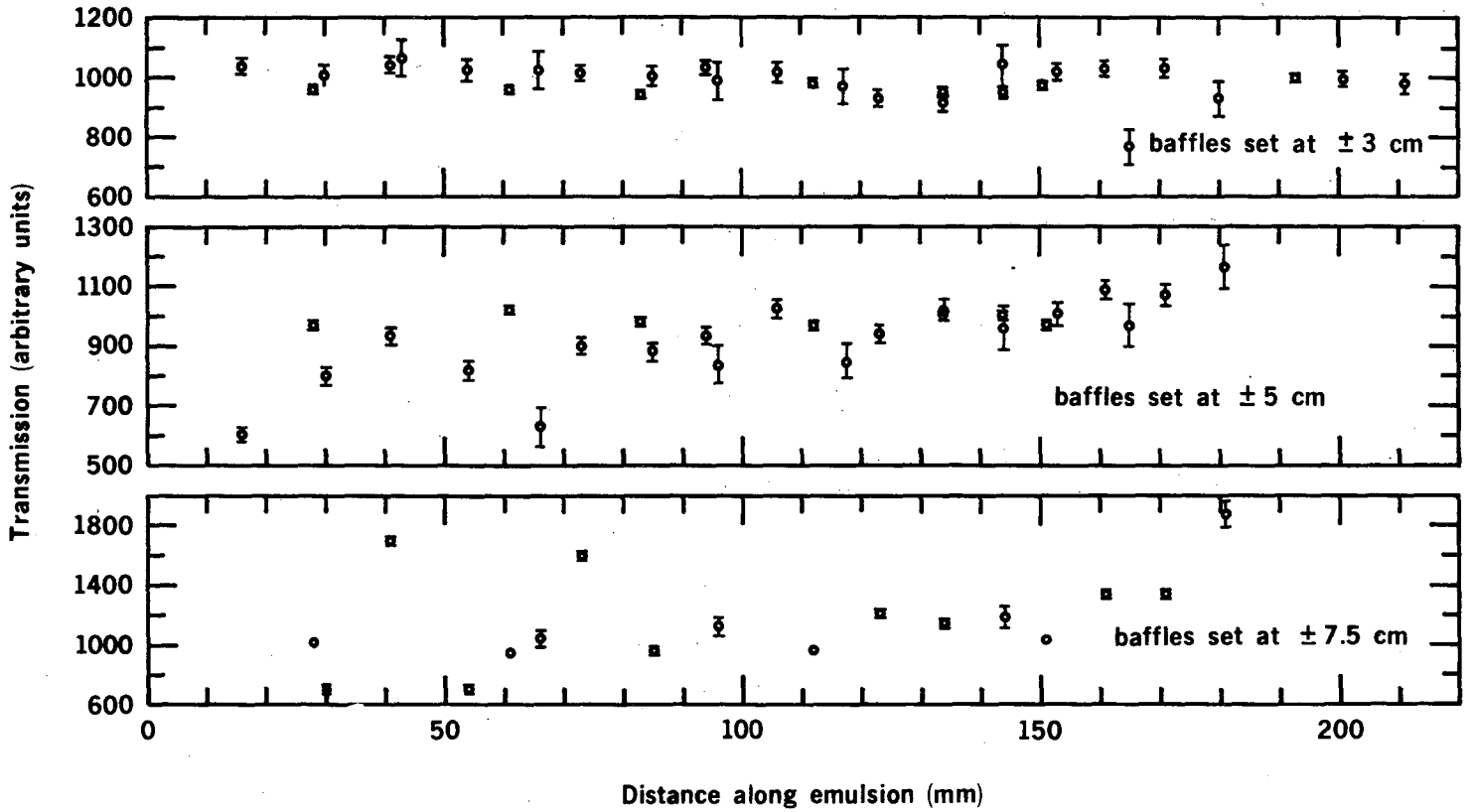

XBL 687-1313

Figure 48. Transmission of the 180 deg double focussing spectrograph in arbitrary units as a function of the distance along the emulsion for three different baffle settings.

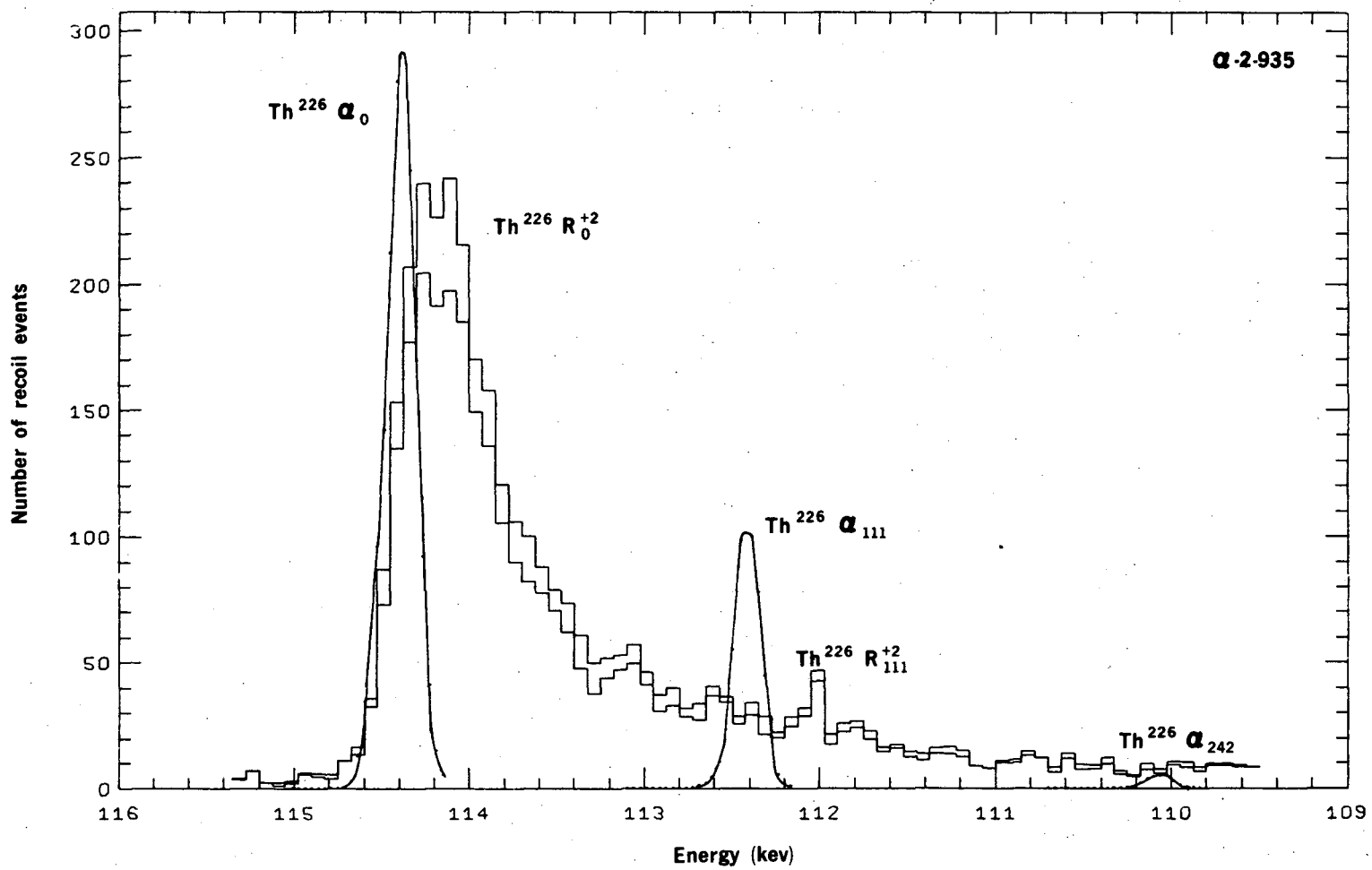

XBL 687-1220

Figure 49. $Th^{226}R^{+2}$ spectrum taken with alpha particle spectrograph in "regular plate" configuration. Alpha peak is reduced by a factor of 30. The lower curve shows 2-pronged events only, and the upper curve shows 2- plus 3-pronged events.

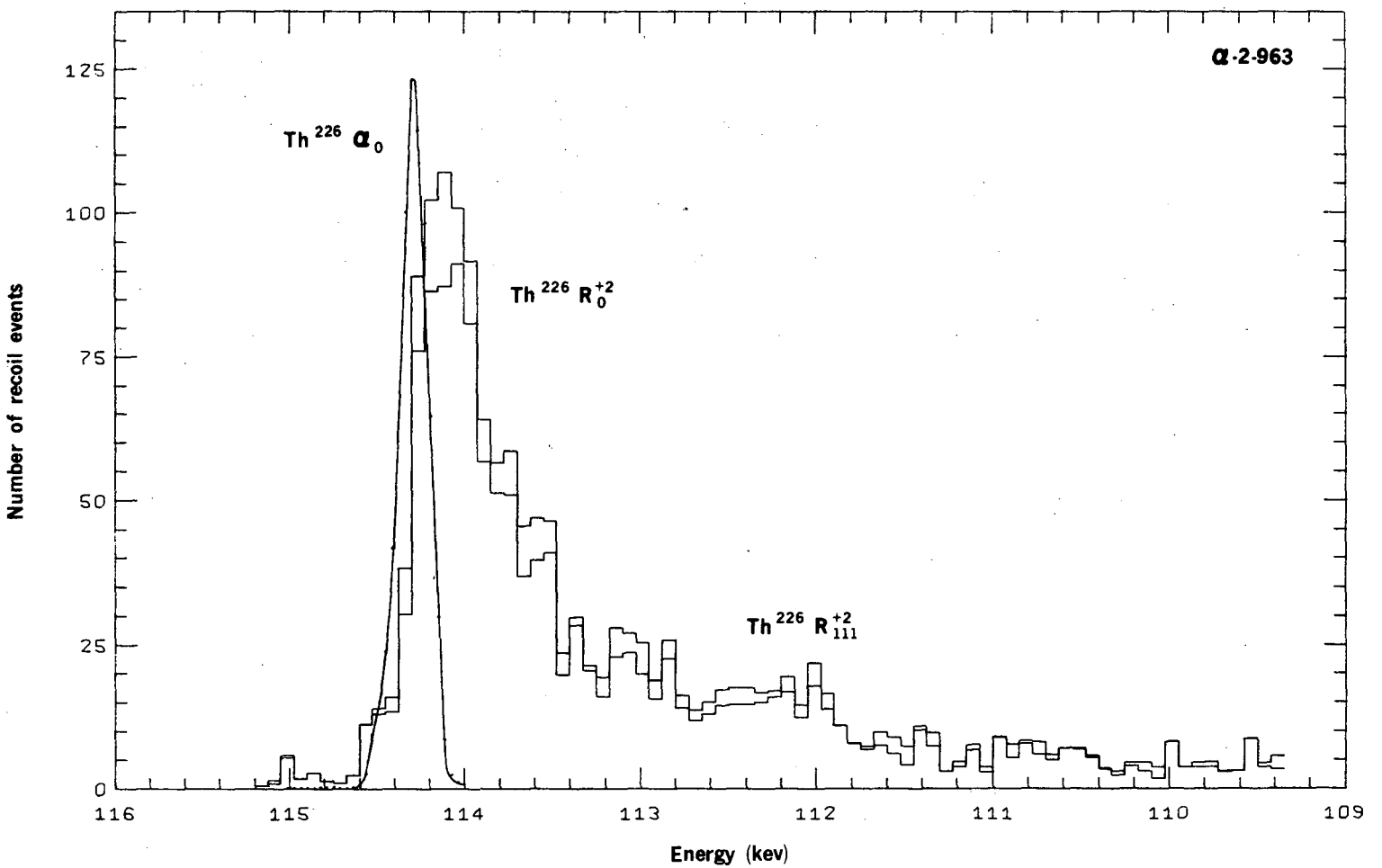

XBL 687-1236

Figure 50. $Th^{226}R^{+2}$ spectrum taken with alpha particle spectrograph in "regular plate" configuration. Alpha peak is reduced by a factor of 32. The lower curve shows 2-pronged events only, and the upper curve shows 2-plus 3-pronged events.

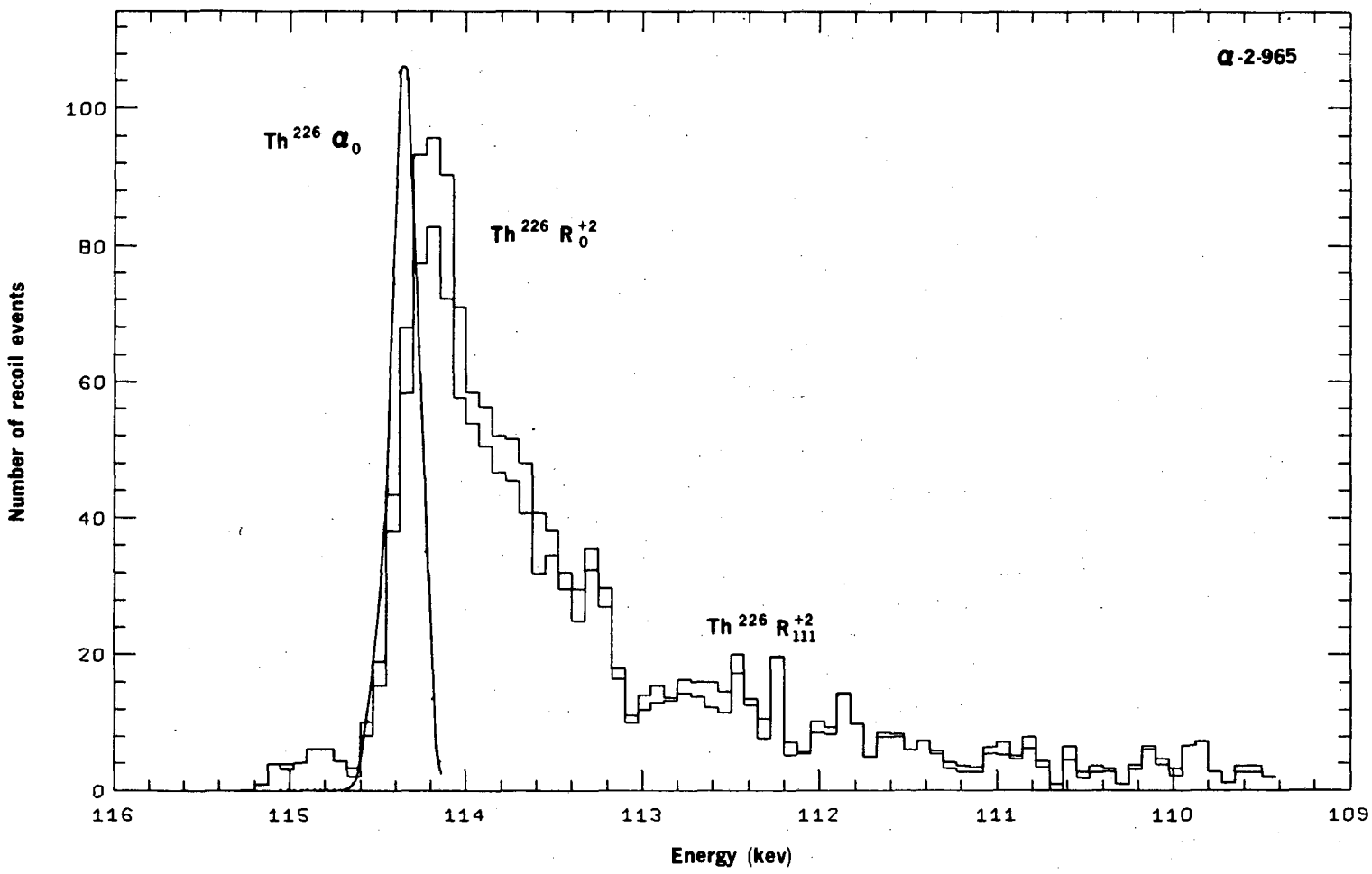

XBL 687-1237

Figure 51. $Th^{226}R^{+2}$ spectrum taken with alpha particle spectrograph in "regular plate" configuration. Alpha peak is reduced by a factor of 36. The lower curve shows 2-pronged events only, and the upper curve shows 2-plus 3-pronged events.

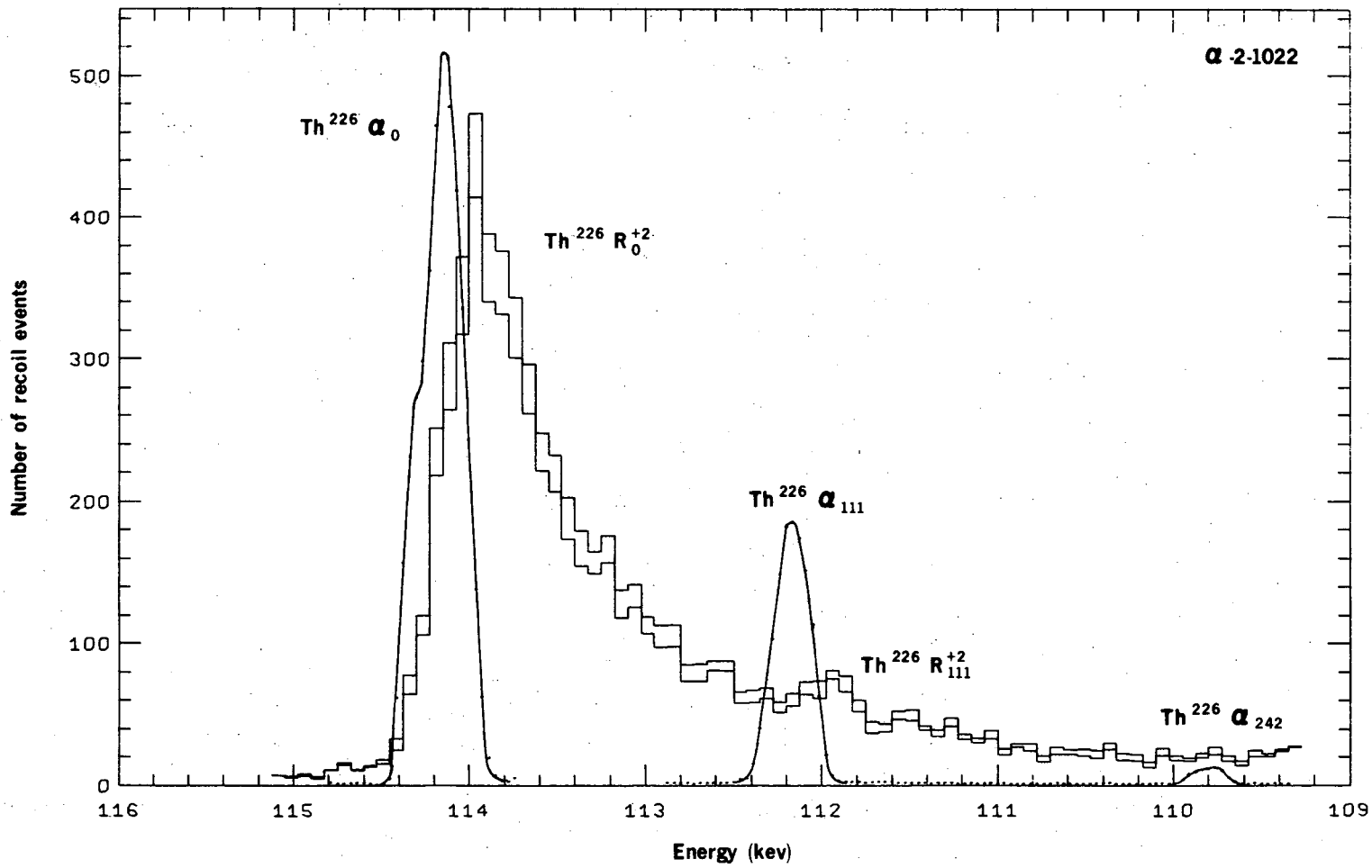

XBL 687-1223

Figure 52. The $^{226}R^{+2}$ spectrum taken with alpha particle spectrograph in "regular plate" configuration. Alpha peak is reduced by a factor of 27. The lower curve shows 2-pronged events only, and the upper curve shows 2- plus 3-pronged events.

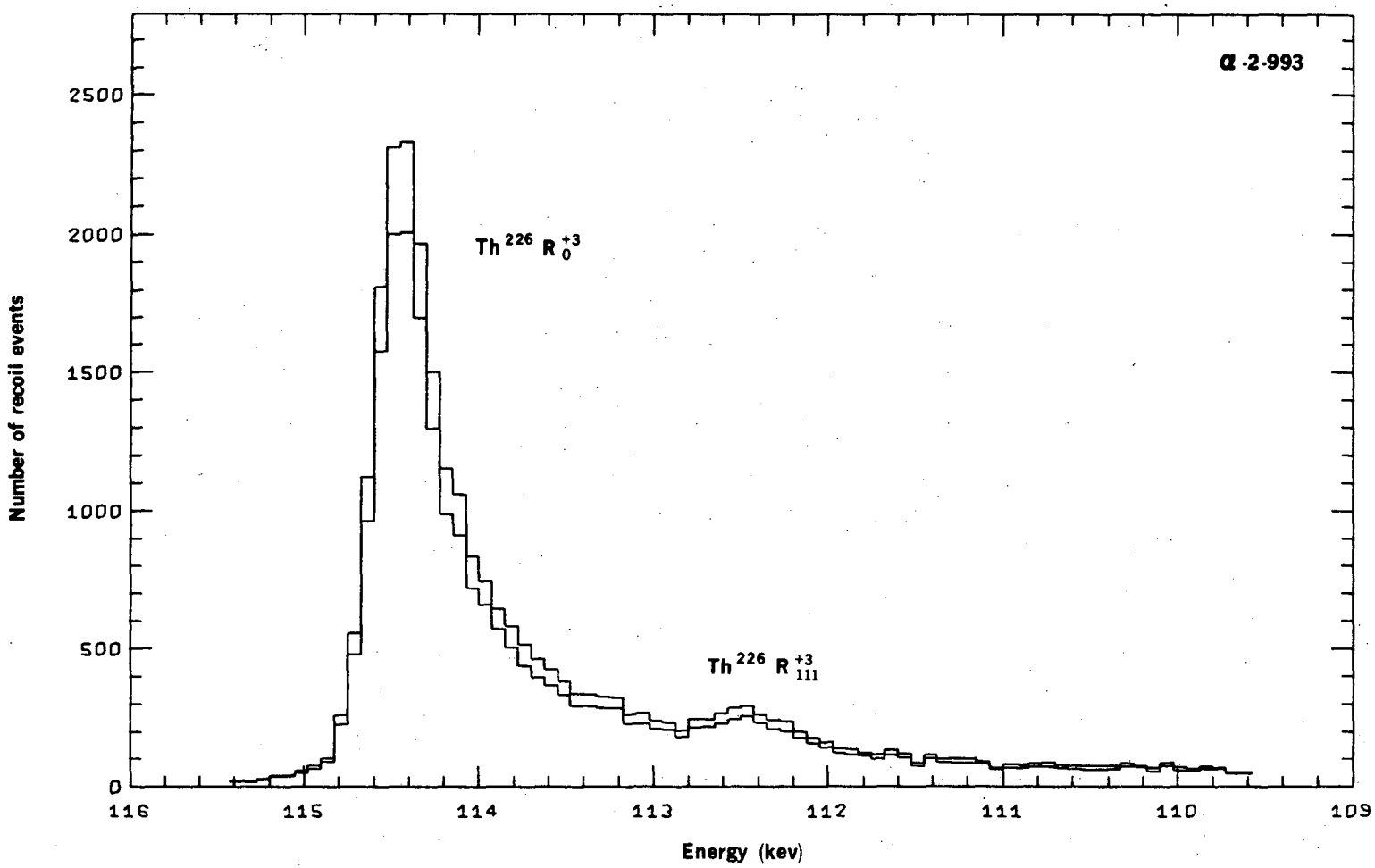

XBL 687-1235

Figure 53. $Th^{226}R^{+3}$ spectrum taken with alpha particle spectrograph in "regular plate" configuration. The lower curve shows 2-pronged events only, and the upper curve shows 2- plus 3-pronged events.

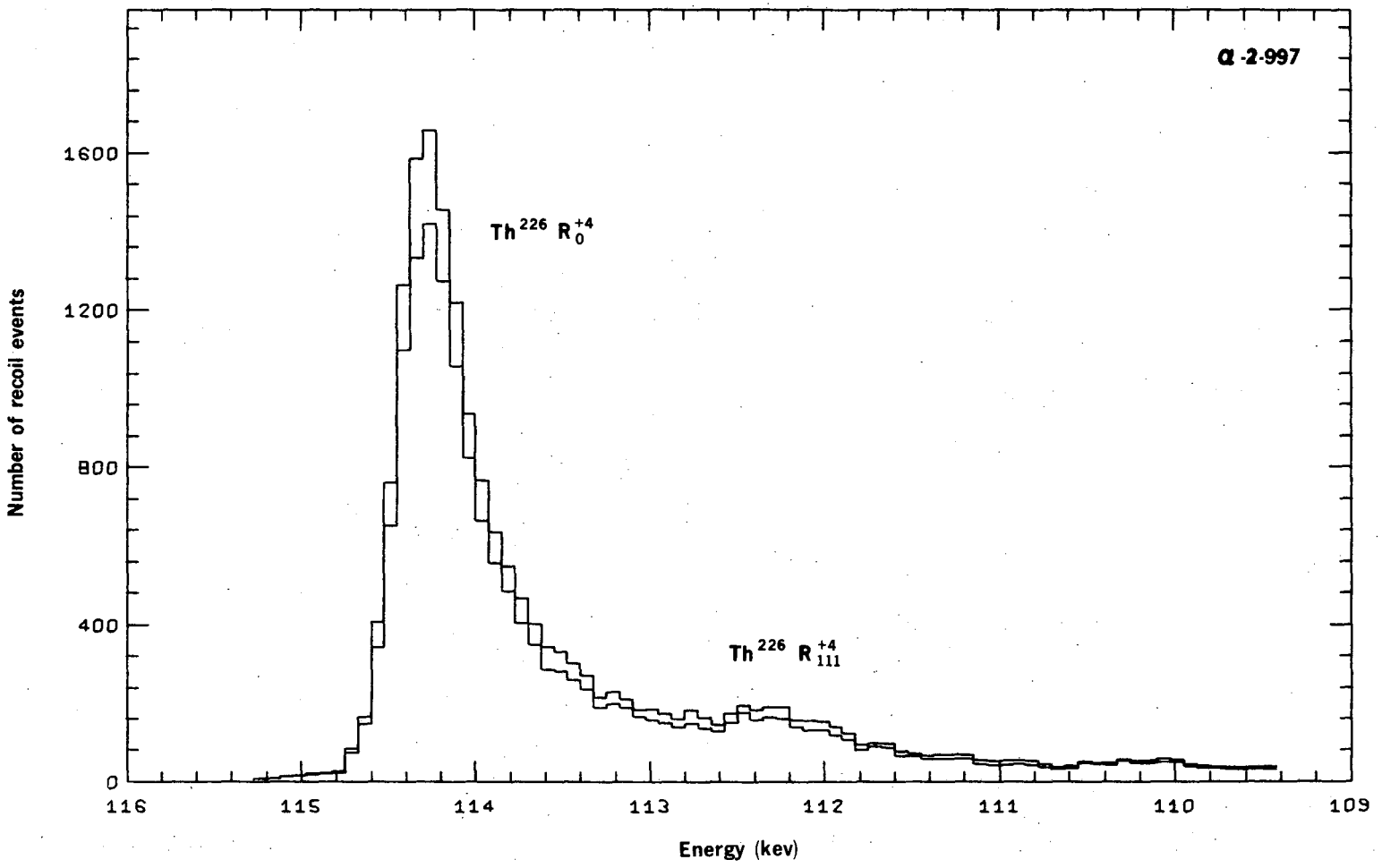

XBL 687-1234

Figure 54. $Th^{226}R^{+4}$ spectrum taken with alpha particle spectrograph in "regular plate" configuration. The lower curve shows 2-pronged events only, and the upper curve shows 2- plus 3-pronged events.

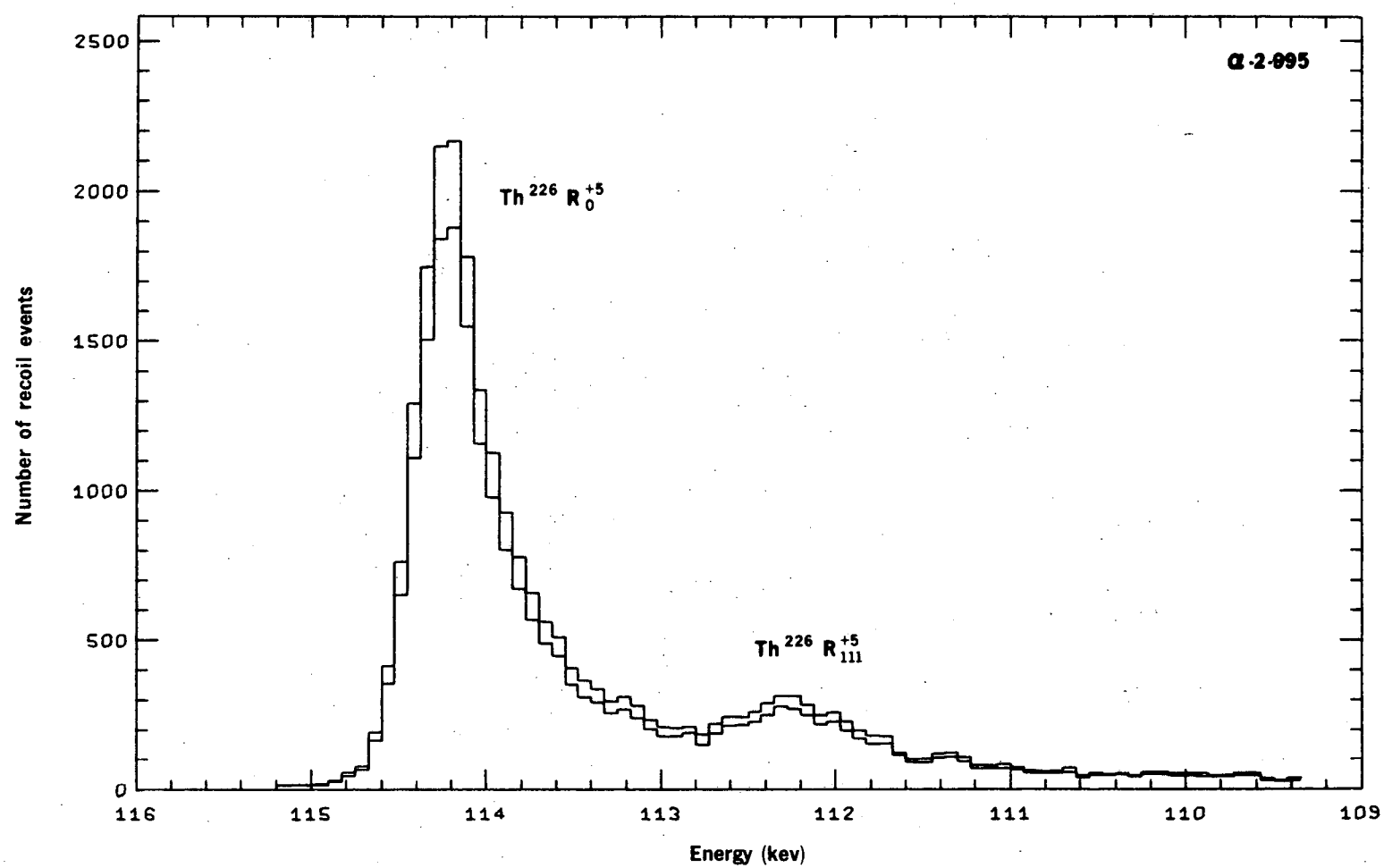

XBL 687-1233

Figure 55. $Th^{226}R^{+5}$ spectrum taken with alpha particle spectrograph in "regular plate" configuration. The lower curve shows 2-pronged events only, and the upper curve shows 2- plus 3-pronged events.

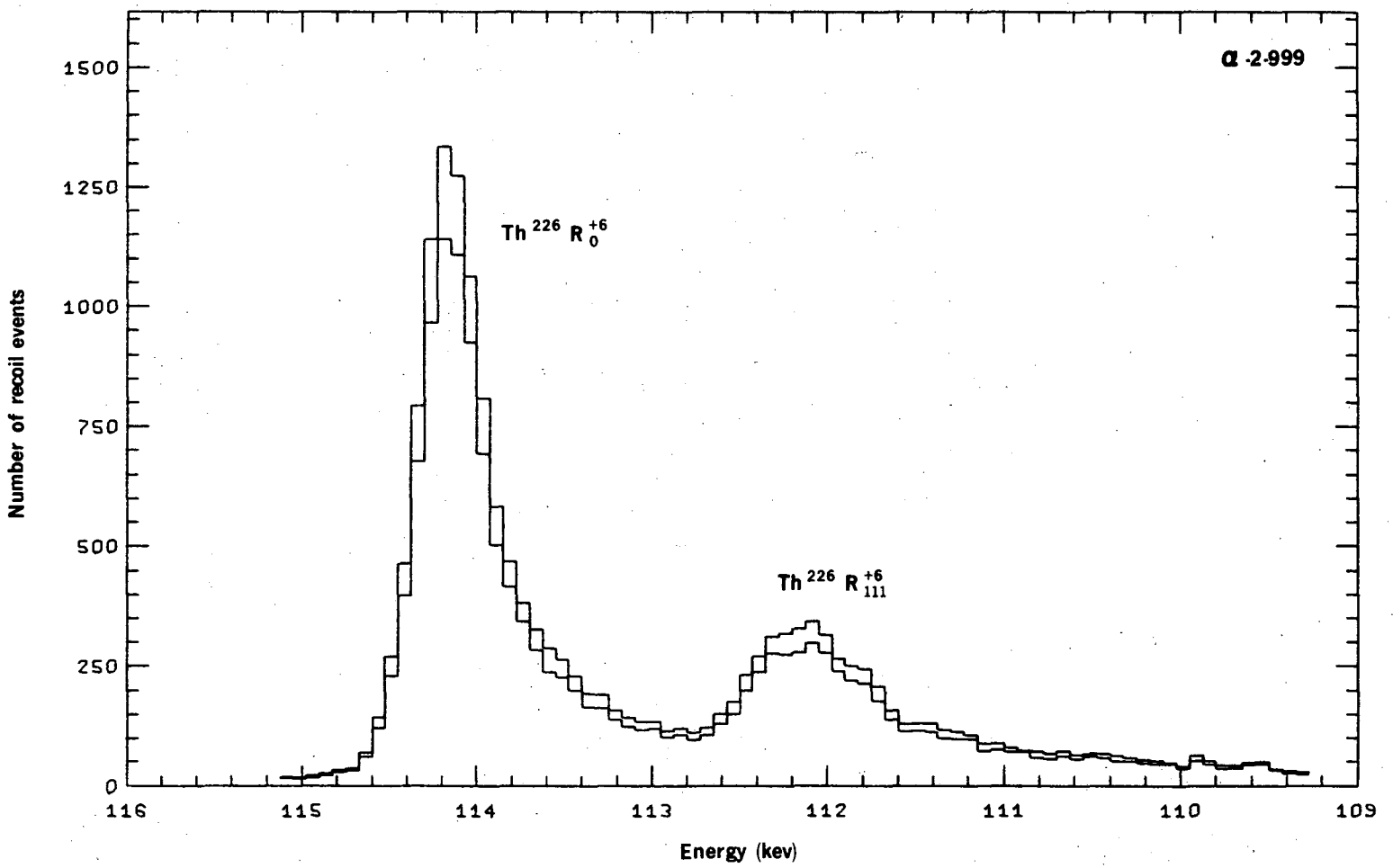

XBL 687-1232

Figure 56. $Th^{226}R^{+6}$ spectrum taken with alpha particle spectrograph in "regular plate" configuration. The lower curve shows 2-pronged events only, and the upper curve shows 2- plus 3-pronged events.

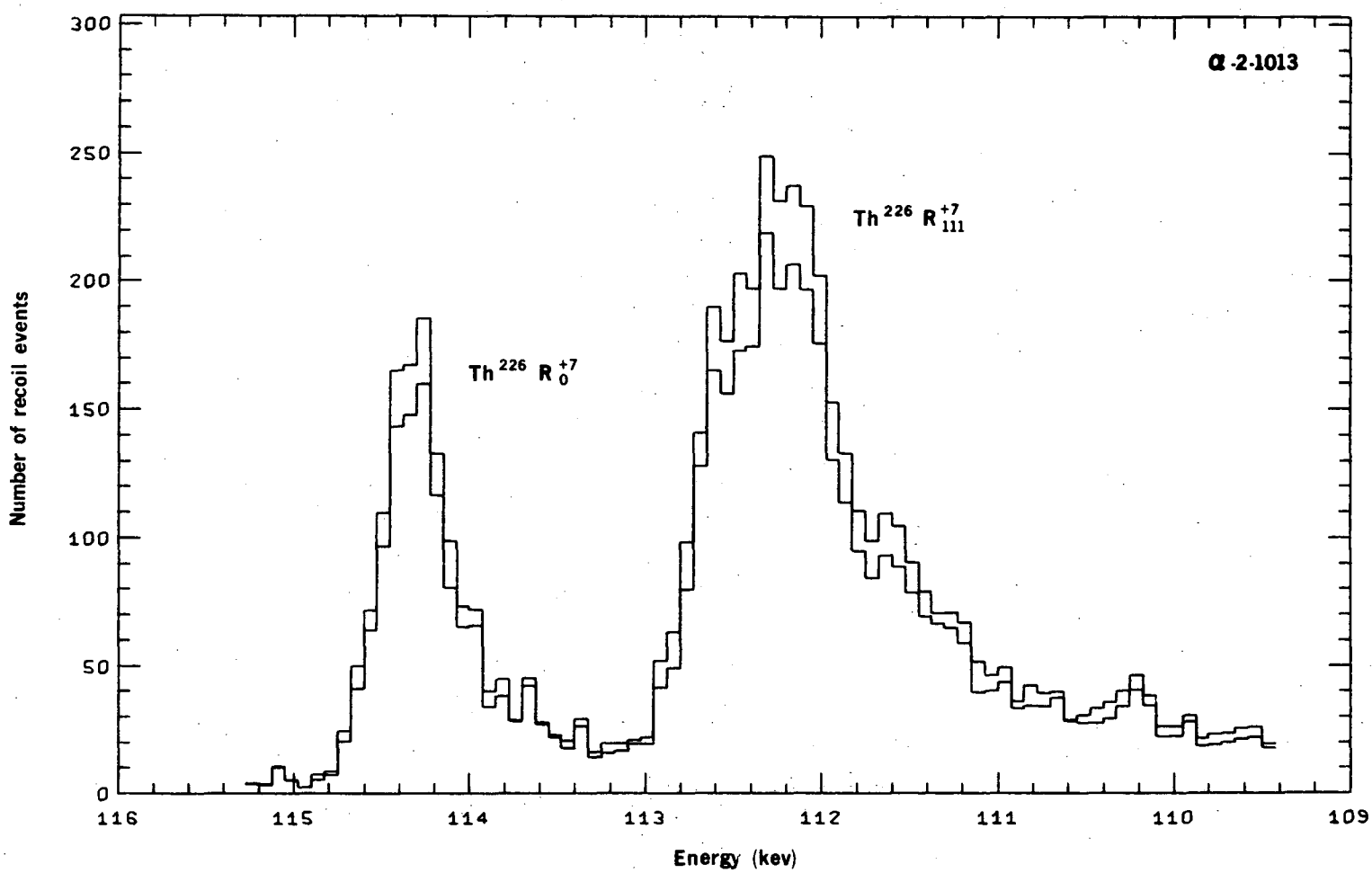

XBL 687-1231

Figure 57. $Th^{226}R^{+7}$ spectrum taken with alpha particle spectrograph in "regular plate" configuration. The lower curve shows 2-pronged events only, and the upper curve shows 2- plus 3-pronged events.

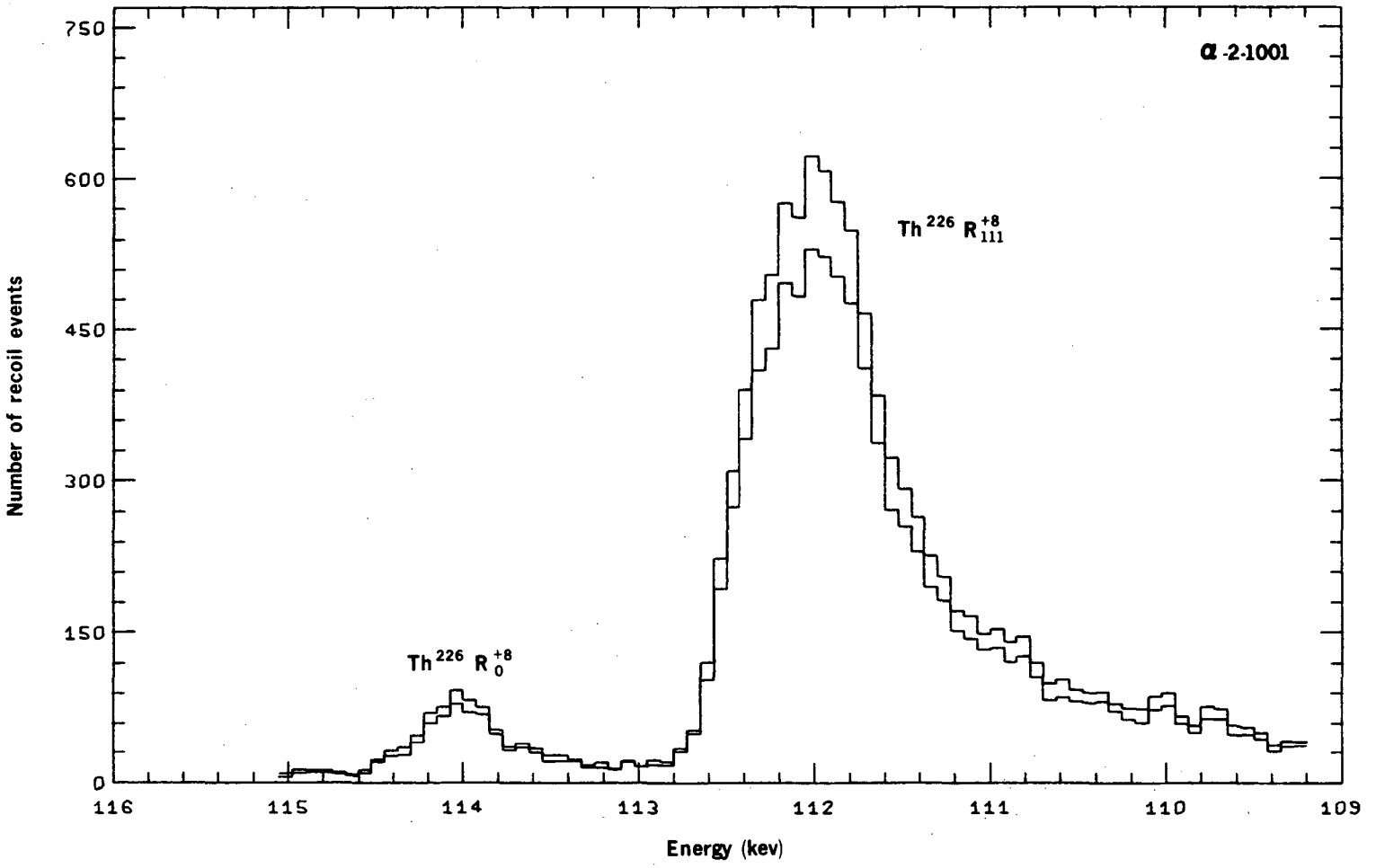

XBL 687-1230

Figure 58. $Th^{226}R^{+8}$ spectrum taken with alpha particle spectrograph in "regular plate" configuration. The lower curve shows 2-pronged events only, and the upper curve shows 2- plus 3-pronged events.

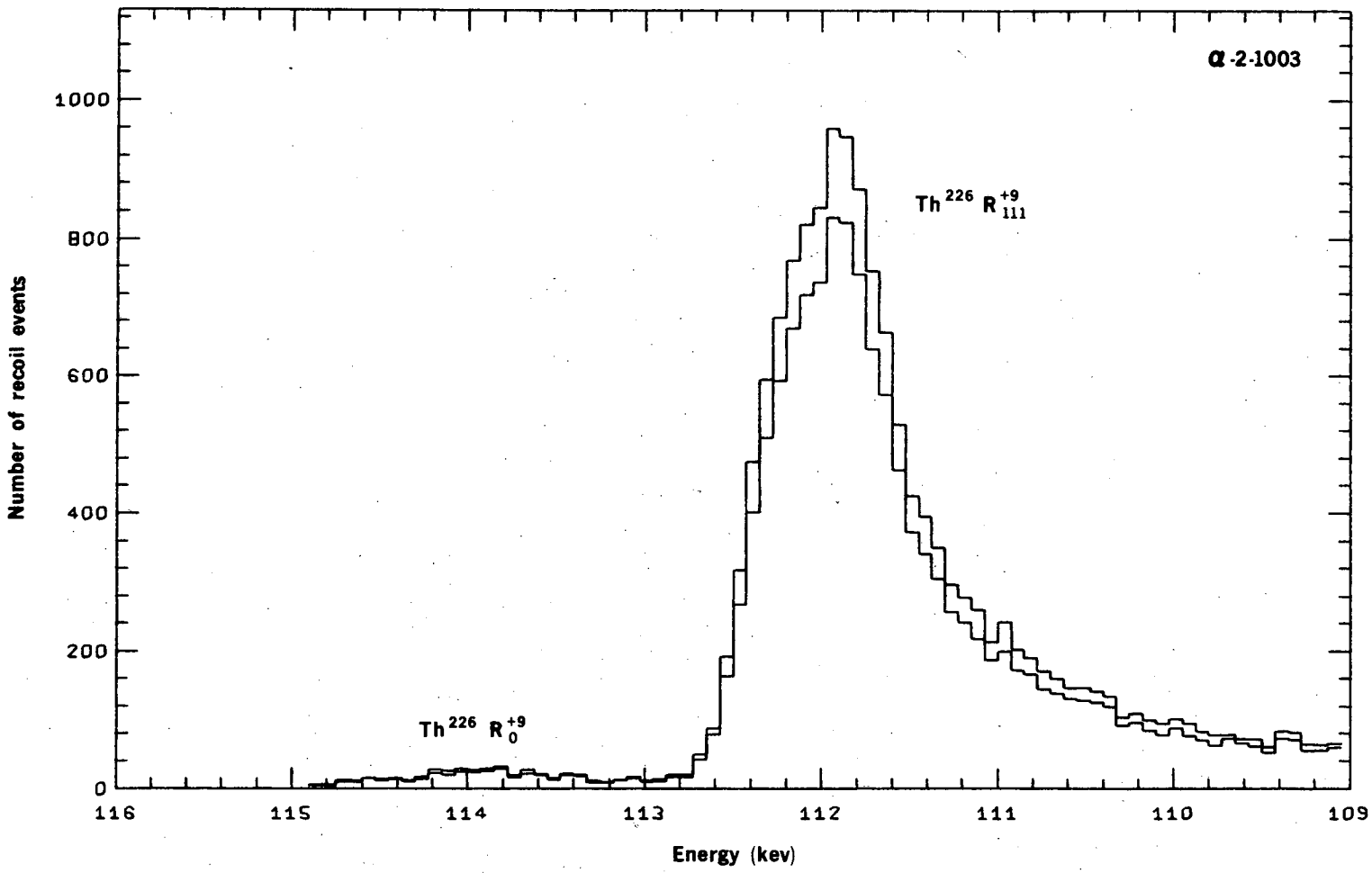

XBL 687-1229

Figure 59. $Th^{226}R^{+9}$ spectrum taken with alpha particle spectrograph in "regular plate" configuration. The lower curve shows 2-pronged events only, and the upper curve 2- plus 3-pronged events.

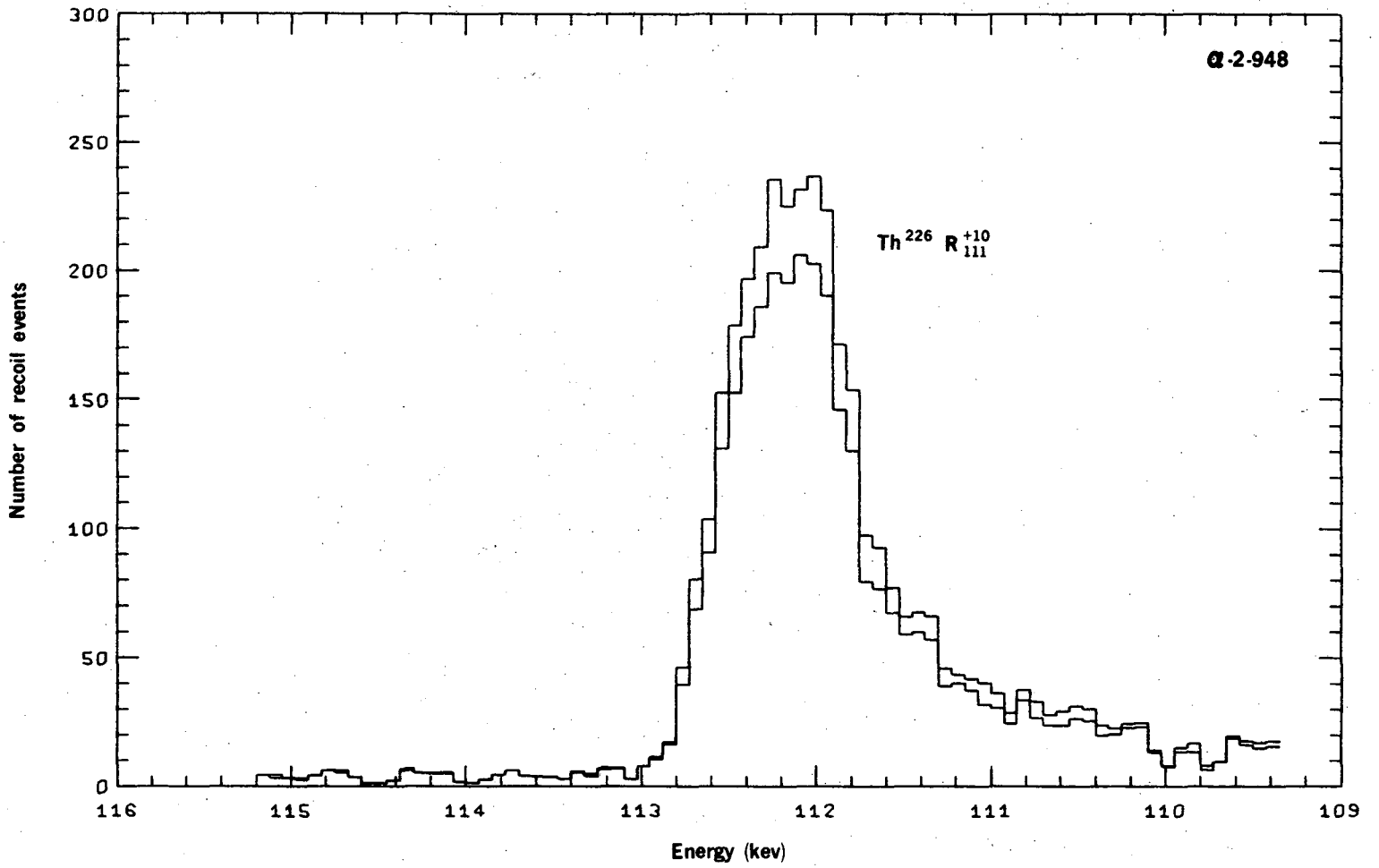

XBL 687-1228

Figure 60. $Th^{226}R^{+10}$ spectrum taken with alpha particle spectrograph in "regular plate" configuration. The lower curve shows 2-pronged events only, and the upper curve shows 2- plus 3-pronged events.

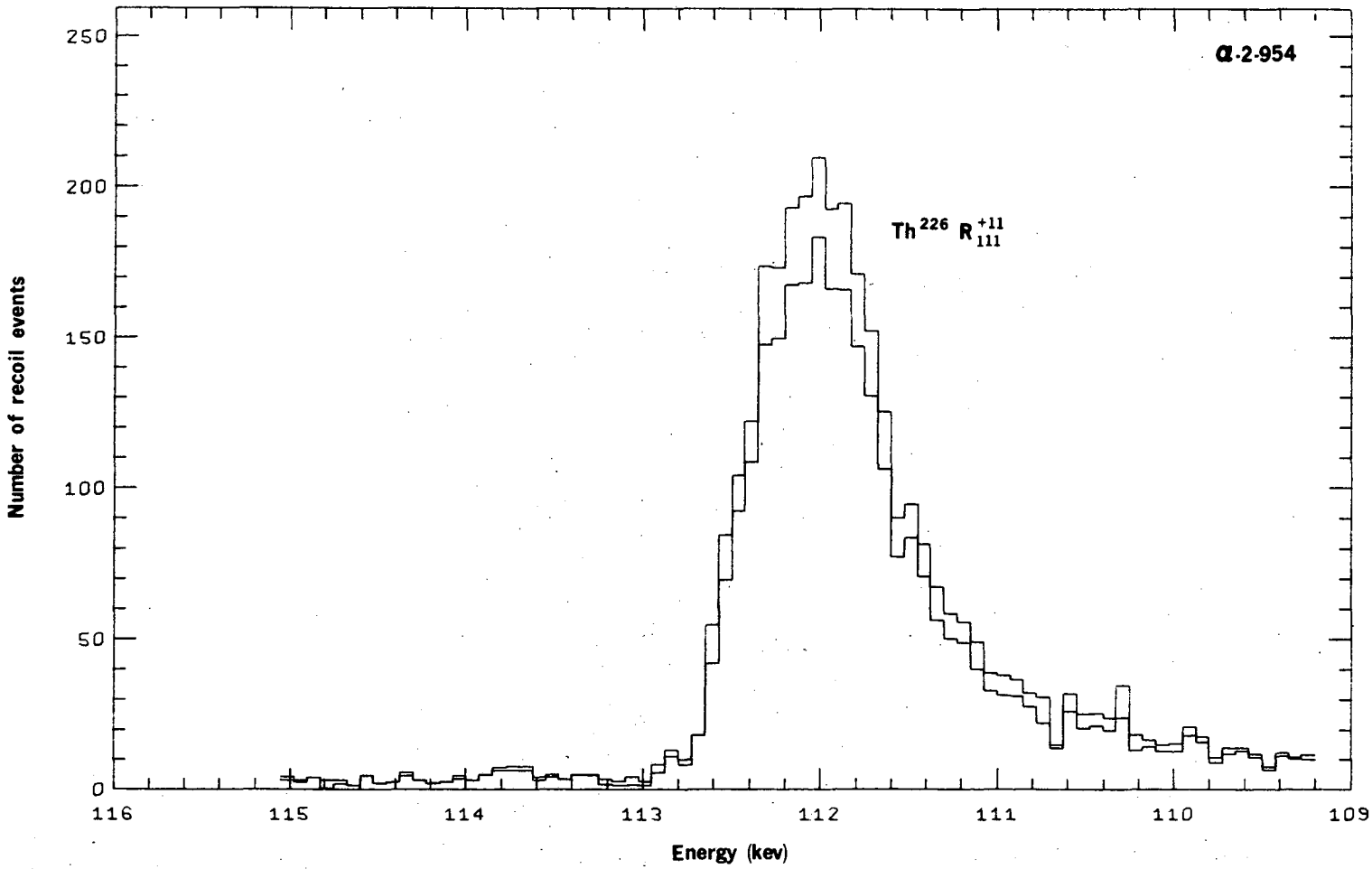

XBL 687-1248

Figure 61. $Th^{226}R^{+11}$ spectrum taken with alpha particle spectrograph in "regular plate" configuration. The lower curve shows 2-pronged events only, and the upper curve shows 2- plus 3-pronged events.

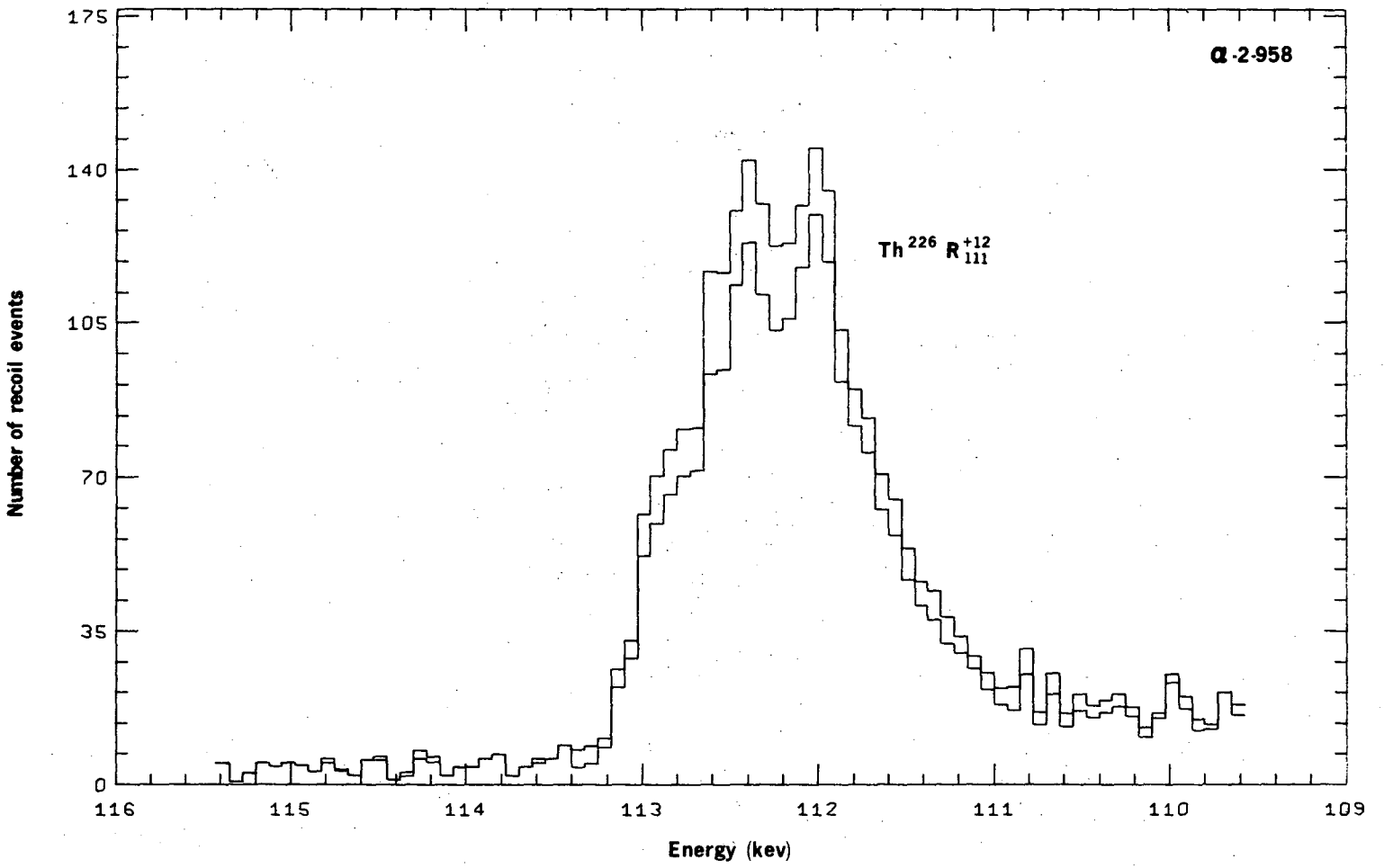

XBL 687-1247

Figure 62. $Th^{226}R^{+12}$ spectrum taken with alpha particle spectrograph in "regular plate" configuration. The lower curve shows 2-pronged events only, and the upper curve shows 2- plus 3-pronged events.

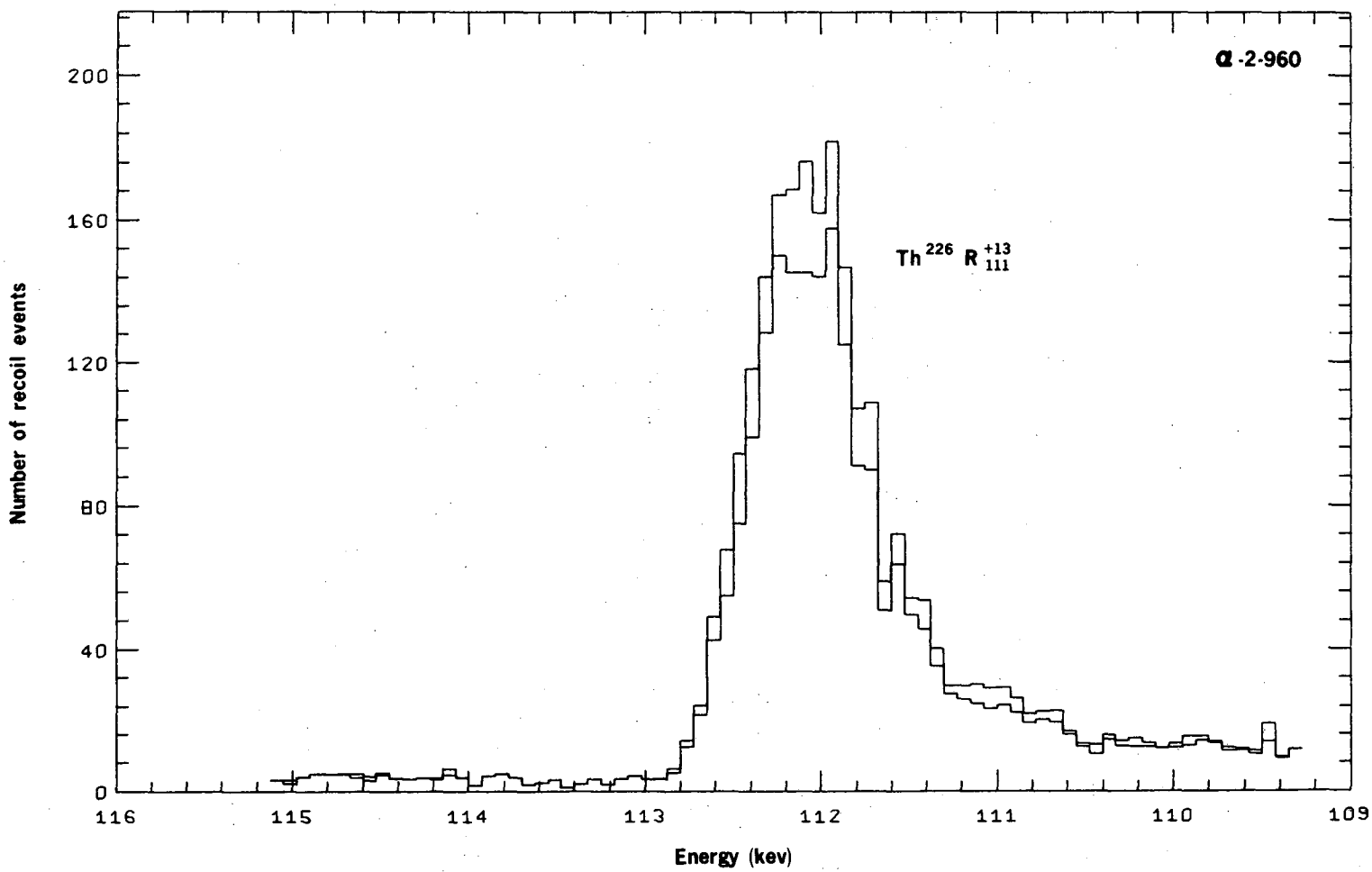

XBL 687-1246

Figure 63. $Th^{226}R^{+13}$ spectrum taken with alpha particle spectrograph in "regular plate" configuration. The lower curve shows 2-pronged events only, and the upper curve shows 2- plus 3-pronged events.

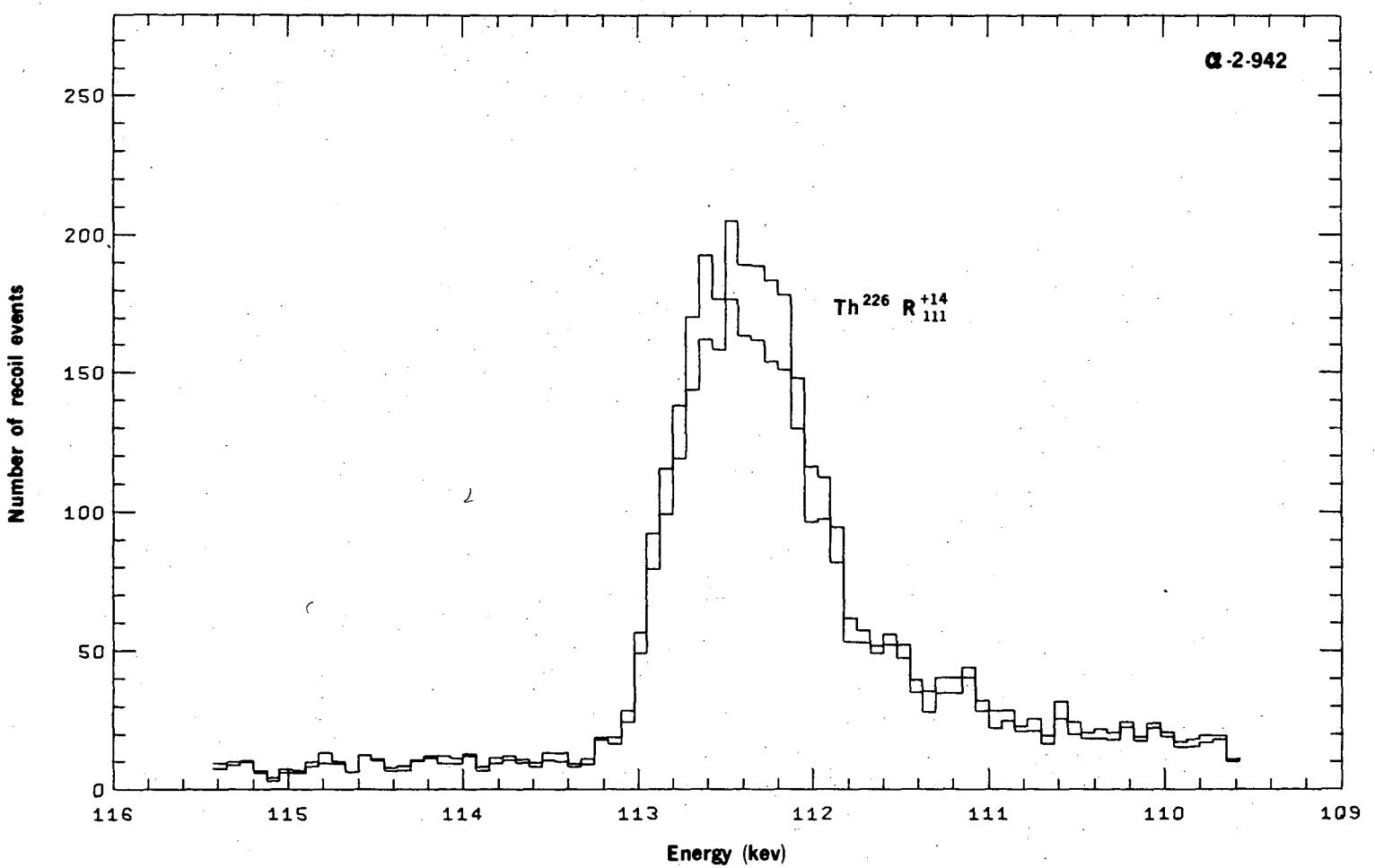

XBL 687-1245

Figure 64. $Th^{226}R^{+14}$ spectrum taken with alpha particle spectrograph in "regular plate" configuration. The lower curve shows 2-pronged events only, and the upper curve shows 2- plus 3-pronged events.

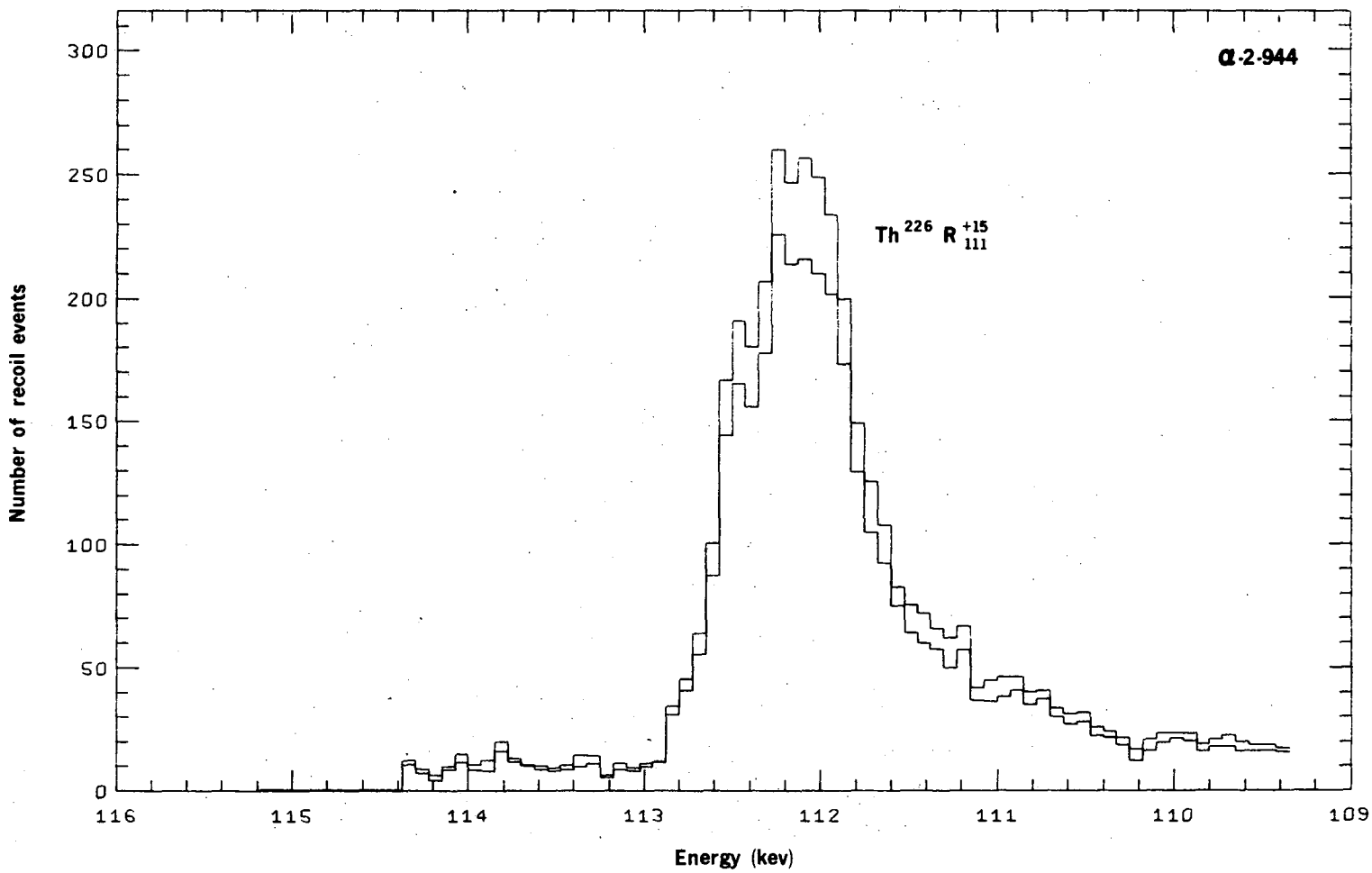

XBL 687-1244

Figure 65. $Th^{226}R^{+15}$ spectrum taken with alpha particle spectrograph in "regular plate" configuration. The lower curve shows 2-pronged events only, and the upper curve shows 2- plus 3-pronged events.

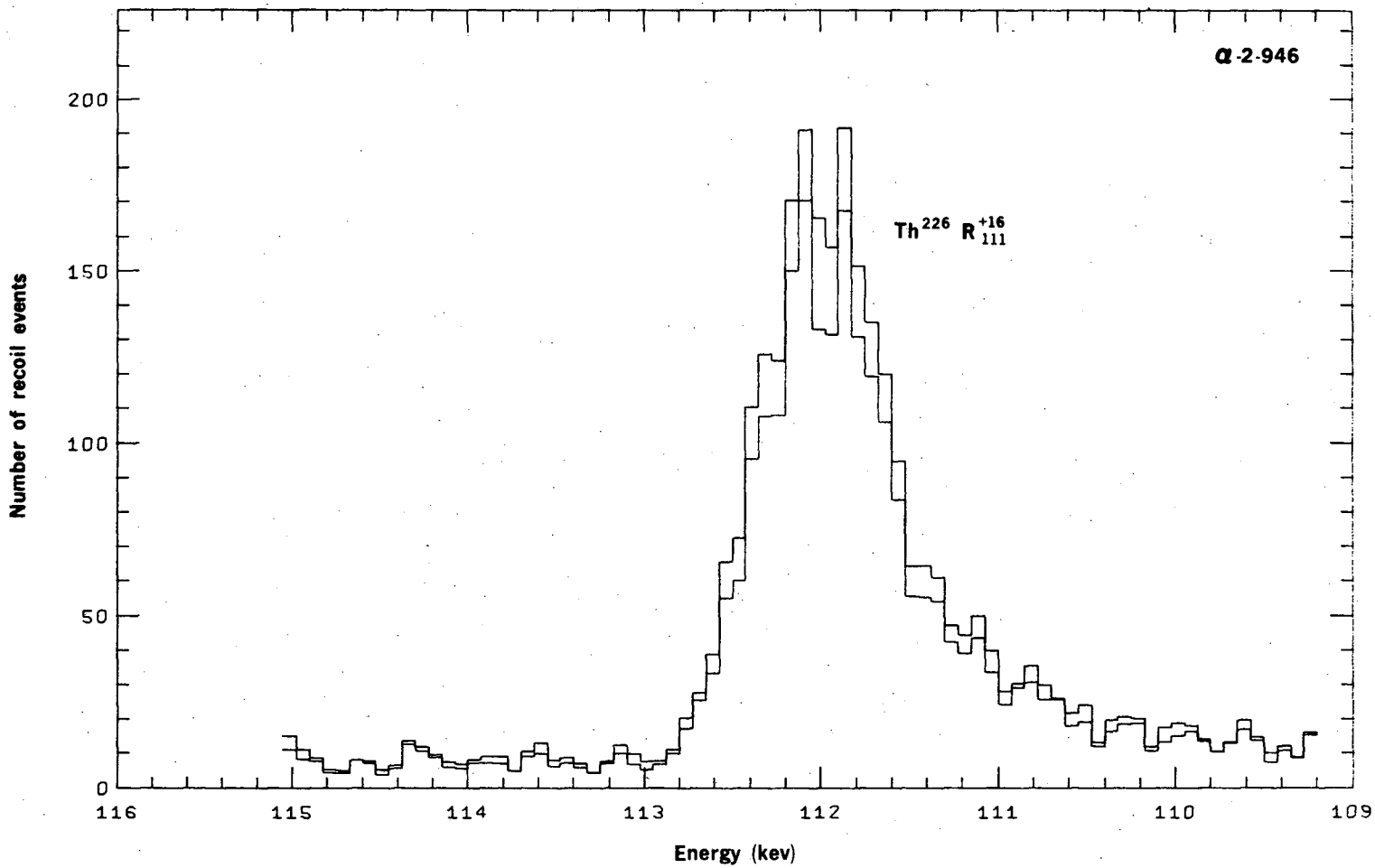

XBL 687-1243

Figure 66. $Th^{226}R^{+16}$ spectrum taken with alpha particle spectrograph in "regular plate" configuration. The lower curve shows 2-pronged events only, and the upper curve shows 2- plus 3-pronged events.

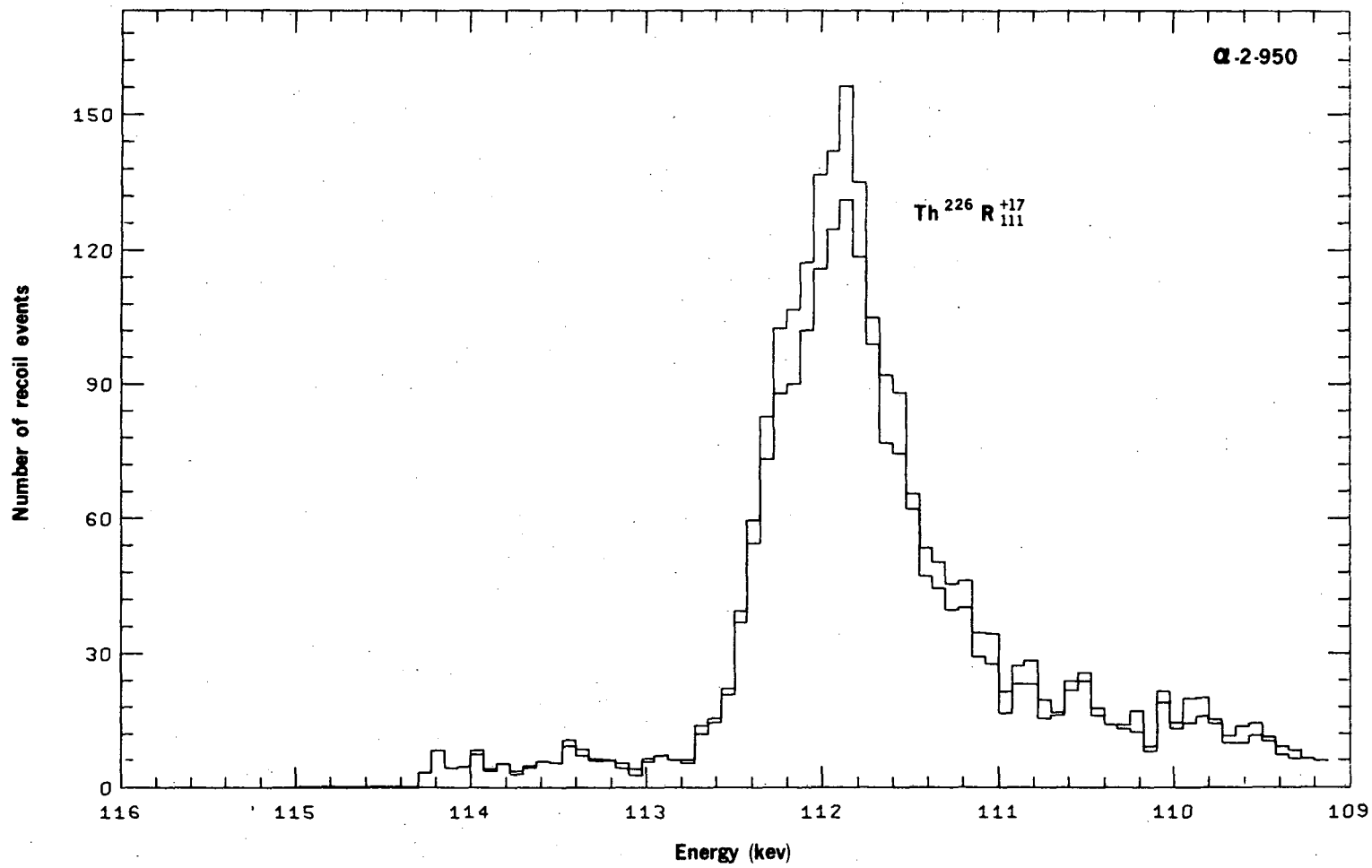

XBL 687-1242

Figure 67. $Th^{226}R^{+17}$ spectrum taken with alpha particle spectrograph in "regular plate" configuration. The lower curve shows 2-pronged events only, and the upper curve shows 2- plus 3-pronged events.

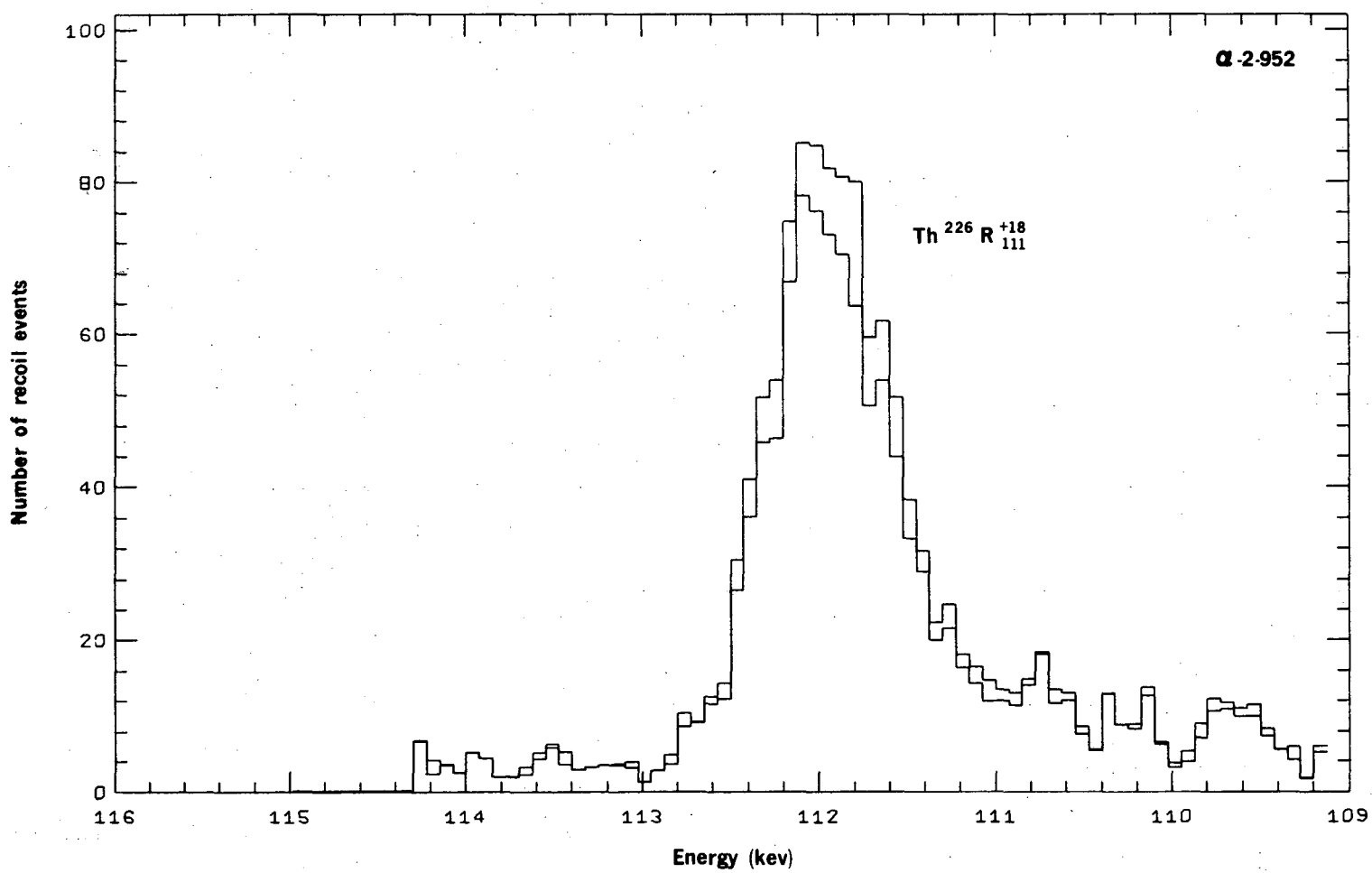

XBL 687-1241

Figure 68. $Th^{226}R^{+18}$ spectrum taken with alpha particle spectrograph in "regular plate" configuration. The lower curve shows 2-pronged events only, and the upper curve shows 2- plus 3-pronged events.

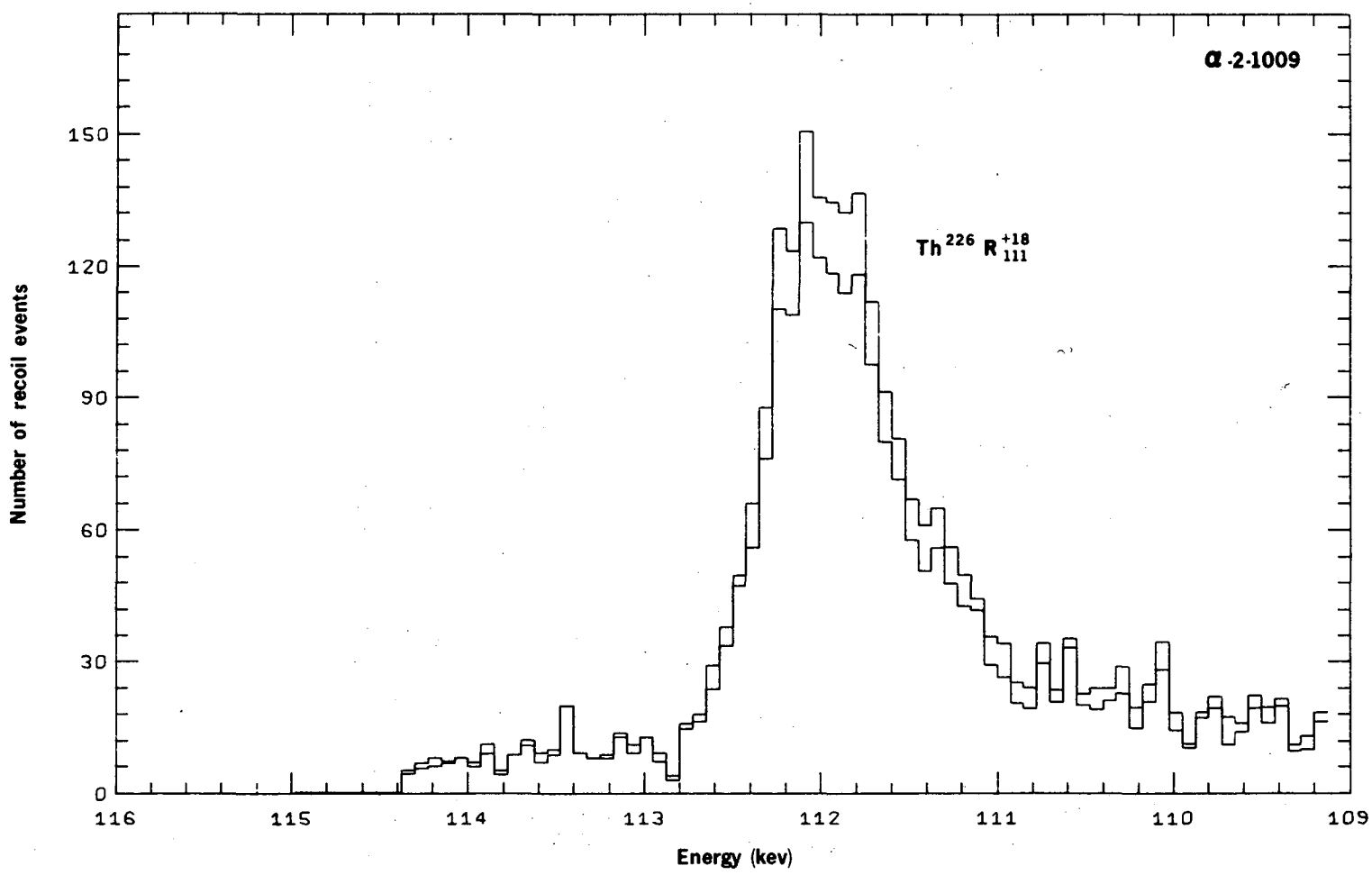

XBL 687-1240

Figure 69. $Th^{226}R^{+18}$ spectrum taken with alpha particle spectrograph in "regular plate" configuration. The lower curve shows 2-pronged events only, and the upper curve shows 2- plus 3-pronged events.

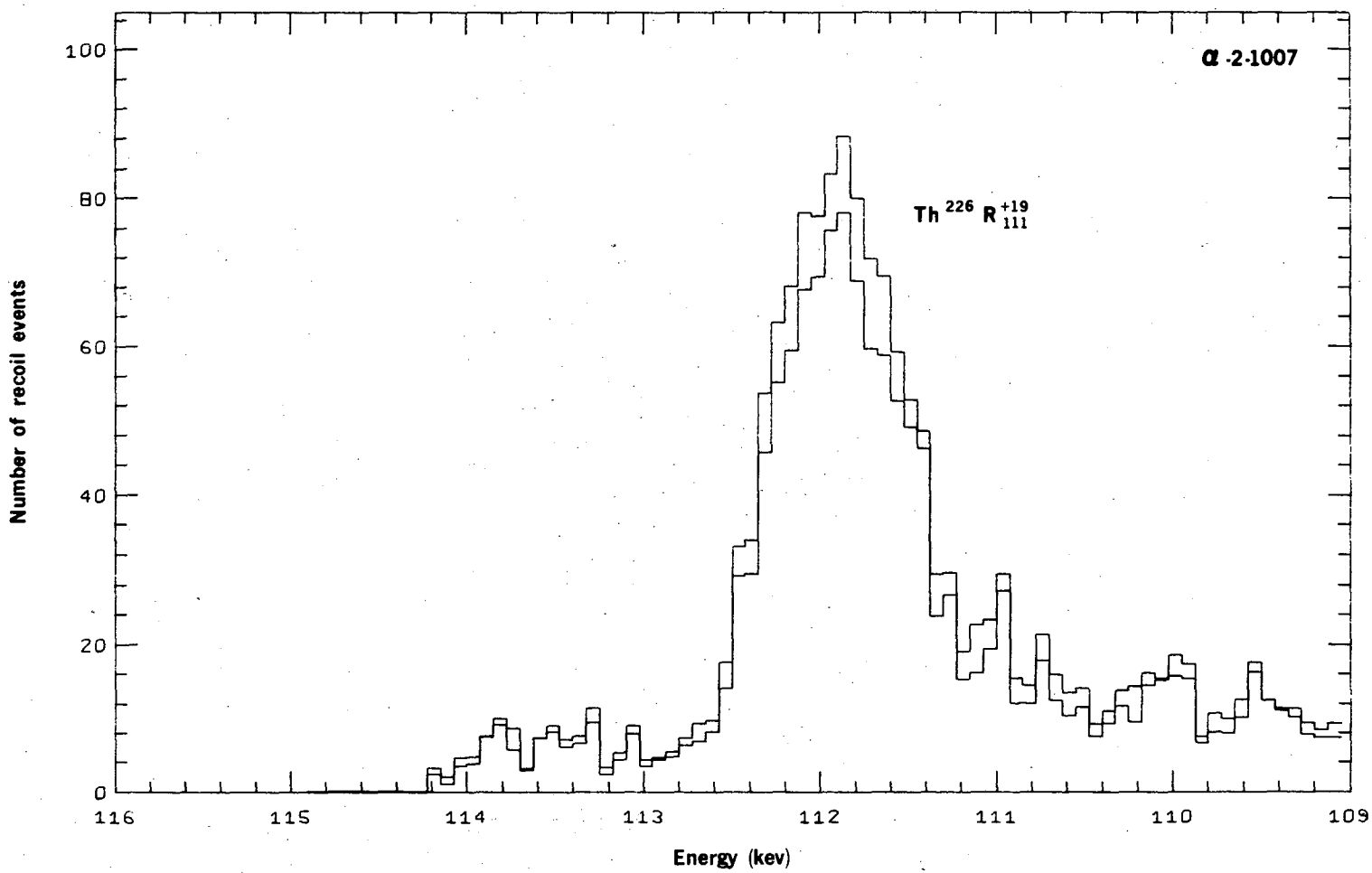

XBL 687-1226

Figure 70. $Th^{226}R^{19}$ spectrum taken with alpha particle spectrograph in "regular plate" configuration. The lower curve shows 2-pronged events only, and the upper curve shows 2- plus 3-pronged events.

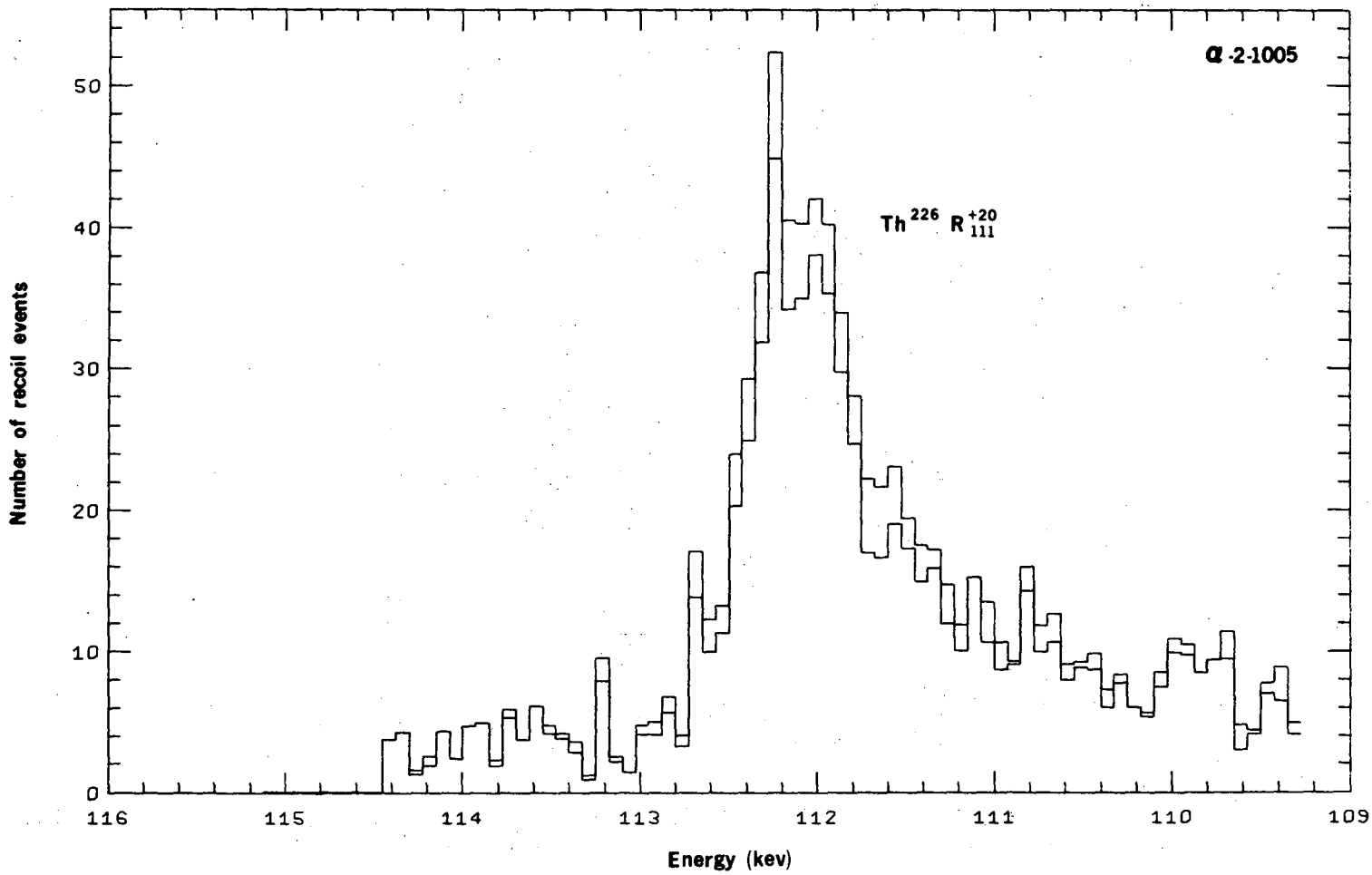

XBL 687-1227

Figure 71. $Th^{226}R^{+20}$ spectrum taken with alpha particle spectrograph in "regular plate" configuration. The lower curve shows 2-pronged events only, and the upper curve shows 2- plus 3-pronged events.

counting the $Th^{226}\alpha_0$ for ratio purposes in addition to the fact that more intense alpha peaks make it impossible to distinguish the recoils associated with them. The existence of these four peaks makes it possible to compare the variation in charge and energy distributions for completely different sources. This was also the purpose in including two $Th^{226}R^{+18}$ spectra. Each of these spectra except the one for Th^{226} R^{+12} accurately reflects the actual energy distributions even though the half width is the composite of the half width due to the physical width of the source and the "intrinsic" half width of the recoil peak because the physical half width is always less than half the "intrinsic" half width. The $Th^{226}R^{+12}$ spectrum is an exception to this because a field change occurred during the time the spectrum was being made which caused broadening of the peak beyonds its "intrinsic" half width.

The $Th^{226}R^{+n}$ spectra are composed of the following three peaks: $Th^{226}R_0{}^{+n}$, $Th^{226}R_{111\gamma}{}^{+n}$ and $Th^{226}R_{111e}{}^{+n}$. Thus in order to discuss the charge and energy distributions of these three recoil groups, it is necessary to find some means of separating them. In order to do this the following assumptions were made:

1) $Th^{226}R_0$ and $Th^{226}R_{111\gamma}$ have exactly the same charge and energy distribution except that the energy peak of $Th^{226}R_{111\gamma}$ is displaced towards lower energies by the difference in the initial recoil energies of 2 keV which is small compared with the 114 keV. This assumption is justified by the fact that the charge and energy distributions are the result of atomic processes which can not distinguish between a nucleus which is excited and one that is not. Since for $Th^{226}R_{111\gamma}$, the nucleus de-excites by the emission of a gamma ray, the atomic electrons will not be affected by the de-excitation process either.

2) The energy distribution of $Th^{226}R_{111e}{}^{+n}$ is the same regardless of the value of n. This assumption appears to be confirmed by a comparison of the energy distributions of $Th^{226}R_{111e}{}^{+n}$ for n = +10 through +20 with the exception of n = +12. These energy distributions are clearly all that appears in the $Th^{226}R^{+n}$ spectra for $n \geq +10$. (See Figs. 60 through 71 and compare them with Fig. 59, for example.)

3) The low energy distribution side of any peak should be a smoothly descending curve.

Using these three assumptions and the fact that $Th^{226}\alpha_{111\gamma}/Th^{226}\alpha_0 = \frac{.0288}{.761} = 0.0378$, the separation of $Th^{226}R_0$, $Th^{226}R_{111\gamma}$ and $Th^{226}R_{111e}$ was accomplished in the following way. The background was removed from all of the data since it can affect the shape of the low energy tail. The composite peak $Th^{226}R^{+3} + Th^{226}R^{+4}$ was assumed to contain no $Th^{226}R_{111e}$ and so the $Th^{226}R_{111\gamma}$ component was removed from the peak by assuming that it had exactly the same shape as $Th^{226}R_0$ reduced by a factor of 0.0378 and shifted down in energy by 2 keV. This resulted in an "ideal" $Th^{226}R_0$ tail. The $Th^{226}R_0{}^{+9}$ peak was then assumed to have the same shape tail and it was used to remove the $Th^{226}R_0{}^{+9}$ and $Th^{226}R_{111\gamma}{}^{+9}$ peaks from the $Th^{226}R^{+9}$ spectrum leaving the $Th^{226}R_{111e}{}^{+9}$ energy distribution. This energy distribution was then used as the "ideal" $Th^{226}R_{111e}$ energy distribution because it had the best statistics of the $Th^{226}R_{111e}$ peaks. This peak was then used to remove the $Th^{226}R_{111e}$ component from the $Th^{226}R_{111e}{}^{+5}$ spectrum by assuming various heights and positions for the $Th^{226}R_{111e}{}^{+5}$ peak, removing a $Th^{226}R_{111e}$ of this height and position, removing the $Th^{226}R_{111\gamma}{}^{+5}$ as discussed above and then assuming that the correct height and position would yield a tail on the $Th^{226}R_0{}^{+5}$ peak that best fit assumption No. 3. This process yielded a new "ideal" $Th^{226}R_0$ tail which was used to find a new "ideal"

$Th^{226}R_{111e}$ energy distribution from the $Th^{226}R^{+9}$ spectrum. This process was then repeated twice more yielding the energy distribution of $Th^{226}R_{111e}{}^{+9}$ shown in Fig. 72, which was assumed to be the "ideal" $Th^{226}R_{111e}$ energy distribution, and also yielding the energy distribution of $Th^{226}R_0{}^{+5}$ shown in Fig. 73. This "ideal" $Th^{226}R_{111e}$ spectrum was then used to find the $Th^{226}R_0{}^{+n}$ spectra for n = +2 through +6 in the same way that $Th^{226}R_0{}^{+5}$ was found, i.e. the $Th^{226}R_{111e}{}^{+n}$ spectra for n = +2 through +6 was assumed to have exactly the same energy distribution as $Th^{226}R_{111e}{}^{+9}$. When a comparison was made between the $Th^{226}R_0{}^{+n}$ curves produced this way (see Figs. 73 through 76), it was noticed that $Th^{226}R_0{}^{+3}$, $Th^{226}R_0{}^{+4}$, $Th^{226}R_0{}^{+5}$ and $Th^{226}R_0{}^{+6}$ had practically the same energy distribution, particularly in the tails.

Hence, it is likely that this is also true for the tails of $Th^{226}R^{+n}$ for n = +7 and +8 which is usefull since an attempt to remove $Th^{226}R_{111e}{}^{+n}$ from the $Th^{226}R^{+n}$ spectra for n = +7 and +8 was not too successful because of the low intensity of the $Th^{226}R_0{}^{+n}$ peaks for these charges. So, the $Th^{226}R_0{}^{+n}$ spectra for n = +6, +7 and +8 were found by assuming that they all had "ideal" tails where the "ideal" tail used was that of the $Th^{226}R_0{}^{+5}$ energy distribution. (See Figs. 77, 78, and 79.) The $Th^{226}R_0{}^{+9}$ spectrum which was obtained in the same way is shown in Fig. 80.

Using these curves, it was then possible to obtain the energy distributions of $Th^{226}R_{111e}{}^{+n}$ for n = +6, +7 and +8. (See Figs. 81, 82, and 83.) The energy distributions of $Th^{226}R_{111e}{}^{+n}$ for n = +2, +3, +4 and +5 are not shown since they are identical to that of $Th^{226}R_{111e}{}^{+9}$.

Once the separation of the various spectra was accomplished, it became possible to compare their energy distributions. The following are the results.

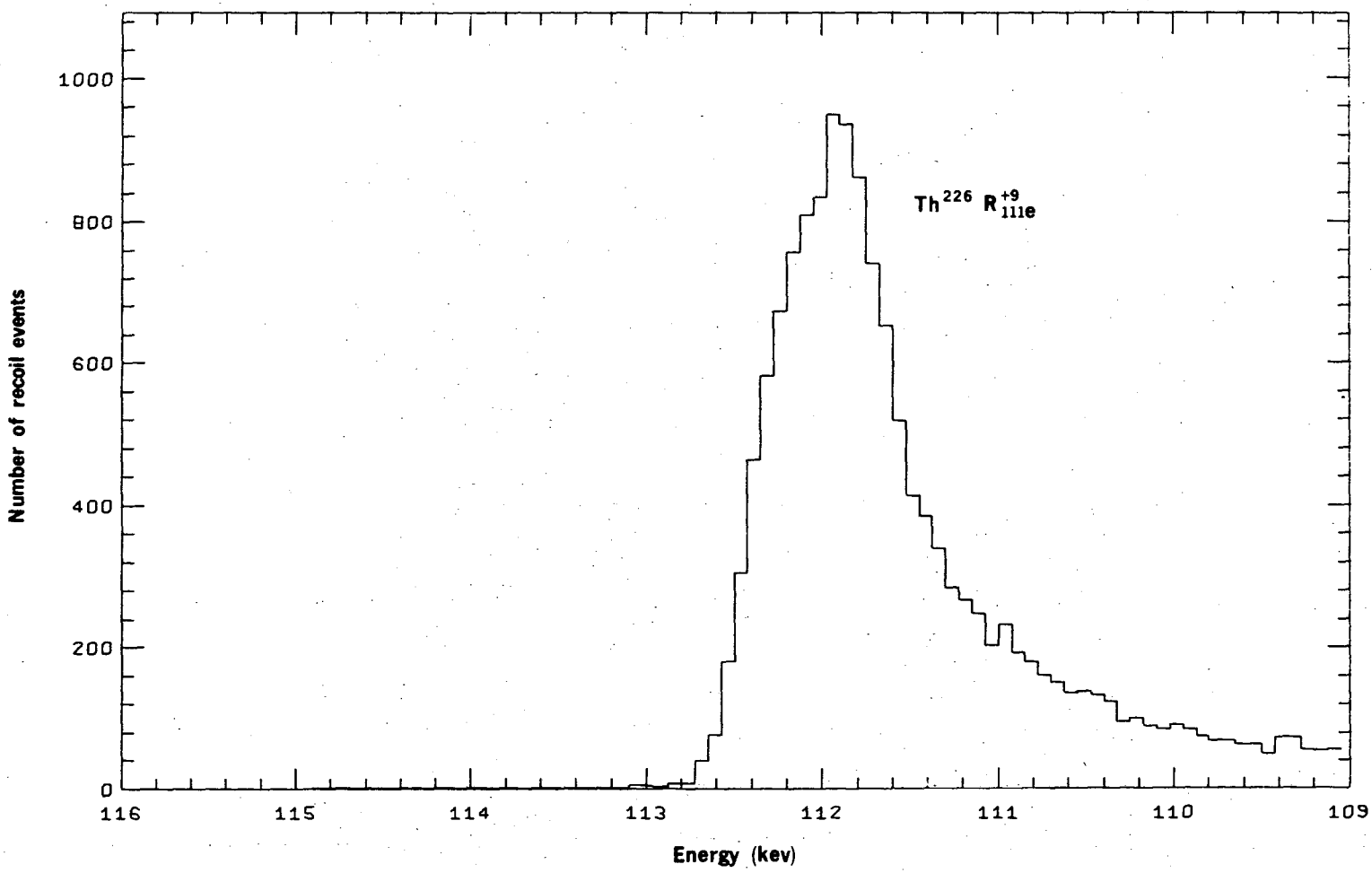

XBL 687-1249

Figure 72. $Th^{226}R_{111e}^{+9}$ spectrum which was separated from the $Th^{226}R^{+9}$ spectrum shown in Fig. 59, as discussed in the text. The number of recoil events indicated is the sum of 2- and 3-pronged events per 75 eV.

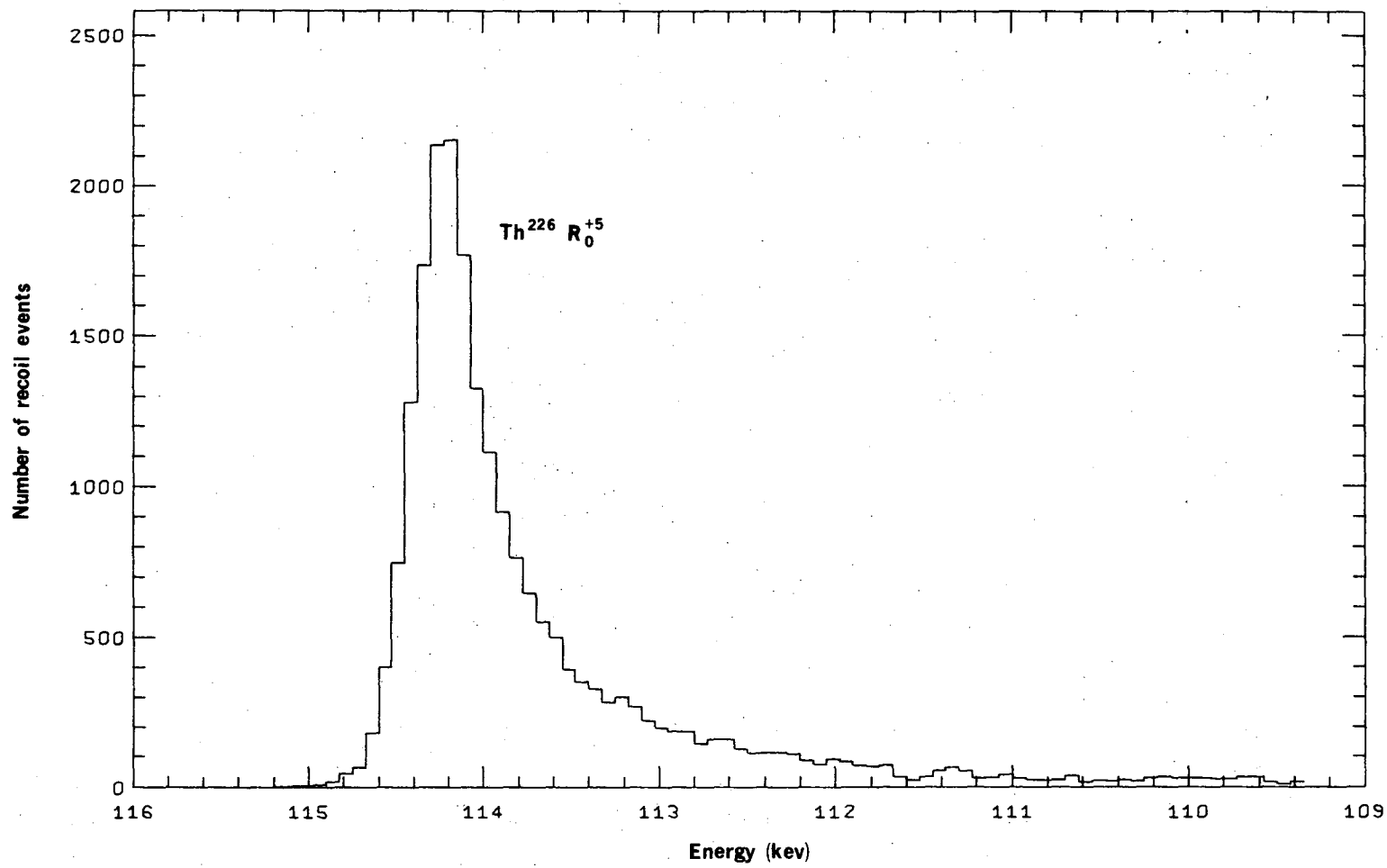

XBL 687-1258

Figure 73. $Th^{226}R_0^{+5}$ spectrum which was separated from the $Th^{226}R^{+5}$ spectrum shown in Fig. 55, as discussed in the text. The number of recoil events indicated is the sum of 2- and 3-pronged events per 75 eV.

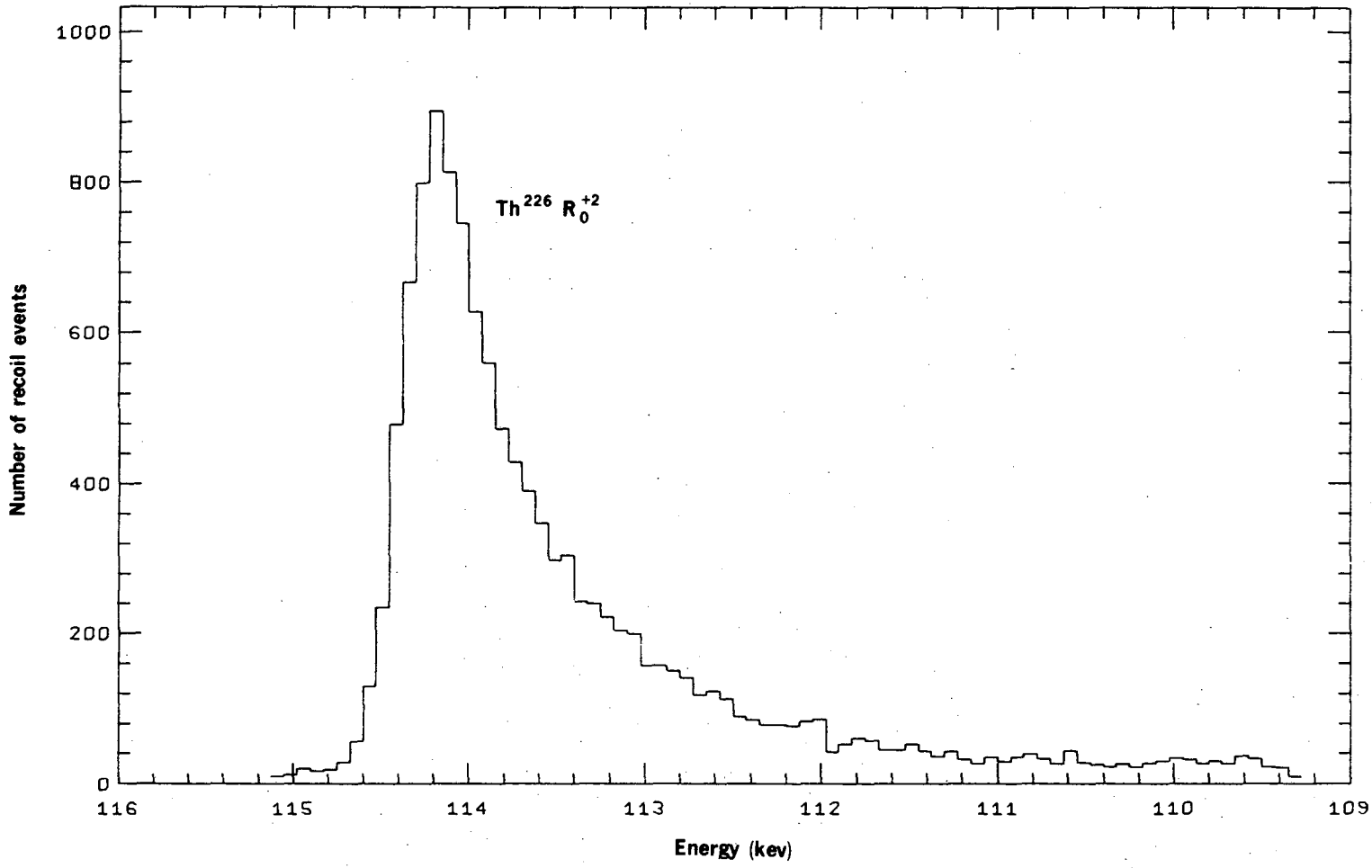

Figure 74. $Th^{226}R_0^{+2}$ spectrum which was separated from the $Th^{226}R^{+2}$ spectrum as discussed in the text. The number of recoil events indicated is the sum of 2- and 3-pronged events per 75 eV.

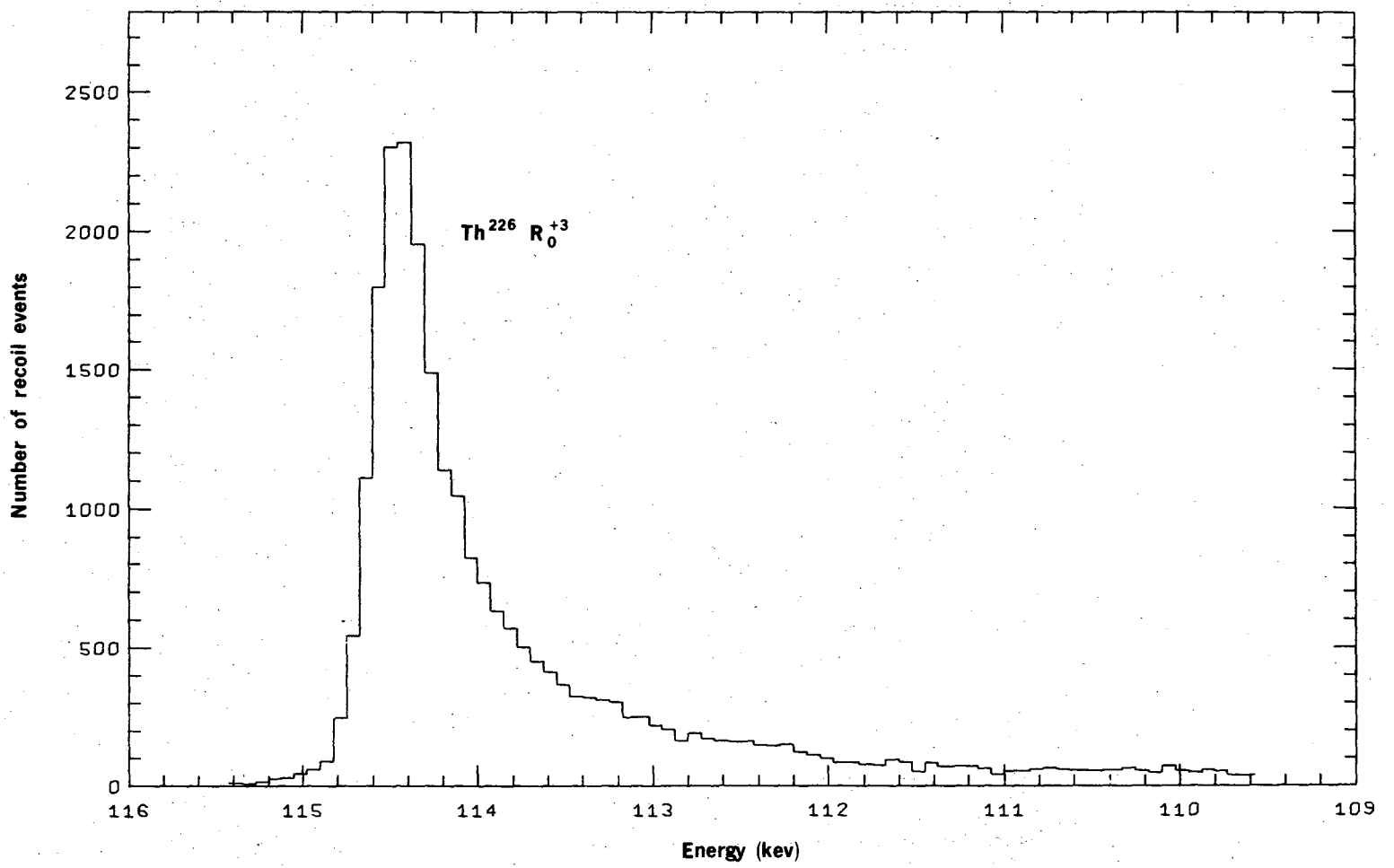

XBL 687-1262

Figure 75. $Th^{226}R_0^{+3}$ spectrum which was separated from the $Th^{226}R^{+3}$ spectrum shown in Fig. 53 as discussed in the text. The number of recoil events indicated is the sum of 2- and 3-pronged events per 75 eV.

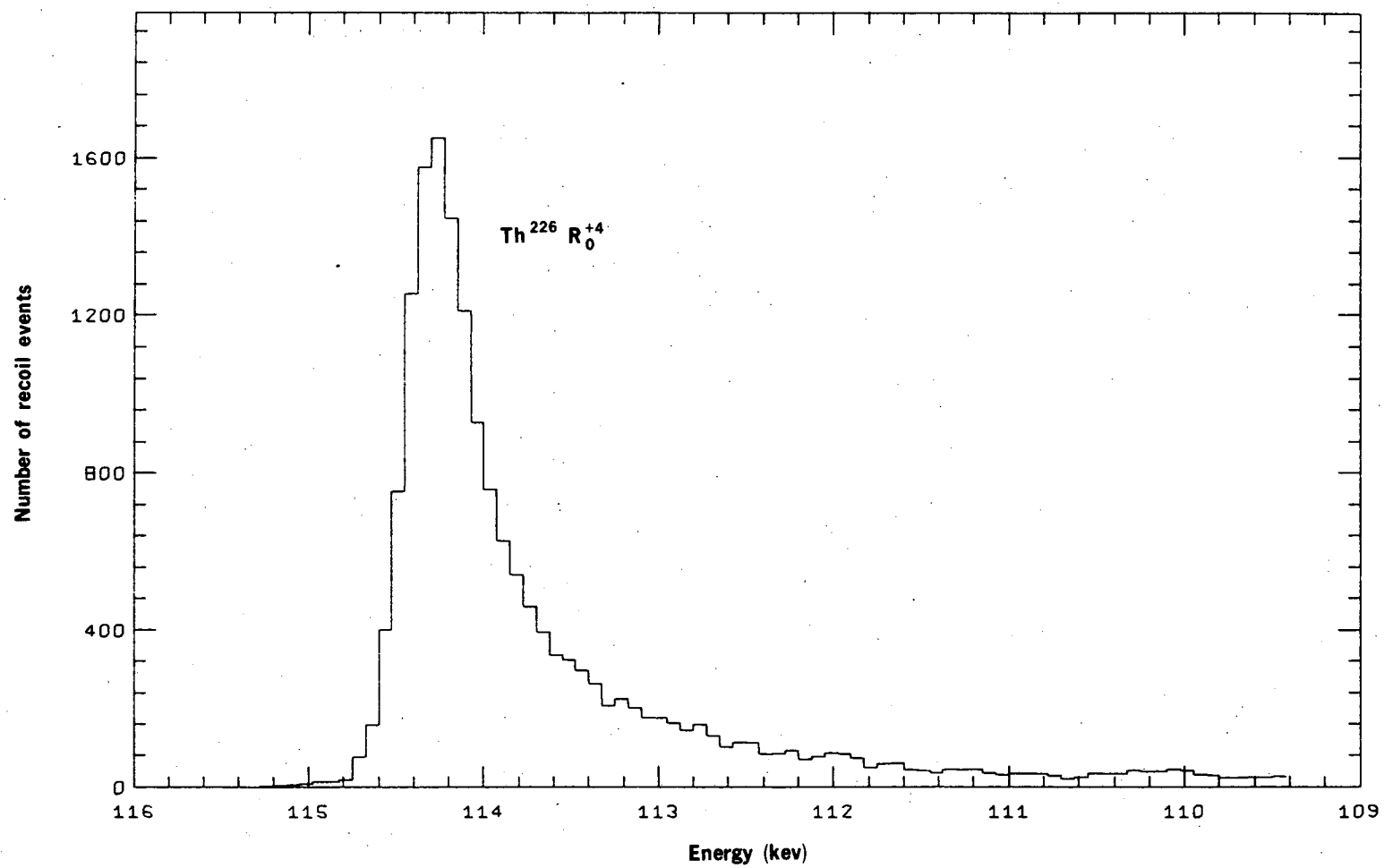

Figure 76. $Th^{226}R_0^{+4}$ spectrum which was separated from the $Th^{226}R^{+4}$ spectrum shown in Fig. 54 as discussed in the text. The number of recoil events indicated is the sum of 2- and 3-pronged events per 75 eV.

XBL 687-1260

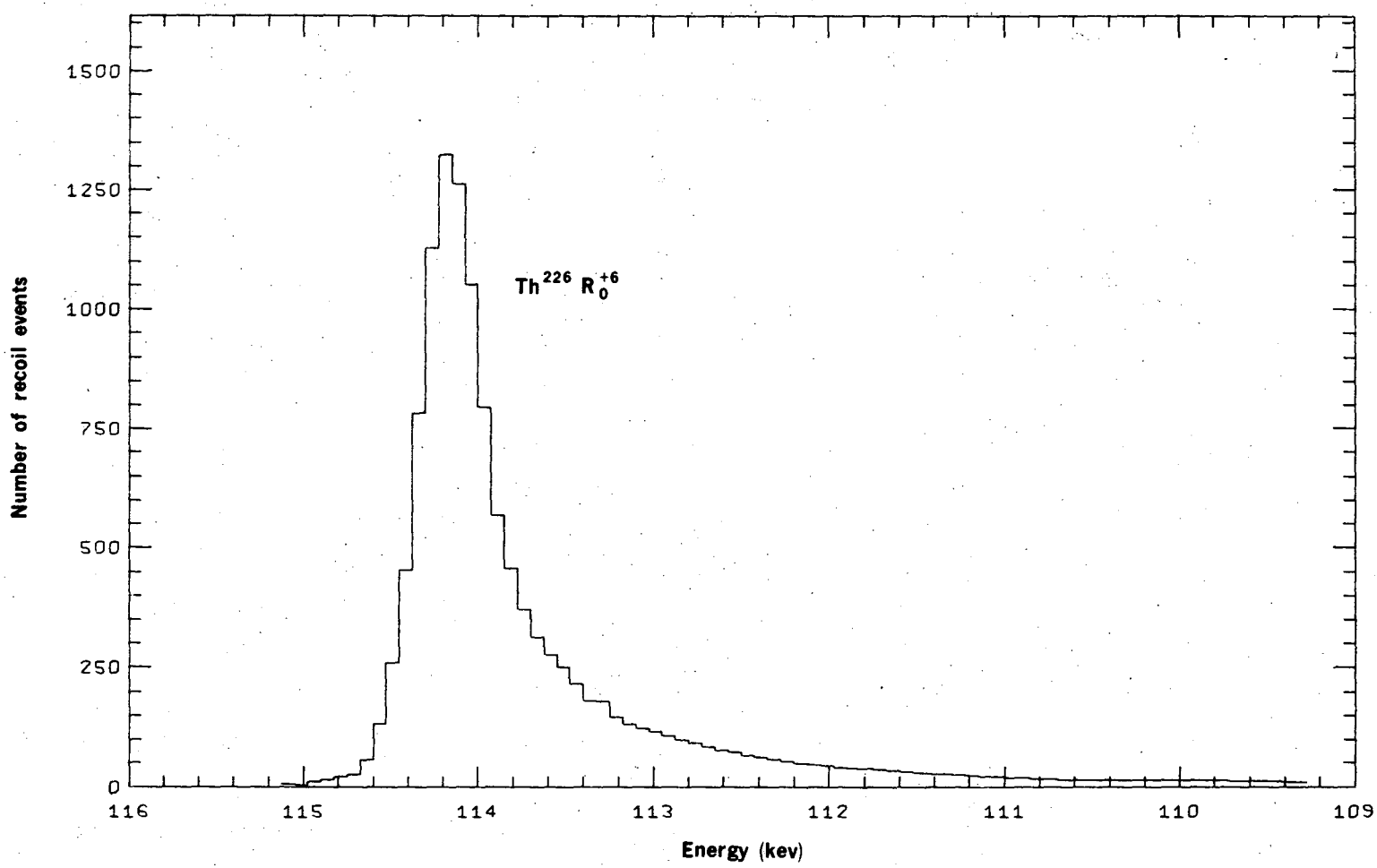

XBL 687-1256

Figure 77. $Th^{226}R_0^{+6}$ spectrum which was separated from the $Th^{226}R^{+6}$ spectrum shown in Fig. 56, as discussed in the text. The number of recoil events indicated is the sum of 2- and 3-pronged events per 75 eV.

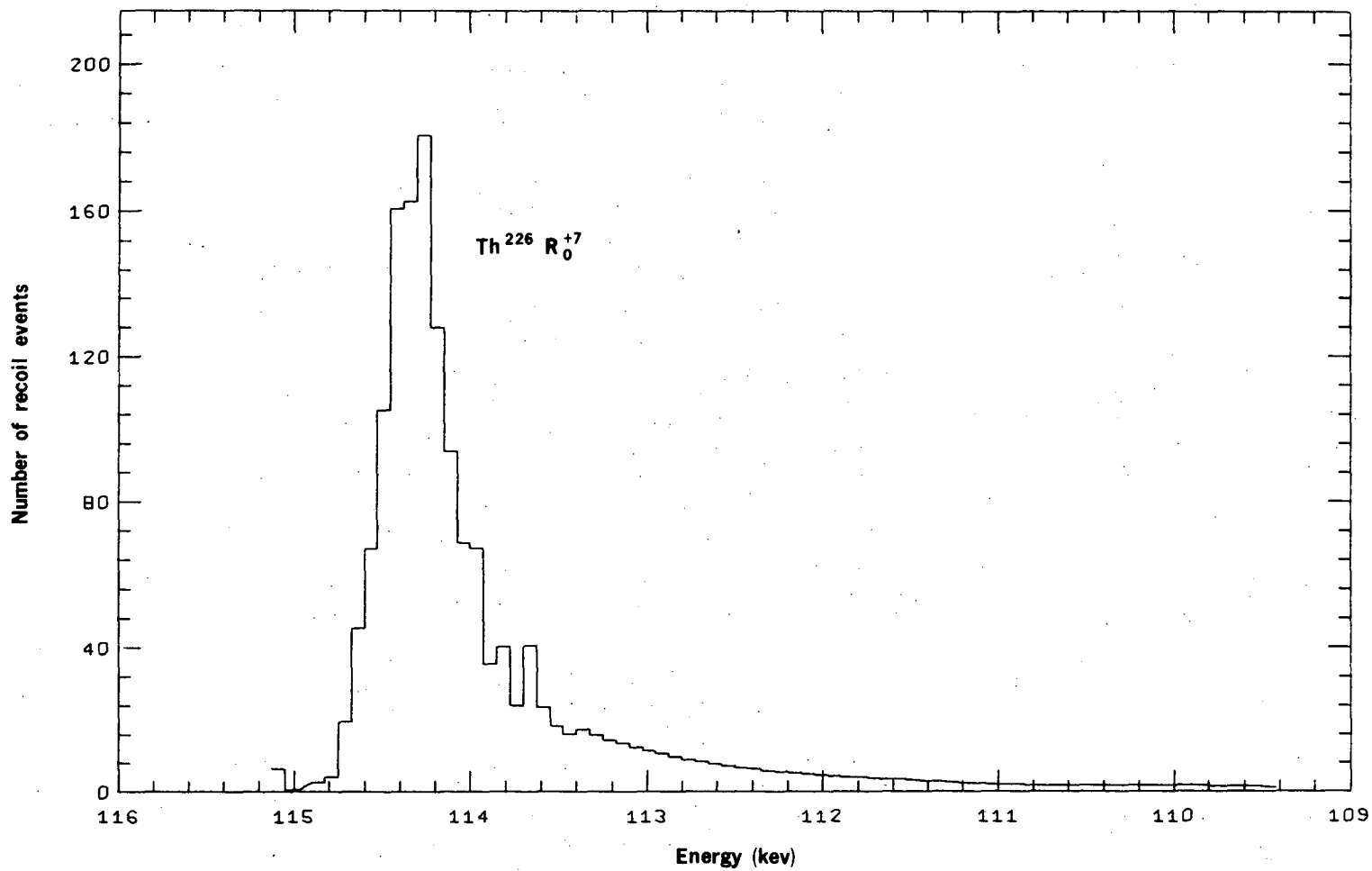

XBL 687-1254

Figure 78. $Th^{226}R_0^{+7}$ spectrum which was separated from the $Th^{226}R^{+7}$ spectrum shown in Fig. 57, as discussed in the text. The number of recoil events indicated is the sum of 2- and 3-pronged events per 75 eV.

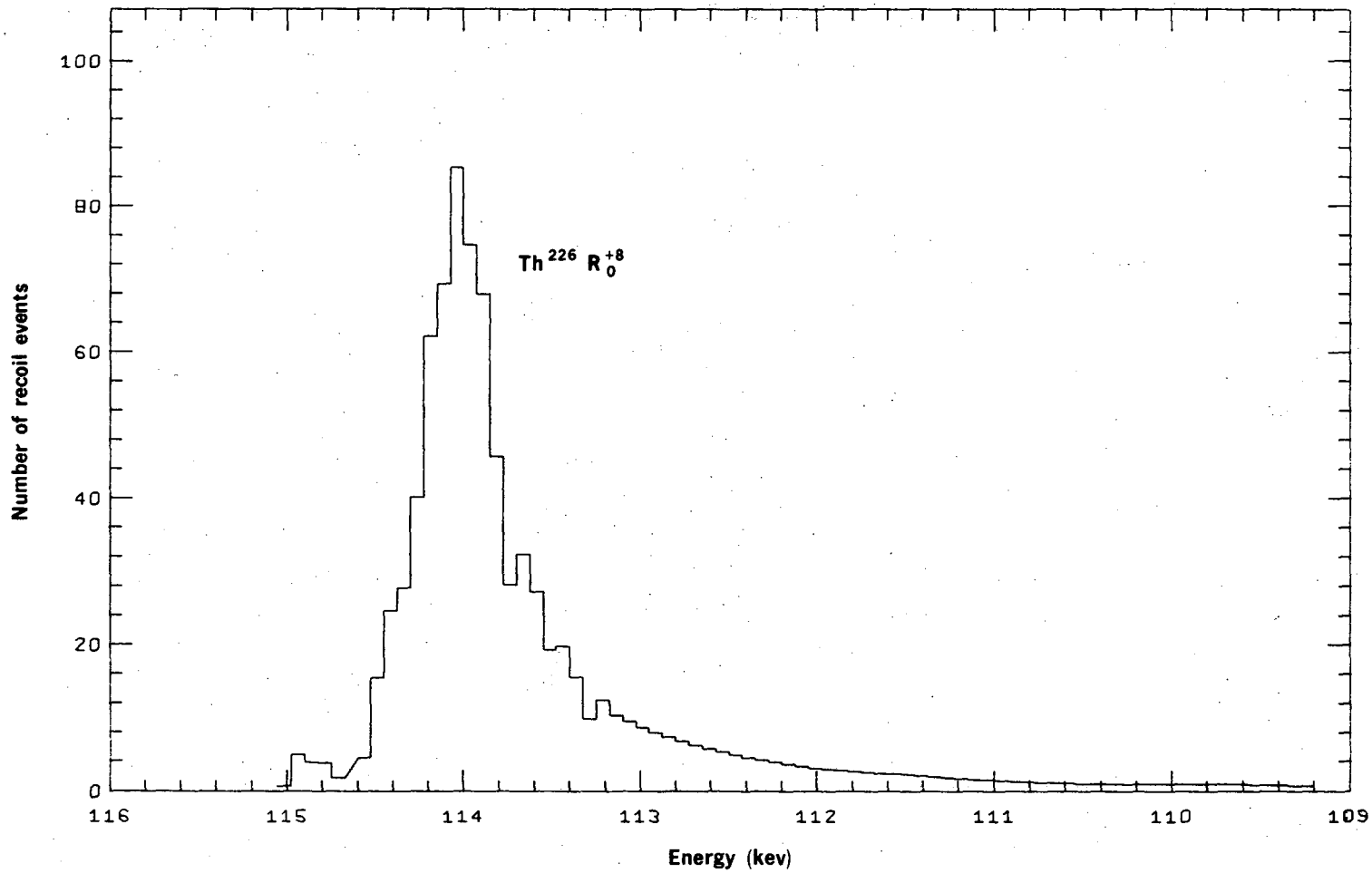

XBL 687-1252

Figure 79. $Th^{226}R_0^{+8}$ spectrum which was separated from the $Th^{226}R^{+8}$ spectrum shown in Fig. 58, as discussed in the text. The number of recoil events indicated is the sum of 2- and 3-pronged events per 75 eV.

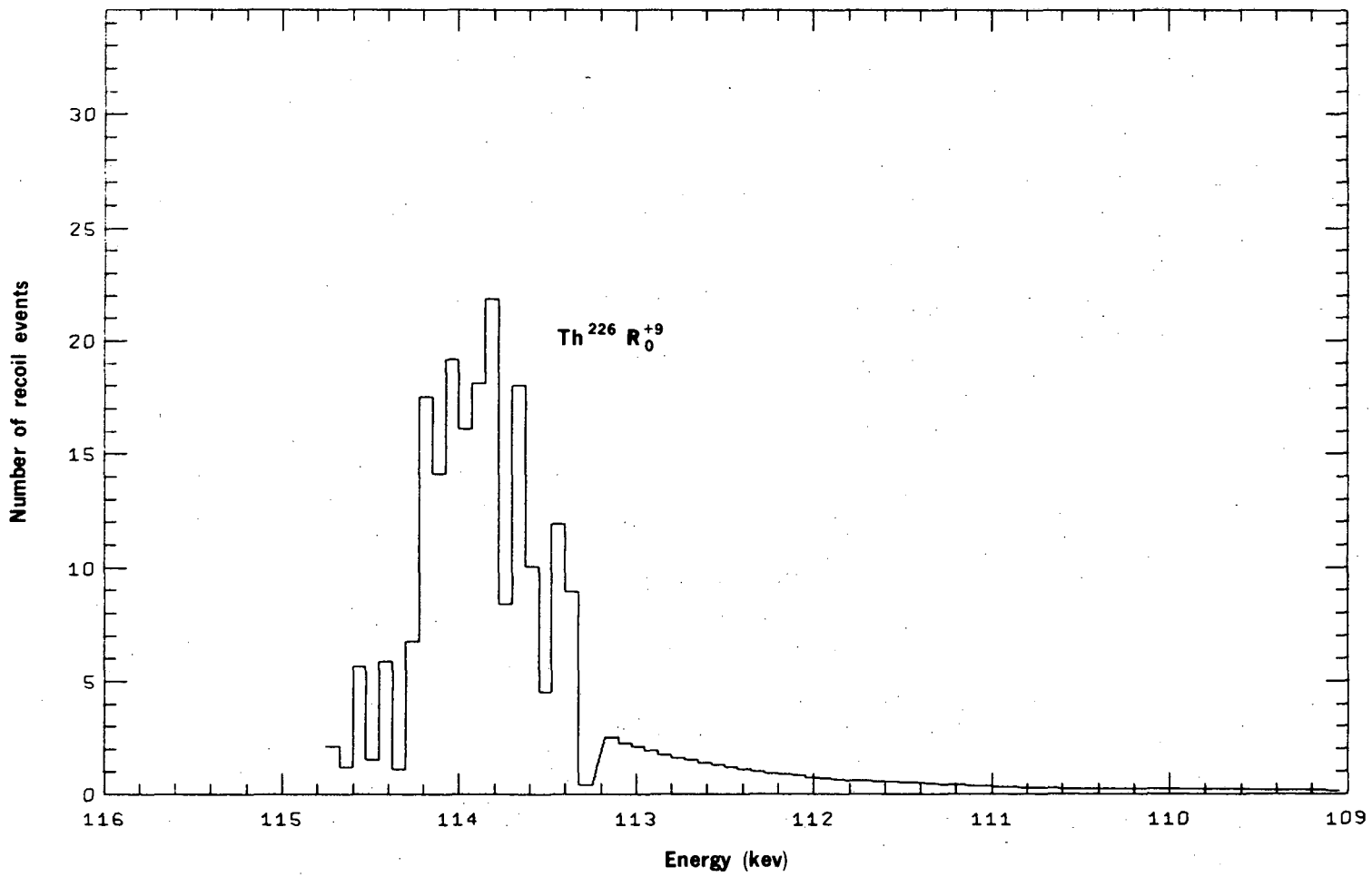

XBL 687-1250

Figure 80. $Th^{226}R_0^{+9}$ spectrum which was separated from the $Th^{226}R^{+9}$ spectrum shown in Fig. 59, as discussed in the text. The number of recoil events indicated is the sum of 2- and 3-pronged events per 75 eV.

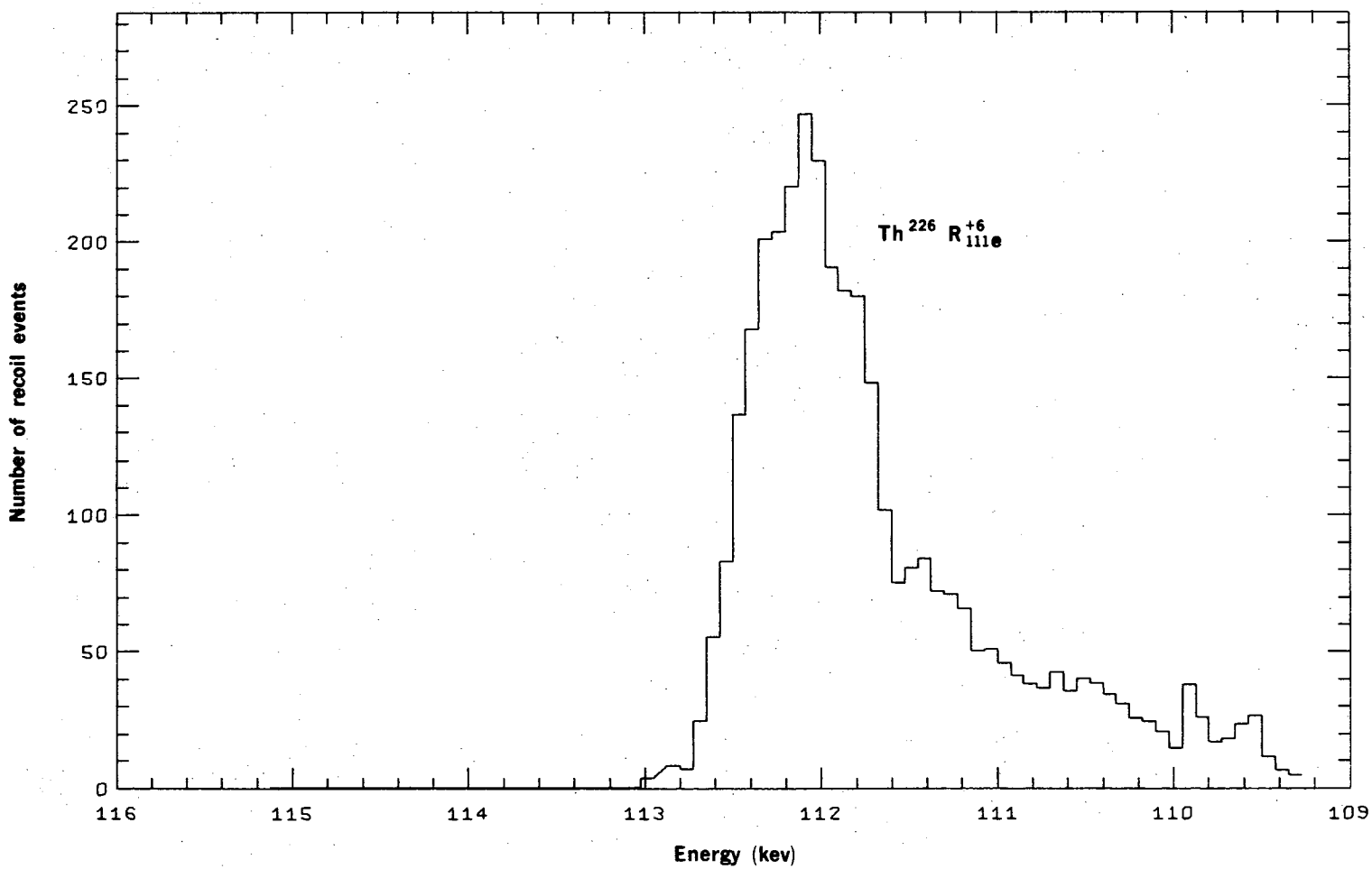

XBL 687-1255

Figure 81. $Th^{226}R_{111e}^{+6}$ spectrum which was separated from the $Th^{226}R^{+6}$ spectrum shown in Fig. 56, as discussed in the text. The number of recoil events indicated is the sum of 2- and 3-pronged events per 75 eV.

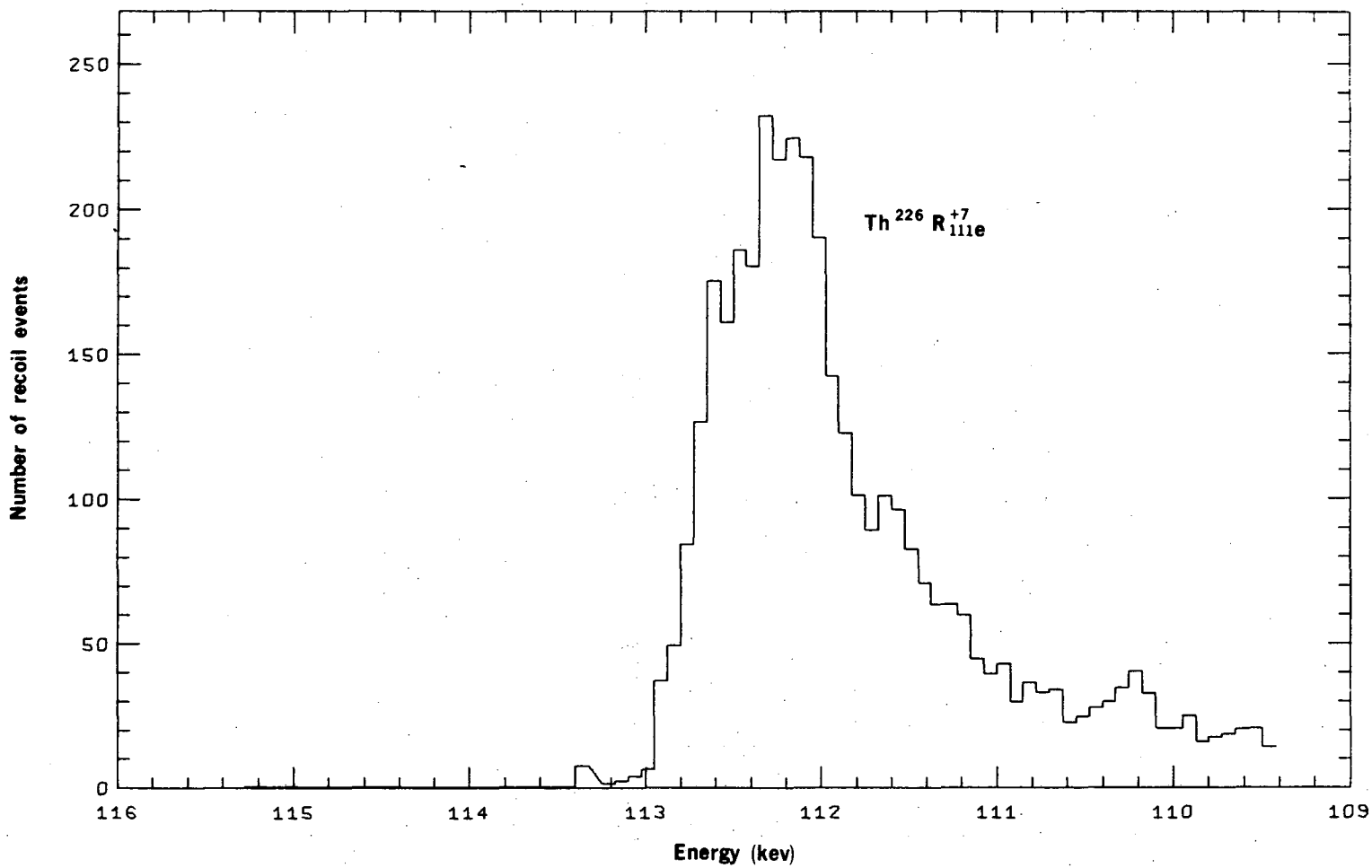

XBL 687-1253

Figure 82. $Th^{226}R_{111e}^{+7}$ spectrum which was separated from the $Th^{226}R^{+7}$ spectrum shown in Fig. 57, as discussed in the text. The number of recoil events indicated is the sum of 2- and 3-pronged events per 75 eV.

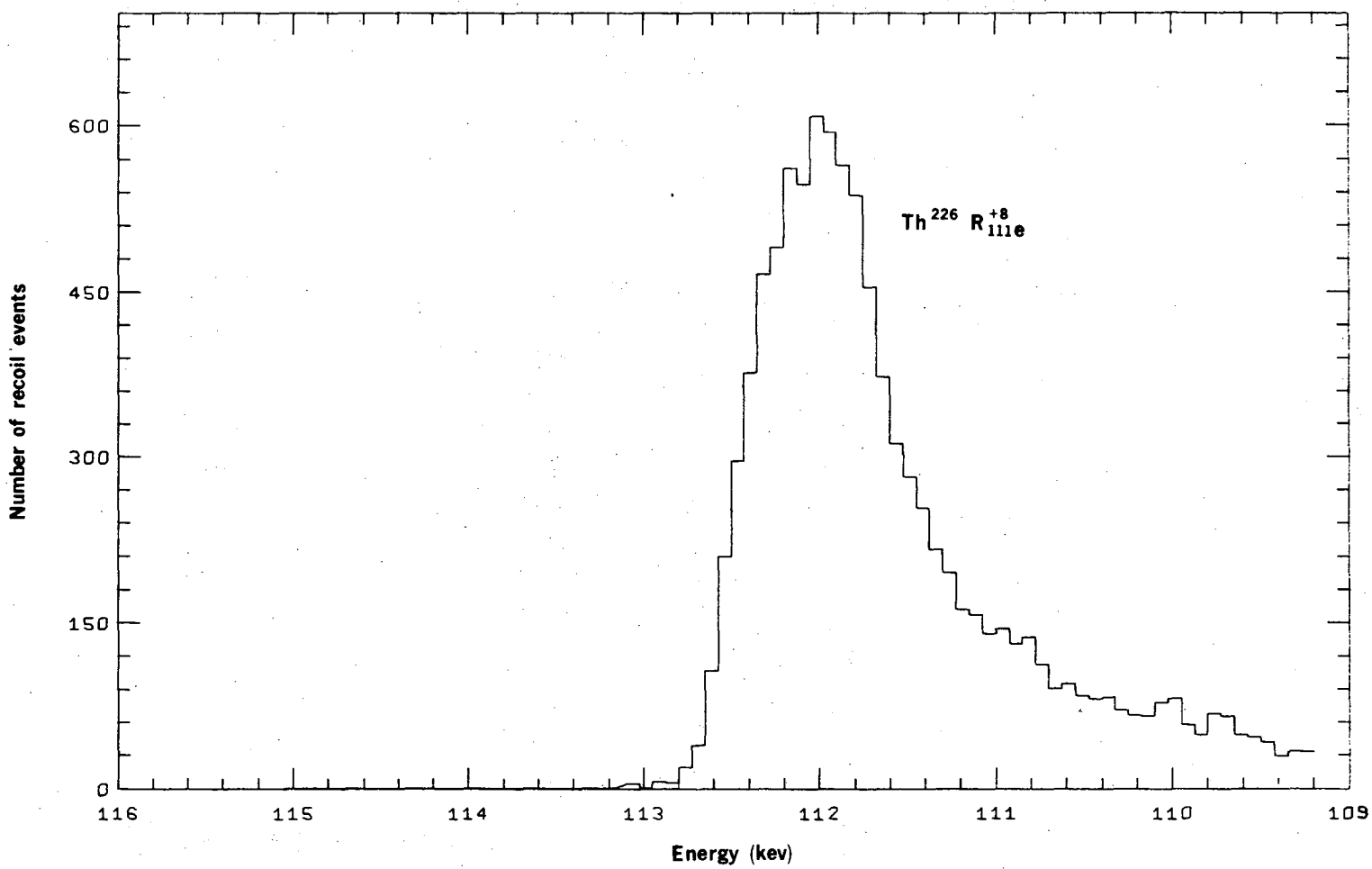

XBL 687-1251

Figure 83. $Th^{226}R_{111e}^{+8}$ spectrum which was separated from the $Th^{226}R^{+8}$ spectrum shown in Fig. 58, as discussed in the text. The number of recoil events indicated is the sum of 2- and 3-pronged events per 75 eV.

1) The energy distributions of all of the $Th^{226}R_{111e}{}^{+n}$ for n = +2 through +20 are the same with a half width of approximately 900 eV.

2) The energy distributions of $Th^{226}R_0{}^{+n}$ are the same with half-widths of approximately 490 eV <u>except</u> for the $Th^{226}R_0{}^{+2}$ which had a long low energy tail and a resultant half-width of 675 eV.

The total number of recoils in these curves (minus background) was then counted for use in calculating the ratios No. $Th^{226}R_0{}^{+n}(2\alpha + 3\alpha)$/ No. $Th^{226}\alpha_0$ and No. $Th^{226}R_{111e}{}^{+n}(2\alpha + 3\alpha)$/No. $Th^{226}\alpha_{111e}$. Obviously, all of the recoils in these spectra cannot be counted, because the low energy tail extends beyond the end of the photographic plate in many cases. It was desirable to find the smallest region that needed to be counted in order to prevent a distortion of the resulting charge distribution. This was a accomplished in the following manner. Starting at the center line of the recoil peak, each peak was counted out to a distance where the tail begins to merge with the background for all the peaks in the recoil group of interest. This number was then arbitrarily designated as being equal to all of the 2- and 3-pronged events in that peak. Ratios of the number of 2- and 3-pronged events in various subintervals with respect to the number of such events in the total interval were then compared for all of the recoil peaks in a given group (either the $Th^{226}R_0$ group or the $Th^{226}R_{111e}$ group). The minimum necessary counting interval was then designated as the smallest interval for which all of the ratios in a group were equal in the error limits involved plus the smallest interval necessary to include the front portion of all of the peaks in a group. This interval corresponds to the region from the center-line of the recoil peak plus 0.975 keV (£ + 0.975 keV) to £ - 3.000 keV for the $Th^{226}R_{111e}$ peaks and from £ + 0.975 keV to £ - 4.800 keV for the $Th^{226}R_0$ peaks. The number of

alphas was obtained by using the technique outlined in Sec. I.C. along with the ratio No. $Th^{226}\alpha_{111e}$/No. $Th^{226}\alpha_0 = \frac{.195}{.761} = 0.256$ where necessary. Using these numbers, the ratios No. $Th^{226}R_0{}^{+n}(2\alpha + 3\alpha)$/No. $Th^{226}\alpha_0$ and No. $Th^{226}R_{111e}{}^{+n}(2\alpha + 3\alpha)$/No. $Th^{226}\alpha_{111e}$ were calculated for n = +2 through +10 and +2 through +20 respectively. (See Table V and Figs. 84 and 85.)

Table V. Experimental ratios obtained from the regular plates.

n	$\frac{\text{No. } Th^{226}R_0{}^{+n}(2\alpha + 3\alpha)}{\text{No. } Th^{226}\alpha_0}$	$\frac{\text{No. } Th^{226}R_{111e}{}^{+n}(2\alpha + 3\alpha)}{\text{No. } Th^{226}\alpha_{111e}}$
+2	$(5.60 \pm 0.11) \times 10^{-2}$	$(5.6 \pm 3.8) \times 10^{-3}$
+3	$(1.378 \pm 0.076) \times 10^{-2}$	$(1.09 \pm 0.58) \times 10^{-3}$
+4	$(9.70 \pm 0.54) \times 10^{-3}$	$(1.23 \pm 0.59) \times 10^{-3}$
+5	$(8.17 \pm 0.45) \times 10^{-3}$	$(2.89 \pm 0.34) \times 10^{-3}$
+6	$(3.64 \pm 0.21) \times 10^{-3}$	$(4.20 \pm 0.34) \times 10^{-3}$
+7	$(8.44 \pm 0.47) \times 10^{-4}$	$(8.04 \pm 0.51) \times 10^{-3}$
+8	$(3.64 \pm 0.21) \times 10^{-4}$	$(1.67 \pm 0.10) \times 10^{-2}$
+9	$(7.4 \pm 1.3) \times 10^{-5}$	$(1.94 \pm 0.10) \times 10^{-2}$
+10	$\leq (1.8 \pm 4.1) \times 10^{-5}$	$(2.49 \pm 0.12) \times 10^{-2}$
+11		$(2.49 \pm 0.13) \times 10^{-2}$
+12		$(2.42 \pm 0.13) \times 10^{-2}$
+13		$(2.24 \pm 0.12) \times 10^{-2}$
+14		$(1.252 \pm 0.069) \times 10^{-2}$
+15		$(1.168 \pm 0.070) \times 10^{-2}$
+16		$(8.57 \pm 0.55) \times 10^{-3}$
+17		$(6.99 \pm 0.47) \times 10^{-3}$
+18		$(3.68 \pm 0.27) \times 10^{-3}$
+19		$(2.21 \pm 0.19) \times 10^{-3}$
+20		$(1.11 \pm 0.12) \times 10^{-3}$

(Note: The No. $Th^{226}R_0{}^{+10}(2\alpha + 3\alpha)$ was calculated by determining the background count well in front of the $Th^{226}R_0{}^{+10}$ peak and then subtracting the background from the total number of 2- and 3-pronged events in the

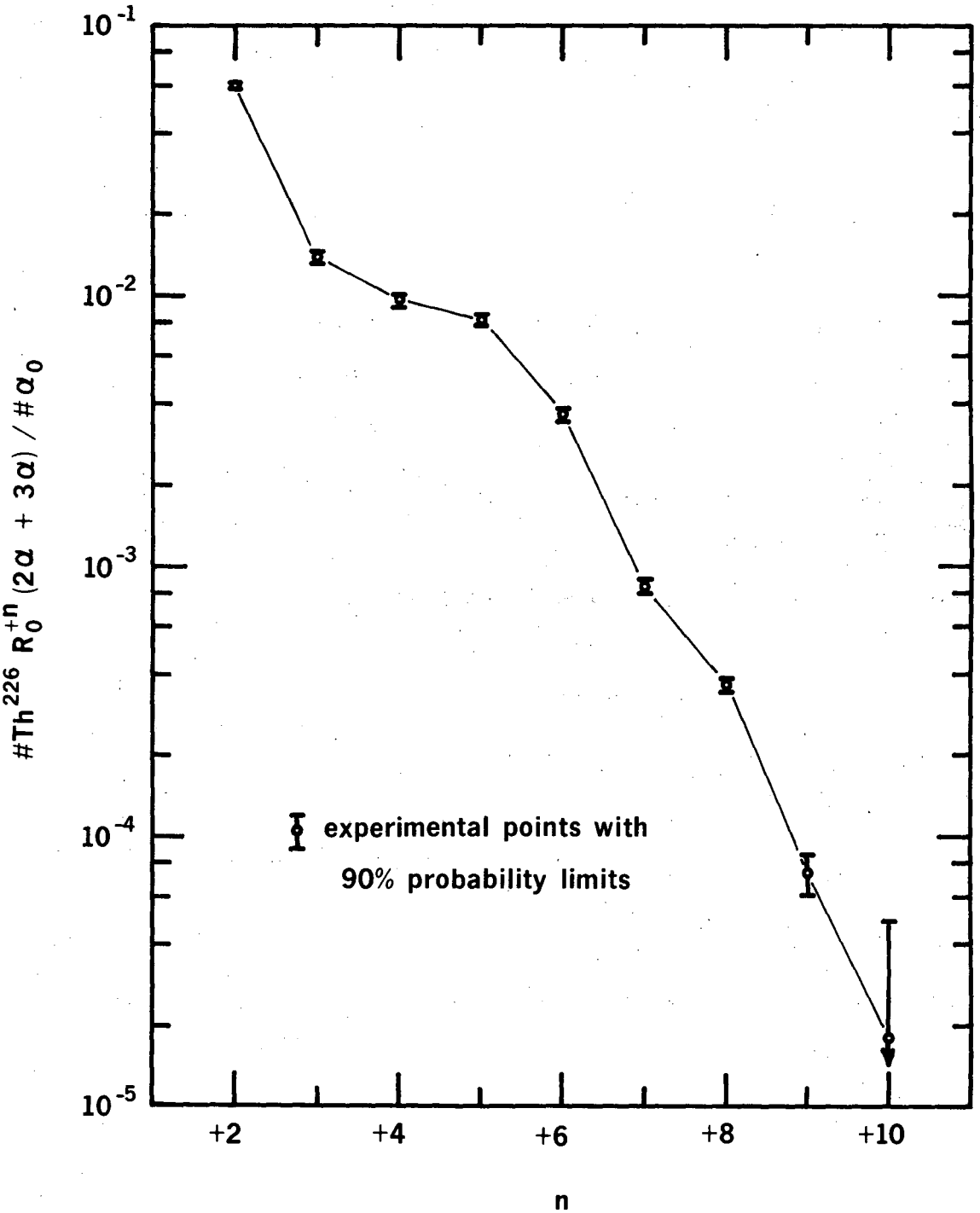

Figure 84. Experimental charge distribution of $Th^{226}R_0$ as obtained from the regular plates.

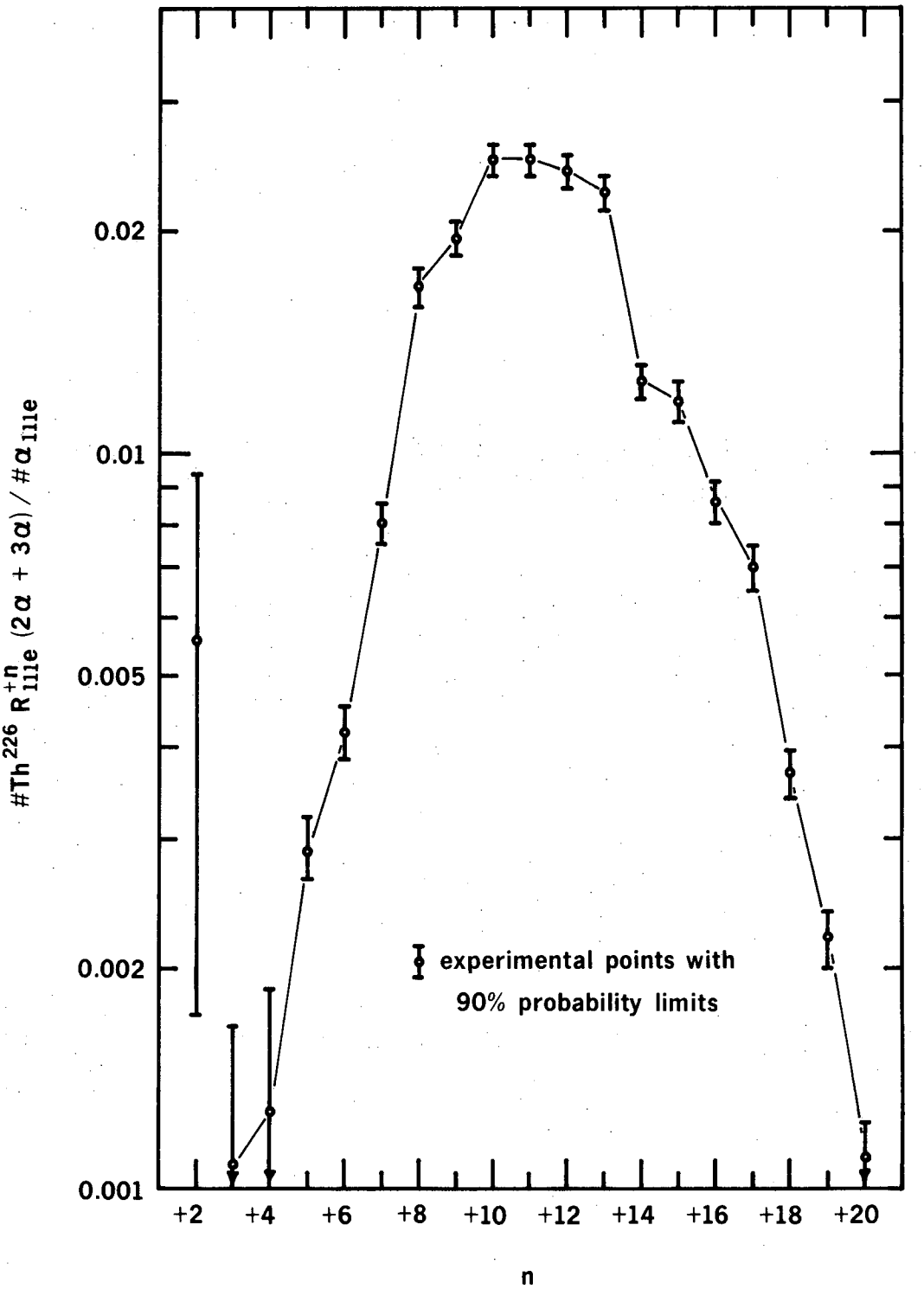

Figure 85. Experimental charge distribution of $Th^{226}R_{111e}$ as obtained from the regular plates.

region from $\mathcal{E}_{Th^{226}R_0}$ + 0.375 keV to $\mathcal{E}_{Th^{226}R_0}$ - 1.125 keV which accounts for about 90% of the peak. This number was then corrected from the n + .5 data and represents the upper limit shown in Table V. Because of the absence of any peak and the fact that No. $Th^{226}R_0^{+n}$ for n > +10 must be less than No. $Th^{226}R_0^{+10}$, no values for these n's are given in Table V.)

As has been previously discussed, the information concerning charges -2, ±1 and 0 had to be obtained from the "thin" plates. The experimental ratio No. $Th^{226}R_0(2\alpha + 3\alpha)$/No. $Th^{226}\alpha_0$ was obtained in the following way. A study of Figs. 84 and 85 shows that No. $Th^{226}R^{+2} \approx$ No. $Th^{226}R_0^{+2}$ + No. $Th^{226}R_{111\gamma}^{+2}$ = No. $Th^{226}R_0^{+2}(1.0378)$. Therefore it is probably true that this statement also holds true for charges ±1, -2 and 0, particularly since it is probable that the point shown for charge +2 in Fig. 85 should actually be below those of charges +3 and +4. This is borne out by the evidence from previous studies on the charge distribution resulting from inner shell vacancies,[25] in addition to the fact that the $Th^{226}R_{111e}^{+2}$ composite peak represents a peak which is 15 events high on a tail which is 100 events high and hence could easily be caused by statistical fluctuations. This is not so much the case for $Th^{226}R_{111e}^{+3}$ and $Th^{226}R_{111e}^{+4}$ since they are peaks whose heights are 30 and 35 events respectively on tails which are 150 and 100 events high.

The ratios No. $Th^{226}R_0^{+n}(2\alpha + 3\alpha$, regular plate angle)/No. $Th^{226}\alpha_0$ for n = -2, ± 1 and 0 were obtained in the following manner: for a given plate, the $Th^{226}R^{+n}(3\alpha)$ was obtained for charges ±2, ±1, and 0 when present. From this, a constant β times the No. $Th^{226}R_{exp}^{+n}$ was obtained by using the experimental Prob(3α) curve that was determined in Sec. II.D.4. (see Fig. 22) since βNo. $Th^{226}R_{exp}^{+n}$ = No. $Th^{226}R^{+n}(3\alpha, \beta$ deg)/Prob(3α, β deg) where No. $Th^{226}R_{exp}^{+n}$ is total number of recoils of charge +n given off in an

unknown solid angle. For the ▫ thin plates such as α-2-985 and α-2-990 (see Figs. 86 and 87), this unkown solid angle was the same for each peak and so

$$\left(\frac{\text{No. } Th^{226}R^{+n}}{\text{No. } Th^{226}R^{+2}}\right)_{▫} = \left(\frac{\beta \text{ No. } Th^{226}R_{exp}^{+n}}{\beta \text{ No. } Th^{226}R_{exp}^{+2}}\right)_{▫}$$

for these plates since the β's cancel. This fact can be confirmed by calculating this ratio for n = 0, +1 and +3 using data from the "30 deg"▫$_{cold}$ plate α-2-985 (see Fig. 86) and comparing it with the corresponding ratio found from the data of the "90 deg"▫$_{cold}$ plate α-2-990 (see Fig. 87). This is not true for the ▯ plates (compare the heights of the various peaks in Figs. 86 and 88); however, the ratios of the correction factors C^{+n} for the various peaks can be found from the relation

$$\left(\frac{\beta \text{ No. } Th^{226}R_{exp}^{+n}}{\beta \text{ No. } Th^{226}R_{exp}^{+2}}\right)_{\text{"}\alpha\text{ deg"}▫_{cold}} = \left(\frac{C^{+n}_{\text{"}\alpha\text{ deg"}▯}}{C^{+2}_{\text{"}\alpha\text{ deg"}▯}}\right)\left(\frac{\beta \text{ No. } Th^{226}R_{exp}^{+n}}{\beta \text{ No. } Th^{226}R_{exp}^{+2}}\right)_{\text{"}\alpha\text{ deg"}▯_{cold}}$$

It was necessary to do this because all of the "warm" plates were ▯ in addition to the plate which contained the $Th^{226}R^{-2}$ and $Th^{226}R^{-1}$ peaks, and it was believed that the data from the warm plates more nearly represents the normal room temperature situation, i.e. the regular plate situation, than do the cold plates (compare Figs. 88 and 89). Thus, the ratios $(\text{No. } Th^{226}R^{+n}/\text{No. } Th^{226}R^{+2})_{warm}$ for n = 0 and +1 were found in the following manner

$$\left(\frac{\text{No. } Th^{226}R^{+n}}{\text{No. } Th^{226}R^{+2}}\right)_{warm} = \left(\frac{\text{No. } Th^{226}R^{+n}}{\text{No. } Th^{226}R^{+2}}\right)_{\text{"30 deg" warm}}$$

$$= \left(\frac{C^{+n}_{\text{"30 deg"}▯}}{C^{+2}_{\text{"30 deg"}▯}}\right)\left(\frac{\beta \text{ No. } Th^{226}R_{exp}^{+n}}{\beta \text{ No. } Th^{226}R_{exp}^{+2}}\right)_{\text{"30 deg"}▯_{warm}}$$

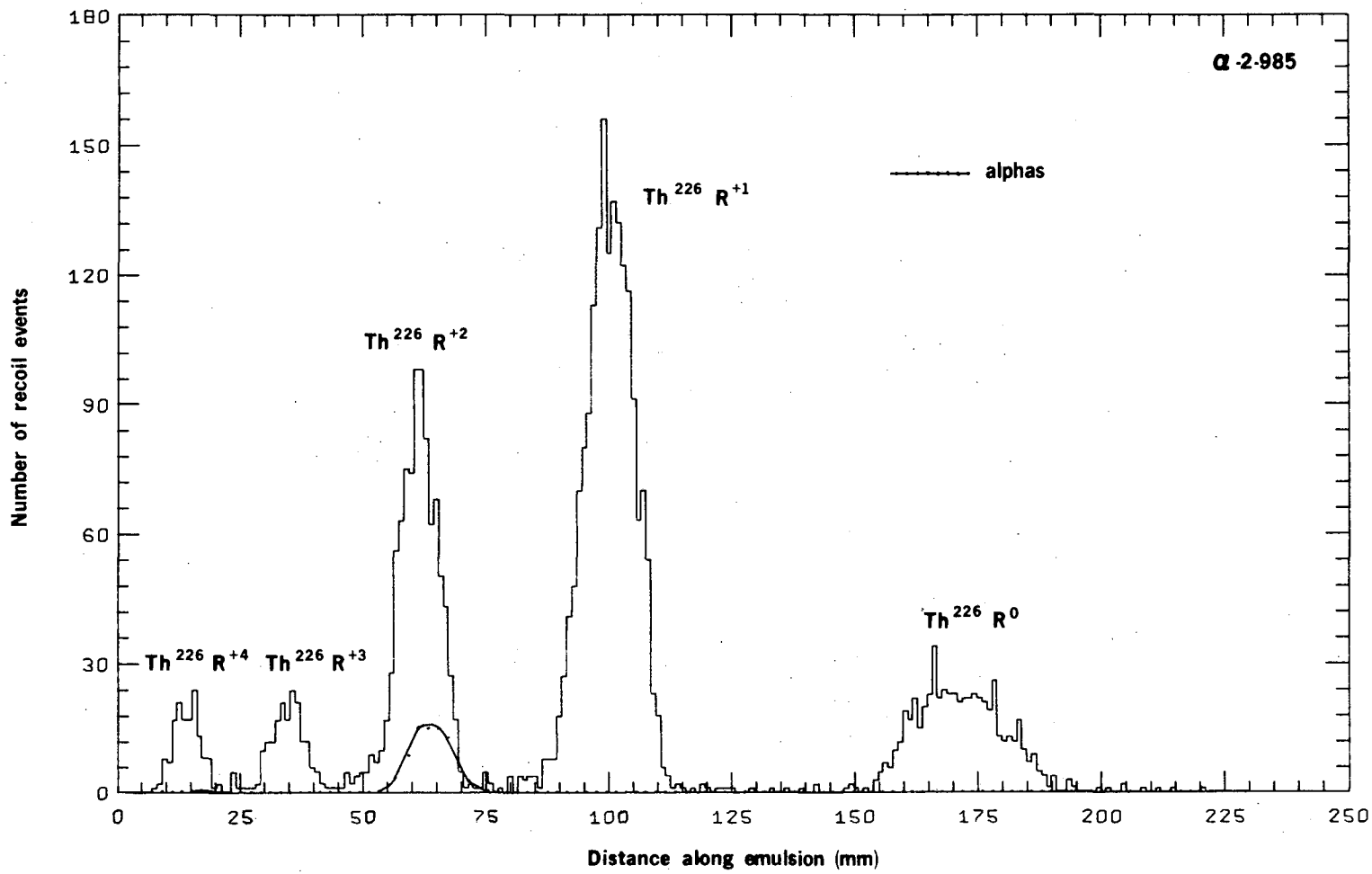

XBL 687-1222

Figure 86. Recoil spectrum of Th^{226} taken with alpha particle spectrograph in the "thin plate" configuration where only the number of 3-pronged events is shown. Alpha peak is reduced by a factor of 250. α-2-985 is a "30 deg" α_{cold} plate.

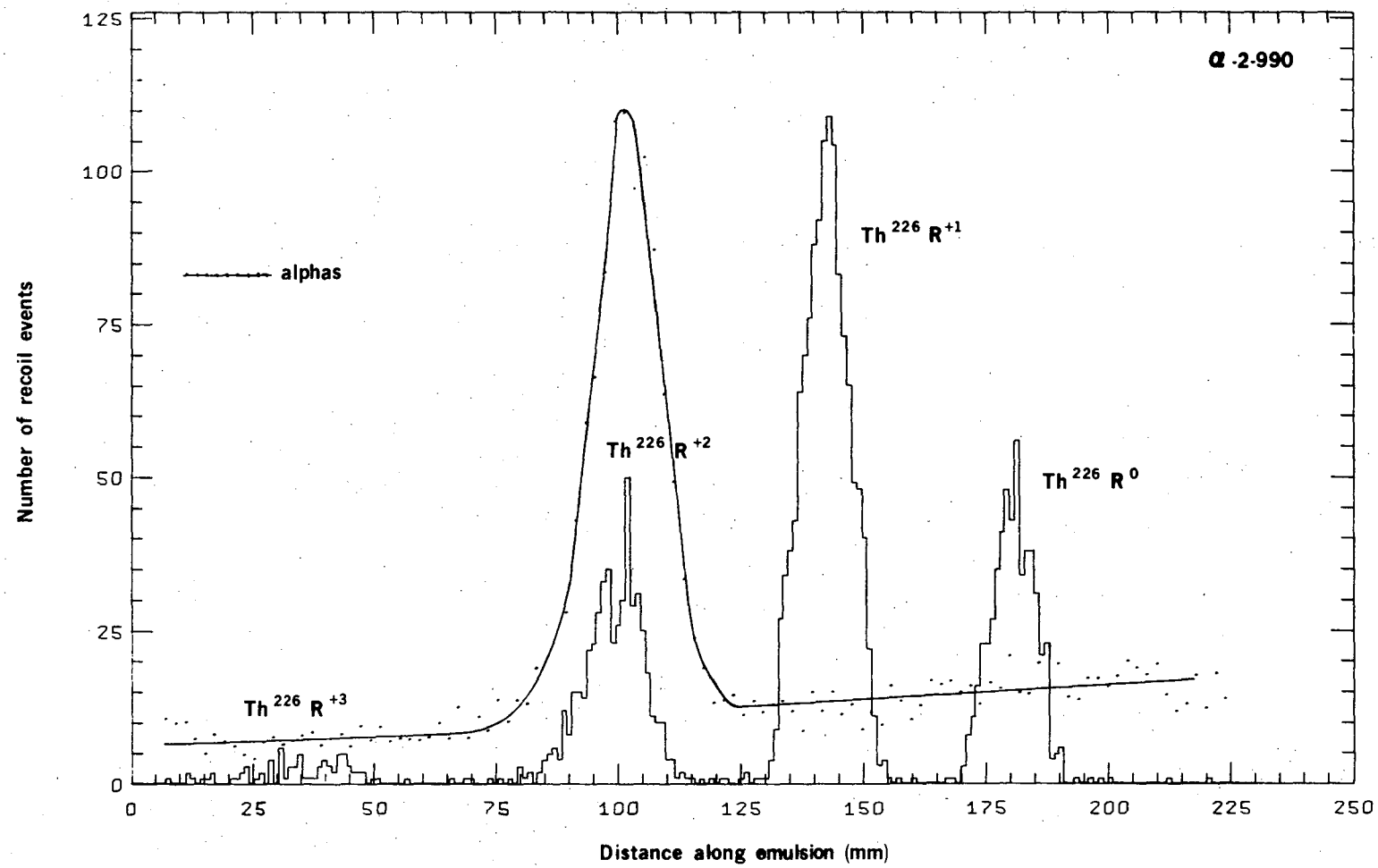

XBL 687-1221

Figure 87. Recoil spectrum of Th^{226} taken with alpha particle spectrograph in the "thin plate" configuration where only the number of 3-pronged events is shown. Alpha peak is reduced by a factor of 6. α-2-990 is a "90 deg" α_{cold} plate.

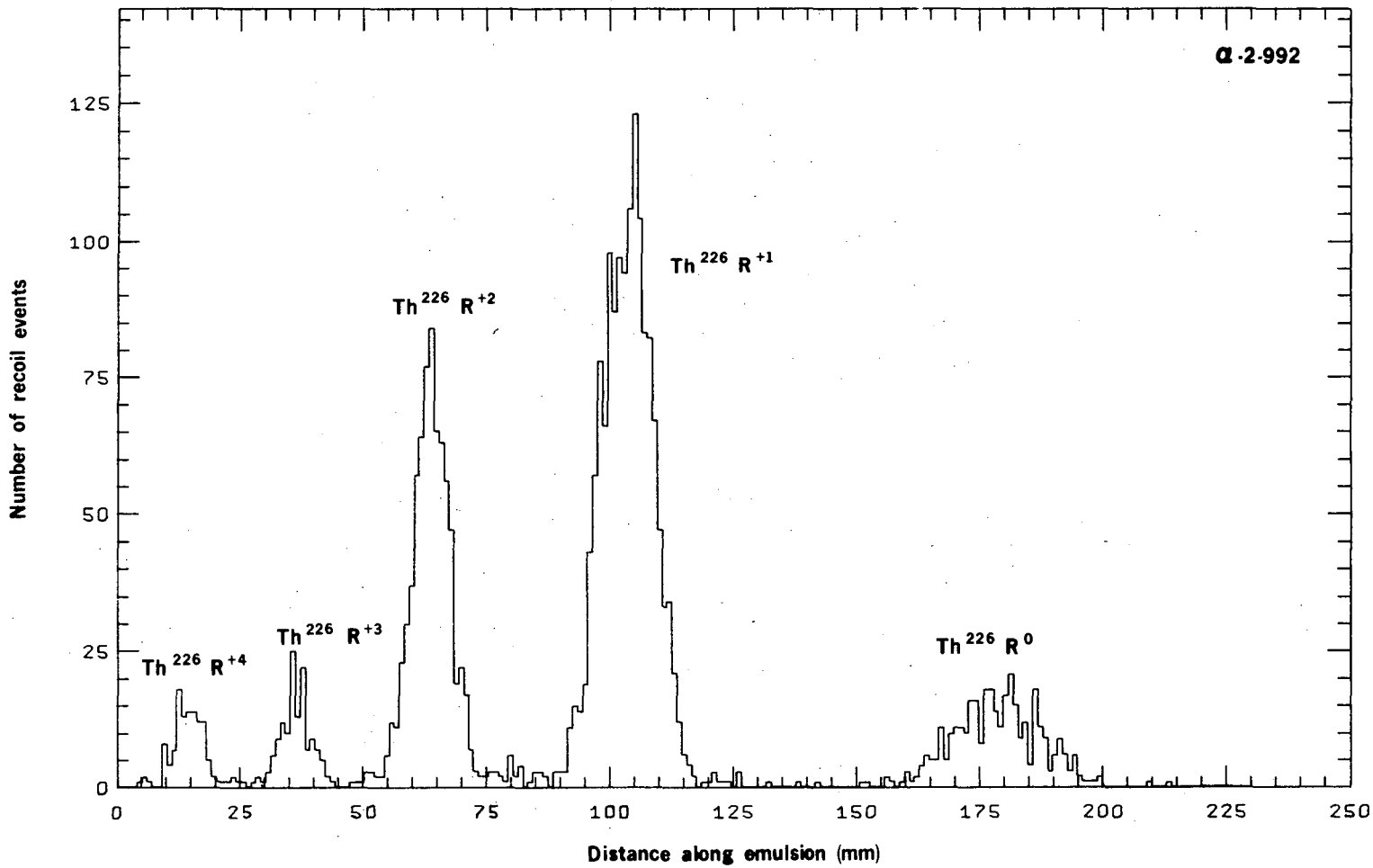

XBL 687-1219

Figure 88. Recoil spectrum of Th^{226} taken with alpha particle spectrograph in the "thin plate" configuration where only the number of 3-pronged events is shown. α-2-992 is a "30 deg"∥ cold plate.

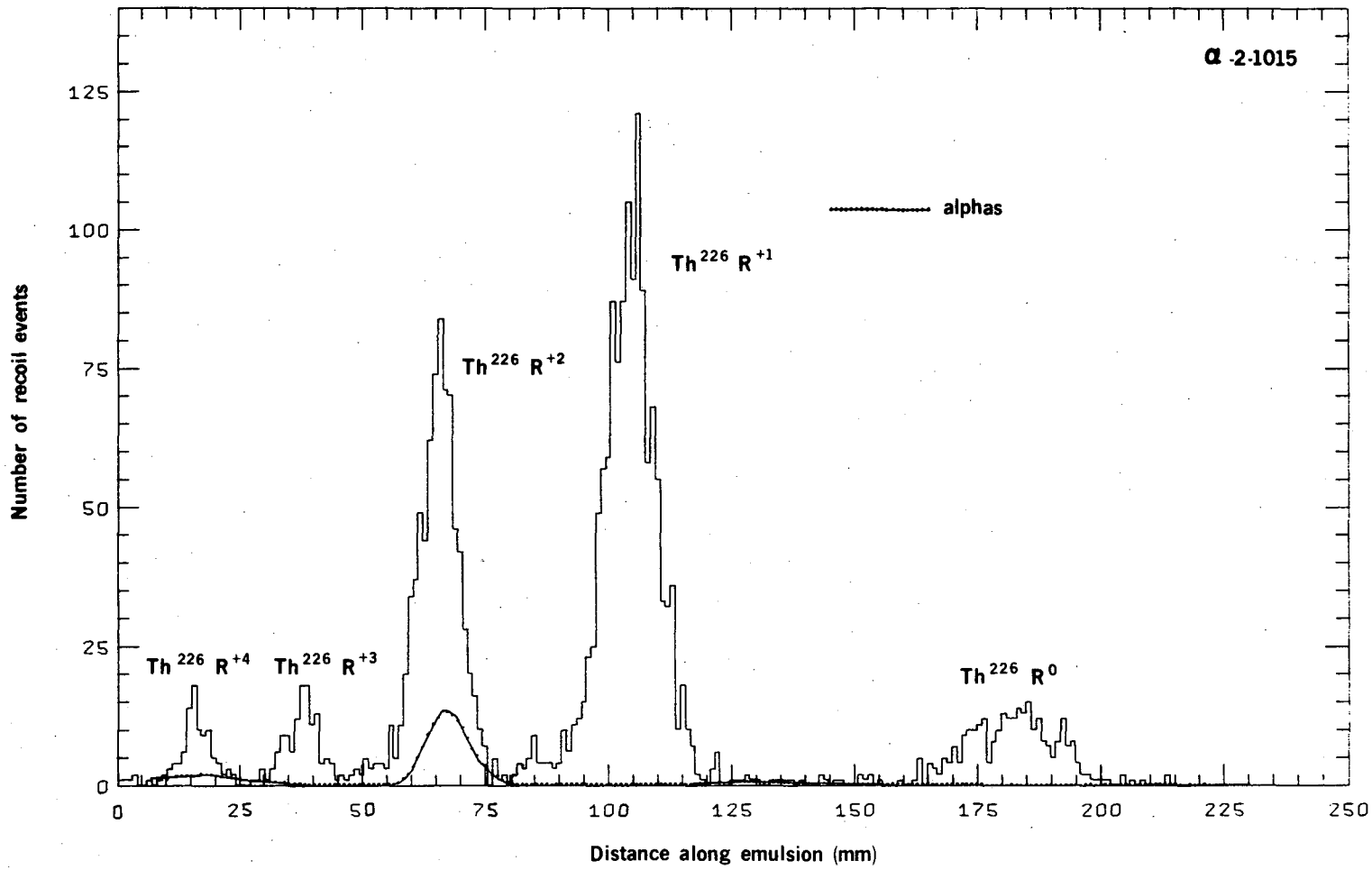

XBL 687-1224

Figure 89. Recoil spectrum of Th^{226} taken with alpha particle spectrograph in the "thin plate" configuration where only the number of 3-pronged events is shown. Alpha peak is reduced by a factor of 250. α-2-1015 is a "30 deg" ℓ_{warm} plate.

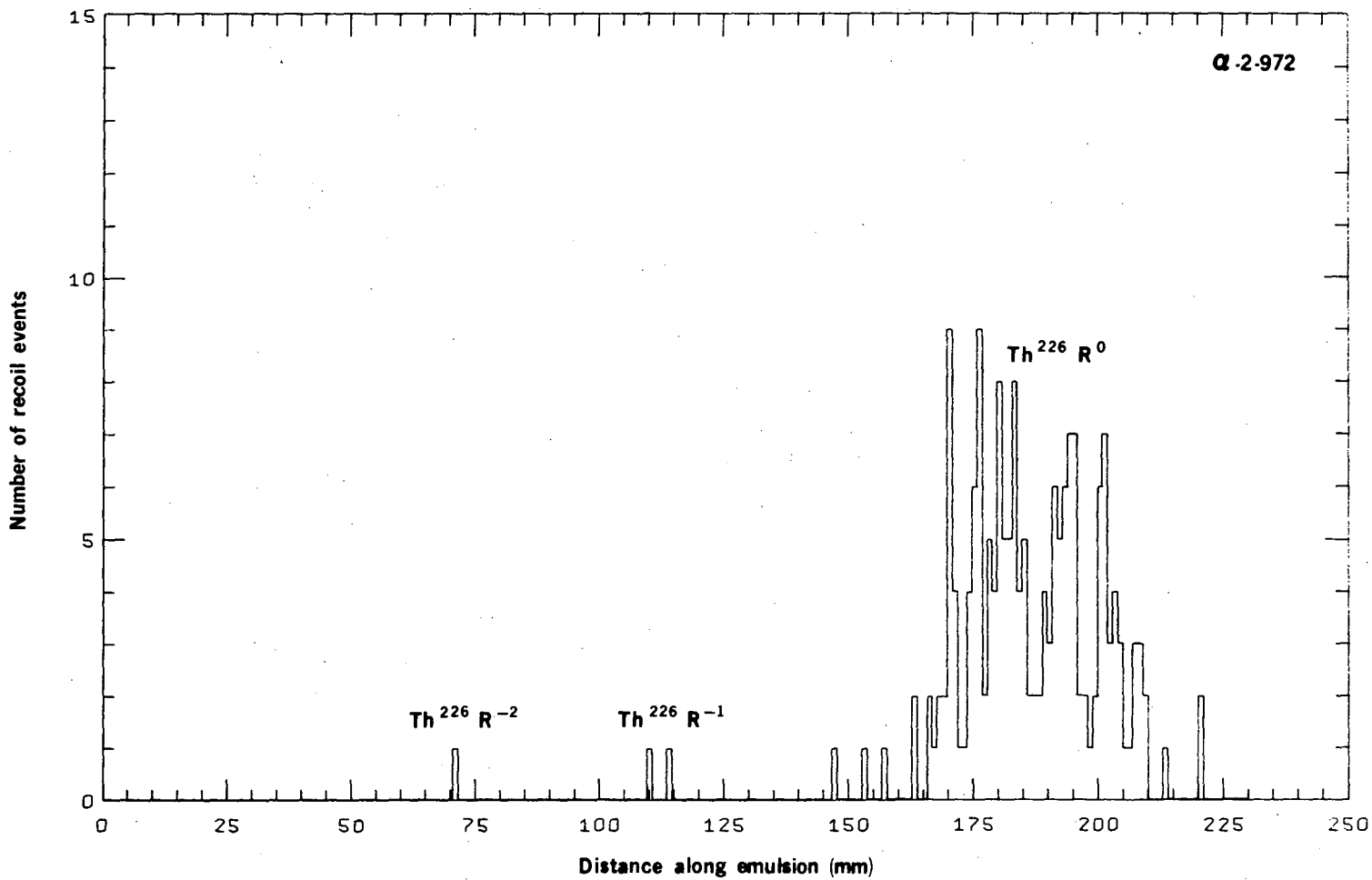

XBL 687-1239

Figure 90. Recoil spectrum of Th^{226} taken with alpha particle spectrograph in the "thin plate" configuration where only the number of 3-pronged events is shown. α-2-972 is a "30 deg" σ_{cold} plate.

where $\left(C^{+n}\text{"30 deg"}[]/C^{+2}\text{"30 deg"}[] \right)$ is obtained from the relation given previously. In a similar way the ratios $(\text{No. } Th^{226}R^{+n}/\text{No. } Th^{226}R^{0})_{cold}$ for n = -1 and -2 were obtained (see Fig. 90), and used to calculate $(\text{No. } Th^{226}R^{+n}/\text{No. } Th^{226}R^{+2})_{warm}$ by assuming that

$$\left(\frac{\text{No. } Th^{226}R^{+n}}{\text{No. } Th^{226}R^{+2}} \right)_{warm} \approx \left(\frac{\text{No. } Th^{226}R^{+n}}{\text{No. } Th^{226}R^{0}} \right)_{cold} \left(\frac{\text{No. } Th^{226}R^{0}}{\text{No. } Th^{226}R^{+2}} \right)_{warm}$$

for these two values of n. Since

$$\frac{\text{No. } Th^{226}R^{+n}(2\alpha + 3\alpha,\ \gamma \text{ deg})}{\text{No. } Th^{226}R^{+2}(2\alpha + 3\alpha,\ \gamma \text{ deg})} = \frac{\text{No. } Th^{226}R^{+n}}{\text{No. } Th^{226}R^{+2}} \quad \text{for the thin plates}$$

$$\approx \frac{\text{No. } Th^{226}R_0^{+n}\ (2\alpha + 3\alpha,\ \gamma \text{ deg})}{\text{No. } Th^{226}R_0^{+2}\ (2\alpha + 3\alpha,\ \gamma \text{ deg})},$$

we have

$$\left(\frac{\text{No. } Th^{226}R_0^{+n}(2\alpha + 3\alpha)}{\text{No. } Th^{226}\alpha_0} \right)_{\text{reg. plate}} \approx \left(\frac{\text{No. } Th^{226}R^{+n}}{\text{No. } Th^{226}R^{+2}} \right)_{warm}$$

$$\text{times} \quad \left(\frac{\text{No. } Th^{226}R_0^{+2}(2\alpha + 3\alpha)}{\text{No. } Th^{226}\alpha_0} \right)_{\text{reg. plate}}$$

for n = -2, ± 1 and 0. The ratios obtained in this manner are shown in Table VI.

Table VI. Experimental ratios obtained from the thin plates in conjunction with the experimental Prob(3α) curve and the ratio No. $Th^{226}R_0^{+2}(2\alpha + 3\alpha)$/No. $Th^{226}\alpha_0$ obtained from the regular plates.

n	No. $Th^{226}R_0^{+n}(2\alpha + 3\alpha)$/No. $Th^{226}\alpha_0$
-2	$(1.16 \pm 1.34) \times 10^{-4}$
-1	$(2.60 \pm 3.07) \times 10^{-4}$
0	$(3.92 \pm 1.14) \times 10^{-2}$
+1	$(1.17 \pm 0.17) \times 10^{-1}$

If there were no pressure effects (see Sec. III.B.) then we would have

$$\text{Prob}(2\alpha + 3\alpha)_{\text{for reg. plates}} = \sum_{n=-2}^{+10} \left(\frac{\text{No. } Th^{226}R_0{}^{+n}(2\alpha + 3\alpha)}{\text{No. } Th^{226}\alpha_0} \right)$$

$$= \sum_{n=+3}^{+20} \left(\frac{\text{No. } Th^{226}R_{111e}{}^{+n}(2\alpha + 3\alpha)}{\text{No. } Th^{226}\alpha_{111e}} \right) .$$

However, the former = 0.253 ± 0.21 and the latter = 0.1967 ± 0.0033 which indicates that the pressure effects discussed in Sec. II.B. are not negligible. Hence, in order to obtain (No. $Th^{226}R_0{}^{+n}$/No. $Th^{226}\alpha_0$) and (No. $Th^{226}R_{111e}{}^{+n}$/No. $Th^{226}\alpha_{111e}$) it is necessary to assume that the above numbers are actually Prob($2\alpha + 3\alpha$) times c_1 or c_2 respectively. The above numbers ($\text{Prob}(2\alpha + 3\alpha)_{c1}$ = 0.253 ± 0.21 and $\text{Prob}(2\alpha + 3\alpha)c_2$ = 0.1967 ± 0.0033) were then used to obtain the ratios (No. $Th^{226}R_0{}^{+n}$/ No. $Th^{226}\alpha_0$) and No. $Th^{226}R_{111e}{}^{+n}$/No. $Th^{226}\alpha_{111e}$) shown in Table VII and illustrated in Figs. 91 and 92.

Table VII. Calculated ratios for $Th^{226}R_0$ and $Th^{226}R_{111e}$.

n	$\frac{\text{No. } Th^{226}R_0{}^{+n}}{\text{No. } Th^{226}\alpha_0}$	$\frac{\text{No. } Th^{226}R_{111e}{}^{+n}}{\text{No. } Th^{226}\alpha_{111e}}$
-2	$(4.6 \pm 5.3) \times 10^{-4}$	
-1	$(1.03 \pm 1.20) \times 10^{-3}$	
0	$(1.55 \pm 0.40) \times 10^{-1}$	
+1	$(4.62 \pm 0.53) \times 10^{-1}$	
+2	$(2.37 \pm 0.20) \times 10^{-1}$	$< 5.5 \times 10^{-3}$
+3	$(5.44 \pm 0.53) \times 10^{-2}$	$(5.5 \pm 3.0) \times 10^{-3}$
+4	$(3.83 \pm 0.38) \times 10^{-2}$	$(6.5 \pm 3.0) \times 10^{-3}$
+5	$(3.23 \pm 0.32) \times 10^{-2}$	$(1.47 \pm 0.17) \times 10^{-2}$
+6	$(1.44 \pm 0.14) \times 10^{-2}$	$(2.14 \pm 0.17) \times 10^{-2}$
+7	$(3.33 \pm 0.33) \times 10^{-3}$	$(4.09 \pm 0.26) \times 10^{-2}$
+8	$(1.44 \pm 0.15) \times 10^{-3}$	$(8.49 \pm 0.47) \times 10^{-2}$
+9	$(2.93 \pm 0.58) \times 10^{-4}$	$(9.84 \pm 0.52) \times 10^{-2}$
+10	$\leq (7.0 \pm 16.0) \times 10^{-5}$	$(1.266 \pm 0.059) \times 10^{-1}$
+11		$(1.265 \pm 0.060) \times 10^{-1}$
+12		$(1.228 \pm 0.060) \times 10^{-1}$
+13		$(1.141 \pm 0.058) \times 10^{-1}$
+14		$(6.36 \pm 0.35) \times 10^{-2}$
+15		$(5.94 \pm 0.35) \times 10^{-2}$
+16		$(4.36 \pm 0.28) \times 10^{-2}$
+17		$(3.56 \pm 0.24) \times 10^{-2}$
+18		$(1.87 \pm 0.14) \times 10^{-2}$
+19		$(1.12 \pm 0.10) \times 10^{-2}$
+20		$(5.64 \pm 0.63) \times 10^{-3}$

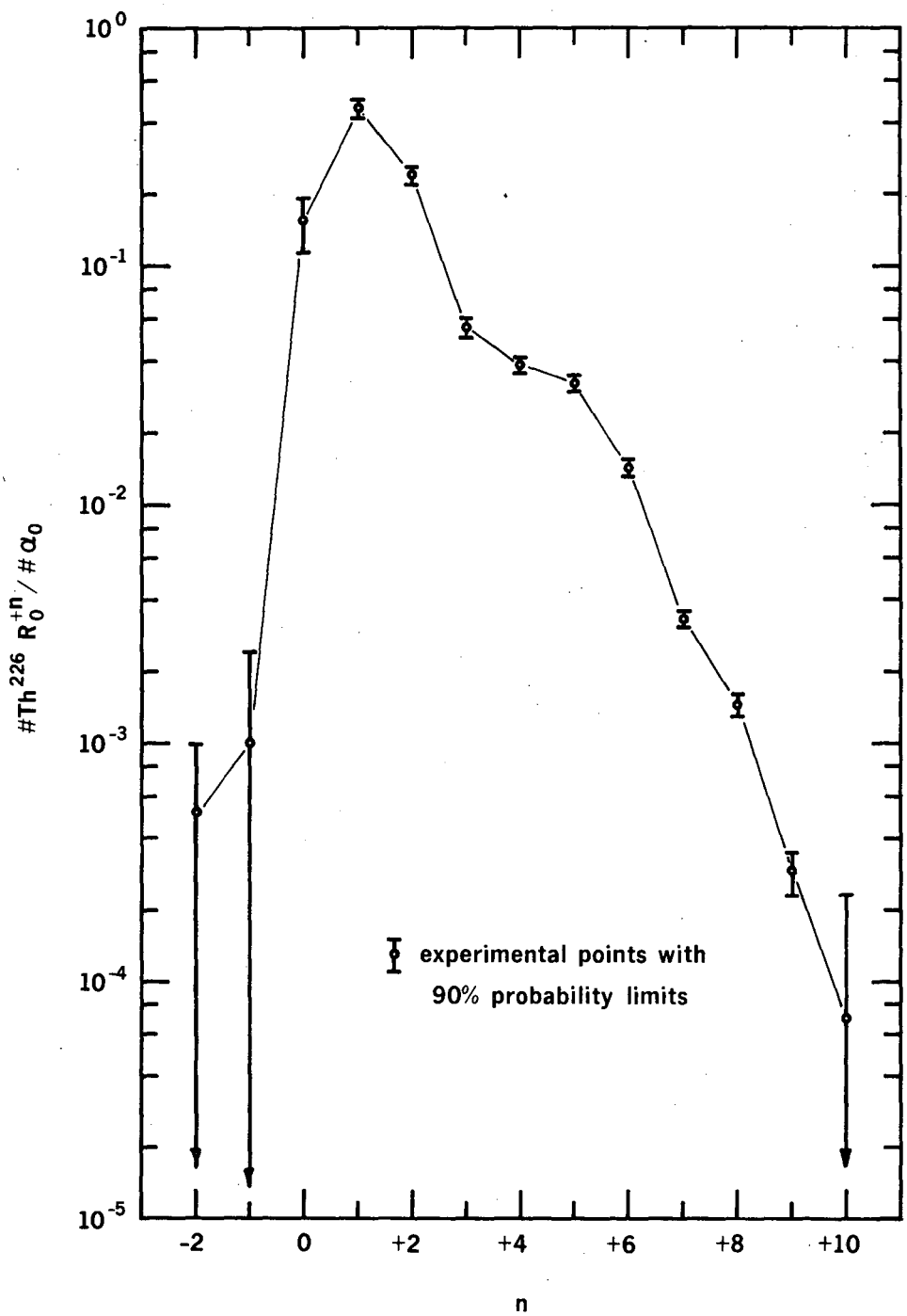

Figure 91. Calculated charge distribution of $Th^{226}R_0$.

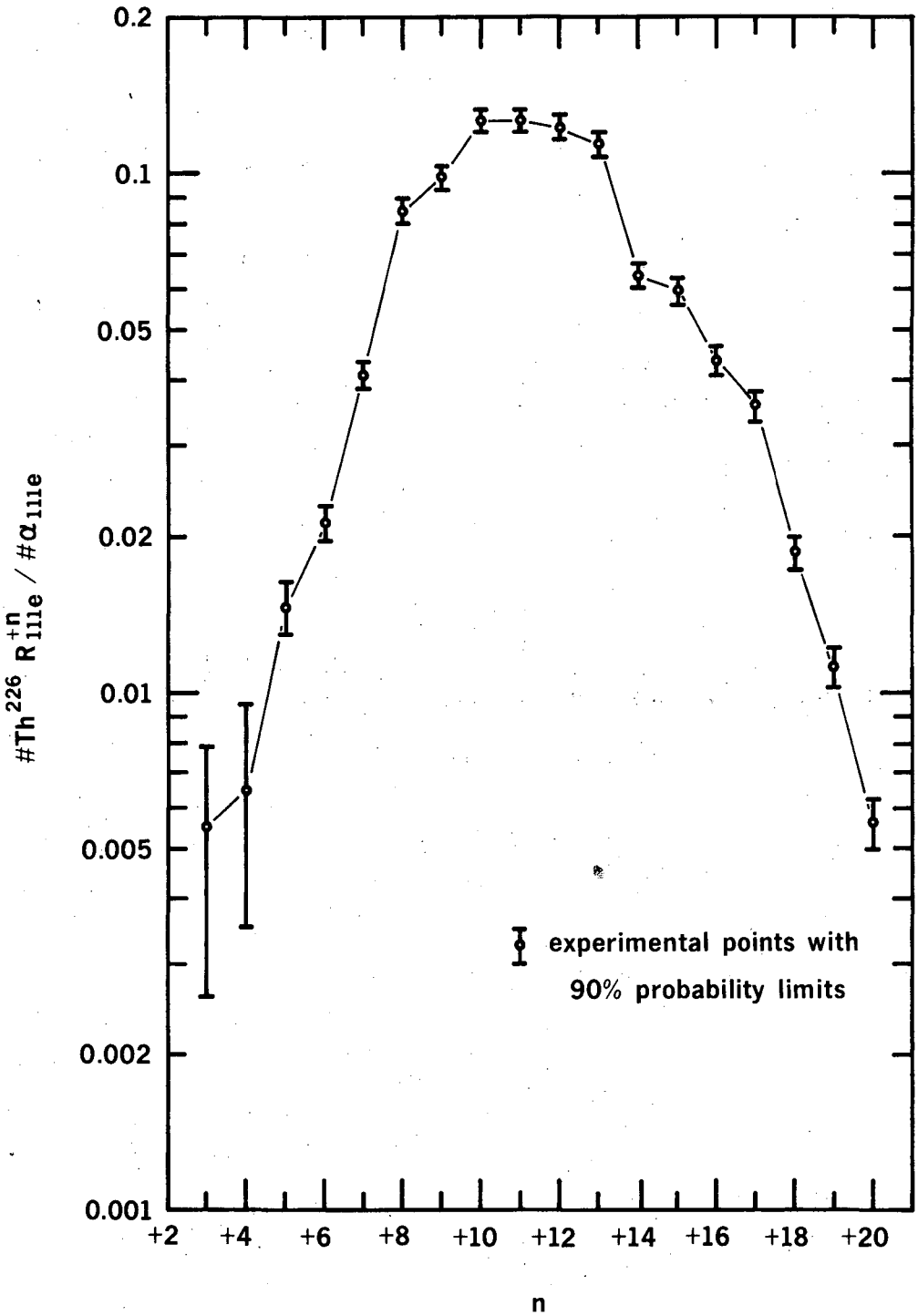

XBL 687-1504

Figure 92. Calculated charge distribution of $Th^{226}R_{111e}$.

2. Theory

The energy distributions obtained for the various recoil groups result not directly from the alpha decay but rather from the interactions between the recoils and the collector plate material and contamination as well as from possible pressure effects. It is clear from the data on $Th^{226}R^{+2}$ (see Figs. 49, 50, 51 and 52) that the distribution can not be the result of variations in the amount of energy carried off by the alpha particle, for this would give energy distributions for recoils the same as those for the alphas. Thus, any variation in the momentum distribution of recoils from that of the alphas due to the alpha decay process, must be caused by the atomic electrons. However, Migdal[1] and Lev nger[2] showed that the energy of the free electrons which result from the "shake off" effect or direct collisions with the alpha particle is very small. Therefore these electrons do not account for the discrepancy between the momentum distributions of the alphas and the recoils. The only other electrons connected with the alpha decay process which could be responsible for this discrepancy are the Auger electrons which are given off when the "holes" created by the "shake off" effect or direct collisions are filled. However, these holes are most likely to occur in the outer-most electron shells as can be seen by comparing the actual charge distribution of $Th^{226}R_0$ (see Fig. 91) with the charge distributions which would result from holes in any particular electron shell of Th^{226} as discussed by Carlson, Hunt and Krause.[25] Thus it is unlikely that any substantial number of holes occur in any shell deeper than the N shell in the direct alpha decay process. Assuming a 1s electron hole in the N shell is filled by a Q electron with another Q electron escaping with the excess energy, the free electron so produced will have a maximum of 1.3 keV in the center of mass system. An electron of maximum energy 1.3 keV in the

center of mass system of the atom can cause a change of only 39 eV in the 114 keV laboratory kinetic energy of the recoil, and so the Auger electrons can not account for the energy distributions of $Th^{226}R_0$. In addition, all of the processes mentioned would create symmetric energy distributions which was not the case at all. Therefore, the half widths of the $Th^{226}R_0^{+n}$ peaks (675 eV for n = +2, 490 eV for n = +3, +4 and +5, and 450 eV for n = +6) must be the result of collision processes both in the source plate and in the path through the spectrograph as discussed in Sec. III. The greater half width and larger tail of the $Th^{226}R_0^{+2}$ can be caused by two things: first, $Th^{226}R^{+2}$ will have suffered more collisions than recoils with higher charges since they are less likely to change their charge, and second, $Th^{226}R^{+2}$ recoils can suffer a large change in energy (small impact parameter)without a charge change whereas recoils with higher charges can not. If this is the case, $Th^{226}R_0^{+1}$ could have even greater collision losses and so its energy distribution would be even broader than that of $Th^{226}R_0^{+2}$. As was discussed previously, in Sec. III.A., this postulated energy distribution is probably what accounts for the identical broad energy distributions of the $Th^{226}R_{111e}^{+n}$ peaks. The recoils which make up these peaks were predominantly of charge +1 before the conversion electron escaped with the resulting increase in charge from Auger processes. The $Th^{226}R_{111e}^{+n}$ peaks will have the energy distribution of $Th^{226}R_0^{+1}$ modified by the energy and momentum carried off by the conversion and Auger electrons. The half width of the R_{111e} peaks, of the order of 900 eV, is consistent with the half width value expected from the R_0 peaks and the half width due to the recoil from the conversion electrons.

Since a complete theory of the effects of alpha decay on the atomic electrons is not presently in existence, it is impossible to make any comparisons between theory and experiment other than to say that the experimental charge distribution for $Th^{226}R_0$ indicates that alpha decay primarily affects the outer shell electrons.

Source and pressure effects on the charge distribution have already been discussed in Sec. III. and will not be repeated here.

3. Conclusions and Future Experiments

It is difficult to draw any strong conclusions concerning the results of Sec. IV. C. other than to say that the energy distributions obtained are not the result of the alpha decay but rather the result of interactions between the recoils and the source. This suggests that such recoils could be used to study various surface effects along with the interactions of heavy atoms or ions with various other materials since both the charge distributions and energy distribution are very sensitive to such effects and interactions. They could also be used to determine the possible composition of the surface contaminant by deliberately placing known amounts of various possible contaminants on the surface of the recoil source plate. In order to analyze such results it would be very desirable to obtain the intrinsic charge distribution of the recoils by setting up an atomic beam type experiment to eliminate source effects entirely. All of these experiments, of course, should be carried out in better vacuums than were used here in order to eliminate pressure effects.

Two other experiments that should be carried out to test some of the theories proposed in this thesis are as follows. First, a study should

be made of the effects of source temperature on the charge and energy distributions of $Th^{226}R_0$. Second, pressure effects of the charge and energy distributions of recoil sources should be studied by using the same parallel plate collected recoil source for as many different pressures as possible in order to separate source effects from pressure effects. The same, of course, holds true for the study of the effects of source temperature.

In addition, it may be possible to make α-γ angular correlation studies in vacuum by selecting the charge of the recoil involved in any particular α-γ angular correlation. This could be done by detecting alphas, gamma rays and charge +n recoils and requiring a coincidence between all three where the charge +n recoils could be separated from recoils of different charges by means of a magnetic field. The lower charged or neutral recoils should be in a limited number of electron configurations. Hence the resulting magnetic field at the nucleus might not be so variable as to destroy the α-γ correlation as has apparently been the case when all charge states of the recoil were included.[47]

V. ERROR ANALYSIS

As was mentioned in a footnote, practically all of the errors mentioned in this thesis were $\pm$ 90% probability limits. Usually, the only source of error considered was the statistical error introduced by counting a finite number of events with a finite background. The exceptions to this rule were as follows:

1. A counting error was introduced in the process of counting the alphas and 2- and 3-pronged events on the photographic plates and was included in the error calculations. These counting errors were determined by making several counts of the same plate. The resulting counting errors were $\pm$ 0.5% for alphas and recoils.

2. An attempt was made to include the error involved in arbitrarily choosing the best smooth curve for separating $Th^{226}R_{111e}$ from $Th^{226}R_0$ where necessary. This was done by finding the largest and smallest $Th^{226}R_{111e}$ peak heights for which it could still be said that the resulting $Th^{226}R_0$ tails were reasonably smooth. However, no term was included in calculating the total error that covered the possibility that the apparent $Th^{226}R_{111e}$ peak in the tail of a $Th^{226}R_0$ peak was simply a statistical fluctuation in this tail. This omission will be important only for separating the $Th^{226}R_{111e}{}^{+2}$ peak from the $Th^{226}R_0{}^{+2}$ peak and such a fluctuation is, in fact, the likely cause of the high value obtained for the ratio No. $Th^{226}R_{111e}{}^{+2}(2\alpha + 3\alpha)$/No. $Th^{226}\alpha_{111e}$ given in Table V.

3. The times at which various plates were run entered into the calculation of the ratios No. $Th^{226}R^{+n}(2\alpha + 3\alpha)$/No. $Th^{226}\alpha$ for $n > +2$ since the alphas and recoils were not on the same plate. The errors involved in measuring the actual times were assumed to be on the order of $\pm$ 10 sec.

4. Since the shape and ordinates of the experimental Prob(3α) curve

(see Fig.22) could not be determined exactly, its possible variations were included as a source of error in calculating the errors for the ratios No. $Th^{226}R_0{}^{+n}$/No. $Th^{226}R_0{}^{+2}$ for n = -2, $\pm$ 1 or 0.

No systematic errors were known to exist and hence no such errors were included in the error analysis. Hence the total error for $f(x_1, x_2, \ldots x_n)$ was assumed to be as follows:

$$\sigma^2 \left[f(x_1, x_2, \ldots x_n)\right] = \sum_{i=1}^{n} \left(\frac{\partial f(x_1, x_2, \ldots x_n)}{\partial x_i}\right)^2 \sigma^2(x_i)$$

where the x_i's are independent quantities and $\sigma^2(x_i)$ is the standard deviation for each of these quantities. Then

$\pm$ 1.6 $\sigma \left[f(x_1, x_2, \ldots x_n)\right]$ gives the 90% probability limits of the quantity $f(x_1, x_2, \ldots x_n)$.

ACKNOWLEDGEMENTS

I wish to thank Dr. Frank Asaro who supervised the day to day work involved in this experiment, Professor A. C. Helmholz who directed this study and provided a great deal of help in the final stages, and Miss Miriam Machlis who gave invaluable assistance in typing up rough drafts and the final copy.

I would also like to thank Mrs. Helen Michel, Mr. Eldred Calhoon, Mr. Alton Minter and Mr. George Driscoll for their help in the chemistry involved and Mr. James Arnold for keeping the alpha spectrograph in working condition.

REFERENCES

1. A. Migdal, J. Phys. IV, 5, 449 (1941).

2. J. S. Levinger, Phys. Rev. 90, 1, 11 (1953).

3. H. M. Schwartz, Phys. Rev. 100, 1, 135 (1955).

4. Alex E. S. Green, Phys. Rev. 107, 6, 1646 (1957).

5. E.H. S. Burhop, The Auger Effect and Other Radiationless Transitions (Cambridge University Press, 1952).

6. W. N. Asaad and E. H. S. Burhop, Proc. Phys. Soc. (London) 71, 3, 369 (1958).

7. Max Wolfsberg and Morris L. Perlman, Phys. Rev. 99, 6, 1833 (1955).

8. S. Szucs and J. M. Delfose, Phys. Rev. Letters 15, 4, 163 (1965).

9. Gilber L. Cano and Ralph W. Dressel, Phys. Rev. 139, 6A, A1883 (1965).

10. MM. Nils Perrin et Wladyslaw de Wieclawik, Cr. Acad. Sc. Paris, 262, Series B, 511 (1966).

11. T. A. Carlson, A. H. Snell, P. Pleasonton, and C. H. Johnson, Chemical Effects of Nuclear Transformations (International Atomic Energy Agency, Vienna, 1961) Vol. I, p. 155.

12. T. A. Carlson, Phys. Rev. 130, 6, 2361 (1963).

13. T. A. Carlson, Physics Division Annual Progress Report, ORNL-3268, p. 65 (Jan. 31, 1962).

14. Arthur H. Snell and Frances Pleasonton, Phys. Rev. 111, 5, 1338 (1958).

15. T. A. Carlson, Frances Pleasonton, and C. H. Johnson, Phys. Rev. 129 5, 2220 (1963).

16. William Rubinson, CONF 233-1, BNL-7333, p. 510.

17. W. Rubinson, W. Bernstein, Phys. Rev. 86, 545 (1952).

18. William Rubinson, Phys. Rev. 130, 5, 2011 (1963).

19. A. H. Snell, F. Pleasonton, and T. A. Carlson, Chemical Effects of Nuclear Transformations (Int. Atomic Energy Agency, Vienna, 1961) Vol. I, p. 147.

20. Thomas A. Carlson and Manfred O. Krause, Phys. Rev. 137, 6A, A1655 (1965).

21. Frances Pleasonton and A. H. Snell, Proc. Roy. Soc. (London) A241, 141 (1957).

22. Manfred O. Krause, Marvin L. Vestal, and William H. Johnston, Phys. Rev. 133, 2A, 385A (1964).

23. Thomas A. Carlsen and Manfred O. Krause, CONF-233, 3, p. 494.

24. R. A. Rubenstein (Thesis), University of Illinois (1955).

25. Thomas A. Carlson, W. E. Hunt, and Manfred O. Krause, Phys. Rev. 151, 1, 41 (1966).

26. R. C. Pilger, Nuclear Decay Schemes in the Actinium Family (Ph. D. Thesis), UCRL-3877 (1957).

27. Carl Phillip Ruiz, Alpha Decay Studies in the Families of the Light Uranium Isotopes, (Ph. D. Thesis) UCRL-9511 (1961).

28. D. L. Judd and S. A. Bludman, Nucl. Inst. 1, 46 (1957).

29. W. Wayne Meinke, High Energy Bombardment Products of Thorium, (Thesis), UCRL-483 (1949).

30. E. W. Valyocsik, Range and Range Straggling of Heavy Recoil Atoms (M. A. Thesis) UCRL-8855 (1959).

B. G. Harvey, Recoil Techniques in Nuclear Reaction and Fission Studies, UCRL-9151 (1960).

31. P. W. Benjamin, Nuc. Instr. and Meth. 26, 179-181 (1964).

32. J. Rotblat, J. Catala, and W. M. Gibson, Nature 167, 550-552, (April 7, 1951).

33. W. H. Barkas, Nuovo Cimento, VIII, 2, 201-214 (1958).

34. W. H. Barkas, P. H. Barrett, P. Cüer, H. Heckman, F. M. Smith and H.K. Ticho, Nuovo Cimento VIII, 2, 185-200 (1958).

35. Albert T. Oliver, Rev. Sci. Instr. 25, 4, 326-330 (1954).

36. M. Debeauvais, E. Piccotto and S. Wilgain, Nuovo Cimento 5, (10) 260-5 (1957).

37. N. Marongue, Nuovo Cimento (10) 6, 1102-5 (1957).

38. Leopold Vigneron, Jeannine Genin and Raymond Chastel, Compt. Rend. 240, 1423-25 (1955).

39. E. H. S. Burhop and H. S. W. Massey, Electronic and Ionic Impact Phenomena (Clarendon Press, Oxford, 1952).

40. F. Asaro, Lawrence Radiation Laboratory (private communication).

41. R. S.Hager and E. C. Seltzer, Internal Conversion Tables, Part I. K. L. M-Shell Conversion Coefficients, California Institute of Technology report CALT-63-60 (1967).

42. Hans-Christian Pauli, Tables of Internal Conversion Coefficients and Particle Parameters, Princeton University Report COO-1420-137 (1967).

43. C. M. Lederer, J. M. Hollander, I. Perlman, Table of Isotopes, (John Wiley and Sons, Inc., 6th Ed. 1967).

44. E. Segre, Nuclei and Particles (W. A.Benjamin, Inc. 1964).

45. J. M. Meek and J. D. Craggs, Electrical Breakdown of Gases, (Clarendon Press, Oxford, 1953).

46. J. O. Cobine, Gaseous Conductors (McGraw-Hill, 1941).

47. Eileen Flamm, Perturbation of Alpha-Gamma Angular Correlations in Transuranium Isotopes (Ph. D. Thesis) UCRL-9325 (1960).